Peroxisomal membrane dynamics in health and disease

Submitted by **Josiah Benjamin Passmore** to the University of Exeter as a thesis for the degree of **Doctor of Philosophy in Biological Sciences** in October 2019.

I certify that all material in this thesis which is not my own work has been identified and that no undeclared material has previously been submitted and approved for the award of a degree by this or any other University.

Signature: ……..

Abstract

Peroxisomes are oxidative subcellular organelles present in the majority of eukaryotic cells, with key functions in lipid metabolism, reactive oxygen species (ROS) homeostasis, and production of ether phospholipids (myelin lipids). Modulation of peroxisome number in the cell through coordinated proliferation and degradation is crucial for supporting these functions, with peroxisomes rapidly responding to environmental changes in order to maintain cell vitality. As a result, patients with defects in peroxisome proliferation present with a range of symptoms and severity, with vision/hearing loss, neurological defects, seizures, and organ dysfunction being common in peroxisome biogenesis disorders.

To proliferate, peroxisomes follow a multi-step process of growth and division, whereby (i) the peroxisome membrane is elongated, (ii) this elongation is constricted at several points to produce a 'beads on a string' morphology, and (iii) the membrane undergoes scission at these constriction points to produce new peroxisomes. This process requires extensive remodelling of the peroxisomal membrane, through the action of dedicated division machinery. Our knowledge of the key processes underlying the regulation of this membrane remodelling and the contribution of alterations to membrane dynamics to health and disease are still not well understood.

In this thesis, a literature review is presented describing knowns and unknowns in the peroxisome field, with particular focus on the role peroxisome membrane dynamics play in maintaining peroxisome function, and the role of these dynamics in human health and disease.

Results chapters begin first by investigating alterations to peroxisomal membrane dynamics in response to the mitochondrial respiratory chain inhibitor rotenone, to understand the resistance of peroxisomes to mitochondria-derived ROS. Surprisingly, alterations to the peroxisome compartment are due to the microtubule-destabilising ability of rotenone, and peroxisomes are unaffected by mitochondrial ROS, despite this not being the case *vice versa*. The implication of these findings in understanding the peroxisome-mitochondria redox relationship are discussed, in addition to highlighting the importance of investigating

peroxisome membrane dynamics in *in cellulo* models of disease. Second, alterations to peroxisomal membrane dynamics in response to lack of division protein MFF are investigated. It is revealed that despite completely normal biochemical parameters, there are more underlying alterations to the peroxisomes than hyper-elongation, and that MFF has a crucial role in the maturation of peroxisomes. In addition, these findings suggest that peroxisomal import complex protein PEX14 may play a role in peroxisomal membrane dynamics, by stabilising elongated peroxisomal tubules through interaction with the cytoskeleton. Third, an interdisciplinary, combined experimental-modelling approach is used to characterise alterations to peroxisomal membrane dynamics, using peroxisomes with a block in division (loss of function of MFF), and peroxisomes with altered membrane dynamics (elongation through expression of Rho GTPase MIRO1), as case studies. The key cellular processes underlying the regulation of peroxisome growth and division are highlighted, and findings from this chapter provide a proof-of-concept that this interdisciplinary approach is useful not only for characterisation and understanding mechanisms of membrane dynamics, but as a prediction tool to help suggest future therapeutics.

Finally, a discussion of the key findings of this thesis and their implications is presented, highlighting the real importance of studying peroxisome membrane dynamics through interdisciplinary approaches such as the ones employed here.

Acknowledgements

Firstly, to my supervisor Prof. Michael Schrader, I express my gratitude for the support during my time in the lab, from backing me for a Masters, to my upgrade to PhD, and following. Under your guidance and mentoring I have learnt a great deal about what it means to be successful in science.

Thank you to Dr. David Richards, whose support and teaching with modelling has opened my eyes to interdisciplinary research. Also, thanks for the many off-tangent conversations, making our meetings twice as long as they should be but twice as interesting.

Every one of the Schrader lab taught me something invaluable, from the basics down to the little time-saving tips. Particularly Joe Costello and Tina Schrader; I arrived in the lab with barely any experience and without your continued support I would not have got very far! Also thanks the rest of the lab members and visitors who have been in the group; Afsoon, Paula, Alexa, Suzan, Maki, Ruth & Beatriz, you all have taught me a great deal, as well as being great friends.

To those in Lab 211, thanks for making every day different and ensuring that I never got bored. Thanks for slacker's club, the beach trips, the quizzes and the all-you-can-eat Chinese.

To my friends and family, thank you for the support, care packages, questions, interest and much confusion about what I am really doing. Particularly thanks to Kelly for being my motivation in this journey.

Additional thanks and recognition go to those colleagues who, through collaboration on various projects, provided exceptional data that is included in this thesis as described in the Author's Declarations.

Finally, funding for this work was provided by UoE, The Sidney Perry Foundation and from Zellweger UK (https://www.zellweger.org.uk/). It has been a pleasure to get to know Tash at ZUK over the past few years and am thankful not just for funding, but for allowing us to see the more personal side of the work that we do in the lab, providing much encouragement.

List of Contents

List of Figures

List of Tables

Author's Declarations

Chapter 1

Part of the literature review in this chapter (section 1.1.10) has resulted in the publication of a review article:

Costello JL, **Passmore JB**, Islinger M, Schrader M. (2018) Multi-localized proteins: the peroxisome-mitochondria connection. Subcell Biochem. 89:382-415. DOI: 10.1007/978-981-13-2233-4_17.

Chapter 2

This chapter is comprised of published data, with figures and some text (materials and methods) that are included in the following manuscript:

Passmore JB, Pinho S, Gomez-Lazaro M, Schrader M. (2017) The respiratory chain inhibitor rotenone affects peroxisomal dynamics via its microtubule-destabilising ability. *Histochem Cell Biol*. 148(3), 331-341. DOI: 10.1007/s00418-017-1577-1.

More specifically, the complete materials and methods, contribution to the other sections of the manuscript, and preparation of all figures for this manuscript were performed by me.

Similar results as those presented in Figures 2.1-2.3 were previously reported in the master's thesis of Sónia Pinho (Pinho 2010), and results were independently confirmed by me (cell culture, drug treatment, immunofluorescence, microscopy, analysis, and figures) for this study.

Figures 2.4 and 2.5 are novel data generated by me and allow a more complete picture of the effects of rotenone on the peroxisomal and mitochondrial compartments.

Chapter 3

This chapter is comprised of original data; an edited version of a manuscript submitted to *Biochimica et Biophysica Acta – Molecular Cell Research* at the

point of thesis submission. Figure numbers have been changed to integrate into this thesis; much of the text is unaltered. Please note that removed from the text is data regarding the modelling of MFF-deficient fibroblasts with a mathematical model; this data is presented as part of Chapter 4 (section 4.3.3.1), but does not take away from the overall message of this chapter. My specific contributions to this manuscript are outlined below:

- The complete first draft of all aspects of the manuscript, including putting together all figures, and subsequent editing.
- Cell culture of control (C109) and MFF-deficient fibroblasts, used in Figures 3.1, 3.3, 3.4E-G, and 3.6.
- Immunofluorescence and confocal images of MFF-deficient fibroblasts for Figure 3.1C.
- Analysis of immunofluorescence and electron micrographs for Figures 3.1D-F.
- With the exception of transfection and microscopy of Figures 3.3A-B, all data contained in Figure 3.3, including immunofluorescence, protein distribution analysis, siRNA transfection, SDS-PAGE and immunoblotting, and drug treatment.
- Measurement of peroxisomal pH using ImageJ for Figures 3.4E-G.
- All data contained in Figure 3.6, including transfection, immunofluorescence, analysis, HBSS treatment, SDS-PAGE and immunoblotting.
- Computer generation of control and MFF-deficient peroxisome populations for the calculations used for Figure 3.7.

Contributions by collaborators for figures shown in this chapter are below:

- Luis Godinho performed the transfection (where appropriate), immunofluorescence and microscopy of control and MFF-deficient patient fibroblasts for Figures 3.1A, 3.3A-B, and 3.4E.
- Sacha Ferdinandusse performed the biochemical analysis shown in Table 3.3 and Figure 3.2.
- Celien Lismont and Marc Fransen performed redox measurements of control and MFF-deficient fibroblasts for Figure 3.4A-D.
- Yunhong Wang and Markus Islinger performed the knockdown of MFF in neuronal cells for Figure 3.5.
- Christian Hacker performed the electron microscopy shown in Figure 3.1B.

The full authorship list for the manuscript is as follows:

Passmore JB, Godinho LF, Ferdinandusse S, Lismont C, Wang Y, Hacker C, Islinger M, Fransen M, Richards DM, Freisinger P, Schrader M.

Chapter 4

This chapter is comprised of original and published data, all of which was generated by me in collaboration with Dr David Richards, as an expert in this mathematical modelling approach.

Similar, more basic results to those in Figures 4.4, 4.10, 4.15 and 4.16, in addition to a brief description of the model can be found in the following manuscript:

Castro IG, Richards DM, Metz J, Costello JL, **Passmore JB**, Schrader TA, Gouveia A, Ribeiro D, Schrader M. (2018) A role for MIRO1 in motility and membrane dynamics of peroxisomes. *Traffic*. 19(3):229-242. DOI: 10.1111/tra.12549

The full MATLAB code used for this study is available upon request to Dr David Richards (david.richards@exeter.ac.uk), or Professor Michael Schrader (m.schrader@exeter.ac.uk).

Abbreviations

3-MA	3-methyladenine
ABCD	ATP-binding cassette transporters, subfamily D
ACBD	acyl-CoA binding domain containing protein
ACOX	Acyl-CoA oxidase
ACSL	long-chain acyl-CoA synthetase
AGP	1-O-alkyl G3P
ALOX15	arachidonate 15-lipoxygenase
ARD	adult refsum disease
ATAD1	ATPase family AAA domain-containing protein 1
ATG	autophagy related protein
ATM	ataxia telangiectasia mutated kinase
ATP	adenosine triphosphate
BAAT	bile acid-CoA: aminoacid transferase
BAK	Bcl-2 homologous antagonist/killer
Bcl-2	B-cell lymphoma 2
BSA	bovine serum albumin
CDP-DAG	cytidine diphosphate diacylglycerol
CL	cardiolipin
DAG	diacylglycerol
DBP	D-bifunctional protein
DHA	docosahexaenoic acid
DHAP	dihydroxyacetone phosphate
DHAPAT	dihydroxyacetone phosphate acyltranferase
DHCA	dihydroxycholestanoic acid
DEHP	di(2-ethylhexyl) phthalate
DMEM	Dulbecco’s modified Eagle medium
DMSO	dimethyl sulfoxide
DNML1	dynamin-1-like protein gene
DRP1	dynamin-related protein 1
DYNAMO	dynamin-based ring motive-force organizer 1
E. coli	Escherichia coli
EPHX2	epoxide hydrolase 2
ER	endoplasmic reticulum
ERAD	ER-associated degradation
ERMES	ER-mitochondria encounter structure
E-Syts	extended synaptotagmin
FAD	flavin adenine dinucleotide
FALDH	fatty aldehyde dehydrogenase
FAR1	fatty acyl-CoA reductase
FIS1	mitochondrial fission 1 protein 1
FPP	farnesyl diphosphate
Fzo1p	fuzzy onions homolog 1
G3P	glycerol-3-phosphate

GDAP	ganglioside-induced differentiation-associated protein
Gem1	GTPase EF-hand protein of mitochondria 1
GFP	green fluorescent protein
GSH	reduced glutathione
GSSG	glutathione disulphide
GSTK1	glutathione S-transferase kappa
GTP	guanosine triphosphate
H_2O_2	hydrogen peroxide
HBSS	Hank's balanced salt solution
HCMV	human cytomegalovirus
HIF	hypoxia-inducible factor
HIV	human immunodeficiency virus
HSP	heat shock protein
IgG	immunoglobulin G
KifC3	Kinesin Family Member C3
LBP	L-bifunctional protein
LC3	microtubule-associated proteins 1A/1B light chain 3B
LIR	LC3 interacting region
LONP	Lon peptidase
MAP2	microtubule-associated protein 2
MAVS	mitochondrial antiviral signalling protein
MDS	molecular dynamics simulations
MDV	mitochondrial-derived vesicle
MEF	mouse embryonic fibroblast
MFF	mitochondrial fission factor
MiD	mitochondrial dynamics protein
MIRO	mitochondrial Rho GTPase
mPTS	peroxisome membrane protein targeting signal
Msp1	mitochondrial sorting of proteins 1
mTORC1	mammalian target of rapamycin complex 1
NAC	N-acetyl cysteine
NBR1	neighbour of breast cancer type 1 susceptibility protein 1 gene protein 1
NO·	nitric oxide
NOC	nocodazole
$O_2{\cdot}^-$	superoxide
$ONOO^-$	peroxynitrite
PA	phosphatidic acid
PBD	peroxisome biogenesis disorder
PBS	phosphate-buffered saline
PC	phosphatidylcholine
PE	phosphatidylethanolamine
PED	peroxisomal enzyme deficiency
PEX	peroxin
PG	phosphatidylglycerol
PGC-1α	peroxisome proliferator-activated receptor gamma coactivator 1α
PI	phosphatidylinositol
PI(4,5)P2	phosphatidylinositol 4,5-bisphosphate

PMP	peroxisomal membrane protein
PPAR	peroxisome proliferator-activated receptor
PPRE	peroxisome proliferator response element
PRDX5	peroxiredoxin 5
PS	phosphatidylserine
PTS	peroxisomal targeting signal
PUFA	poly-unsaturated fatty acid
PXMP2	peroxisomal membrane protein 2
RADAR	receptor accumulation and degradation in the absence of recycling
RCDP	rhizomelic chondriodysplasia punctata
RIG	retinoic acid-inducible gene
RING	really interesting new gene
RLR	RIG-I-like Receptor
RNS	reactive nitrogen species
ROS	reactive oxygen species
ROT	rotenone
RXR	retinoid X receptor
SDS-PAGE	sodium dodecyl sulfate polyacrylamide gel electrophoresis
SM	sphingomyelin
SQSTM1	sequestosome 1
SV40	polyomavirus simian virus 40
TA	tail-anchored
TAX	paclitaxel
TCA	tricarboxylic acid
THCA	trihydroxycholestanoic acid
TMD	transmembrane domain
TNKS	tankyrase
TOM20	translocase of outer membrane protein 20
TRAK	trafficking kinesin protein
TRiC	T-complex protein-1 ring complex
Tysnd	trypsin domain containing protein
UBXD8	ubiquitin-regulatory X domain-containing protein 8
UPR	unfolded protein response
UPS	ubiquitin proteasome system
USP30	ubiquitin-specific-processing protease 30
VAP	vesicle-associated membrane protein-associated protein
VHL	Von Hippel-Lindau tumor suppressor
VLACS	very long-chain acyl-CoA synthetase
VLCFA	very long-chain fatty acid
vMIA	HCMV-encoded viral mitochondria-localised inhibitor of apoptosis
VPS35	vacuolar protein sorting-associated protein 35
X-ALD	X-linked adrenoleukodystrophy
ZSD	Zellweger spectrum disorder

Chapter 1 Introduction

1.1 Peroxisomes

1.1.1 Overview

Peroxisomes are ubiquitous, single-membrane bound organelles with a wide variety of functions, including lipid metabolism, maintenance of reactive oxygen species (ROS), and production of ether phospholipids. They are responsive, highly dynamic, crucial for proper cell function, and are therefore hugely important in health and disease. A thorough understanding of not only the peroxisome's many functions, but the actual maintenance of the peroxisomal population is work which, in the future, will allow for better therapeutic intervention for peroxisomal and peroxisome-related disorders.

This thesis explores the dynamics of the peroxisome membrane; literature review and results particularly focussing on mammalian cells, with some discussion on different aspects of peroxisome dynamics in other cell types and organisms. The introduction will cover the formation of the peroxisome lipid bilayer including its integral membrane proteins (sections 1.1.3-1.1.4), and the remodelling of the peroxisomal membrane during the maintenance of peroxisome number (sections 1.1.5-1.1.7) and motility (section 1.1.8). The peroxisome membrane plays a crucial role in compartmentalising the organelle from the rest of the cell in order to carry out its many functions, which are summarised in section 1.1.9. A common theme of this thesis is the interaction of peroxisomes with the mitochondria, including in maintenance of ROS (Chapter 2), and the sharing of division proteins (Chapter 3). An overview of peroxisome-mitochondria interaction is discussed in section 1.1.10. Finally, the importance of peroxisomes and peroxisomal membrane dynamics in human health and disease is presented in section 1.1.11.

1.1.2 History

Peroxisomes were first described as 'microbodies' in mouse kidney proximal tubule cells in 1954, in a PhD thesis by Swedish doctoral student Johannes Rhodin (Rhodin 1954). The characterisation of peroxisomes as an organelle came through the work of Christian De Duve and others, who, through sedimentation assays, identified many of the key peroxisomal enzymes (De Duve and Baudhuin 1966). Since then, our understanding of peroxisome function,

maintenance, and characteristics has improved in leaps and bounds, but much still remains to be discovered.

1.1.3 The Peroxisomal Membrane

The initial building blocks of all organelles are membrane lipids. The lipid composition of biological membranes affects the functioning of membrane-associated activities, the integrity of the organelles themselves, carries different properties to enable dynamic processes, and acts to compartmentalise cellular functions. This compartmentalisation is especially important for the peroxisomes; allowing them to function as ROS-scavengers to reduce oxidative stress to the rest of the cell (Schrader and Fahimi 2006a; Fransen et al. 2012). The peroxisomal membrane is also highly dynamic, with deformation of the membrane occurring during the growth and division process of peroxisome proliferation (see section 1.1.5.2). The properties of the membrane that facilitate this process and the extent that peroxisomal proteins deform the peroxisomal membrane biophysical properties remain to be discovered.

Lipids making up organelle membranes are typically, in order of cellular abundance: phosphatidylcholine (PC), phosphatidylethanolamine (PE), phosphatidylinositol (PI), phosphatidylserine (PS), sphingomyelin (SM), cardiolipin (CL), phosphatidic acid (PA) and phosphatidylglycerol (PG) (Vance 2015). Other lipids present include cholesterol and glycosphingolipids, both typically enriched in the plasma membrane compared to other organelles (Vance 2015).

Phospholipid biosynthesis requires the precursors diacylglycerol (DAG), and cytidine diphosphate DAG (CDP-DAG), synthesised from PA (Yang et al. 2018). DAG and CDP-DAG are made either on the ER membrane or on both the ER and mitochondrial membranes, respectively, through the action of PA-phosphatase-1 and CDP-DAG synthase. CDP-DAG is used as a substrate for production of PI and PS on the ER membrane, or PG on the mitochondrial membrane. PS can also be transferred to mitochondria, where it can be decarboxylated by PS decarboxylase to produce mitochondrial PE (Shiao et al. 1995). DAG is important in the Kennedy pathway (Gibellini and Smith 2010) on the ER membrane, to produce PE and PC *de novo* from CDP-ethanolamine and CDP-choline, respectively. Further PC can be made from the methylation of PE.

PC can then form the basis for SM, where a family of SM synthases on the Golgi or plasma membrane transfer a phosphocholine headgroup from PC to ceramide, producing SM in addition to DAG (Marggraf et al. 1981; Huitema et al. 2004). Finally, CL is produced on the mitochondrial inner membrane, requiring the addition of another phosphatidyl residue from CDP-DAG to PG, catalysed by CL synthase 1 in humans (Chen et al. 2006).

The phospholipid composition of peroxisomes in mammalian cells was discovered through isolation of rat liver peroxisomes with two-dimensional thin-layer chromatography (Hardeman et al. 1990), obtaining the following phospholipid composition: PC 56.4%, PE 27.5%, plasmalogen PE 2.1%, PS 3%, PI 4.7%, SM 3.7%, other 2.6% (not including cardiolipin).

How then do these lipids get to the peroxisome? The vast majority of peroxisomal lipids are synthesised in the ER. Several PMPs have been suggested to be targeted to the ER and inserted to peroxisomes through a vesicular pathway (see section 1.1.4.2), and peroxisomes can be formed *de novo* from the ER (see section 1.1.5.1). This may play a role in supplying phospholipids to the peroxisome. Indeed, through targeting of the *E. coli* PS decarboxylase to the peroxisomal membrane in yeast cells lacking the enzyme, it was shown that PS is efficiently transferred to the peroxisomes from the ER to be converted into PE, and that synthesised PE can transfer back to the ER from peroxisomes (Raychaudhuri and Prinz 2008). However, this ER to peroxisome PS transport still occurred under conditions of disturbed ER vesicular transport, suggesting a non-vesicular pathway for phospholipid transfer from the ER to peroxisomes. This was further shown by the conversion of PS to PE *in vitro* following mixing PS-containing microsomes with purified PS decarboxylase-containing peroxisomes, removing the possibility for a vesicular pathway (Raychaudhuri and Prinz 2008). While PS is not the most abundant peroxisomal membrane phospholipid (Hardeman et al. 1990), it is likely that due to the high efficiency of transfer and close apposition of their membranes, the majority of phospholipid transfer to the peroxisome will follow this non-vesicular pathway.

Therefore, as can be expected, the phospholipid profile of the peroxisome largely resembles that of the ER. It is also similar to that of mitochondria, except for the absence of cardiolipin. Cardiolipin is supposedly specific to mitochondria, with the

presence of cardiolipin in non-mitochondrial fractions attributed to contamination (Vance 2015). Interestingly, the peroxisomal phospholipid composition does seem to include cardiolipin in yeast, shown by two separate studies (Zinser et al. 1991; Wriesnegger et al. 2007). As there may be a *de novo* pathway of peroxisome biogenesis from mitochondria under certain conditions (Sugiura et al. 2017) (see section 1.1.5.1), this may play a role in supplying membrane lipid including cardiolipin to the peroxisome in yeast. However, deletion of cardiolipin synthase in *Saccharomyces cerevisiae* has no effect on peroxisome biogenesis and abundance (Kawałek et al. 2016), suggesting either cardiolipin itself or *de novo* synthesis from mitochondria is not needed to maintain peroxisomes in yeast. The lack of cardiolipin in mammalian peroxisomes possibly suggests that the *de novo* synthesis of peroxisomes in mammalian cells from mitochondria only occurs under certain conditions, or that mitochondrial-derived pre-peroxisomal vesicles are devoid of cardiolipin. How the phospholipid profile differs between an established population of peroxisomes and newly-formed peroxisomes formed from pre-peroxisomal vesicles could shed some light on this.

The phospholipid composition of the membrane can affect not only membrane properties, but also affect protein interaction with organelles (Bigay and Antonny 2012). The distribution of charged lipids such as PS and PI(4,5)P_2 in the membrane affects membrane electrostatics, in turn affecting the targeting of proteins with charged residues (Yeung et al. 2008). For example, changes in levels of PS or PI(4,5)P_2 in the phagosomal membrane during maturation, directs different G proteins with positively charged residues to the membrane (Magalhaes and Glogauer 2010). Indeed, variations in the tail charge of tail-anchored (TA) proteins affects their organelle localisation, with a high charge clearly promoting a peroxisomal localisation (Costello et al. 2017a). It was shown that this high charge promotes PEX19 interaction (required for TA protein membrane insertion), and loss of charge causes mistargeting to the mitochondria. It is possible that the membrane phospholipid composition plays a role in this, with the percentage of mitochondrial PS and PI being relatively low and preferentially orienting to the inner membrane space (Horvath and Daum 2013). This possibly increases the membrane charge facing the cytosol, reducing mistargeting of tail-anchored peroxisomal proteins to the mitochondria.

Membrane phospholipids also affect organelle shape via mechanical properties, causing changes in membrane tension, elasticity, bending and curvature (Janmey and Kinnunen 2006). Conical shaped lipids promote negative curvature (e.g. PE and DAG), inverted conical shaped lipids (e.g. PI variants) promote positive curvature, and cylindrical shaped lipids prefer flat membrane structures (e.g. PC and SM) (Janmey and Kinnunen 2006). The overall ratio of lipids in the peroxisome membrane will then affect peroxisome shape and morphology, regardless of external factors. It is then possible that the membrane phospholipid composition alters locally in specific areas of the peroxisome as a prerequisite to peroxisome elongation, for example.

The peroxisomal membrane itself is a fascinating yet relatively understudied area of peroxisome biology. It is highly likely that the composition not only affects biophysical properties of the peroxisome, but that these biophysical properties are altered under various conditions; growth and division, *de novo* biosynthesis, intracellular conditions and cell stress may all have an effect. This in turn can then have further consequences on protein interaction and function at the peroxisomal membrane. An in-depth analysis of peroxisomal membrane composition, biophysical properties and alterations under various conditions is certainly needed in the future.

1.1.4 Peroxisomal Membrane Proteins

The phospholipid/protein ratio in purified rat liver peroxisomes has been reported to have values ranging from 36 to 153 $nmol.mg^{-1}$ (Donaldson et al. 1972; Appelkvist et al. 1981; Fujiki et al. 1982; Hardeman et al. 1990), of which ~26% appear to be membrane proteins (Hardeman et al. 1990). Peroxisomal membrane proteins (PMPs) are typically indispensable for peroxisome function, with loss of PMPs contributing to devastating conditions in humans (see section 1.1.11), mainly due to their roles in controlling the import and export of peroxisomal matrix enzymes (Walter and Erdmann 2019), and the import of fatty acid substrates by the membrane-bound ATP-binding cassette transporters, subfamily D (ABCDs) (Baker et al. 2015) (Figure 1.1C).

1.1.4.1 Control of matrix protein import by PMPs

Peroxisomal matrix proteins are synthesised on free, rather than membrane-bound ribosomes (Goldman and Blobel 1978). Shuttling receptors PEX5 (either short (PEX5(S)) or long (PEX5(L)) isoform) or PEX5(L) with PEX7 bind cargo in the cytosol harbouring a peroxisomal targeting signal (PTS). PTS type 1 (typically the C-terminal tripeptide SKL) and type 2 (typically the loose consensus N-terminal nonapeptide RLXXXXX(Q/H)L), are recognised by PEX5 and PEX7, respectively (Braverman et al. 1998). Following cargo binding, the receptor proteins dock to the peroxisomal membrane via PMPs PEX14 and PEX13, releasing their cargo into the peroxisomal lumen (Schell-Steven et al. 2005). Monoubiquitination by PEX2, PEX10 and PEX12 enables receptor protein recycling back to the cytosol through the action of the PEX1 and PEX6 hexamer anchored to the membrane by PMP PEX26 (Platta et al. 2005) (Figure 1.1C).

1.1.4.2 PMP peroxisomal targeting and membrane insertion

How PMPs target and insert into the peroxisomal membrane is a relatively well-studied area of peroxisome biology, although is still somewhat uncharacterised, with several unknowns and apparent conflictions. Many disorders associated with loss of peroxisomal function typically still harbour peroxisome ‘ghosts’, peroxisomes incapable of matrix protein import but still with an intact membrane (Santos et al. 1988). Therefore, the sorting of PMPs to the peroxisome appears to require separate components to those involved in matrix import. The exceptions to this rule appear to be in loss of the peroxins PEX3, PEX16, and PEX19, in which peroxisomes are absent, but can be formed *de novo* following expression of the missing protein (Honsho et al. 1998; Matsuzono et al. 1999; South and Gould 1999; Shimozawa et al. 2000). This *de novo* formation in the absence of pre-existing peroxisomes appears to be primarily an ER-derived pathway (see section 1.1.5.1). In general, the insertion of a particular PMP into the peroxisomal membrane follows one of two pathways, directly via PEX19, or indirectly via other subcellular organelles (Kim and Hettema 2015; Mayerhofer 2016).

Direct PMP insertion to existing peroxisomal membranes

As with matrix proteins, proteins destined for the peroxisomal membrane also appear to be synthesised on cytosolic ribosomes and sorted post-translationally

to the peroxisome (Suzuki et al. 1987). The classical pathway for targeting and insertion of PMPs to the peroxisomal membrane involves recognition and shuttling by cytosolic PEX19, which upon binding facilitates insertion of the PMP in the peroxisome membrane (Sacksteder et al. 2000) (Figure 1.1C). Recognition by PEX19 is via a peroxisome membrane protein targeting signal (mPTS) on the PMP (Jones et al. 2001, 2004), consisting of a motif of at least 11 basic and hydrophobic amino acids (Rottensteiner et al. 2004; Halbach et al. 2005), with no apparent preference for mPTS localisation on the protein. TA proteins, i.e. those with a single transmembrane domain in close apposition to the C-terminal tail, also interact with PEX19 for membrane insertion (Costello et al. 2017a). Interestingly, reduction in only TA protein tail charge is sufficient for mistargeting of peroxisome proteins to the mitochondria and the ER, with the peroxisomal isoform of ER-localised protein FALDH differing only in having a more positively charged C-terminal tail (Costello et al. 2017a). While it is unknown if the mPTS motif was altered in this study, PEX19 contains a hydrophobic domain, of which mutations disturb PMP binding (Schueller et al. 2010; Chen et al. 2014b). Therefore, it is possible that the mPTS combined with tail charge and TMD hydrophobicity of PMPs facilitates PEX19 binding and subsequent insertion into the membrane, with alterations in this affecting PEX19 binding and causing mistargeting to other organelles. The exact relationship between TA protein properties, PEX19 binding and insertion into the membrane is still unclear.

Contrasting a simple cytosol-peroxisome shuttle model for PEX19, recently Pex19p has been suggested to be involved in TA insertion into the mitochondrial membrane in budding yeast, demonstrated by a reduction in the mitochondrial pool of dual-localised peroxisome-mitochondria proteins Fis1p and Gem1p after deletion of Pex19p (Cichocki et al. 2018), although this was not observed for mammalian FIS1 (Delille and Schrader 2008). In addition, farnesylated PEX19 is required for the insertion of newly synthesised lipid droplet/ER protein UBXD8 into the ER membrane (Schrul and Kopito 2016), with farnesylation of PEX19 not required for the restoration of peroxisomes in PEX19 deficient cells (Vastiau et al. 2006), but required for PMP binding (Rucktäschel et al. 2009). It is therefore likely that other factors such as post-translational modifications of PEX19 can influence PMP binding, targeting and localisation.

The PEX19-PMP complex has the capability to interact and dock with integral PMP PEX3 at the peroxisomal membrane (Fang et al. 2004), with PMP bound PEX19 having a higher affinity for PEX3 than PEX19 alone (Pinto et al. 2006). PEX3 may facilitate PMP insertion upon binding to the PEX19-PMP complex by perturbing the lipid bilayer, as the C-terminal cytosolic domain can strongly associate with membrane lipids *in vitro*, possibly altering membrane properties (Pinto et al. 2009). The final peroxin indispensable for formation of an intact peroxisomal membrane in mammalian cells is PEX16, which can act as a receptor for a PEX19-PEX3 complex, inserting it into the peroxisomal membrane (Matsuzaki and Fujiki 2008) (Figure 1.1C). Therefore, as PEX19-dependent PEX3 import requires PEX16 at the membrane, and PEX19-dependent PEX16 import should require PEX3 at the membrane, it would appear that in order to build a complete peroxisome, it is required to start with either PEX3 or PEX16 already at the membrane. Therefore, this would suggest that in order to form peroxisomes *de novo*, PMPs – or at the minimum either PEX3 or PEX16 – must be targeted and inserted into membranes via an alternative pathway.

Indirect PMP insertion via other organelles

Several PMPs have been observed at the ER membrane, with only a small subset shown under endogenous conditions in mammalian cells, including PEX13 and PMP70 (Geuze et al. 2003). For yeast, particularly *Saccharomyces cerevisiae*, many more PMPs may be trafficked to peroxisomes via the ER under endogenous levels of expression (van der Zand et al. 2010), although this observation does not appear consistent with the mislocalisation of PMPs to the cytosol, not the ER, in *S. cerevisiae* cells devoid of Pex3p or Pex19p (Hettema et al. 2000). As previously mentioned, either PEX3 or PEX16 should be required in the peroxisomal membrane in order to import PMPs via the PEX19-dependent pathway. Indeed, both PEX16 and PEX3 in mammalian cells have been implicated in shuttling of PMPs to the peroxisome via the ER and mitochondria, respectively (Sugiura et al. 2017; Schrader and Pellegrini 2017) (Figure 1.1A, C). In mammalian cells lacking peroxisomes due to loss of PEX19 or PEX3, expressed PEX16 is mislocalised solely at the ER membrane, and a low percentage is found in the ER of wild-type COS-7 cells when expressed (Kim et al. 2006). In wild-type COS-7 cells, expressed ER-bound PEX16 was shown by pulse-chase experiments to move to peroxisomes dependent on its mPTS, and

also rescue the lack of peroxisomes in PEX16-deficient cells. The PEX16 at the ER membrane had the ability to recruit other PMPs to the ER, including PEX3 (Kim et al. 2006), presumably through PEX19 interacting with PEX16. Finally, Kim *et al.* also showed a heterogeneous population of peroxisomes using photoactivatable GFP-SKL; mature peroxisomes (labelled by the first round of photoactivation) continued to import GFP-SKL (increasing in fluorescence in a second round of photoactivation), but a subset of peroxisomes were only labelled in the second round, implying *de novo* formation (Kim et al. 2006). It may then therefore be possible for PMPs to enter peroxisomes indirectly, via the ER, instead of PEX19 shuttling directly from free ribosomes. Indeed, ER-targeted PEX3 (which in contrast to yeast Pex3p, does not target to the ER under overexpression in mammalian cells), appears to be inserted into the membrane of pre-existing peroxisomes at a similar rate to PEX16, although slower than PEX3 and PMP34, which are not known to be inserted via the ER (Aranovich et al. 2014). However, while PEX16 can recruit PEX3 (Matsuzaki and Fujiki 2008), which should then be enough to insert the rest of the PMPs, targeting PEX3 to the ER membrane is not sufficient to complement PEX16 deficient cells (Aranovich et al. 2014). This suggests that the role that PEX16 plays in PMP recruitment possibly through *de novo* peroxisome biogenesis is more than that of just PEX3 recruitment, and possibly plays a role in the formations of the pre-peroxisomal vesicles themselves.

If PEX3 does not follow an ER-derived pathway but is still required to form peroxisomes *de novo*, how then does PEX3 contribute to *de novo* peroxisome biogenesis and PMP import? Suguira *et al.* provided evidence that PEX3 is first inserted into the mitochondrial membrane, along with PEX14 before budding off in mitochondrial-derived vesicles (MDVs) in peroxisome-deficient cells (Sugiura et al. 2017) (Figure 1.1A). These MDVs were positive for peroxisomal membrane and matrix proteins PMP70 and catalase, suggesting that they mature into functional peroxisomes. Interestingly, PEX16-containing pre-peroxisomal vesicles from the ER appear to fuse directly with PEX3/14-containing MDVs, which would build a PEX3 and PEX16 positive vesicle then capable of importing PMPs via PEX19. While previously identifying that MDV transport to the peroxisomes with an unknown function required the vesicle cargo sorting protein VPS35 (Neuspiel et al. 2008; Braschi et al. 2010), the authors showed that the

MDVs involved in PMP import were independent of VPS35 (Sugiura et al. 2017), suggesting functionally independent MDV subtypes.

It is therefore likely that no individual PMP is preferentially constrained to a single pathway, and in fact that environmental conditions, the presence of functional peroxisomes, or requirements of the cell, influence the trafficking of PMPs to the peroxisome either through the PEX19 or ER pathway. As peroxisomes both in mammals and yeast primarily appear to regulate their number through growth and division over *de novo* synthesis (see section 1.1.5), it could be expected that the PEX19 pathway is the predominant way in which the peroxisomal membrane is supplied with membrane proteins.

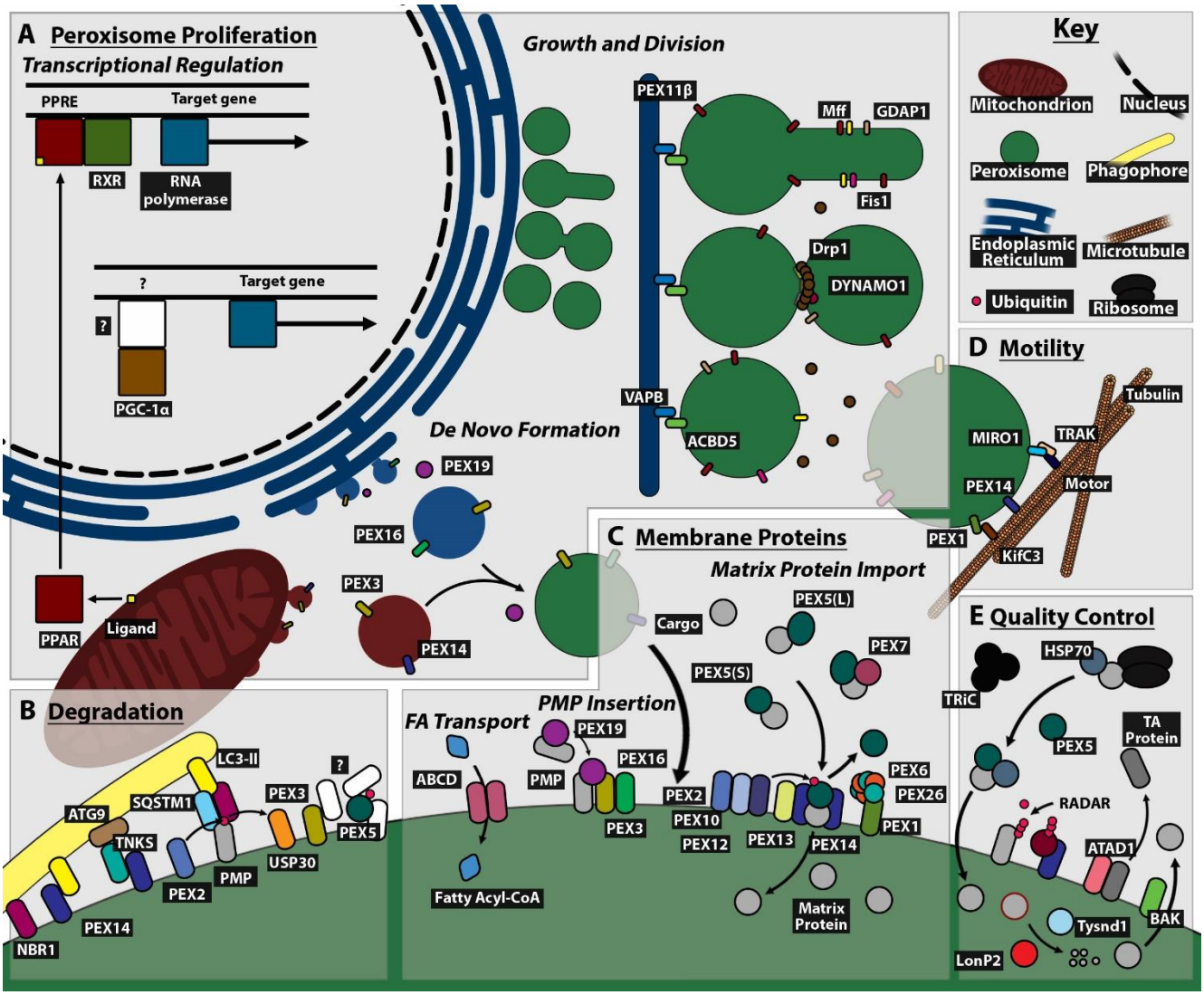

Figure 1.1: An overview of the regulation of peroxisomal membrane dynamics. (A) Peroxisome proliferation (section 1.1.5) through the control of transcriptional regulation, the growth and division process, and *de novo* peroxisome biogenesis. **(B)** The degradation of peroxisomes through the recruitment of the phagophore membrane

(section 1.1.7). **(C)** Peroxisomal membrane proteins (PMPs) (section 1.1.4) control the import of matrix enzymes and substrates, and the insertion of the PMPs themselves. **(D)** The motility and dynamics of the peroxisome as a whole are primarily controlled by microtubule-binding factors (section 1.1.8). **(E)** Quality control proteins maintain peroxisomal dynamics, extracting or degrading damaged or accumulated proteins (section 1.1.6).

1.1.5 Peroxisome Proliferation

1.1.5.1 *De Novo* Formation

Peroxisomes are highly responsive organelles, which, in addition to constantly proliferating and degrading to maintain a stable basal peroxisome number, need to be able to rapidly increase in number in response to certain environmental conditions. This may be particularly important in those cell types that are sensitive to oxidative stress, such as inner-ear hair cells and primary auditory neurons (Delmaghani et al. 2015).

Proliferation by biogenesis of peroxisomes can form through a *de novo* pathway in the absence of a population of functional peroxisomes, or through growth and division of existing peroxisomes. In the current model of *de novo* synthesis, PMPs are initially inserted into the ER or mitochondria, and exit the organelle membrane generating “pre-peroxisomal” vesicles, which fuse with other pre-peroxisomal vesicles or directly with mature peroxisomes (Farré et al. 2019) (Figure 1.1A).

As discussed previously (see section 1.1.4), some peroxisomal membrane proteins may take an ER-derived pathway prior to insertion into the peroxisomal membrane. In addition to PEX16 and PEX19 acting in budding off vesicles from the ER in order to target sorted PMPs to the peroxisome, these ER-derived pre-peroxisomes could also play a role in peroxisome biogenesis through *de novo* formation of peroxisomes under certain physiological conditions. The mitochondria also appear to play a role in peroxisome *de novo* formation and PMP supply, with mitochondria-derived pre-peroxisomal vesicles containing PEX3 and PEX14 being formed in a PEX19-dependent manner (Sugiura et al. 2017). Although currently not shown, the fusion of these pre-peroxisomal vesicles, with the presence of major components of the peroxisomal membrane protein insertion and matrix protein import machinery should, therefore, be enough to mature into fully functional, metabolically active peroxisomes.

While this process has been extensively studied in yeast (Jansen and van der Klei 2019), there are many unknowns, including precise roles of PEX3 and PEX19 in peroxisome *de novo* biogenesis and PMP sorting, the mechanism of pre-peroxisomal fusion and maturation, and the role of other organelles in addition to the ER.

1.1.5.2 Growth and Division

The peroxisomal growth and division pathway, maintaining basal peroxisome intracellular number and regulating their dynamics, can be described by three major steps (Schrader et al. 2016b); (i) membrane deformation to form an elongated peroxisomal tubule from the peroxisome 'mother', (ii) constriction of the peroxisomal elongation at localised points along the tubule, and (iii) scission of the peroxisomal membrane at constriction sites to release 'daughter' peroxisomes (Figure 1.1A). This process is tightly regulated, requiring several dedicated division proteins and relying on interplay with other organelles and the cytoskeleton (Costello and Schrader 2018).

The initiation of peroxisome elongation requires the peroxin PEX11β. PEX11β shows a strong association with membrane lipids, with its N-terminal amphipathic helices being sufficient to oligomerise, localise at specific sites on the membrane and cause deformation (Opaliński et al. 2011; Bonekamp et al. 2013a; Yoshida et al. 2015; Su et al. 2018). PEX11β oligomerisation and peroxisome elongation can be induced through supplementation with docosahexaenoic acid (DHA) (Itoyama et al. 2012), suggesting DHA plays a role in peroxisome proliferation in collaboration with PEX11β. The concentration of PEX11β at the peroxisomal membrane appears to correlate with peroxisome area, and it can be found on all actively-importing peroxisomes (Galiani et al. 2016). Therefore, it may be possible that there is a trigger for peroxisome proliferation induced by PEX11β when the peroxisome reaches a certain size. When the peroxisome reaches this size, the increased concentration of PEX11β on the membrane could initiate proliferation, or it is also possible that at a certain size the curvature properties of the membrane may then reach optimal conditions for deformation by PEX11β.

Following membrane elongation, constriction and fission of the physical membrane must occur to form 'daughter' peroxisomes (Figure 1.1A). This is achieved through the action of the GTPase dynamin-related protein 1 (DRP1).

DRP1 oligomerises at constriction sites, facilitated by direct interaction with recruitment factors mitochondrial fission 1 (FIS1) and mitochondrial fission factor (MFF) (Yoon et al. 2003; Koch et al. 2005; Otera et al. 2010; Liu and Chan 2015). FIS1 and MFF interact with PEX11β on the peroxisomal membrane (Kobayashi et al. 2007; Koch and Brocard 2012). A third recruitment factor, ganglioside-induced differentiation-associated protein (GDAP1), can also mediate peroxisomal division in a DRP1-dependent manner (Huber et al. 2013), although a direct GDAP1-DRP1 interaction has not been shown. PEX11β itself can also interact with DRP1 and activate it due to its GTPase activating activity (Williams et al. 2015). DRP1 then forms oligomeric helices to induce constriction and fission of the peroxisomal membrane, reducing the diameter of the DRP1 helix to deform the membrane and finally pinch off new peroxisomes (Li and Gould 2003; Motley et al. 2008; Mears et al. 2011). This process requires a large amount of GTP, and it has been shown using the unicellular algae *Cyanidioschyzon merolae* that the GTP generator DYNAMO1 forms a complex with DRP1 to locally supply DRP1 with GTP and increase the magnitude of the constricting force (Imoto et al. 2018).

The peroxisomal membrane protein acyl-CoA binding domain containing protein 5 (ACBD5) facilitates physical tethering of the peroxisome to the ER (Costello et al. 2017b; Hua et al. 2017) (Figure 1.1A), likely supplying membrane lipids to the peroxisome to facilitate membrane expansion for peroxisome growth and division. Lipid supply from the ER may also work in combination with pulling forces from the cytoskeleton to mediate peroxisome proliferation, utilising the adaptor for microtubule-based motility mitochondrial Rho GTPase 1 (MIRO1) (Castro et al. 2018). Further evidence for the role of the cytoskeleton in peroxisome proliferation through growth and division is shown by the peroxisome response to microtubule-destabilising drugs. In addition to altering peroxisomal dynamics through disrupting their cellular localisation and inducing clustering (see section 1.1.8; Chapter 2), microtubule-destabilising drugs also induce peroxisomal elongation (Schrader et al. 1996; Wiemer et al. 1997). How and why elongation is triggered following depolymerisation of microtubules is unknown.

Whether *de novo* or through growth and division, the primary way in which peroxisomes increase in number under physiological conditions is still controversial (Agrawal and Subramani 2016). In order to maintain peroxisome

number, increasing peroxisome abundance when required is likely performed through the coordinated interplay between the two pathways. Further work remains to elucidate whether the different mechanisms are required under different conditions, as growth and division appears more prominent under basal conditions, particularly in yeast (Motley and Hettema 2007; Hettema et al. 2014). When this balance of peroxisome biogenesis against degradation is disturbed, peroxisome homeostasis is disrupted, causing further cellular consequences (see section 1.1.11).

1.1.5.3 Transcriptional Regulation

Transcriptional regulators mediate peroxisome proliferation by inducing the transcription of genes involved in peroxisome biogenesis and function, commonly through the peroxisome proliferator-activated receptors (PPARs) (Ma et al. 2008; Schrader et al. 2012) (Figure 1.1A).

Three PPAR subtypes have been described, PPARα, PPARβ/δ and PPARγ. These subtypes vary in tissue specificity and response to activation and are activated by peroxisome proliferators, typically fatty acids or fibrates (Schrader et al. 2012). Following activation by ligand binding, the PPAR translocates to the nucleus to up-regulate expression of target genes by interacting with Retinoid X Receptor-α (RXRα), binding to a peroxisome proliferator response element (PPRE) in the promoter region, and causing co-activators and co-repressors to be exchanged in order to induce gene expression (Berger and Moller 2002; Rakhshandehroo et al. 2010). The PPARs can be activated when needed according to cellular demand or environmental conditions; for example, PPARα stimulates the proliferation of peroxisomes in hypoxic conditions. Following hypoxia, PPARα localises to the nucleus, and peroxisomal proteins known to be under PPARα transcriptional control are upregulated, accompanied by an increase in peroxisomal abundance (Laurenti et al. 2011).

In addition to PPAR transcriptional control, other pathways have also been shown to play a role in the regulation of peroxisome proliferation, although with unknown mechanisms independent of the PPARs. For example, the transcriptional coactivator PGC-1α is also a coordinator of peroxisome biogenesis (Bagattin et al. 2010), and overexpression increases peroxisomal and mitochondrial activity (Huang et al. 2017). PGC-1α expression is sufficient to increase peroxisome

abundance, and following exposure to cold conditions, peroxisomes proliferate in a PGC-1α-dependent manner, although despite being a PPARγ coactivator, the effect was PPAR-independent (Bagattin et al. 2010). In addition, a high-throughput screening identified novel compounds that induce peroxisome proliferation independent of PPAR (Sexton et al. 2010). It still remains to be clarified what the exact role of the PPARs are in peroxisome proliferation, as well as their target genes and activation under specific conditions. In addition, peroxisome regulation through PPAR-independent mechanism such as PGC-1α remains to be elucidated, such as the unknown transcription factor facilitating PGC-1α transcriptional control.

1.1.6 Quality Control

Functional peroxisomes rely on coordination between many membrane and matrix proteins, loss of which can be devastating (see section 1.1.11). Therefore, multiple quality control mechanisms have evolved to stabilise, correct or rescue peroxisomal protein dysfunction in order to ensure cell survival (Figure 1.1E).

Quality control mechanisms can act on proteins destined for the peroxisome before insertion into the membrane, if, for example, misfolding occurs prior to peroxisomal localisation. Peroxisomes carry the capacity to import fully folded proteins across the peroxisomal membrane, suggesting that the quality control of the misfolding of these proteins likely occurs in the cytosol. For example, the heat shock protein (proteins typically involved in stabilisation of newly synthesised proteins) HSP70 has been shown to associate with proteins being imported into the peroxisomal matrix, increase in levels during peroxisome proliferation, and interact with PEX5 (Walton et al. 1994; Harano et al. 2001). The cytosolic chaperonin T-complex protein-1 ring complex (TRiC) also has been shown to have the ability to form a complex with PMPs (Pause et al. 1997). The action of PEX5 in translocation of matrix proteins across the matrix also likely involves a chaperone activity (Freitas et al. 2011). Similarly, the PMP import receptor PEX19 binds to newly synthesised PMPs, and can also act as a chaperone (Jones et al. 2004).

Once inside the peroxisomal matrix, high ROS levels lead to an increased risk of damaged, oxidised and misfolded proteins (Fransen et al. 2012). Proteases in

the peroxisomal matrix likely degrade these damaged proteins. The peroxisomal protease Lon peptidase 2 (LONP2) is involved in degradation of peroxisomes through degrading β-oxidation enzymes (Yokota et al. 2008; Okumoto et al. 2011) (see section 1.1.7.1) and can work cooperatively with the protease trypsin domain containing protein 1 (Tysnd1) in the peroxisomal matrix (Okumoto et al. 2011).

PMPs themselves once inserted into the peroxisomal membrane are also subject to quality control mechanisms. Ubiquitination of the import receptor PEX5 is typically a mechanism for enabling recycling of the import receptor (see section 1.1.4.2). However, when recycling of PEX5 is impaired, the Receptor Accumulation and Degradation in the Absence of Recycling (RADAR) system polyubiquinates PEX5, thus likely targeting it for degradation by the Ubiquitin Proteasome System (UPS) (Kiel et al. 2005). This correlates with a decrease in PEX5 in patients lacking a component of the receptor recycling complex (Dodt and Gould 1996). This process likely also affects other PMPs, as the turnover of several PMPs can be extended by inhibition of the UPS (Huybrechts et al. 2009).

The yeast AAA ATPase mitochondrial sorting of proteins 1 (Msp1p) identifies and extracts excess tail-anchored membrane proteins on the mitochondrial and peroxisomal membrane. The human homologue ATPase family AAA domain-containing protein 1 (ATAD1) has been shown to have conserved function and also dual mitochondrial-peroxisomal localisation (Chen et al. 2014a; Weir et al. 2017).

Some PMPs appear to be sorted to the ER prior to peroxisomal *de novo* biogenesis, or PMP supply to mature peroxisomes (see section 1.1.4.2). The ER-associated degradation (ERAD) pathway is a quality control system for ER membrane proteins; ubiquitinated ERAD substrates are extracted from the ER membrane, triggering the Unfolded Protein Response (UPR), enhancing protein folding and degradation (Hwang and Qi 2018). Therefore, it is possible that the ERAD system also plays a role in quality control of ER-sorted peroxisomal proteins.

Finally, the mitochondrial protein Bcl-2 homologous antagonist/killer (BAK) is capable of targeting to peroxisomes (Hosoi et al. 2017). When localised to peroxisomes, an increase in cytosolic peroxisomal matrix proteins, including

catalase, was observed. BAK can, therefore, increase the membrane permeability of peroxisomes, possibly to balance cellular redox signalling.

Quality control mechanisms like the ones mentioned above certainly help to maintain peroxisome and cell viability. In addition to basal mechanisms, certain mechanisms kick into action under dangerous conditions. For example, peroxisomes are large contributors of ROS to the intracellular environment. Under high ROS levels, peroxisomal degradation is induced, likely to counter these high ROS levels. These are discussed in section 1.1.7.2.

1.1.7 Peroxisome Degradation

1.1.7.1 Basal Mechanisms

Selective Autophagy (Pexophagy)

As previously mentioned, maintaining a constant peroxisome number is performed through a combination of peroxisome proliferation by biogenesis, and peroxisome degradation. A constant basal level of peroxisome degradation ensures this stable number, but peroxisome degradation is also triggered under certain conditions (see section 1.1.7.2). The primary way in which peroxisomes are degraded is via autophagy, the removal and recycling of organelles by the cell.

General autophagy (Khaminets et al. 2016) is described as formation and elongation of the phagophore, sequestration of cargo and phagophore closure preceding maturation into the autophagosome, and autophagosome-lysosome fusion, promoting cargo degradation by lysosome hydrolases. Peroxisome-specific selective autophagy is denoted pexophagy (Eberhart and Kovacs 2018) (Figure 1.1B).

The precise mechanism of initiation of pexophagy in mammalian cells appears somewhat unclear, varying between cell types and under certain conditions. Expression of autophagy receptors neighbour of breast cancer type 1 susceptibility protein 1 gene protein 1 (NBR1) and sequestosome 1 (SQSTM1) induce peroxisome clustering and degradation (Deosaran et al. 2013). Both contain a ubiquitin-associated domain to bind to ubiquitinated targets on the peroxisomal membrane, and a phagophore-resident protein microtubule-

associated proteins 1A/1B light chain 3B (LC3) interacting region (LIR), enabling the receptors to bring the phagophore membrane in close apposition to the peroxisomes to facilitate engulfment and subsequent degradation (Kirkin et al. 2009). Indeed, artificial overexpression of peroxisomal proteins PMP34 and PEX3 mono-ubiquitinated at their cytosol-facing C terminus has been shown to trigger pexophagy in an SQSTM1-dependent manner (Kim et al. 2008). NBR1 may also localise to peroxisomes independently of ubiquitin via its J domain, which enables direct binding to the peroxisomal lipid bilayer (Deosaran et al. 2013).

RING-finger E3 ubiquitin ligase PEX2 is typically involved in the PEX5 import cycle but also plays a role in basal pexophagy; overexpression triggers NBR1-dependent loss of peroxisome abundance (Sargent et al. 2016). Inhibition of the autophagy-inhibiting protein complex mammalian target of rapamycin complex 1 (mTORC1) increases PEX2 levels (Sargent et al. 2016), with activated mTORC1 possibly increasing the degradation of PEX2 by the proteasome to prevent unintended pexophagy. A fraction of the mitochondrial deubiquitylase ubiquitin-specific-processing protease 30 (USP30) is also localised to peroxisomes (Marcassa et al. 2018). USP30 could possibly suppress pexophagy by reversing the activity of PEX2 and deubiquitinating peroxisomal membrane proteins before they are targeted by NBR1/SQSTM1. Knockdown of USP30 in this study increased pexophagy rate but had no effect on peroxisome abundance, suggesting that peroxisome biogenesis was also increased (Marcassa et al. 2018). However, peroxisome abundance has recently been shown to be reduced with USP30 knockdown in another study (Riccio et al. 2019).

Loss of the AAA ATPase complex (PEX1, PEX6, PEX26) leads to an increase in ubiquitinated PEX5 at the peroxisomal membrane, where it can be recognised by NBR1 to attract the phagophore (Law et al. 2017). Mono-ubiquitinated PEX5 has been shown to trigger pexophagy in SV40 large T-antigen-transformed MEFs, although interestingly without requiring NBR1 and SQSTM1 (Nordgren et al. 2015).

Overexpression of PEX3 induces NBR1-mediated pexophagy, although without a direct PEX3-NBR1 interaction (Yamashita et al. 2014). This may suggest PEX3 plays a role in facilitating the ubiquitination of other peroxisomal membrane

proteins to recruit NBR1. In addition, the expression of an N-terminal fragment of PEX3 is sufficient to cause extensive peroxisome degradation (Soukupova et al. 1999) (see Chapter 3).

PEX14 has also been shown to interact with LC3-II *in vivo*, despite a lack of LIR domain for classical LC3 binding (Jiang et al. 2014), suggesting the presence of PEX14 can also attract the phagophore membrane to facilitate pexophagy. The tankyrases TNKS and TNKS2 are also associated with PEX14 through a TNKS binding motif and have a peroxisomal localisation (Li et al. 2017). Overexpression of TNKS/TNKS2 reduced the number of peroxisomes, however, this is independent of ubiquitin, NBR1 and SQSTM1 (Li et al. 2017), suggesting an alternate pathway. This could possibly include autophagy-related protein 9 (ATG9), which delivers lipids to the forming phagosome (Mercer et al. 2018) and also associates with TNKS/TNKS2 (Li et al. 2017).

Finally, the yeast autophagy protein Atg37p, required for phagophore formation during pexophagy, is a homologue of human ACBD5, required for tethering peroxisomes to the ER, facilitating membrane expansion (see section 1.1.5.2). ACBD5 was reported to be essential for pexophagy (Nazarko et al. 2014), however, no further evidence has since been described (Yagita et al. 2017; Ferdinandusse et al. 2017).

Therefore, there are many pathways in the cell with the capacity to initiate pexophagy at basal conditions. Many involve ubiquitination, however, there are possible alternative pathways for pexophagy. In mammalian liver cells, it was suggested that 70-80% of peroxisomes are degraded by pexophagy, based on the degradation of peroxisomes following proliferation from treatment with DEHP (Iwata et al. 2006). The other 20-30% are likely degraded by other degradation pathways.

ALOX15-mediated autolysis

In the recovery period from peroxisome proliferation, a population of peroxisomes show disruption of the peroxisomal membrane, and the peroxisomal crystalline cores were seen free in EM (Fahimi 1973). ALOX15 binds to organelle membranes, disturbs their structure and releases their contents, resulting in degradation of the organelle (van Leyen et al. 1998). It has been shown that

ALOX15 can localise to peroxisomes and ALOX15 inhibitors can rescue peroxisomal membrane disturbance (Yokota et al. 2001). Therefore, it is likely that ALOX-15 mediated autolysis is another pathway of peroxisomal degradation.

LONP2 proteolysis

LONP1 is a major protease located in the mitochondrial matrix, degrading proteins that get damaged from ROS generated by the mitochondrial respiratory chain (Bota and Davies 2002). While peroxisomal ROS is tightly controlled (Schrader and Fahimi 2006a; Fransen et al. 2012), peroxisomal proteins can still be damaged by un-reduced H_2O_2. Therefore, it is no surprise that there is a peroxisomal isoform of LONP1, denoted LONP2 (Kikuchi et al. 2004). Using the DEHP recovery assay to investigate peroxisome degradation in mammalian liver cells, LONP2 increases after recovery from DEHP, while peroxisomes are being removed (Yokota et al. 2008), suggesting that LONP2 does indeed play a role in peroxisome degradation. It is possible that LONP2 degradation of peroxisomal matrix proteins can lead to degradation of the peroxisome as a whole; however, no study has shown LONP2 expression or knockdown altering peroxisome abundance. Whether LONP2 proteolysis is an alternative pathway in its own right or a contributor to protein removal during peroxisome degradation through other pathways remains to be seen.

1.1.7.2 Pexophagy-Initiating Conditions

Peroxisomal degradation by pexophagy can be initiated and carried out by a number of pathways, the majority using ubiquitinated proteins as a flag. Several physiological conditions induce peroxisome degradation by pexophagy utilising these pathways, including high ROS levels, various types of starvation, and reduced oxygen levels.

ROS Levels

Peroxisomal degradation can be influenced by ROS levels. mTORC1 is an autophagy regulator, with activated mTORC1 preventing autophagy (Rabanal-Ruiz et al. 2017). Several mTORC1 inhibitors are supposed to be peroxisomally localised proteins, and their activation represses mTORC1 to initiate autophagy (Zhang et al. 2013). The kinase ataxia telangiectasia mutated kinase (ATM) is activated under conditions of increased peroxisomal ROS; it not only activates peroxisomal mTORC1 inhibitors to initiate general autophagy (Alexander et al.

2010; Zhang et al. 2015), but also phosphorylates PEX5 at S141, promoting ubiquitination at K209 by the E3 ubiquitin ligases PEX2,10 and 12 (Zhang et al. 2015). PEX5 ubiquitinated at K209 is subsequently recognised by SQSTM1 in order to promote pexophagy (Zhang et al. 2015). Noise overexposure induces oxidative stress and peroxisomal degradation (Delmaghani et al. 2015; Defourny et al. 2019). This peroxisomal degradation is mediated by peroxisomal-localised pejvakin, which contains an LIR domain for LC3 binding and recruitment of the phagophore to peroxisomes.

Starvation

Under nutrient-starved conditions, NBR1 localises to peroxisomes and has been shown to interact with SQSTM1 and PEX14, with decreased NBR1 expression leading to decreased LC3 recruitment to peroxisomes (Jiang et al. 2014). Under nutrient starvation PEX14 has been shown to interact with LC3 itself (Hara-Kuge and Fujiki 2008), suggesting that NBR1 may play a role in facilitating PEX14-LC3 interaction to drive pexophagy under these conditions as well as through direct recruitment with its LIR domain. Catalase knockdown under serum-depleted conditions reduced peroxisome number, increased ROS levels and increased the association of NBR1 with PMP70 (Lee et al. 2018). Treatment with *N*-acetyl-cysteine to reduce the ROS levels produced under catalase inhibition rescued the increased pexophagy under nutrient starvation and catalase knockdown (Lee et al. 2018); suggesting ROS again plays a role in pexophagy under starvation conditions. In amino acid starvation induction of pexophagy, PEX2 has been shown to be upregulated in earlier starvation timepoints and to ubiquitinate PEX5 and PMP70, recruiting NBR1 to peroxisomes (Sargent et al. 2016). It is unknown if the ubiquitination of PEX5 by PEX2 under amino-acid starvation is linked to the ubiquitination of PEX5 following phosphorylation by ATM under periods of increased ROS. Pexophagy under amino-acid starvation conditions can be prevented by expression of USP30, counteracting ubiquitination by PEX2 (Riccio et al. 2019). Interestingly, loss of TNKS/TNKS2 prevented pexophagy under amino-acid starvation conditions (Li et al. 2017), showing again the importance of ubiquitin-independent pathways.

Hypoxia

The cell's adaptive response to hypoxia is mediated by transcription factors HIF-1α and HIF-2α, typically flagged under normoxia by the E3 ubiquitin ligase component VHL to be degraded by the proteasome, but stabilised under conditions of low oxygen (Ohh et al. 2000). The numbers of peroxisomes were reduced in mice deficient in VHL alone (simulating hypoxia) and both VHL and HIF-1α (Walter et al. 2014). The decrease in peroxisome abundance was caused by an increase in HIF-2α mediated pexophagy, as double VHL and HIF-2α knockout mice showed no change in peroxisome abundance (Walter et al. 2014). The decrease in peroxisome number was associated with a decrease in NBR1 and SQSTM1 and could be rescued in VHL knockout mice with the treatment of autophagy inhibitor 3-MA, despite the presence of clustered NBR1 and SQSTM1 at peroxisomes (Walter et al. 2014). The mode-of-action of HIF-2α at peroxisomes remains to be elucidated; it possibly induces ubiquitination of a PMP to attract NBR1/SQSTM1, or it induces post-translational modification of NBR1 if it directly binds to the peroxisome membrane via its J domain. Interestingly, hypoxia has also been linked to peroxisome proliferation via PPARα (Laurenti et al. 2011) (see section 1.1.5.3), leading to the possibility that peroxisome proliferation is triggered to counteract peroxisome degradation in hypoxic conditions.

1.1.8 Peroxisome Motility

Peroxisomes are highly motile (Schrader et al. 2003), with peroxisome distribution being important for the cell cycle (Asare et al. 2017), and during development in neurons; peroxisomes accumulate in the axon during postnatal development but are absent in mature projection neurons (Arnold and Holtzman 1978; Kassmann et al. 2011). Despite this, much of the mechanisms for peroxisome motility are not well understood.

It was initially shown that peroxisomes in mammalian cells have a direct association with the microtubule network (Rapp et al. 1996; Schrader et al. 1996; Wiemer et al. 1997), regulating their intracellular dynamics and motility. Microtubule destabilising drugs lead to clustering and elongation of the peroxisomal compartment, disturb peroxisome cellular distribution and impair peroxisome motility (Rapp et al. 1996; Schrader et al. 1996; Wiemer et al. 1997;

Thiemann et al. 2000; Passmore et al. 2017) (see Chapter 2). Defects in patients affecting the microtubular network have been shown to also affect peroxisomal dynamics. For example, a defect in microtubule-severing protein spastin, which leads to lower cellular levels of acetylated α-tubulin, causes impaired peroxisomal trafficking (Fan et al. 2014; Wali et al. 2016). Interference with the microtubule network via the microtubule-binding protein tau also alters proper localisation of peroxisomes (Stamer et al. 2002). Several studies have investigated peroxisomal movements in more detail, showing that peroxisomes can move bidirectionally along microtubules, and typically exhibit short oscillatory movements (0.05-0.2 $\mu m.s^{-1}$) or more rare (5-10%) long range, microtubule-dependent movements (>0.24 $\mu m.s^{-1}$) (Rapp et al. 1996; Wiemer et al. 1997; Schrader et al. 2000; Bharti et al. 2011; Fan et al. 2014; Castro et al. 2018; Wang et al. 2018). These movements are highly energy-dependent; depletion of ATP and GTP or changes in the intracellular calcium pool causes impaired peroxisome motility (Huber et al. 1997).

As peroxisomal motility is bidirectional, utilising the microtubule network, it can be expected that the microtubule motors kinesin and dynein (minus- and plus-end motors respectively) are involved in peroxisomal trafficking. Indeed, several studies have linked microtubule-interacting molecular motors and adaptors to the motility of peroxisomes (Figure 1.1D). The kinesin family member KifC3 can interact with peroxisomal membrane protein PEX1, and knockdown of KifC3 induces perinuclear clustering (Dietrich et al. 2013). Overexpression of the dynactin subunit dynamitin, inhibiting dynein-based motility, inhibits the movement of peroxisomes and reduces their ability to recover an even cellular distribution after treatment with microtubule destabilising drugs (Schrader et al. 2000). The MIRO1 Ras GTPase was recently identified as an adaptor for microtubule-based motility (Castro et al. 2018). In addition, three distinct splice variants of MIRO1 (MIRO1-var2, MIRO1-var3 and MIRO1-var4) were identified (Okumoto et al. 2018) MIRO1-var2 and MIRO1-var4 are localised to peroxisomes, and play a role in the longer-range movement. MIRO1 forms a motility complex with the trafficking kinesin proteins TRAK1 and TRAK2, and both dynein and kinesin themselves (Wang and Schwarz 2009).

Microtubule-dependent peroxisomal motility possibly involves PEX14, as peroxisome motility may be impaired in cells deficient in PEX14 (Bharti et al. 2011; Castro et al. 2018; Okumoto et al. 2018). PEX14 has been shown to interact with tubulin via direct binding mediated by its N-terminal domain (Bharti et al. 2011), suggesting it plays a role as a membrane anchor for microtubules. In addition, knockdown of PEX14 disturbs highly elongated peroxisomal tubules in MFF-deficient cells, further suggesting that it stabilises these tubules via microtubule binding (see Chapter 3).

Expression of peroxisome-ER tethering protein ACBD5 inhibits proper peroxisomal motility (Costello et al. 2017b; Wang et al. 2018). It is likely that ACBD5 plays a role in the coordination of peroxisome motility, by releasing peroxisomes from the ER to facilitate movement along microtubules.

It is clear that peroxisome motility is a tightly regulated process, involving the coordinated interplay of peroxisomal membrane proteins, adaptors and motors in order to maintain an even distribution of peroxisomes in the cell but with the capability to perform directed long-range movement when required. Proper peroxisome motility is important for cellular function and involved in health and disease (see section 1.1.11). Therefore, elucidating the finer details of peroxisome motility and dynamics will be important future work.

1.1.9 Peroxisome Functions

1.1.9.1 Overview

Previous sections have described various aspects of peroxisomal dynamics; peroxisome number, morphology, and motility. These dynamics help to maintain the peroxisomes, allowing them to carry out their many functions inside the cell, including fatty acid oxidation, reactive oxygen species homeostasis, and the production of ether-linked phospholipids, bile acid intermediates and docosahaexanoic acid. These functions and more are discussed further here, and the consequences of loss-of-function of peroxisomes and peroxisomal proteins are discussed in section 1.1.11.

1.1.9.2 Fatty Acid Oxidation

A major function of the peroxisome is the degradation of fatty acids (Figure 1.2A). In Zellweger patients, those lacking functional peroxisomes, very long-chain fatty acids (VLCFAs) accumulate in plasma (Brown et al. 1982). The oxidation of VLCFAs by peroxisomes prevents this accumulation, which can lead to ER stress and lipoapoptosis in adrenoleukodystrophy (van de Beek et al. 2017). Peroxisomes can catalyse the oxidation of those fatty acids that cannot be broken down in mitochondria, including C24:0 and C26:0 VLCFAs, the branched-chain fatty acid pristanic acid, and the long-chain dicarboxylic acids (Wanders et al. 2016). Peroxisomes also cooperate with mitochondria for the degradation of fatty acids; both organelles can oxidise the long-chain fatty acids palmitic acid, linoleic acid and linolenic acid. Substrates for β-oxidation are activated to form fatty acyl-CoAs by long-chain acyl-CoA synthetases (ACSLs), or very long-chain acyl-CoA synthetase (VLACS) (Mashek et al. 2017). The fatty acids then enter the peroxisome via the membrane-bound ABCD proteins (Baker et al. 2015).

β-oxidation is the chain shortening of acyl-CoA esters (Poirier et al. 2006), with each cycle releasing two carbon atoms. Acyl-CoA oxidase (ACOX) enzymes catalyse the initial step, desaturating acyl-CoAs to 2-trans-enoyl-CoAs, and also resulting in the production of ROS (see section 1.1.9.3). The peroxisomal multifunctional enzymes L- and D-bifunctional protein (LBP and DBP) hydrate 2-trans-enoyl-CoAs to 3-hydroxyacyl-CoAs, then subsequently dehydrogenate this to 3-ketoacyl-CoAs. Finally, the thiolytic cleavage of 3-ketoacyl-CoA to acyl-CoA by 3-ketoacyl-CoA thiolases releases two carbons as acetyl-CoA. Transfer of chain-shortened lipids and β-oxidation products out of the peroxisome and to the mitochondria for use in energy production is provided through short- and medium-chain carnitine acyltransferases and acyl-CoA thioesterases in a complementary system (Westin et al. 2008).

Bile Acid Synthesis

β-oxidation in peroxisomes also plays a role in the production of primary bile acids (Ferdinandusse et al. 2009b) (Figure 1.2A). The C24 bile acids cholic acid and chenodeoxycholic acid are produced by β-oxidation of the C27 fatty acids di- and trihydroxycholestanoic acid (DHCA and THCA), converting the bile acid's CoA-esters to glycine or taurine esters by bile acid-CoA: aminoacid transferase

(BAAT), which also produces propionic acid as a by-product. The β-oxidation of C27 bile acid intermediates is crucial to reducing toxicity, as mature C24-bile acids are significantly less cytotoxic than DHCA and THCA (Ferdinandusse et al. 2009a).

Docosahexaenoic Acid Production

Peroxisomal β-oxidation is also required for the formation of docosahexaenoic acid (DHA) (Figure 1.2A). DHA is an omega-3 poly-unsaturated (C22:6) fatty acid (PUFA), generated from β-oxidation of newly imported C24:6-CoA, requiring both ACOX1 and DBP (Su et al. 2001). DHA is important for brain and retinal development and function (Anderson et al. 1990), highlighting the importance of β-oxidation not only in the breakdown of fatty acids to reduce toxicity and aid the mitochondria in acetyl-CoA production, but also in the production of other crucial metabolites.

Phytanic Acid Oxidation

In addition to the β-oxidation of fatty acids, peroxisomes also carry out α-oxidation, primarily of phytanic acid (Wanders et al. 2011) (Figure 1.2A). Phytanic acid is a 3-methyl fatty acid, obtained from the diet only, and the methyl group at the 3-position prohibits β-oxidation. Therefore, activated phytanic acid (phytanoyl-CoA) can undergo one round of α-oxidation, consisting of hydroxylation by phytanoyl-CoA 2-hydroxylase, cleavage to pristanal, and the conversion of pristanal to pristanic acid. Pristanic acid can then undergo β-oxidation.

Phytanic acid can not only be α-oxidised in order to pass into the β-oxidation pathway, but also ω-oxidised (Komen et al. 2005). In this pathway, phytanic acid is hydroxylated at the ω-end, which is then converted to an aldehyde and dehydrogenated by cytochrome P450 enzymes to form a carboxyl group, producing phytanedioic acid. Phytanedioic acid can be degraded by β-oxidation at the ω-end. ω-oxidation of phytanic acid is likely key for reducing phytanic acid levels in Adult Refsum Disease (ARD) patients, which have a deficiency in α-oxidation primarily through mutation of phytanoyl-CoA 2-hydroxylase (Jansen et al. 1997).

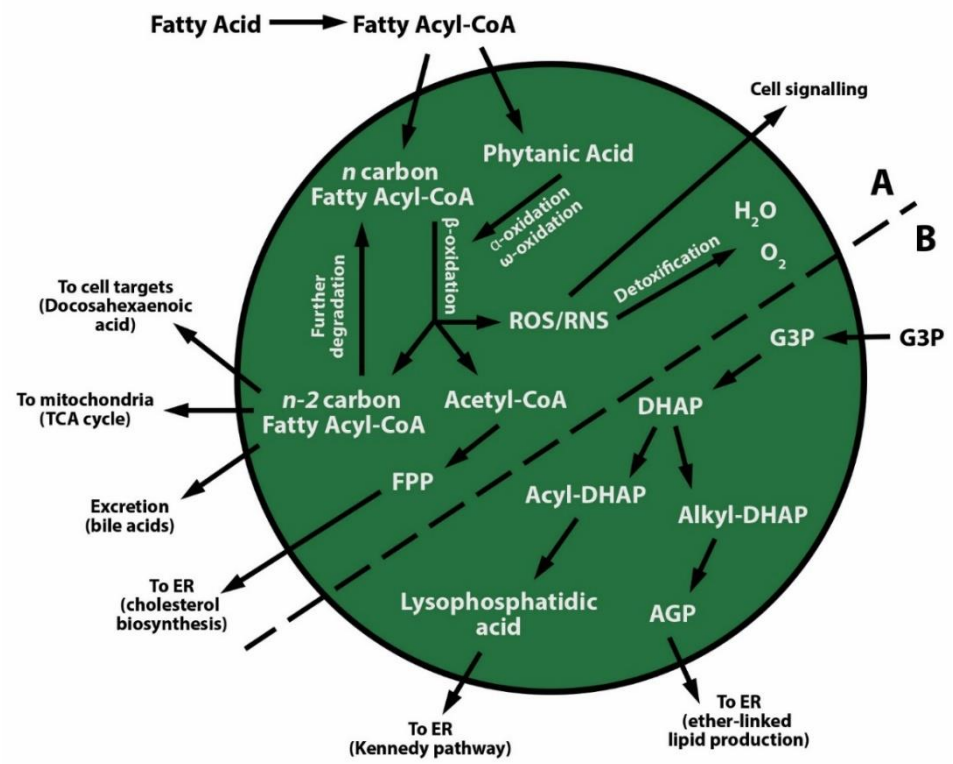

Figure 1.2: An overview of the main peroxisomal metabolic substrates and products. (A) Fatty acid degradation and ROS homeostasis (see sections 1.1.9.2 and 1.1.9.3). **(B)** The production of lipid precursors to be passed to the ER (see section 1.1.9.4).

1.1.9.3 Reactive Oxygen and Nitrogen Species Homeostasis

Several peroxisomal enzymes are oxidases, producing reactive oxygen species (ROS) as a by-product in the form of hydrogen peroxide (H_2O_2) (Schrader and Fahimi 2004) (Figure 1.2A). For example, during β-oxidation the reoxidation of reduced FAD (flavin adenine dinucleotide) to oxidised FAD in the activity of ACOX enzymes generates H_2O_2. A few exceptions produce other reactive species, for example xanthine oxidase and the inducible nitric oxide synthase can produce superoxide ($O_2\cdot^-$) and the reactive nitrogen species (RNS) nitric oxide ($NO\cdot$) in addition to H_2O_2 (Zhang et al. 1998; Stolz et al. 2002; Galbusera et al. 2006). ROS and RNS species can also readily react; $O_2\cdot^-$ can react with $NO\cdot$ to form peroxynitrite ($ONOO^-$), and H_2O_2 can be decomposed to produce hydroxyl radicals ($OH\cdot$) (Fransen et al. 2012). This build-up of ROS/RNS can lead to protein modifications and the inactivation of peroxisomal enzymes, and disturbance of the peroxisomal membrane through lipid peroxidation (Fransen et al. 2012).

Therefore, in order to reduce highly damaging build-up of ROS/RNS, peroxisomes contain various scavenging/detoxification enzymes (Walker et al. 2018) (Figure 1.2A). Several enzymes catalyse the metabolism of H_2O_2; peroxiredoxin 5 (PRDX5) (Walbrecq et al. 2015), also involved in the breakdown of $ONOO^-$ (Trujillo et al. 2007), catalase, which can detoxify H_2O_2 either by conversion into oxygen and water, or reducing H_2O_2 into water via an electron donor (Sepasi Tehrani and Moosavi-Movahedi 2018); and peroxisomal glutathione peroxidase, converting H_2O_2 into water via oxidation of GSH (reduced glutathione) to GSSG (glutathione disulphide) (Singh et al. 1994; Djordjević 2004). The breakdown of $O_2{\cdot}^-$ requires the peroxisomal superoxide dismutases, which rapidly convert $O_2{\cdot}^-$ to the more manageable H_2O_2 (Keller et al. 1991). Other peroxisome-localised enzymes to reduce damaging oxidative metabolites include the epoxide hydrolase 2 (EPHX2) and glutathione S-transferase kappa (GSTK1) (Fransen et al. 2012). In addition, peroxisomes are involved in the synthesis of plasmalogens (see section 1.1.9.4), which carry antioxidant properties.

While at high concentrations reactive species can damage cellular proteins and membranes, at low concentrations they have the capacity to act as important intracellular signalling molecules (Walker et al. 2018). This is especially evident for H_2O_2, which has been shown as important for many cellular functions including cell proliferation, differentiation, migration, microbial defence in the phagosome, and the regulation of protein function through targeted oxidative inactivation (Rhee 2006). Therefore, in maintaining ROS and RNS homeostasis, peroxisomes are important organelles not only for detoxification, but also in crucial cell signalling.

1.1.9.4 Ether Phospholipid Biosynthesis

Ether-linked lipids are glycerophospholipids with an ether-linked alkyl chain attached to the glycerol backbone at position *sn-1* instead of the classical ester-linked chain. Plasmalogens (Nagan and Zoeller 2001) make up the majority of ether-linked lipids and are those that show a *cis* double bond on the alkyl chain adjacent to the ether bond, and typically appear with an ethanolamine head group (plasmanylethanolamine).

Ether lipid levels are reduced in peroxisome-deficient patients (Heymans et al. 1983), suggesting a role of peroxisomes in their synthesis. Ether phospholipid

synthesis begins in the peroxisome through the production of dihydroxyacetone phosphate (DHAP) from glycerol-3-phosphate (G3P) (Wanders et al. 2016) (Figure 1.2B). G3P likely enters the peroxisome with the help of channel forming peroxisomal membrane protein PXMP2 (PMP22) (Rokka et al. 2009; Antonenkov and Hiltunen 2012). Acyl-CoA from fatty acid synthase-mediated *de novo* lipogenesis is then either used by the enzyme dihydroxyacetone phosphate acyltransferase (DHAPAT) to produce acyl-DHAP, or is reduced to a fatty alcohol by fatty acyl-CoA reductase on the peroxisomal membrane and used in the next step to form alkyl-DHAP by alkyl-DHAP synthase (Dean and Lodhi 2018), using a fatty alcohol generated by fatty acyl-CoA reductase (FAR1). Acyl-DHAP and alkyl-DHAP are both ether phospholipid precursors, and can be reduced to 1-acyl G3P (lysophosphatidic acid) or the ether-linked analogue 1-O-alkyl G3P (AGP), respectively (LaBelle and Hajra 1974). The final steps in the conversion to ether phospholipids take place in the ER, with lysophosphatidic acid forming a basis for diacylglycerol (DAG) used for production of diacyl phospholipids in the Kennedy pathway (see section 1.1.3) (Gibellini and Smith 2010), and AGP forming the basis for the ether-linked lipids, following acylation, removal of the phosphate group, and attachment of the head group by phosphotransferases (Figure 1.2B). To make the plasmalogen form of ether-linked lipids, the *cis* double bond on the alkyl chain is created by plasmanylethanolamine desaturases (Nagan and Zoeller 2001).

Plasmalogens have many important roles. Their physical properties allow for the formation of non-bilayer structures, possibly resulting in increased membrane ion leakage and promotion of membrane fusion (Glaser and Gross 1994). The alkyl chain double bond appears to be important to convey an antioxidant property to protect the cell from ROS (Zoeller et al. 1999). These structural and protective roles likely explain the high presence of plasmalogens in multilamellar membranes with high risk of exposure to oxidative stress, such as myelin (Luoma et al. 2015), and sarcolemma (Post et al. 1988). They may also play roles in storage of polyunsaturated fatty acids, release of arachidonic acid, and cell signalling (Nagan and Zoeller 2001).

1.1.9.5 Anti-viral signalling

Peroxisomes are not only metabolic organelles, and one of the most recent discoveries of a peroxisomal function is that of anti-viral defence, primarily through the discovery of a peroxisomal localisation of tail-anchored membrane protein mitochondrial antiviral signalling (MAVS) (Dixit et al. 2010). Following viral infection, the RIG-I-like Receptor (RLR) family of proteins detect viral RNA, and induce a signalling pathway that triggers expression of Type I interferons and other antiviral genes (Loo et al. 2011). This expression of host defence genes requires MAVS as an adaptor protein for the RLR (Xu et al. 2005; Meylan et al. 2005; Kawai et al. 2005). Peroxisomal-localised MAVS has been confirmed to be a site of signal transduction for anti-viral defence, and it was revealed that the peroxisomal localisation is required for rapid induction of antiviral genes, at a faster rate than mitochondrial MAVS (Dixit et al. 2010), implying different signalling cascades at the different organelles. Infection from viruses has been shown multiple times to affect peroxisomes (Wong et al. 2018; Cook et al. 2019), possibly as a way to subvert the peroxisomal role in the cell's antiviral defence. Cells infected with human immunodeficiency virus (HIV) show altered expression of microRNAs, decreasing expression of peroxisomal proteins and reducing peroxisome number (Xu et al. 2017). Similarly, human cytomegalovirus (HCMV)-encoded viral mitochondria-localised inhibitor of apoptosis (vMIA), has been shown to localise to peroxisomes (Magalhães et al. 2016), inducing peroxisome fragmentation and inhibiting the peroxisomal-dependent antiviral signalling pathway. HCMV infection also induces upregulation of the peroxisomal proteome (Jean Beltran et al. 2018). Herpes simplex virus 1 also targets peroxisomal MAVS as a way to dampen the immediate early antiviral response (Zheng and Su 2017). Therefore, the protective role of peroxisomes is not limited to ROS or VLCFA scavenging, but also in combatting viral infection in the immune response. This also leads to the possibility of peroxisomes as targets for anti-viral therapies in the future.

1.1.9.6 Further Roles

In addition to those listed in detail above, several other roles for peroxisomes have been demonstrated. Peroxisomes have been shown to contain a number of enzymes involved in cholesterol biosynthesis (Faust and Kovacs 2014),

converting acetyl-CoA from VLCFA oxidation to mevalonate (requiring acetoacetyl thiolase), and then to farnesyl diphosphate (FPP) with the mevalonate kinases (Figure 1.2A). FPP is a sterol precursor and is converted to cholesterol in the ER. Peroxisomes may also be involved in cholesterol shuttling from lysosomes to the ER (Chu et al. 2015; Xiao et al. 2019). The degradation of several amino acids can also take place in the peroxisome; including a range of D-amino acids by the enzymes D-amino acid oxidase and D-aspartate oxidase, and L-pipecolic acid by L-pipecolic acid oxidase (Wanders et al. 2016). Other metabolic pathways include, but are not limited to; metabolism of glyoxylate to glycine (Fodor et al. 2012), polyamines (Beard et al. 1985), sarcosine (Reuber et al. 1997), purines such as xanthine (Yeldandi et al. 1996), all-*trans*-retinol and 3-keto-C_{19}/C_{21}-steroids (Matsunaga et al. 2008), and prostaglandins (Diczfalusy et al. 1991), all of which it is extremely important to regulate to maintain cellular function.

1.1.10 The Peroxisome-Mitochondria Connection

1.1.10.1 Peroxisome-Organelle Interaction

In recent years, the field of organelle-organelle communication and membrane contact sites has grown massively, with the peroxisome being no exception (Schrader et al. 2019). While it has long been known that peroxisomes interact with other organelles, the physical tethering proteins were unknown, but have now recently began to be identified. For example, ER-peroxisome membrane contact sites are now much more well understood, with the ER-resident VAPs interacting with peroxisomal ACBD4 and ACBD5 to regulate lipid exchange (Costello et al. 2017b, c; Hua et al. 2017), and cholesterol transport from the ER to the peroxisome being facilitated by binding of extended synaptotagmin (E-Syts) on the ER membrane to peroxisomal lipid PI(4,5)P_2 (Xiao et al. 2019). Other peroxisome-organelle contact sites and proteins, including peroxisome-lysosome (Chu et al. 2015; Hu et al. 2018) and peroxisome-lipid droplet (Chang et al. 2019), have also been identified and characterised. In this thesis, the cooperation and interplay of peroxisomes and mitochondria are probed in more detail, including the response of peroxisomes to mitochondrial-derived ROS (see Chapter 2), and the extent to which shared peroxisome-mitochondrial proteins affect peroxisomal membrane dynamics (see Chapter 3; Chapter 4). Therefore, an overview of

current “knowns” and “unknowns” of this peroxisome-mitochondria connection is presented below.

1.1.10.2 Peroxisome-Mitochondria Functional Cooperation

As previously mentioned, peroxisomes work closely with mitochondria in the degradation of fatty acids and ATP generation, with peroxisomes chain-shortening those VLCFAs unable to be degraded by the mitochondria by β-oxidation before shuttling them to the mitochondria for the production of acetyl-CoA for use in the tricarboxylic acid (TCA) cycle (see section 1.1.9.2). In addition to this, peroxisomes and mitochondria also functionally cooperate in other metabolic pathways (Fransen et al. 2017) (Figure 1.3). Mitochondria are major producers of ROS, of which both mitochondria and peroxisomes contain several catalytic enzymes to reduce the levels of (see section 1.1.9.3). In the production of primary bile acids, peroxisomal enzymes catalyse the β-oxidation of the C27 fatty acids DHCA and THCA (see section 1.1.9.2). Both DHCA and THCA are formed in the mitochondria by mitochondrial cytochrome P450, before being passed to the peroxisomes following activation by ER bile acid-CoA ligase (Russell 2003). During the hydroxylation step of phytanic acid α-oxidation in peroxisomes, catalysed by phytanoyl-CoA 2-hydroxylase, the hydroxylation of phytanoyl-CoA is driven by 2-oxoglutarate, and produces succinate as a by-product (McDonough et al. 2005). In the TCA cycle in mitochondria, 2-oxoglutarate is produced, which can enter peroxisomes and be converted to succinate to aid in α-oxidation. Succinate can then re-enter the mitochondria for further use in the TCA cycle. Glyoxylate metabolism also requires peroxisome-mitochondria cooperation; the breakdown of glyoxylate produces both glycine and pyruvate (Wang et al. 2013b), both of which are metabolised in mitochondria. Peroxisomes have been implicated in the regulation of mitochondria-dependent apoptosis, as peroxisome deficiency through PEX3 or PEX5 depletion induces mitochondrial fragmentation, and thus cytochrome *c* release into the cytosol (Tanaka et al. 2019). However, as peroxisomes and mitochondria share components of their division machinery, possibly competitively, it may be likely that without peroxisomes, this division machinery is overly targeted to the mitochondria in order to induce this fragmentation. Finally, as previously discussed (see section 1.1.4), the mitochondria have been implicated in

peroxisome membrane protein supply, contributing to peroxisomal *de novo* biogenesis (Sugiura et al. 2017).

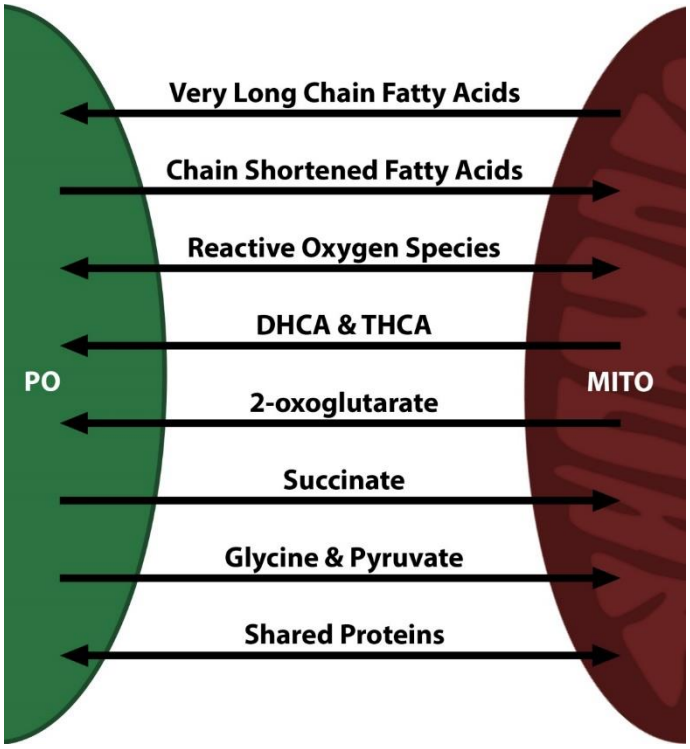

Figure 1.3: An overview of peroxisome-mitochondria functional cooperation. Peroxisomes (PO) and mitochondria (MITO) exchange several factors (see section 1.1.10.2), including fatty acids for degradation, key metabolites for their functions, and proteins involved in organelle dynamics.

1.1.10.3 Peroxisome-Mitochondria Physical Contact

Peroxisomes and mitochondria share many membrane proteins (Costello et al. 2018); including those involved in organelle division (FIS1, MFF, DRP1) (see section 1.1.5.2), organelle motility (MIRO1) (see section 1.1.8), and anti-viral signalling (MAVS) (see section 1.1.9.5). Despite this, and frequent observation of mitochondria in close apposition to peroxisomes in electron micrographs (Fransen et al. 2017), physical tethering proteins for peroxisome-mitochondria membrane interactions are far less characterised. In yeast, contact site proteins have been identified in mitochondrial Fzo1p and PMP Pex34p (Shai et al. 2018), linking peroxisomal β-oxidation with mitochondrial ATP generation. Pex11p has also been implicated in peroxisome-mitochondria contact in yeast, through its role in interacting with the mitochondria-ER tethering complex ERMES, where peroxisomes have been found to localise to upon Pex11p expression (Cohen et al. 2014; Mattiazzi Ušaj et al. 2015). While PEX11β in mammalian cells has not

yet been identified as a peroxisome-mitochondrial tethering protein, it was identified as co-regulated with enzymes involved in mitochondrial ATP generation/respiration, and expression of PEX11β increases peroxisome-mitochondria interaction through induction of peroxisomal membrane protrusions (Kustatscher et al. 2019). In addition, knockout of PEX11β leads to mistargeting of peroxisomal matrix and membrane proteins to the mitochondria, possibly to the inner-membrane space (Lismont et al. 2019a), suggesting PEX11β may play a role in preventing the mitochondrial localization of peroxisomal proteins. Towards the identification of mammalian tethering proteins, steroid biosynthesis in mouse Leydig tumour cells requires peroxisome-mitochondria interaction, which appears to be dependent on the dual targeted membrane protein ACBD2 (Fan et al. 2016). As peroxisome-mitochondria functional cooperation is so crucial for cell metabolism (see section 1.1.10.2), it will be important for future research to further identify tethering components, and identify the roles that they play in maintaining cell function.

1.1.11 The Role of Peroxisomes in Health and Disease

Due to the their vast array of metabolic functions (see section 1.1.9), peroxisomes play crucial roles in health and disease, with a range of symptoms and severity (Waterham et al. 2016). Disorders of peroxisomal function are commonly grouped into either peroxisomal enzyme deficiencies (PEDs) or peroxisome biogenesis disorders (PBDs); the most common of which are discussed here. In addition, several newly discovered disorders comprising of those with a defect in peroxisomal dynamics are discussed.

1.1.11.1 Peroxisomal Enzyme Deficiencies

PEDs include the loss of PMPs important for peroxisome metabolism in addition to peroxisomal matrix enzymes. The most common PED is X-linked adrenoleukodystrophy (X-ALD), a deficiency of the VLCFA transporter ABCD1 (Kemp et al. 2012). As a result, peroxisomal β-oxidation is severely impaired, and patients typically present with brain abnormalities including neuronal degeneration and demyelination and white matter inflammation, loss of cognitive function, peripheral neuropathy and myelopathy, ultimately resulting in loss of mobility, speech, cognitive function, and death within a few years. These symptoms are some of the classical hallmarks of a peroxisomal disorder, and

other PEDs due to a defect in various enzymes involved in β-oxidation have similar clinical presentations, including those arising from mutations in ACOX1 and DBP (see section 1.1.9.2). In addition to β-oxidation defects, a loss of phytanoyl-CoA 2-hydroxylase (catalysing the first step in α-oxidation (see section 1.1.9.2)), leads to adult Refsum disease (Wanders et al. 2006). In contrast to defects of β-oxidation, adult Refsum disease is typically less severe and carries a better prognosis; with loss of sight, smell, and hearing, neuropathy, and ataxia being the hallmarks. PEDs affecting ether lipid biosynthesis (see section 1.1.9.4) result in rhizomelic chondriodysplasia punctata (RCDP) types 2-4, from mutations in key enzymes of the peroxisomal ether phospholipid pathway DHAPAT, alkyl-DHAP synthase, and FAR1, respectively. Due to the marked decrease in crucial ether-linked phospholipids such as plasmalogens, patients often present with severe symptoms, including arthrogryposis, hypotonia, dwarfism and rhizomelia, and stippled bone and cartilage calcification (chondriodysplasia punctata) (Braverman and Moser 2012). Finally, other PEDs include loss of catalase-dependent H_2O_2 metabolism in acatalasemia, glyoxylate metabolism in primary hyperoxaluria type 1, and loss of bile acid synthesis with specific enzyme deficiencies.

1.1.11.2 Peroxisome Biogenesis Disorders

In contrast to the PEDs, PBDs represent mutations in any one of the human PEX genes, resulting in either a reduction of peroxisomal import, the presence of dysfunctional, import-incompetent, peroxisomal remnants (or “ghosts”), or a complete loss of peroxisomal structures. As with PEDs, PBD patients’ clinical presentations are broad, ranging from extensive neurological problems in neonates to slowly-progressing degenerative disease (Braverman et al. 2016). Two subtypes represent the PBDs: (i) the Zellweger spectrum disorders (ZSDs), denoted infantile Refsum disease, neonatal ALD, and Zellweger syndrome in order of increasing severity (with considerable overlap in symptoms), and (ii) RCDP types 1 and 5 (Argyriou et al. 2016). ZSDs arise from mutations in integral PMPs, for example loss of one of the three indispensable PMPs for peroxisome membrane assembly (PEX3, PEX16, PEX19; see section 1.1.4), and are typically on the more severe end of the spectrum, due to the complete lack of peroxisomes. The most common disease-causing PMP mutations are in PEX1 or

PEX6, parts of the PEX5 and PEX7 recycling complex (see section 1.1.4), and are found mutated in over three-quarters of PBD patients (Waterham and Ebberink 2012). RCDP type 1 is a consequence of mutations in PTS2 receptor PEX7, and due to the role of PEX7 in importing crucial matrix enzymes of the ether-linked lipid biosynthesis pathway, show near identical symptoms as those of RCDP type 2-4 discussed previously (Braverman et al. 1993). Similarly, RCDP type 5 arises from mutations in PEX5L, a co-receptor for PTS2 import (Barøy et al. 2015).

1.1.11.3 Disorders of peroxisomal dynamics

While peroxisome dynamics also appear disturbed in PED or PBD patients (e.g. peroxisomes are less abundant in ACOX1 deficiency and can be rescued with treatment with DHA (Itoyama et al. 2012)), a relatively new group of peroxisomal disorders are those that arise from dysfunction in proteins involved in maintenance of peroxisomal membrane dynamics (see section 1.1.5.2). The peroxin PEX11β, and the shared peroxisomal-mitochondrial proteins MFF, GDAP1 and DRP1 have all been associated with disease (Waterham et al. 2007; Shamseldin et al. 2012; Ebberink et al. 2012; Huber et al. 2013). These patients show mitochondrial and peroxisomal elongation (due to a block in organelle fission) and present with typical symptoms of mitochondrial and peroxisomal disorders (including microcephaly, neuropathy, hypotonia, retinal dystrophy etc.), however, display no consistent abnormality in peroxisomal (or mitochondrial) metabolism (Waterham et al. 2007; Shamseldin et al. 2012; Ebberink et al. 2012; Koch et al. 2016; Nasca et al. 2018) (see Chapter 3). It is therefore important to fully understand peroxisomal membrane dynamics and the role that it plays in cellular processes and their links to disease, for example peroxisomal elongation, proliferation and dynamics affecting cell fate (Asare et al. 2017), and carrying protection to the auditory system against noise-induced ROS (Delmaghani et al. 2015). A thorough understanding of the role of membrane dynamics in disease, combined with a detailed characterisation of the key processes underlying peroxisomal membrane dynamics to maintain protective functions, will pave the way for future therapeutics and the way in which they are approached.

1.2 Thesis Overview

1.2.1 Aims and Objectives

As previously discussed, the dynamics of the peroxisomal compartment encompasses not only motility, but also the maintenance of peroxisome number and morphology. How these dynamics relate to peroxisomal function, and *vice versa*, is still a relatively new field. How does altering the membrane dynamics of the peroxisomal compartment contribute to the cellular pathophysiology in disorders of peroxisome dynamics? To what extent are peroxisomal membrane alterations a cause or a consequence of cellular alterations? Which cellular processes are most altered in these conditions, and what should we target in order to rescue alterations of peroxisome membrane dynamics?

Through an interdisciplinary, combined experimental-modelling approach, this thesis will explore these questions, aiming to further elucidate the role that peroxisomal membrane dynamics have in health and disease.

1.2.2 Results Chapters

To address the above questions/aims, this thesis consists of three distinct results chapters, finally culminating in a brief discussion chapter, helping to explain how peroxisome dynamics and peroxisomal alterations contribute to cellular pathophysiology.

Chapter 2 explores the response of the peroxisomal membrane to stress, by looking at how induced alterations to another organelle – the mitochondrion – have consequential effects on peroxisomal morphology. Chapter 3 takes this peroxisome-mitochondrion interplay further, by investigating the role that the dual-localised division protein MFF has in maintaining peroxisomal membrane dynamics, and the further, unexpected, peroxisomal alterations that arise in patients with a defect in these dynamics.

Throughout these studies, the overall picture of how peroxisomal dynamics are altered has become clearer. In Chapter 4, a biophysical, mathematical model is presented of peroxisomal membrane dynamics. This model takes into account alterations of the peroxisomal compartment in terms of morphological changes, as well as peroxisome number.

Finally, the conclusion in Chapter 5 discusses how the previous results chapters come together into a coherent story and evaluate this interdisciplinary approach to organelle biology.

Chapter 2 ROS and Peroxisomal Membrane Dynamics

2.1 Introduction

As previously discussed (see section 1.1.9.3), peroxisomes are crucial players in the maintenance of ROS levels inside the cell, acting as both a source and a sink of ROS, and cooperating extensively with the mitochondria for ROS homeostasis (see section 1.1.10.2). ROS are generated in mitochondria primarily through the generation of ATP. The main mitochondrial ROS is $O_2{\cdot}^-$, produced primarily through the action of complex I (NADH CoenzymeQ1 reductase) in the mitochondrial respiratory chain, with the flavin mononucleotide prosthetic group in the active site carrying out the reduction of O_2 (Hirst et al. 2008).

This redox-sensitive relationship between peroxisomes and the mitochondria may have impact on age-related and degenerative disorders (Titorenko and Terlecky 2011; Fransen et al. 2013; Nordgren and Fransen 2014). A reduction in peroxisomal catalase is linked to ageing in mammalian cells, and results in functionally impaired mitochondria (Koepke et al. 2008; Ivashchenko et al. 2011), likely a result of increased cellular H_2O_2 levels (Walton and Pizzitelli 2012).

It is known that mitochondria are responsive to ROS alterations in peroxisomes; generation of excess ROS in peroxisomes using peroxisome-localised KillerRed perturbs mitochondrial redox balance, not seen with cytosolic KillerRed (Ivashchenko et al. 2011; Wang et al. 2013a). Peroxisomes have also been shown to be somewhat resistant to oxidative stress generated elsewhere in the cell, not responding to KillerRed unless inside of the peroxisomes themselves (Ivashchenko et al. 2011). However, how peroxisomes respond to oxidative stress in the mitochondria is largely unknown. Several drugs that target mitochondria induce mitochondrial ROS, including the mitochondria respiratory chain inhibitor rotenone (Barrientos and Moraes 1999), widely used to produce Parkinson's-like symptoms in animal and cellular models (Betarbet et al. 2000; Alam and Schmidt 2002; Mounsey and Teismann 2011). Inhibition of complex I with rotenone is likely to increase mitochondrial ROS levels by resulting in a backup of electrons onto the flavin mononucleotide group, producing more $O_2{\cdot}^-$ (Votyakova and Reynolds 2008).

It has previously been reported that rotenone has an effect on peroxisomes, inducing elongation and clustering, and that this may be independent of the ROS produced by rotenone (Pinho 2010). It was also noted that rotenone induced

microtubule depolymerisation. However, the precise mechanism whereby rotenone induces peroxisome alteration is still unclear. Similarly, rotenone appears to induce mitochondrial morphological alterations (Pinho 2010), but it is unknown if this is through the same alterations to the intracellular environment that affect peroxisomes. Revealing these mechanisms will shed further light into the complex ROS-sensitive relationship between peroxisomes and mitochondria, in addition to providing valuable insight into the manner in which rotenone affects the intracellular environment.

2.2 Materials and Methods

2.2.1 Antibodies

Antibodies were used as follows: rabbit polyclonal antibody against PEX14 (1:1400, kindly provided by D. Crane, Griffith University, Brisbane, Australia) (Nguyen et al. 2006; Grant et al. 2013), mouse monoclonal antibodies against α-tubulin (Sigma, T9026) and acetylated α-tubulin (Sigma, T6793) (both used at 1:200 for immunofluorescence, 1:1000 for immunoblotting), and TOM20 (1:200 for immunofluorescence) (BD Transduction Laboratories, San Diego, USA; 612278). Secondary anti-IgG antibodies against rabbit (Alexa 488, 1:500; A21206) and mouse (Alexa 488, 1:400, A21202 and Alexa 594, 1:1000, A21203) were obtained from Molecular Probes (as part of Invitrogen Life Technologies, Eugene, USA). Anti-mouse IgG antibodies conjugated to HRP (1:5000, 170-6516) were obtained from Bio-Rad (Munich, Germany). The specificity of all antibodies has been validated in several previous studies.

2.2.2 Cell Culture and Drug Treatment

COS-7 cells (African green monkey kidney cells; ATCC CRL-1651) were cultured in DMEM, high glucose (4.5 g/L) supplemented with 10% FBS, penicillin and streptomycin (all from Life Technologies) at 37 °C with 5% CO_2 and 95% humidity (HERACell 240i CO_2 incubator). Cells were seeded onto glass coverslips (Fisher Scientific, 19 mm Ø, 0.13–0.17 mm thickness) at a defined density (1×10^5 cells/mL). 24 h after seeding, the culture medium was aspirated, and cells were treated for different time intervals (3, 6 and 24 h) with a range of concentrations of rotenone (Sigma, R8875) (100 nM, 1 µM, 10 µM, 100 µM,

1 mM). For pre-treatment with the microtubule-stabilising drug paclitaxel (taxol) (Sigma, T7402), cells were first incubated with 20 µM paclitaxel for 6 h before the addition of rotenone. For pre-treatment with the antioxidant N-acetyl cysteine (NAC) (Sigma, A7250), cells were first incubated with 10 mM NAC for 1 h before the addition of rotenone. Stock concentrations of 100 mM rotenone and 2 mM paclitaxel were prepared in dimethyl sulfoxide (DMSO) (Sigma, D8418) and dilutions prepared in culture medium. A stock concentration of 100 mM NAC was prepared always fresh in culture medium, and diluted in culture medium following pH neutralisation and sterilisation by filtration of the stock.

2.2.3 Immunofluorescence and Microscopy

Cells grown on glass coverslips were washed twice with phosphate-buffered saline (PBS). Cells to be stained with organelle markers (e.g. PEX14 or TOM20) were fixed using 4% paraformaldehyde, pH 7.4 for 20 min at room temperature as previously described (Bonekamp et al. 2013b) as peroxisome morphology is sensitive to alcoholic fixation (Schrader et al. 1995). Cells to be stained with cytoskeletal markers (e.g. α-tubulin or acetylated α-tubulin) were fixed with ice-cold methanol for 15 min at −20 °C. Following fixation, cells were washed 3 times in PBS, membranes were permeabilised with 0.2% (w/v) Triton X-100 for 10 min at room temperature (permeabilisation was omitted for methanol-fixed cells), washed again three times in PBS and blocked with 2% (w/v) bovine serum albumin (BSA) for 10 min at room temperature. Cells were then incubated for 1 h with primary antibodies diluted in PBS, washed three times in PBS and incubated for 1 h with secondary antibodies diluted in PBS. In controls, where the primary antibodies were omitted, no staining reactions were observed. To mount coverslips on slides, cells were washed three times in PBS, dipped in dH_2O and mounted (after removal of excess water) in Mowiol 4-88 containing *n*-propyl galate as an anti-fading (Bonekamp et al. 2013b). Cell imaging was performed using an Olympus IX81 microscope with an UPlanSApo 100x/1.40 Oil objective (Olympus Optical, Hamburg, Germany), eGFP ET filter set (470/40 Et Bandpass filter, Beamsplitter T495 LPXR and 525/50 ET Bandpass filter [Chroma Technology GmbH, Olching, Germany]), TxRed HC Filter Set (562/40 BrightLine HC Beamsplitter HC BS 593, 624/40 BrightLine HC [Semrock, Rochester, USA]). Images were taken with a CoolSNAP HQ2 CCD camera (150–300 ms exposure,

gain 3, bin 1, gamma 1) and MetaMorph 7 (Molecular Devices, USA) was used to adjust for contrast and brightness.

2.2.4 Gel Electrophoresis and Immunoblotting

Following drug treatment, cells were trypsinised, washed in PBS and centrifuged at 500×*g* for 3 min. Cell pellets were lysed [25 mM Tris–HCl, pH 8.0, 150 mM NaCl, 0.5% (w/v) sodium deoxycholate, 1.5 mM Triton X-100 and a protease-inhibitor mix (Roche Diagnostics)] and protein concentrations were determined using the Bradford assay (Bradford 1976) (Bio-Rad Protein Assay Dye Reagent Concentrate, 5000006). Equal amounts of protein were separated by SDS-PAGE on 12.5% polyacrylamide gels, transferred to nitrocellulose membrane (Amersham Bioscience, Arlington Heights, IL, USA) using a semi-dry apparatus (Trans-Blot SD, Bio-rad) and analysed by immunoblotting using the corresponding primary antibodies and horseradish peroxidase-conjugated secondary antibodies and enhanced chemiluminescence reagents (Amersham Bioscience, Arlington Heights, IL, USA).

2.2.5 Quantification and Statistical Analysis of Data

Analysis of statistical significance was performed using GraphPad Prism 5 software. A two-tailed unpaired *t* test was used to determine statistical difference against the indicated group. $*p < 0.05$, $**p < 0.01$, $***p < 0.001$. For analysis of organelle distribution and morphology, a minimum of 150 cells were examined per condition, and organelle parameters (e.g. tubular, elongated morphology, intracellular distribution/clustering) were microscopically assessed in at least three independent experiments. The analysis was made blind and in different areas of the coverslip. Data are presented as mean ± SD.

2.3 Results

2.3.1 Rotenone alters peroxisome morphology and distribution

To assess the effect of rotenone on peroxisome morphology in mammalian cells, COS-7 cells were treated with a range of concentrations of rotenone, and peroxisome morphological characteristics observed following immunofluorescence using an antibody against PEX14. Cells were treated for 6 and 24 hours prior to immunofluorescence. Control COS-7 cells showed an even distribution of peroxisomes, with the typical spherical/punctate morphology (Figure 2.1A). As reported previously (Pinho 2010), cells following drug treatment showed either an elongated (Figure 2.1B) or clustered (Figure 2.1C) peroxisome population, an uneven distribution in the cell (Figure 2.1D), or a combination of all three. Both peroxisomal elongation and peroxisomal clustering was observed in a concentration-dependent manner of rotenone (Figure 2.1E, F).

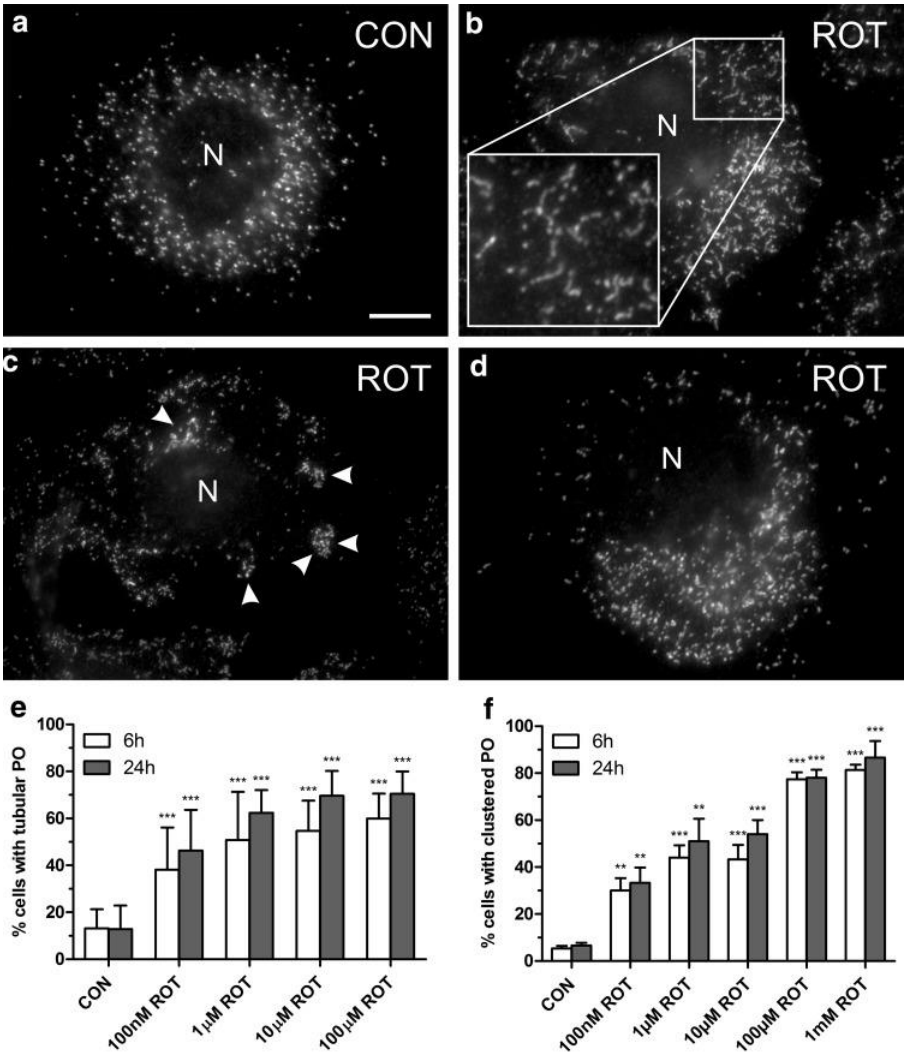

Figure 2.1: Rotenone induces alterations in peroxisome morphology and distribution. COS-7 cells were treated with solvent (CON) or rotenone (ROT) for 6 and 24 h and processed for immunofluorescence microscopy using antibodies directed to PEX14, a peroxisomal membrane protein. **A-D)** Representative examples. **A)** Control (CON). Note the elongated tubular peroxisomes in **B** (1 mM ROT, 6 h), the formation of peroxisomal clusters (**(C)** arrowheads) (100 µM ROT, 6 h), and the non-uniform distribution of peroxisomes **(D)** (100 µM ROT, 6 h) in contrast to **A**. Boxed region in **B** shows higher magnification view. **E, F)** Qualitative assessment of peroxisome elongation **(E)** and cluster formation **(F)**. A minimum of 150 cells were examined per condition, and organelle morphology and distribution were microscopically assessed. Values represent mean ± SD of at least three independent experiments. N, nucleus. Bar, 10 µm.

2.3.2 Rotenone-induced intracellular ROS are not the major cause of peroxisome alterations in COS-7 cells

Rotenone treatment is known to result in an increase in intracellular ROS levels (Barrientos and Moraes 1999), and it is also known that pre-treatment of cells with the antioxidant N-acetyl cysteine (NAC) inhibits this rise in intracellular ROS levels (Pinho 2010; Bonet-Ponce et al. 2016). To assess whether the effect of rotenone on the peroxisomal compartment is due to an increase in ROS levels, or some other factor, COS-7 cells were treated with NAC prior to rotenone treatment (Figure 2.2). In line with previous observations (Pinho 2010), peroxisomes still displayed a concentration-dependent clustered phenotype in response to rotenone treatment (Figure 2.2). This suggests that surprisingly, despite the close redox-sensitive relationship between peroxisomes and mitochondria, mitochondria-derived ROS is not a cause of peroxisomal alterations in COS-7 cells with rotenone treatment.

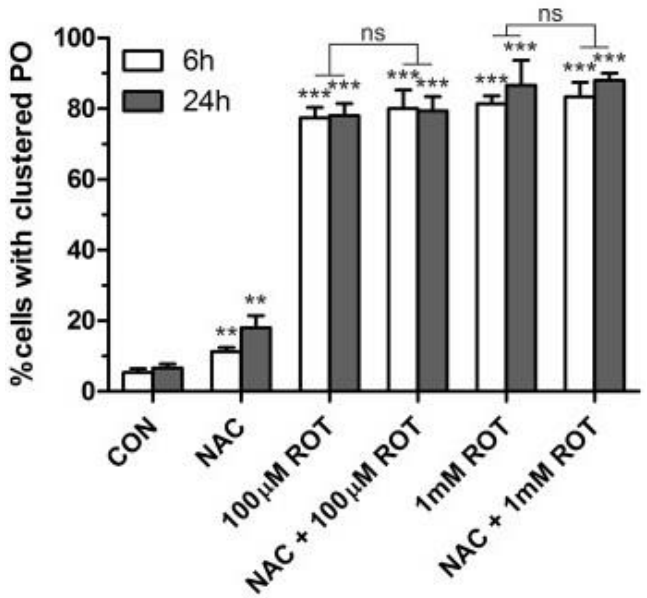

Figure 2.2: Antioxidant treatment does not prevent peroxisomal clustering. Cells were treated as indicated and processed for immunofluorescence microscopy using antibodies directed to PEX14. Values represent mean ± SEM of at least three independent experiments qualitatively assessing peroxisome cluster formation.

2.3.3 Rotenone exerts a microtubule-destabilising activity in COS-7 cells

The morphological phenotypes seen in response to rotenone treatment closely resemble those seen under conditions of microtubule depolymerisation (Schrader et al. 1996; Wiemer et al. 1997), as microtubules are crucial for peroxisome motility and distribution (see section 1.1.8). In addition, rotenone has been shown to interfere with microtubule polymerisation by binding to tubulin, in a similar manner to nocodazole (Marshall and Himes 1978). This then results in an arrest of cell cycle progression at mitosis (Meisner and Sorensen 1966; Brinkley et al. 1974; Srivastava and Panda 2007). Therefore, it may be possible that the peroxisomal morphological alterations seen following rotenone treatment are a result of a microtubule-destabilising activity. To confirm that rotenone induces microtubule depolymerisation in COS-7 cells, cells were treated with the same range of concentrations of rotenone used in Figure 2.1 (Figure 2.3). In controls (Figure 2.3A) and low concentrations of rotenone (Figure 2.3B, C), microtubules show a typical distribution, radiating from one point (the microtubule organising centre). At increasing concentrations of rotenone (10 µM – 100 µM) (Figure 2.3D-E), microtubules began to depolymerise, up to complete depolymerisation (1 mM) (Figure 2.3F). At low concentrations, although staining with an antibody against α-tubulin did not reveal any microtubule abnormalities, staining with an antibody against acetylated α-tubulin revealed an increase in microtubule acetylation with rotenone treatment compared to controls (Figure 2.3G-J). Acetylation of microtubules plays a role in their stabilisation (Piperno 1987), and is likely increased under rotenone treatment to counteract the tubulin-binding, microtubule-destabilising ability of rotenone. These results confirm the effect of rotenone on microtubule stabilisation, which may be a factor in causing the peroxisome abnormalities seen in rotenone-treated COS-7 cells.

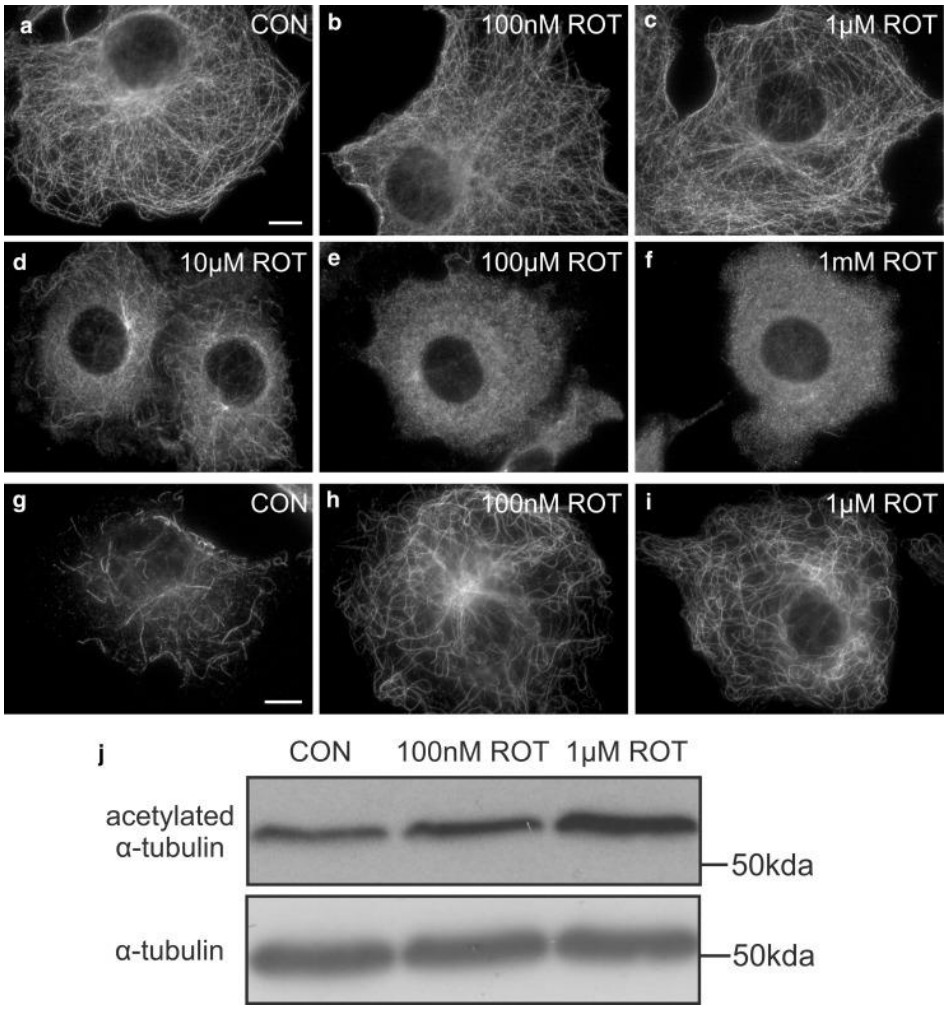

Figure 2.3: Rotenone induces microtubule depolymerisation and acetylation of α-tubulin in COS-7 cells. A-F) Cells were treated with solvent **(A)** (CON) or different concentrations of rotenone (ROT) **(B-F)** for 6 h and processed for immunofluorescence microscopy using antibodies directed to α-tubulin. **G-J)** Cells were treated with solvent **(G)** (CON), 100 nM rotenone **(H)** or 1 µM rotenone **(I)** for 3 h and labelled with antibodies directed to acetylated α-tubulin. **J)** Immunoblot of cell lysates showing levels of acetylated α-tubulin after 3 h of rotenone treatment. 50 µg of protein was loaded and the blot probed with acetylated α-tubulin and α-tubulin antibody as indicated. α-tubulin serves as loading control. Bars, 10 µm.

2.3.4 Alterations in peroxisome distribution induced by rotenone are caused by microtubule depolymerisation

To further confirm the hypothesis that rotenone treatment induces alterations to the peroxisome compartment through its microtubule-destabilising ability, COS-7 cells were pre-treated with paclitaxel (taxol) prior to incubation with rotenone (Figure 2.4). Paclitaxel pre-treatment induces microtubule polymerisation and bundling in control cells (Figure 2.4A, B), and after treatment with paclitaxel, microtubules were no longer destabilised, even in response to high concentrations of rotenone (Figure 2.4C, D). Peroxisomes following paclitaxel

treatment showed a small degree of clustering compared to controls (Figure 2.4E, F), but importantly, paclitaxel pre-treatment significantly reduced the degree of clustering with rotenone treatment (Figure 2.4F-I). These results suggest that peroxisome alterations in mammalian cells induced by rotenone are mainly caused by the microtubule-destabilising activity of rotenone rather than via complex I inhibition and oxidative stress.

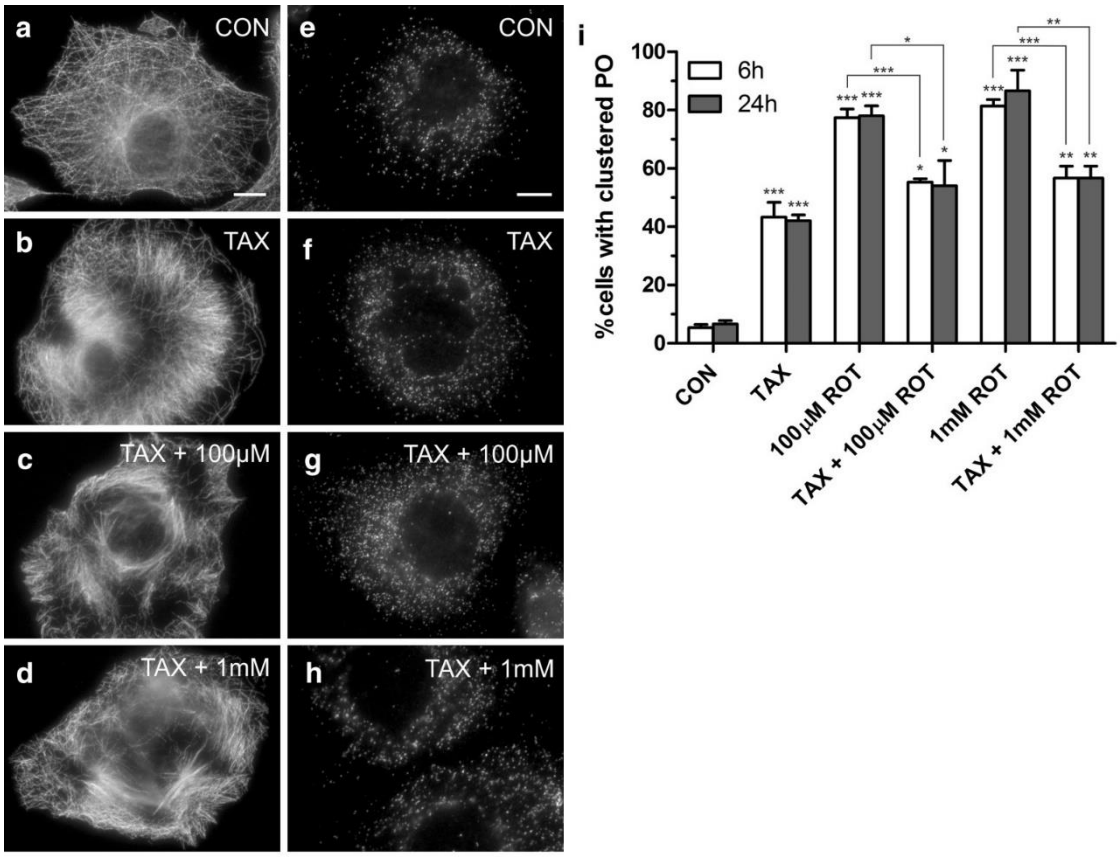

Figure 2.4: Microtubule stabilisation prevents rotenone-induced clustering of peroxisomes. COS-7 cells were treated with solvent (CON) **(A, E)**, paclitaxel (TAX) **(B, F)**, paclitaxel and 100 µM rotenone (ROT) **(C, G)**, or paclitaxel and 1 mM rotenone **(D, H)** for 6 and 24 h. Cells were then processed for immunofluorescence microscopy using antibodies directed to α-tubulin **(A–D)** or PEX14 **(E–H)**. **I)** Qualitative assessment of peroxisome cluster formation. A minimum of 150 cells were examined per condition, and organelle distribution was microscopically assessed. Values represent mean ± SD of at least three independent experiments. *p* values refer to appropriate controls unless indicated. Bars, 10 µm.

2.3.5 Rotenone alters mitochondrial morphology in a ROS dependent manner.

Finally, the effects of rotenone on mitochondrial morphology were investigated. COS-7 cells were treated with rotenone for 6 and 24 hours, and mitochondrial morphology assessed by processing for immunofluorescence using antibody against outer membrane marker TOM20 (Figure 2.5A-D). Control mitochondria typically showed an elongated, tubular morphology (Figure 2.5A), however, following rotenone treatment, mitochondria displayed a rounded, fragmented phenotype in a time- and concentration-dependent manner (Figure 2.5D). To determine if the microtubule-destabilising ability of rotenone was responsible for mitochondrial morphological abnormalities, cells were pre-treated with paclitaxel, as in Figure 2.4 (Figure 2.5E-H). Interestingly, paclitaxel did not prevent the increase in percentage of cells showing a spherical mitochondrial morphology (Figure 2.5H). However, pre-treatment of COS-7 cells with NAC did rescue mitochondrial morphological alterations, preventing mitochondrial fragmentation even at higher concentrations of rotenone (Figure 2.5I-L). These finding suggest that, in contrast to its action on peroxisomes, mitochondrial alterations in mammalian cells induced by rotenone are mainly caused by complex I inhibition and oxidative stress rather than via the microtubule-destabilising activity of rotenone.

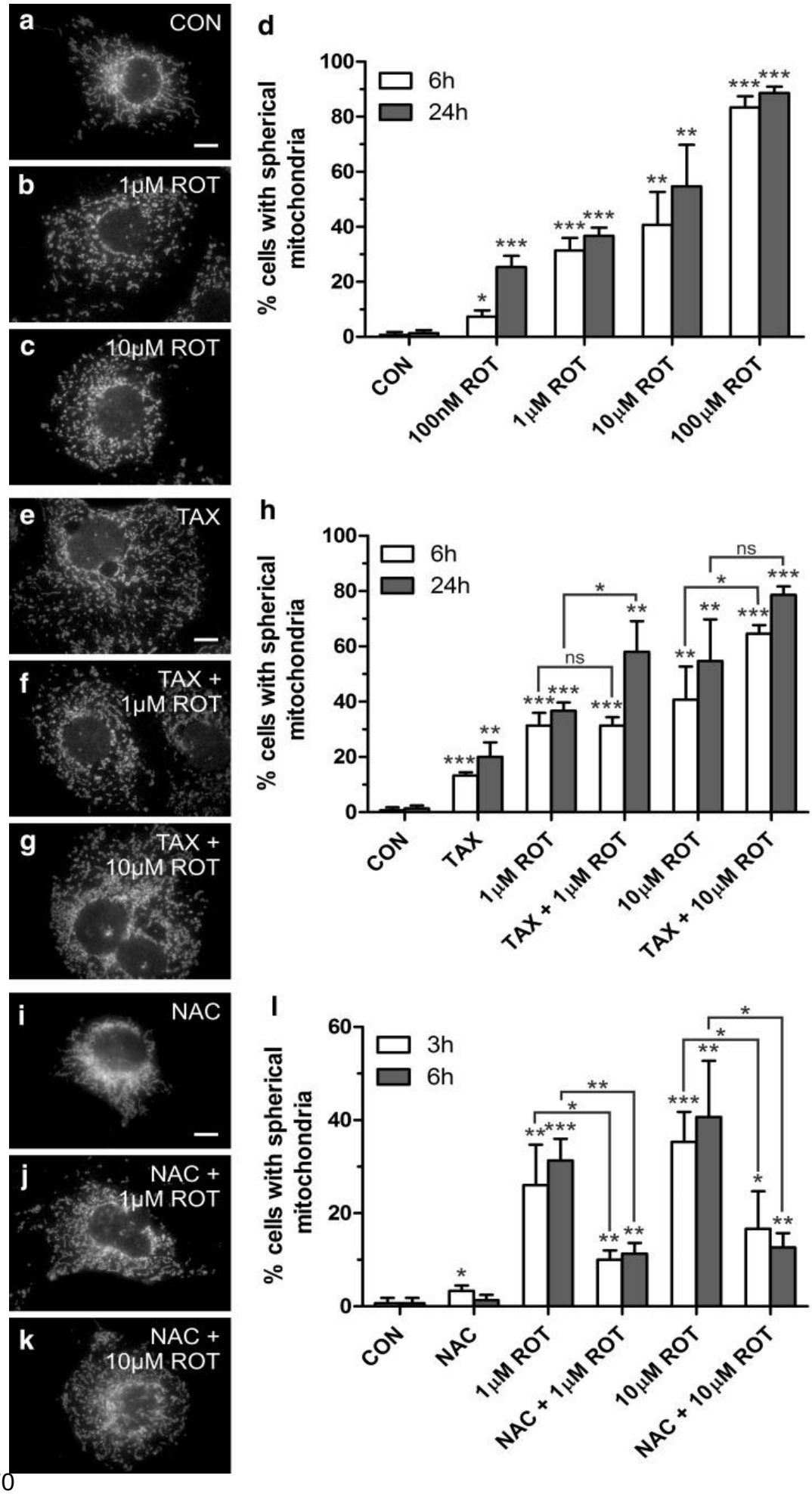
a
CON
b
1μM ROT
c
10μM ROT
d
% cells with spherical mitochondria
6h
24h
CON
100nM ROT
1μM ROT
10μM ROT
100μM ROT
e
TAX
f
TAX + 1μM ROT
g
TAX + 10μM ROT
h
% cells with spherical mitochondria
6h
24h
ns
CON
TAX
1μM ROT
TAX + 1μM ROT
10μM ROT
TAX + 10μM ROT
i
NAC
j
NAC + 1μM ROT
k
NAC + 10μM ROT
l
% cells with spherical mitochondria
3h
6h
CON
NAC
1μM ROT
NAC + 1μM ROT
10μM ROT
NAC + 10μM ROT

Figure 2.5: Rotenone-induced mitochondrial fragmentation can be prevented by antioxidant-treatment but not by microtubule stabilisation. A-D) Rotenone induces the formation of spherical mitochondria. COS-7 cells were treated with solvent (CON) **(A)** or rotenone (ROT) for 6 **(B-D)** and 24 h **(D)** and processed for immunofluorescence microscopy using antibodies directed to TOM20, a mitochondrial outer membrane protein. Note the elongated tubular mitochondria in **A** in contrast to **B, C**. **D)** Qualitative assessment of mitochondrial morphology. A minimum of 150 cells were examined per condition, and organelle morphology was microscopically assessed. Values represent mean ± SD of at least three independent experiments. **E–H)** Microtubule stabilisation does not prevent rotenone-induced mitochondrial fragmentation. COS-7 cells were treated with paclitaxel (TAX) **(E)** or paclitaxel and rotenone (ROT) for 6 **(F-H)** and 24 h **(H)** and labelled with TOM20 antibodies. Note the elongated tubular mitochondria in **E** in contrast to **F, G**. **H)** Qualitative assessment of mitochondrial morphology (see above). **I-L)** Antioxidant-treatment prevents rotenone-induced mitochondrial fragmentation. COS-7 cells were treated with N-acetyl cysteine (NAC) **(I)** or N-acetyl cysteine and rotenone (ROT) for 3 **(J–L)** and 6 h **(L)** and labelled with TOM20 antibodies. Note the elongated tubular mitochondria in **J–L** in contrast to **B, C, F, G**. **L)** Qualitative assessment of mitochondrial morphology (see above). p values refer to appropriate controls unless indicated. Bars, 10 µm.

2.4 Discussion

Peroxisome elongation is a pre-requisite of peroxisome multiplication by growth and division (see section 1.1.5.2) (Schrader et al. 2016a), and is influenced by many factors and can be induced by different stimuli, including culture condition, cell density, growth factors, fatty acids, and ROS (Schrader et al. 1998, 1999, Schrader and Fahimi 2006b, a). In this case, peroxisomal elongation and clustering was surprisingly not stimulated by ROS levels, but by microtubule depolymerisation. These results highlight that peroxisomes are highly resistant to oxidative stress, whereas mitochondria are far more sensitive. This is in line with published findings of the resistance of peroxisomes to oxidative bursts from KillerRed, whereas generation of excess ROS inside peroxisomes with KillerRed perturbed the mitochondrial redox balance and led to mitochondrial fragmentation and cell death (Ivashchenko et al. 2011; Wang et al. 2013a). In addition, the ROS-generating neurotoxin 6-hydroxydopamine (Galindo et al. 2003) induced a mitochondrial fragmentation in SH-SY5Y neuroblastoma cells, but showed no alterations to peroxisome morphology (Gomez-Lazaro et al. 2008). How redox communication between peroxisomes and mitochondria is mediated is currently unclear, but a picture is now becoming clear of a more complex signalling system as opposed to simple diffusion of excess ROS (Fransen and Lismont 2018).

Previous work showed pre-treatment with paclitaxel and stabilisation of microtubules prevented alterations of peroxisome morphology and distribution

caused by microtubule-depolymerising agents such as nocodazole (Schrader et al. 1996). The results in the present study show that rotenone has a similar effect on peroxisomes as other microtubule-depolymerising drugs such as nocodazole, colcemid and vinblastine (Schrader et al. 1996). Why these drugs cause peroxisomal elongation in addition to clustering is still unknown.

Rotenone is often used as an inducer of Parkinson's like symptoms in mice; chronic treatment reproduces features such as motor deficits, protein aggregation, and loss of dopaminergic neurons (Betarbet et al. 2000; Meurers et al. 2009). Inhibiting complex I can deplete ATP levels inducing oxidative stress in cells (Sherer et al. 2003; Testa et al. 2005). This study highlights that results from treatment with rotenone as a model for Parkinson's disease have to be carefully interpreted due to the different effects of rotenone in cells; besides increasing ROS levels, mitochondrial fragmentation, and microtubule depolymerisation, rotenone also effects peroxisome dynamics and distribution. These findings are also in line with observations showing that paclitaxel provides protective effects against rotenone-induced toxicity (Jiang et al. 2006).

Mitochondrial dysfunction is commonly accepted as having a key role in Parkinson's disease, but microtubule alterations are also considered. Another model toxin for Parkinson's disease, 1-methyl-4-phenyl-1,2,3,6-tetrahydropyridine, impacts on microtubule polymerisation besides its effect on mitochondria (Cartelli et al. 2010). Problems with microtubule integrity result in altered vesicular and organelle transport in neurons leading to neuronal death (Ren et al. 2005; De Vos et al. 2008; Cartelli et al. 2010). Peroxisome membrane dynamics and morphology are important for the formation of peroxisomes by growth and division, their intracellular positioning, movement and interaction with other subcellular compartments and have been linked to human health and disease (see section 1.1.11.3) (Ribeiro et al. 2012; Schrader et al. 2015). Patients with Parkinson's disease have reduced levels of plasmalogens (Fabelo et al. 2011), of which the peroxisomes play a major role in the production of (see section 1.1.9.4). Therefore, while mitochondrial dysfunction is accepted as the main cause of Parkinson's disease, loss of peroxisome dynamics and distribution may contribute to this process.

Chapter 3 Mitochondrial Fission Factor (MFF) is a Critical Regulator of Peroxisome Maturation

3.1 Abstract

Peroxisomes are highly dynamic subcellular compartments with important functions in lipid and ROS metabolism. Impaired peroxisomal function can lead to severe metabolic disorders with developmental defects and neurological abnormalities. Recently, a new group of disorders has been identified, which is characterised by defects in the membrane dynamics and division of peroxisomes rather than by loss of metabolic functions. However, the contribution of impaired peroxisome plasticity to the pathophysiology of those disorders is not well understood. Mitochondrial fission factor (MFF) is a key component of both the peroxisomal and mitochondrial division machinery. Patients with MFF deficiency present with developmental and neurological abnormalities. Peroxisomes (and mitochondria) in patient fibroblasts are highly elongated as a result of impaired organelle division. The majority of studies into MFF-deficiency have focused on mitochondrial dysfunction, but the contribution of peroxisomal alterations to the pathophysiology is largely unknown. Here, we show that MFF deficiency does not cause alterations to overall peroxisomal biochemical function. However, loss of MFF results in a reduced import-competence of the peroxisomal compartment and leads to the accumulation of pre-peroxisomal membrane structures. We show that peroxisomes in MFF-deficient cells display alterations in peroxisomal redox state and intra-peroxisomal pH as well as altered peroxisome distribution in neuronal cells. Removal of elongated peroxisomes through induction of autophagic processes is not impaired. The consequences of our findings for the pathophysiology of MFF-deficiency and related disorders with impaired peroxisome plasticity are discussed.

3.2 Introduction

Peroxisomes are highly dynamic membrane-bound organelles with key functions in cellular lipid and ROS metabolism. Defects in peroxisome biogenesis and metabolic function can result in severe disorders with developmental defects and neurological abnormalities (Dorninger et al. 2017; Wanders 2018). Peroxisome biogenesis disorders (PBDs) result from mutations in *PEX* genes, which encode proteins essential for peroxisomal membrane biogenesis and matrix protein import. PBDs, such as Zellweger Spectrum disorders, are usually characterised

by a loss of functional peroxisomes. This impacts on multiple metabolic pathways (e.g., peroxisomal α- and β-oxidation of fatty acids, and the synthesis of ether-phospholipids, which are abundantly present in myelin sheaths) and results in various patient phenotypes and symptoms (Braverman et al. 2016). Peroxisomal single enzyme deficiencies (PEDs) on the other hand are caused by mutations in genes encoding a specific peroxisomal enzyme/protein and usually affect one metabolic pathway or function. The most prominent example is X-linked adrenoleukodystrophy, which is caused by mutations in the *ABCD1* gene, encoding a peroxisomal ABC transporter required for the import of very-long-chain fatty acids (VLCFAs) into the organelle (Raymond et al. 1993). In addition to PBDs and PEDs, a third group of disorders has been identified, which is characterised by defects in the membrane dynamics and division of peroxisomes rather than by loss of metabolic functions (Waterham et al. 2007; Shamseldin et al. 2012; Ebberink et al. 2012; Koch et al. 2016).

Peroxisomes can form and multiply by growth and division, a defined multistep pathway involving membrane elongation of existing peroxisomes, constriction, and membrane fission (Schrader et al. 2016). In mammals, this involves the coordinated interplay of key membrane-shaping and fission proteins such as PEX11β, FIS1, MFF, and DRP1 (encoded by the *DNML1* gene) (Schrader et al. 2016). The peroxisomal membrane protein PEX11β is involved in several steps of peroxisomal growth and division: membrane deformation to facilitate elongation (Delille et al. 2010; Opaliński et al. 2011), recruitment of the division factors MFF and FIS1 to constriction sites (Koch et al. 2005; Koch and Brocard 2012; Itoyama et al. 2013), and activation of the fission GTPase DRP1 (Williams et al. 2015). The tail-anchored membrane proteins MFF and FIS1 act as adaptor proteins for the recruitment of DRP1 to the peroxisomal membrane and interact with PEX11β (Schrader et al. 2016). With the exception of PEX11β, all proteins involved in peroxisome growth and division identified so far are also key mitochondrial division factors. FIS1 and MFF are dually targeted to both peroxisomes and mitochondria, and also recruit DRP1 to the mitochondrial outer membrane (Koch et al. 2005; Gandre-Babbe and van der Bliek 2008; Costello et al. 2017a, 2018). Mitochondria also possess the adaptor proteins MiD49 and MiD51, which are specific to mitochondria and can recruit DRP1 independent of FIS1 and MFF (Palmer et al. 2013). GDAP1 is another tail-anchored membrane

protein shared by mitochondria and peroxisomes, which influences organelle fission in an MFF- and DRP1-dependent manner in neurons (Huber et al. 2013). Recently, also MIRO1, a tail-anchored membrane adaptor for the microtubule-dependent motor protein kinesin, has been shown to localise to mitochondria and peroxisomes and to contribute to peroxisomal motility and membrane dynamics (Castro et al. 2018; Okumoto et al. 2018).

Patients with mutations in DRP1/DNML1, PEX11β, or MFF have been identified and often present with neurological abnormalities (Waterham et al. 2007; Shamseldin et al. 2012; Ebberink et al. 2012; Costello et al. 2018). Loss of DRP1 or MFF function leads to a block in mitochondrial and peroxisomal fission resulting in highly elongated organelles with impaired dynamics. However, the metabolic functions of both peroxisomes and mitochondria are typically not or only slightly altered, indicating that changes in organelle dynamics and plasticity are the main contributors to the pathophysiology of the disease (Waterham et al. 2007; Shamseldin et al. 2012; Koch et al. 2016; Yoon et al. 2016; Vanstone et al. 2016; Nasca et al. 2016, 2018; Gerber et al. 2017; Ladds et al. 2018).

MFF deficiency displays with developmental delay, peripheral neuropathy, optic atrophy, and Leigh-like encephalopathy (Shamseldin et al. 2012; Koch et al. 2016; Nasca et al. 2018). The mitochondria in MFF-deficient patient fibroblasts show no significant alteration in oxidative phosphorylation or mtDNA (Koch et al. 2016; Nasca et al. 2018). Likewise, loss of MFF did not significantly alter the mitochondrial membrane potential, ATP levels or the redox potential of the mitochondrial matrix in neuronal cells (Lewis et al. 2018). While the majority of studies into MFF-deficiency have focused on mitochondrial dysfunction, the contribution of peroxisomal alterations to the pathophysiology is largely unknown. Similarly to DRP1 and PEX11β patients, it appears that peroxisomal metabolic function is unaltered (Koch et al. 2016; Nasca et al. 2018), with the only known peroxisome dysfunction being hyper-elongation. In this study, we assess the extent to which peroxisomal functions and properties are altered in MFF-deficient cells, giving further insight into the pathophysiological consequences of loss-of-function of MFF. We show that loss of MFF impacts on the distribution of peroxisomal marker proteins and causes the accumulation of pre-peroxisomal membrane structures. Furthermore, peroxisomes in MFF-deficient cells display alterations in peroxisomal redox state and intra-peroxisomal pH as well as altered

peroxisome distribution in neuronal cells. Interestingly, elongated peroxisomes in MFF-deficient cells are not fully static, and their dynamics can be modulated, e.g. through the induction of autophagic processes. The consequences of our findings for the understanding of the pathophysiology of MFF-deficiency and related disorders with impaired peroxisome plasticity are discussed.

3.3 Materials and Methods

3.3.1 Plasmids, Antibodies and siRNAs

The plasmids and antibodies used in this study are detailed in Table 3.1 and Table 3.2, respectively. PEX14 siRNA (GAACUCAAGUCCGAAAUUA) (Lee et al. 2017) and MFF siRNA (GACCAGCAGAUCUUGACCU) (Long et al. 2013) were generated by Eurofins as 21-mer siRNAs with 3' dTdT overhangs. siGENOME Non-Targeting siRNA Control Pool (Dharmacon) and siMAX Non Specific siRNA Control 47% GC (AGGUAGUGUAAUCGCCUUG-TT, Eurofins) were used as controls.

Plasmid	Source
EGFP-SKL	Koch et al. 2005
c-roGFP2	Ivashchenko et al. 2011
mt-roGFP2	Ivashchenko et al. 2011
po-roGFP2	Ivashchenko et al. 2011
c-roGFP2-ORP1	Lismont et al. 2019b
mt-roGFP2-ORP1	Lismont et al. 2019b
po-roGFP2-ORP1	Lismont et al. 2019b
pHRed-Cyto	Godinho and Schrader 2017
pHRed-PO	Godinho and Schrader 2017
HsPEX3(1-44)-EGFP	Fransen et al. 2001

Table 3.1: Plasmids used for the study of peroxisomal alterations in MFF-deficient patient fibroblasts.

Antibody	Type	Dilution		Source
		IMF	WB	
ACOX1	pc rb	-	1:1000	Proteintech (10957-1-AP) or gift from T. Hashimoto, Japan
α-Tubulin	mc ms	-	1:1000	Sigma (T9026)
Catalase	pc ms	1:150	-	Abcam (ab88650)
Catalase	mc ms	-	1:250	Abcam (ab179843)
MAP2	pc gp	1:500	-	Synaptic Systems (188004)
PEX14	pc rb	1:1400	1:4000	D. Crane, Griffith University, Brisbane, Australia
PMP70	pc rb	1:100	-	A. Völkl, University of Heidelberg, Heidelberg, Germany
PMP70	mc ms	1:500	-	Sigma (SAB4200181)
Thiolase	pc rb	-	1:2000	Atlas antibodies (HPA007244)
Alexa Fluor 488	dk α-ms	1:500	-	ThermoFisher Scientific (A21202)
Alexa Fluor 488	dk α-rb	1:500	-	ThermoFisher Scientific (A21206)
Alexa Fluor 568	gt α-gp	1:1000	-	Invitrogen (A-11075)
Alexa Fluor 594	dk α-ms	1:500	-	ThermoFisher Scientific (A21203)
Alexa Fluor 594	dk α-rb	1:500	-	ThermoFisher Scientific (A21207)
HRP IgG	gt α-ms	-	1:10000	Bio-Rad (170-6516)
HRP IgG	gt α-rb	-	1:10000	Bio-Rad (172-1013)
IRDye 800 CW	gt α-rb	-	1:12500	Westburg

Table 3.2: Primary and secondary antibodies used for the study of peroxisomal alterations in MFF-deficient patient fibroblasts. Abbreviations: IMF, immunofluorescence; WB, western blot; pc, polyclonal; mc, monoclonal; ms, mouse; rb, rabbit; gp, guinea pig; gt, goat; dk, donkey; HRP, horseradish peroxidase.

3.3.2 Fibroblast Cell Culture and Transfection

For routine culture and morphological experiments, MFF-deficient patient skin fibroblasts and controls (Shamseldin et al. 2012; Koch et al. 2016) were cultured

in Dulbecco's Modified Eagle Medium (DMEM), high glucose (4.5 g/L) supplemented with 10% FBS, 100 U/mL penicillin and 100 µg/mL streptomycin at 37°C (5% CO_2 and 95% humidity). The patient cells showed the following mutations in the MFF gene: c.C190T:p.Q64* (Shamseldin et al. 2012); c.184dup:p.L62Pfs*13 combined with c.C892T:p.R298* (Koch et al. 2016; patient 1); c.453_454del:p.E153Afs*5 (Koch et al. 2016; patient 2). For assessing peroxisome degradation during starvation, cells were cultured in Hanks' Balanced Salt Solution (HBSS) for the time indicated, and recovered in full DMEM. For assessing peroxisome alterations with microtubule depolymerisation, cells were treated with 10 µM Nocodazole (or 0.07% (v/v) DMSO as a control), for four hours prior to fixation. MFF-deficient (MFF^{Q64*}) and control human fibroblasts were immortalised by introduction of the SV40 large T antigen. Immortalised fibroblasts (HUFs-T) were cultured in α-modified Eagle's medium (MEMα) supplemented with 10% FBS, 2 mM Ultraglutamine 1 (Lonza) and 1× MycoZap antibiotics (Lonza) at 37°C (5% CO_2 and 95% humidity). Transfection of fibroblasts was performed using the Neon Transfection System (Thermo Fisher Scientific) as previously described for roGFP2 constructs (Lismont et al. 2017) and siRNA (Schrader and Schrader 2017).

3.3.3 Neuronal Cell Culture and Transfection

Primary hippocampal neuron cultures were prepared from E18 embryonic C57/BL6J mice using a modified protocol of a previously described method (Banker et al. 1998). As standard, pregnant mice [C57BL/6J, delivered at E11 (Janvier Labs, France)] were housed in a 12/12 h light/dark cycle for 1 week, with *ad libitum* access to food and water. Dissected hippocampi were digested by papain enzyme (100 units per ml, Worthington, Biochemical Corp.) for 20 min at 37°C. A homogenous cell suspension was obtained following trituration and filtration, which was then separated from debris by centrifugation [5 min, 180 × g in BSA solution (7.5%, PAN, BIOTECH)]. Animal protocols were approved by the Ruhr-University Animal Research Board and the State of Baden-Württemberg, Germany. Cells were then seeded into coated 24-well plates (Sarstedt) in Neurobasal medium (Gibco, Life Technologies) supplemented with 1% B27 (Gibco, Life Technologies), 1% horse serum, 1% Glutamax (Gibco, Life Technologies) and penicillin/streptomycin (10,000 units/ml). To maintain the

culture, half of the medium was replaced every 2 or 3 times a week by the same medium but containing 2% B27 and without horse serum. For transfection of siRNA and the plasmid encoding EGFP-SKL, the calcium phosphate precipitation method was used at DIV 7 to 9 as described previously (Sun et al. 2013). After 1 hour of incubation at 37 °C, the transfection mixture was washed out of the culture using pre-warmed HBSS (Gibco, Life technologies).

3.3.4 Immunofluorescence and Immunoblotting

Unless otherwise indicated, immunofluorescence was performed 24 hours post-transfection (48 hours for neuronal cells). Cells grown on glass coverslips were fixed for 20 minutes with 4% paraformaldehyde (PFA) in PBS (pH 7.4), permeabilised with 0.2% Triton X-100 for 10 minutes and blocked with 1% BSA for 10 minutes. For neuronal cells, a combined 1 hour permeabilisation and blocking step was used (1% BSA, 0.2% fish skin gelatin, 0.1% Triton X-100). Blocked cells were incubated with primary and secondary antibodies sequentially in a humid chamber for 1 hour. Cells were washed 3 times with PBS between each individual step. Finally, coverslips were washed with ddH_2O to remove PBS and mounted on glass slides in Mowiol 4-88-containing *n*-propyl gallate as an anti-fading (Bonekamp et al. 2013b).

For detection of protein levels, cells were trypsinised, washed in PBS, and centrifuged at 500×*g* for 3 min. Cell pellets were lysed and equal amounts of protein were separated by SDS-PAGE on 12.5% polyacrylamide gels. Transfer to a nitrocellulose membrane (Amersham Bioscience, Arlington Heights, IL, USA) was performed using a semi-dry apparatus (Trans-Blot SD, Bio-rad) and analysed by immunoblotting with enhanced chemiluminescence reagents (Amersham Bioscience, Arlington Heights, IL, USA).

3.3.5 Microscopy

Cell imaging was performed using an Olympus IX81 microscope with an UPlanSApo 100x/1.40 Oil objective (Olympus Optical. Hamburg, Germany). Filters sets eGFP ET (470/40 Et Bandpass filter, Beamsplitter T495 LPXR and 525/50 ET Bandpass filter [Chroma Technology GmbH, Olching, Germany]), and TxRed HC (562/40 BrightLine HC Beamsplitter HC BS 593, 624/40 BrightLine

HC [Semrock, Rochester, USA]) were used. Images were taken with a CoolSNAP HQ2 CCD camera.

Live-cell imaging of roGFP2 constructs in HUFs-T fibroblasts was performed with an Olympus IX81 microscope equipped with an UPlanSApo 100x/1.40 Oil objective (Olympus Optical, Hamburg, Germany), BP390-410 and BP470-495 bandpass excitation filters, a dichromatic mirror with a cut-off at 505 nm, a BA510-550 barrier (emission) filter, and a CCD-FV2T digital black and white camera.

Confocal images of MFF^{Q64*} fibroblasts to assess peroxisomal tubule localisation with microtubules were obtained using a Zeiss LSM 880 inverted microscope, with Airyscan spatial detector array (ChA-T1 5.7, ChA-T2 6.9) for super-resolution imaging. The Alpha Plan Apochromat 100×/1.46 oil DIC M27 Elyra objective was used, with lasers 561 nm (15% power) and 488 nm (3% power).

Confocal images of the pHRed probe in fibroblasts were obtained using a Zeiss LSM 510 META inverted microscope equipped with a Plan Apochromat 63×/1.4 NA (oil/dic) objective (Carl Zeiss), using Argon excitation 458 nm and DPSS561 excitation 561 nm, with emission collection 600–620 nm. For detection of peroxisomal pHRed (pHRed-PO) the HC PL APO CS2 63×/1.4 Oil objective was used. For live-cell imaging, cells were plated in 3.5 cm diameter glass bottom dishes (Cellview; Greiner Bio-One). MetaMorph 7 (Molecular Devices, USA) was used to adjust for contrast and brightness.

Confocal images of neuronal cells were collected using a Nikon 90i upright microscope with a Plan Apo 100×/1.45 NA oil objective (Nikon). Laser lines Argon 488 nm and He 543 nm 633nm were used. Imaging parameters include: 1024*1024 pixels, fixed 0.08µm pixel size, Z-stacks with 4 ~ 7 µm depth and 0.3 µm scanning thickness.

For transmission electron microscopy, fibroblast monolayers were fixed in 0.5% glutaraldehyde in 0.2 M Pipes buffer, pH 7.2, for 15 min at room temperature. Cells were then scraped from the culture dish and pelleted at 17,000 *g* for 10 min. Following three buffer washes, the cell pellet was fragmented and postfixed for 1 h in 1% osmium tetroxide (reduced with 1.5% wt/vol potassium ferrocyanide) in 0.1 M sodium cacodylate buffer, pH 7.2. Following three 5 minute washes in distilled water, the pellet fragments were dehydrated through an ethanol gradient

and embedded in Durcupan resin (Sigma-Aldrich). 70-nm ultrathin sections were collected on pioloform-coated 100-mesh copper EM grids (Agar Scientific) and contrasted with lead citrate before imaging using a JEOL JEM 1400 transmission electron microscope operated at 120 kV.

3.3.6 Measurement of Peroxisomal Body Size, Tubule Size and Length, and Number

The Metamorph 7 (Molecular Devices, USA) region measurements function was used for analysis of peroxisome size in MFF-deficient fibroblasts, following calibration of distances for the magnification used. For measurement of peroxisome body and tubule width, transmission EM images were used at 80,000- and 100,000-fold magnification. For measurement of peroxisome length, immunofluorescence images were used at 100-fold magnification and the Metamorph 7 segmented line tool was used. For calculation of peroxisomal number in control fibroblasts, an in-house ImageJ (Schneider et al. 2012) macro was used, utilising the Analyze Particles function. For MFF-deficient patient fibroblasts, peroxisome number was counted manually.

3.3.7 Marker Protein Distribution Measurements

To measure the fluorescence intensity of PEX14, PMP70, catalase or GFP-SKL over the length of a single peroxisome, cells were first processed for immunofluorescence. After imaging, the Metamorph 7 (Molecular Devices, USA) linescan function was used to assess the distribution of these marker proteins along the peroxisome, with red and green channels overlaid. A 2 pixel width line was drawn along the centre of the peroxisome from the body, along the tubule for a total length of 5 µm. The fluorescence intensity for each colour channel was measured with 65 nm increments, and data were normalised to a 0-1 scale, with 1 representing the value of the pixel with the maximum intensity of unsaturated images. Only peroxisomes which did not overlap with other peroxisomes were analysed.

3.3.8 Metabolic and Biochemical Analyses

Peroxisomal parameters were determined in cultured skin fibroblasts (Ferdinandusse et al. 2016). Concentrations of VLCFAs and C26:0 lysophosphatidylcholine (C26:0 lysoPC) were measured in cultured cells as

described previously (Dacremont et al. 1995; Ferdinandusse et al. 2016). Peroxisomal β-oxidation of the VLCFA hexacosanoic acid (C26:0) and pristanic acid were measured as described (Wanders et al. 1995). A D3-C22:0 loading test was performed by loading cells for 3 days with deuterated (D3) C22:0 followed by fatty acid analysis with tandem mass spectrometry, essentially as previously described (Kemp et al. 2004) but with D3-C22:0 instead of D3-C24:0. Peroxisomal phytanic acid α-oxidation (Wanders and Van Roermund 1993) and the activity of dihydroxyacetone phosphate acyltransferase (DHAPAT), a key enzyme in peroxisomal ether phospholipid synthesis, were measured as described (Ofman and Wanders 1994). Immunoblot analysis was performed with cell homogenates, which were separated by SDS-PAGE and subsequently transferred onto a nitrocellulose membrane using semidry blotting. For visualisation, the secondary antibody IRDye 800 CW goat anti-rabbit was used with the Odyssey Infrared Imaging System (LI-COR Biosciences, Nebraska, USA).

3.3.9 Measurement of Subcellular Redox Dynamics

The procedures involved in the measurement of subcellular redox levels have been previously described in detail (Lismont et al. 2017). In brief, SV40 large T antigen-transformed human fibroblasts (HUFs-T) were transfected with plasmids coding for GSH/GSSG- (roGFP2) or H_2O_2-sensitive (roGFP2-ORP1) reporter proteins targeted to various subcellular compartments [cytosol (c-), mitochondria (mt-), or peroxisomes (po-)]. One day later, the cells were incubated for 30-60 minutes in phenol red-free culture medium and imaging was performed to visualize both the oxidized (excitation 400 nm, emission 515 nm) and reduced (excitation 480 nm, emission 515 nm) states of roGFP2. During image acquisition, the cells were maintained in a temperature-, humidity-, and CO_2-controlled incubation chamber. For cytosolic measurements, the ROI was selected outside the nucleus. The Cell^M/xcellence software module (Olympus) was used to quantify the relative fluorescence intensities of roGFP2 at 400 and 480 nm excitation, giving a ratiometric response.

3.3.10 Measurement of Peroxisomal pH using pHRed

Peroxisomal pH was measured as previously described (Godinho and Schrader 2017). Briefly, MFF-deficient and control fibroblasts were transfected with plasmids coding for a cytosolic or peroxisomal pH-sensitive red fluorescent protein (pHRed-Cyto and pHRed-PO, respectively) (Godinho and Schrader 2017). Twenty four hours after transfection, cells were imaged using excitation wavelengths of 458 and 561 nm. Prior to image acquisition, a controlled temperature chamber was set-up on the microscope stage at 37°C, as well as an objective warmer. During image acquisition, cells were kept at 37°C and in a HEPES-buffered CO_2-independent medium. For calibration, the cells were incubated in solutions of known pH (containing 5 µM nigericin) in a confocal stage chamber. ImageJ (Schneider et al. 2012) was used to calculate the 561/458 ratiometric response.

3.3.11 Statistical Analysis

A two-tailed, unpaired *t*-test was used to determine statistical differences against the indicated group (*, $p < 0.05$; **, $p < 0.01$; ***, $p < 0.001$). Unless indicated otherwise, boxplots are presented with the bottom and top of each box representing the 25th and 75th percentile values, respectively; the horizontal line inside each box representing the median; and the horizontal lines below and above each box denoting the range. Bar graphs are presented as mean ± SEM. In-text data are presented as mean ± SD. Analysis was performed from at least three independent experiments.

3.4 Results

3.4.1 Morphological characterisation of MFF-deficient peroxisomes

To visualize peroxisomes in different MFF-deficient patient skin fibroblasts (Shamseldin et al. 2012; Koch et al. 2016) under similar conditions, we processed the cells for immunofluorescence microscopy using an antibody against PEX14, a peroxisomal membrane protein. In all three MFF-deficient patient cells, peroxisomes were highly elongated, whereas in controls peroxisomes showed a punctate staining pattern typical for human fibroblasts (Figure 3.1A). Mitochondria in patient cells were also reported to be elongated (Shamseldin et al. 2012; Koch et al. 2016). In many cells peroxisomes were extremely long (> 30 µm); elongation was even more pronounced than in DRP1 patient fibroblasts, which also display tubular peroxisomes and mitochondria (Waterham et al. 2007; Nasca et al. 2016). The elongation of peroxisomes in MFF-deficient fibroblasts has been suggested to be the result of a constant lipid flow from the ER to peroxisomes via membrane contact sites which are mediated by peroxisomal ACBD5 and ER-resident VAPB (Costello et al. 2017b). As peroxisomes cannot divide due to the loss of functional MFF, lipid transfer from the ER results in a pronounced growth/elongation of the peroxisomal membrane. Furthermore, re-introduction of MFF has been shown to restore the normal, punctate peroxisomal phenotype in MFF-deficient fibroblasts (Costello et al. 2017b).

Occasionally, peroxisomes in patient fibroblasts appeared to have a constricted, ‘beads-on-a-string’ phenotype (Figure 3.1A, magnifications). Such a phenotype is seen with DRP1 depletion, as peroxisomal constriction can occur independently of DRP1, but fission cannot (Koch et al. 2004). How peroxisomal constriction is mediated is still unclear. A constricted, ‘beads-on-a-string’-like peroxisome morphology in MFF-deficient cells would suggest that peroxisomal constriction can also occur independently of MFF (Ribeiro et al. 2012). However, MFF is also suggested to play a role in the constriction of the peroxisomal membrane, as it localises to peroxisomal constriction sites (Itoyama et al. 2013; Soliman et al. 2018). To confirm constricted peroxisome morphology in MFF-deficient cells, we performed electron microscopy (Figure 3.1B). In contrast to immunofluorescence, constrictions of elongated peroxisomes were not observed in ultrastructural studies (Figure 3.1B). Interestingly, EM revealed the presence

of spherical peroxisome bodies, with a single, smaller tubule protruding from the body (Figure 3.1B). We assume that the “constricted” appearance of peroxisomes in immunofluorescence is likely due to instability of the extremely long, delicate membrane structures during fixation with para-formaldehyde, highlighting the importance of ultrastructural studies to validate light microscopy observations. Ultrastructural studies (Figure 3.1B) and immunofluorescence microscopy (Figure 3.1C) show that the peroxisomal membrane tubules are frequently aligned along microtubules, which may contribute to tubule stability and maintenance.

Measurement of peroxisomes in EM micrographs revealed that peroxisome bodies are significantly larger than peroxisomal tubules (mean width, body: 141 ± 37 nm, tubule: 81 ± 22 nm) (Figure 3.1D). The measured body width is consistent with that of spherical peroxisomes in human fibroblasts from healthy individuals typically being reported to be between 50-200 nm in width (Arias et al. 1985; Galiani et al. 2016). Peroxisome length was also quantified based on immunofluorescence data, with a wide range of lengths being present, from smaller, rod shaped peroxisomes (> 3 µm) up to very highly elongated tubules (> 30 µm) (mean length, 8.73 ± 9.2 µm) (Figure 3.1E). As expected with a defect in division, the peroxisome number was reduced in MFF-deficient fibroblasts in contrast to controls (mean number, control fibroblasts: 244 ± 116, dMFF: 34 ± 25) (Figure 3.1F). Overall, we reveal that peroxisomes in MFF-deficient patient fibroblasts are fewer and consist of two continuous membrane domains: a spherical peroxisome body with typical peroxisome size, and a thin, highly elongated tubular structure protruding from this body.

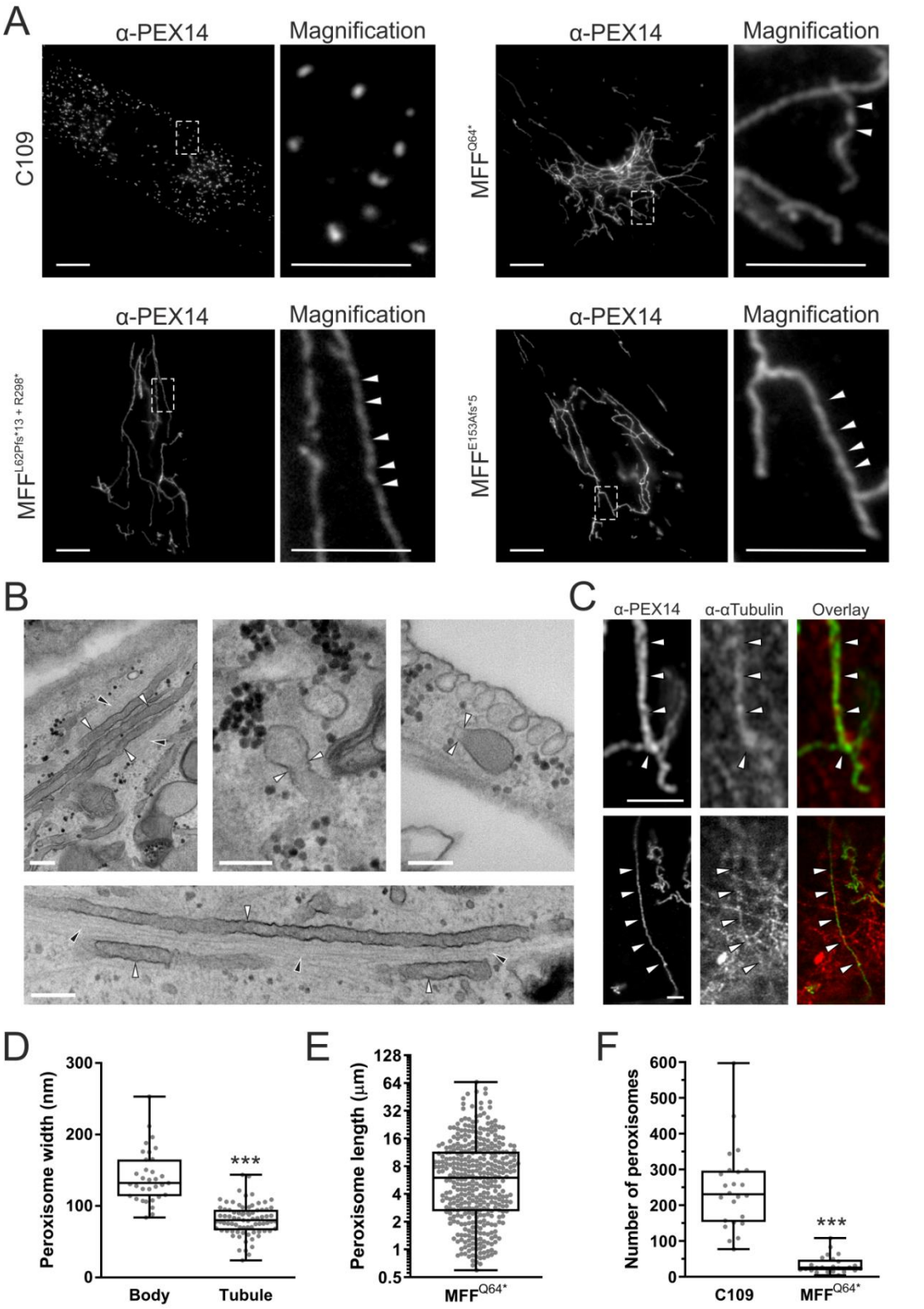

Figure 3.1. Morphological characteristics of peroxisomes in MFF-deficient patient fibroblasts are altered. (**A**) Control fibroblasts (C109) and MFF-deficient patient fibroblasts [mutations Q64* (Shamseldin et al. 2012), L62Pfs*13+R298* (Koch et al. 2016) and E153Afs*5 (Koch et al. 2016)] were processed for immunofluorescence microscopy using antibodies directed to PEX14, a peroxisomal membrane marker. Higher magnification of boxed region is shown. Arrowheads highlight potential membrane constrictions. Scale bars, 10 µm; magnification, 5 µm. (**B**) Electron micrographs of peroxisomes in MFF-deficient cells (MFF^{Q64*}). White arrowheads highlight peroxisomal membrane tubules, black arrowheads indicate microtubules. Scale

bars, 0.2 µm. (**C**) Confocal (Airyscan) images of peroxisomal membrane tubules (anti-PEX14) in MFF^{Q64*} cells co-stained with anti-α-tubulin. White arrowheads indicated co-localisation of peroxisomes and microtubules. Scale bars, 3 µm. (**D**) Measurement of peroxisomal width (nm) of bodies and tubules based on electron micrographs of MFF^{Q64*} fibroblasts [n = 33 (bodies), 79 (tubules)]. (**E**) Measurement of peroxisomal length (µm) from immunofluorescence images of MFF^{Q64*} patient fibroblasts (n = 392). (**F**) Quantification of peroxisome number based on immunofluorescence images of control (C109) and MFF^{Q64*} fibroblasts (n = 24). Data are from at least 3 independent experiments. ***, P < 0.001; two-tailed, unpaired t test.

3.4.2 MFF deficiency does not alter standard biochemical parameters associated with peroxisomal dysfunction

Several biochemical parameters were studied to investigate peroxisomal function in cultured fibroblasts (Table 3.3). Peroxisomal α- and β-oxidation activities were measured with different radiolabelled substrates, i.e. [^{14}C]-phytanic acid, pristanic acid and cerotic acid (C26:0). In addition, very long-chain fatty acid (VLCFA) metabolism was studied with a three day D3-C22 loading test, and total VLCFA levels and C26-lysophosphatidylcholine levels were determined in cell pellets (Ferdinandusse et al. 2016). No notable abnormalities were found in all three MFF-deficient cell lines providing no indication of a disturbed metabolism of VLCFAs or branched-chain fatty acids in peroxisomes. α-oxidation values were slightly higher than the reference range, but this does not indicate any dysfunction. The activity of dihydroxyacetone phosphate acyltransferase (DHAPAT), the first enzyme of the plasmalogen biosynthesis pathway located in peroxisomes, was within reference range. The intra-peroxisomal processing of the peroxisomal β-oxidation enzymes acyl-CoA oxidase 1 (ACOX1) and 3-ketoacyl-CoA thiolase was not altered, suggesting normal peroxisomal matrix protein import and processing activity in contrast to fibroblasts from a patient with a peroxisomal biogenesis disorder (Figure 3.2). This is in line with metabolic and biochemical analyses of plasma from different MFF patients (Shamseldin et al. 2012; Koch et al. 2016; Nasca et al. 2018). We can confirm from these studies that MFF deficiency does not cause alterations to overall peroxisomal biochemical function. This is also in line with reports from other disorders affecting the dynamics and plasticity of peroxisomes (e.g. DRP1- or PEX11β-deficiency) (Waterham et al. 2007; Ebberink et al. 2012).

	MFF$^{L62Pfs*13+R298*}$	MFF^{E153Afs*5}	MFF^{Q64*}	Reference range
VLCFAs (µmol/g protein)				
C26:0	0.30	0.33	0.29	0.16-0.41
C26/C22 ratio	0.06	0.07	0.07	0.03-0.1
C26-lysoPC (pmol/mg protein)	12.3	9.2	7.0	2-14
Alpha-oxidation activity (pmol/(hour.mg protein))	135	104	n.d.	28-95
Beta-oxidation activity (pmol/(hour.mg protein))				
C26:0	2109	1505	n.d.	800-2040
Pristanic acid	1072	1099	n.d.	790-1072
D3C22 loading test (µmol/g protein)				
D3C26 (chain elongation)	0.29	0.3	0.26	0.16-0.66
D3C16/D3C22 ratio (beta-oxidation)	1.25	1.74	2.27	0.64-2.13
DHAPAT activity (nmol/(2hour.mg protein))	9.2	7.1	6.6	5.9-15.5

Table 3.3: Biochemical parameters associated with peroxisomal dysfunction are normal in MFF-deficient patient fibroblasts. Peroxisomal parameters determined in three MFF-deficient patient fibroblast cell lines MFF$^{L62Pfs*13+R298*}$ (Koch et al. 2016), MFF^{E153Afs*5} (Koch et al. 2016), and MFF^{Q64*} (Shamseldin et al. 2012). Very long-chain fatty acid (VLCFA) levels, C26-lysophosphatidylcholine (C26-lysoPC), α- and β-oxidation activity, VLCFA metabolism (D3C22 loading test) and dihydroxyacetone phosphate acyltransferase (DHAPAT) activity were measured. A reference range of control fibroblasts from healthy individuals is shown for comparison. Abbreviations: n.d., not determined; VLCFA, very long-chain fatty acid; C26-lysoPC, C26-lysophosphatdylcholine; DHAPAT, dihydroxyacetone phosphate acyltransferase.

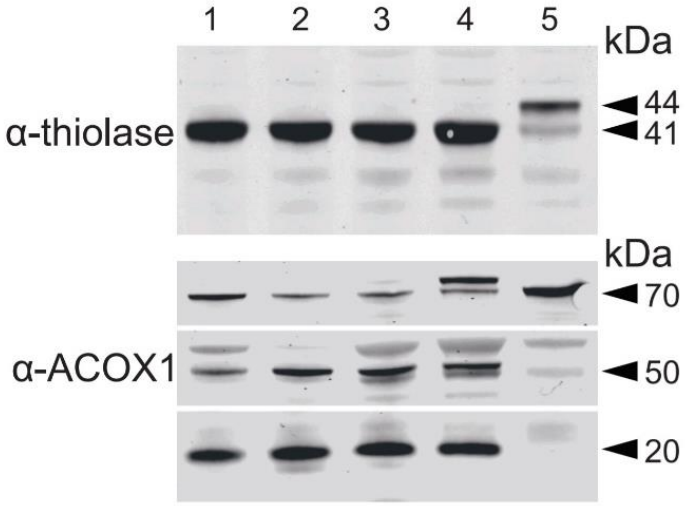

Figure 3.2: Immunoblot analysis of fibroblast homogenates from MFF-deficient patients. Antibodies were directed against peroxisomal 3-ketoacyl-CoA thiolase (upper panel) or peroxisomal acyl-CoA oxidase 1 (ACOX1; lower panel). Lanes 1-3, MFF-deficient patient fibroblasts MFF^{Q64*} (Shamseldin et al. 2012), $MFF^{L62Pfs*13+R298*}$ (Koch et al. 2016) and $MFF^{E153Afs*5}$ (Koch et al. 2016), respectively. Lane 4: control subject, Lane 5: fibroblasts of a patient with Zellweger Spectrum Disorder (ZSD). Results show normal proteolytic processing of 3-ketoacyl-CoA thiolase (40-kDa) and ACOX1 (50- and 20-kDa) in the MFF-deficient cell lines, whereas in the ZSD line the unprocessed bands of 3-ketoacyl-CoA thiolase (44-kDa) and ACOX1 (70-kDa) are present. Note that the protein band above the 70 kDa band of ACOX1 is non-specific.

3.4.3 Protein import into MFF-deficient peroxisomes is impaired in tubular extensions

As globular peroxisomal bodies were visible in ultrastructural studies but surprisingly less visible in immunofluorescence studies with anti-PEX14, which labelled predominantly tubular structures (Figure 3.1A, B), we performed co-localisation studies with anti-catalase, a prominent peroxisomal marker enzyme in the peroxisomal matrix (Figure 3.3A). In contrast to PEX14, endogenous catalase was found to localise primarily to the spherical peroxisome bodies, with weaker fluorescence intensity along the peroxisomal tubules (Figure 3.3A). Analysis of fluorescence intensity along single peroxisomes of both PEX14 and catalase confirmed PEX14 fluorescence primarily along tubules with some localisation in bodies, whereas catalase fluorescence was primarily detected in the peroxisomal body, with reduced intensity along the tubule (Figure 3.3A). Peroxisomes import matrix proteins from the cytosol via dedicated import machinery at the peroxisomal membrane (Francisco et al. 2017). Matrix proteins such as catalase are imported into peroxisomes via a C-terminal peroxisomal targeting signal (PTS1). These steady-state observations imply that catalase is

mainly imported into the spherical bodies, suggesting that those represent mature, import-competent structures. To test this hypothesis, we expressed a GFP-fusion protein with a C-terminal PTS1 signal SKL (GFP-SKL) in MFF-deficient cells. Cells were processed for immunofluorescence after 24 hours and labelled with anti-PEX14 antibodies (Figure 3.3B). Similar to endogenous catalase, exogenously expressed GFP-SKL localised primarily to peroxisomal bodies, with less presence in the peroxisomal tubules (Figure 3.3B). This was confirmed by analysis of fluorescence intensity (Figure 3.3B). Immunofluorescence microscopy with the peroxisomal membrane markers PMP70 and PEX14 revealed co-localisation of both membrane proteins at membrane tubules (Figure 3.3C). PMP70 also localised to the spherical bodies, where PEX14 is less prominent (Figure 3.3C). These findings indicate that the spherical bodies represent mature, import-competent peroxisomes, whereas tubular extensions comprise a pre-peroxisomal membrane compartment which either has not yet fully acquired import competence for matrix proteins, or lacks the capability to retain them.

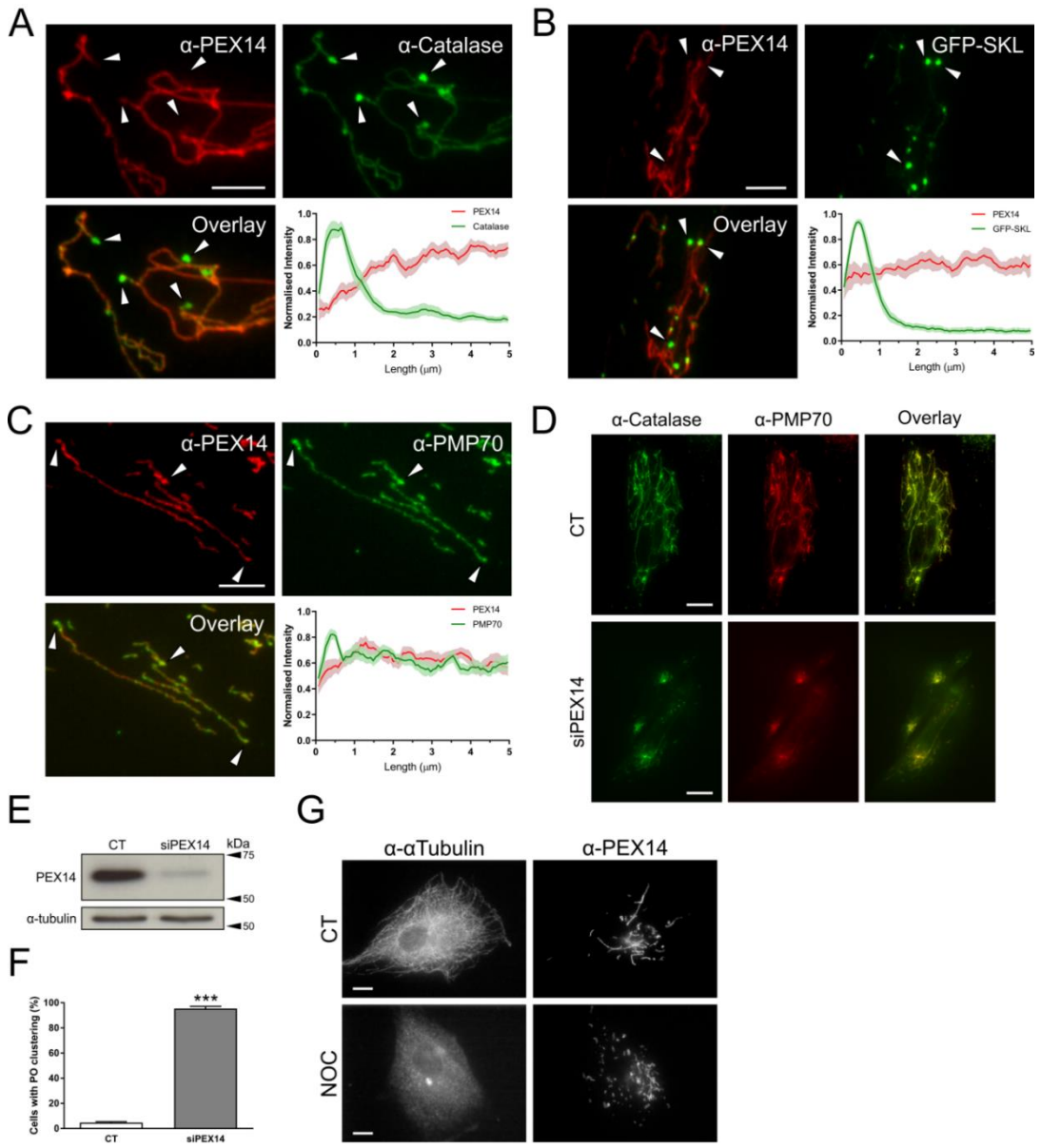

Figure 3.3: Altered marker protein distribution in MFF-deficient patient fibroblasts (MFF^{Q64*}). (**A**) Patient fibroblasts were processed for immunofluorescence microscopy using antibodies against peroxisomal membrane marker PEX14 and matrix marker catalase, and fluorescence intensity measured along 5 um of peroxisome, starting at peroxisome bodies (arrowheads) normalised to the maximum intensity. Shaded area in graphs represents the standard error of the mean (line) (n = 12). Arrowheads highlight peroxisomal bodies. Scale bar, 5 µm. (**B**) Patient fibroblasts were transfected with a plasmid encoding EGFP-SKL and processed for immunofluorescence microscopy using an antibody against PEX14. Quantification was performed as in A, B (n = 12). Arrowheads highlight peroxisomal bodies. Scale bar, 5 µm. (**C**) As in (A), using antibodies against membrane markers PEX14 and PMP70. (**D**) MFF^{Q64*} fibroblasts were transfected with control (CT) or PEX14 siRNA (siPEX14), and processed for immunofluorescence microscopy after 48 hours using antibodies against catalase and PMP70. Scale bars, 10 µm. (**E**) Immunoblotting of control (CT) or PEX14 siRNA (siPEX14) transfected patient fibroblasts, using antibodies against PEX14 and α-tubulin (loading control). (**F**) Quantification of peroxisomal clustering in MFF-deficient fibroblasts either transfected with control (CT) or PEX14 siRNA (siPEX14) (n = 150). Data are from at least 3 independent experiments. ***, P < 0.001; two-tailed, unpaired t test. (**G**) MFF^{Q64*} patient fibroblasts were treated with 0.07% DMSO (CT), or 10 µM nocodazole (NOC) for four hours prior to processing for immunofluorescence microscopy using antibodies against α-tubulin and PEX14. Scale bars, 10 µm.

3.4.4 A role of PEX14 in maintaining peroxisomal tubule stability

As PEX14 is part of the matrix protein import machinery (Brown and Baker 2008), its predominant localisation to the peroxisomal membrane tubules (rather than the import-competent spherical bodies) is unexpected. However, additional functions for PEX14 have been suggested. Peroxisomes interact with and move along microtubules (Thiemann et al. 2000; Schrader et al. 2003; Castro et al. 2018). The N-terminal domain of PEX14 (1-78) has previously been shown to bind tubulin (Bharti et al. 2011; Theiss et al. 2012). Although PEX14 is not essential for microtubule-dependent peroxisomal motility (Castro et al. 2018), it may function as a peroxisomal microtubule docking factor. Indeed, in ultrastructural and confocal studies microtubules were frequently observed in close association with the entire length of peroxisomal tubules in MFF patient cells (Figure 3.1B, C). Furthermore, in a previous study, we showed that highly elongated peroxisomal tubules in fibroblasts are associated with microtubules, and that tubule elongation is reduced in PEX14-deficient cells (Castro et al. 2018). Based on these observations, we hypothesised that PEX14 may be required for the stabilisation of highly elongated peroxisomal tubules. To test this, we depleted PEX14 by siRNA-mediated knock down in MFF-deficient cells (Figure 3.3D-F). Peroxisomal tubules in these cells are typically stretched out in the cell, allowing for easy visualisation. However, when PEX14 was knocked down, peroxisomes lost their tubular morphology and appeared clustered or fragmented (Figure 3.3D) (cells with clustered/fragmented morphology: control siRNA: 4.7 ± 1.2%, PEX14 siRNA: 95.3 ± 3.1%) (Figure 3.3F). The peculiar peroxisome morphology was specific for silencing of PEX14, and was not observed after silencing of PEX11β or ACBD5 in MFF-deficient cells (Costello et al. 2017b). Clustering and fragmentation of elongated peroxisomes in MFF-deficient cells was also observed after depolymerisation of microtubules with nocodazole (Figure 3.3G). These observations suggest a role for PEX14 in facilitating and stabilising peroxisomal membrane extensions by linking the peroxisomal membrane to microtubules. This may explain why PEX14 is predominantly localising to the highly elongated peroxisomal membranes in MFF patient cells.

3.4.5 Peroxisomal redox state and pH levels are altered in MFF-deficient fibroblasts

The metabolic parameters of peroxisomes in MFF-deficient cells were normal, in particular their different functions in lipid metabolism (Table 3.3). As peroxisomes play a role in cellular H_2O_2 metabolism and redox homeostasis, we also investigated these parameters (Figure 3.4). Firstly, we assessed the glutathione disulphide (GSSG) to glutathione (GSH) ratio, a marker of oxidative balance. Therefore, MFF-deficient SV40 large T antigen-transformed human fibroblasts (HUFs-T) were transfected with a plasmid encoding cytosolic, mitochondrial or peroxisome-targeted roGFP2 (Figure 3.4A). RoGFP2 is a highly responsive, pH-independent sensor for the glutathione redox couple, and oxidation causes a shift of its excitation maximum from 488 nm to 405 nm (Ivashchenko et al. 2011; Lismont et al. 2017). Analyses of the 400/480 ratiometric responses of peroxisome-targeted roGFP2 revealed that the intra-peroxisomal pool of glutathione is less oxidized in the MFF-deficient fibroblasts than in the control cells (Figure 3.4B). In contrast, no alterations in the glutathione redox state could be detected in the cytosol or the mitochondrial matrix. To monitor changes in hydrogen peroxide homeostasis, MFF-deficient HUFs-T and controls were transfected with plasmids coding for cytosolic, mitochondrial, or peroxisome-targeted roGFP2-ORP1, a H_2O_2-responsive variant of roGFP2 (Figure 3.4C) (Lismont et al. 2019b). No changes in oxidation state were observed in the cytosol and mitochondria (Figure 3.4D). However, for peroxisomes, a decreased 400/480 nm ratiometric response was seen (Figure 3.4D), indicating reduced levels of H_2O_2 inside peroxisomes in MFF-deficient cells.

In addition, we used peroxisome-targeted pHRed (pHRed-PO), another ratiometric probe, to assess peroxisomal pH in MFF-deficient patient fibroblasts (Tantama et al. 2011; Godinho and Schrader 2017). Importantly, this sensor is insensitive to changes in H_2O_2 levels (Tantama et al. 2011). The pHRed-PO probe successfully targets to peroxisomes in control and MFF-deficient fibroblasts (Figure 3.4E). It mainly distributes to the import-competent spherical peroxisomal bodies, but also to the membrane tubules (Figure 3.4E). Following calibration of the pHRed probe (Figure 3.4F), the intra-peroxisomal pH can be calculated based on the 458/561 nm ratiometric response. Interestingly, intra-peroxisomal pH in MFF-deficient fibroblasts was found to be more alkaline than

in control fibroblasts (Figure 3.4G) (mean peroxisomal pH, control: 7.24 ± 0.30, patient fibroblasts: 8.00 ± 0.29).

Overall, these findings point towards alterations in the peroxisomal redox environment. Specifically, we observed a decrease in the GSSG/GSH ratio and H_2O_2 levels in MFF-deficient fibroblasts. In addition, we have shown that absence of MFF results in a more alkaline intra-peroxisomal pH. This suggests that MFF-deficiency may compromise normal peroxisomal redox regulation.

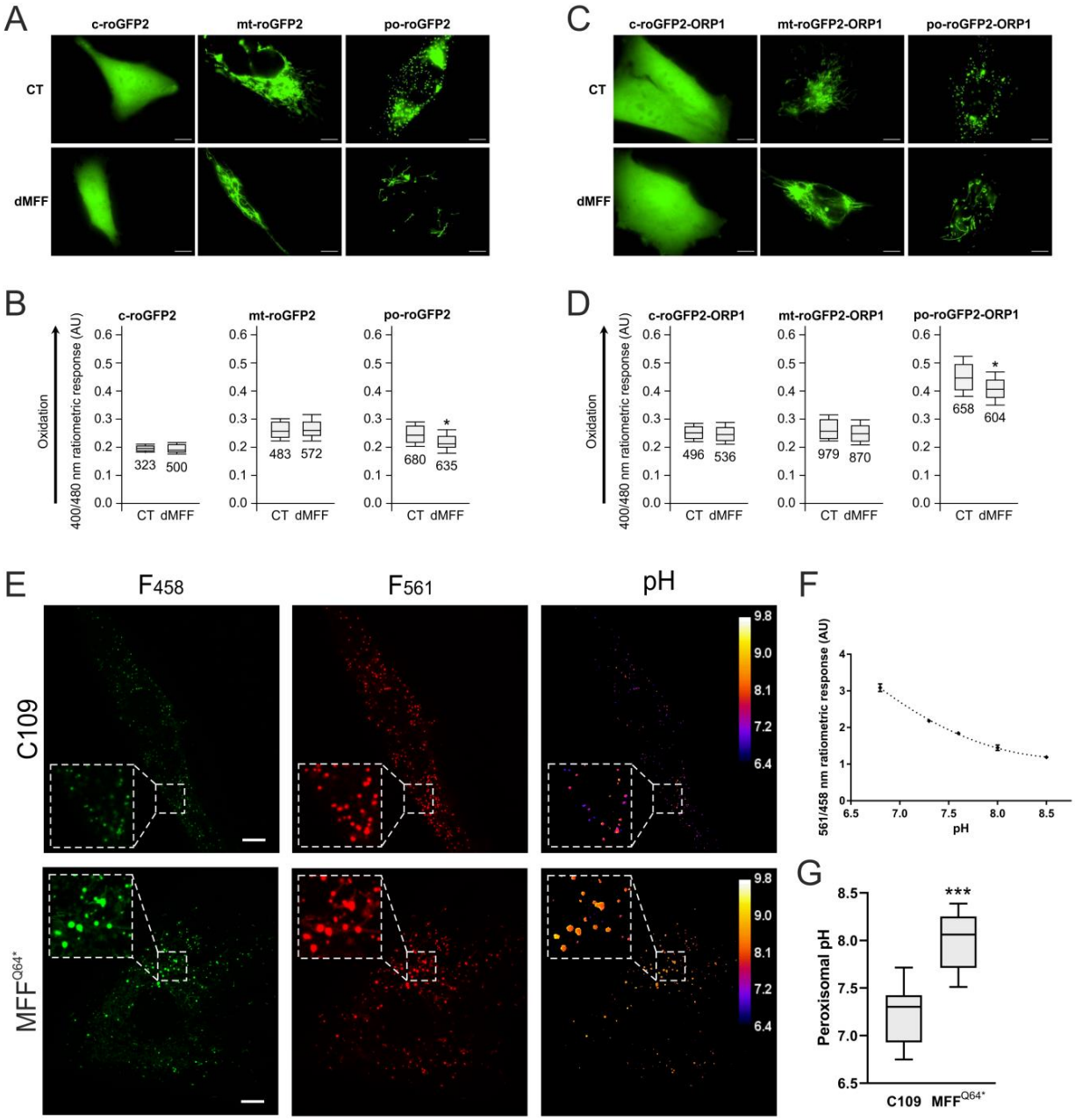

Figure 3.4: Peroxisomal redox state and pH levels are altered in MFF-deficient fibroblasts. Control (CT) or MFF-deficient (dMFF) SV40 large T antigen-transformed human fibroblasts (HUFs-T) were transfected with a plasmid encoding cytosolic (c-), mitochondrial (mt-) or peroxisomal (po-) roGFP2 (**A, B**) or roGFP2-ORP1 (**C, D**). (**A**) Distribution patterns of the respective roGFP2 proteins. (**B**) Box plot representations of the 400/480 nm fluorescence response ratios of the respective roGFP2 proteins. (**C**) Distribution patterns of the respective roGFP2-ORP1 proteins. (**D**) Box plot representations of the 400/480 nm fluorescence response ratios of the respective roGFP2 proteins. The bottom and top of each box represent the 25th and 75th percentile values, respectively; the horizontal line inside each box represents the median; and the horizontal lines below and above each box denote the mean minus and plus one standard deviation, respectively. The total number of measurements (two independent experiments; minimum 15 individual measurements in at least 20 randomly chosen cells) is indicated below each box plot. The data from the dMFF cell line were statistically compared with those from the CT cell line (**, $p < 0.01$). (**E**) Distribution patterns of pHRed-PO in control (C109) and MFF-deficient patient fibroblasts (MFF^{Q64*}) at excitation wavelengths of 458 and 561 nm, along with digital visualisation of individual peroxisomal pH levels. Higher magnification views of boxed regions are indicated. (**F**) Calibration of the pHRed probe using cytosolic pHRed. The 458/561 ratiometric response is given at each pH level. AU, arbitrary units. (**G**) Quantification of peroxisomal pH in control (C109) and MFF^{Q64*} cells, converting the ratiometric response to pH using the calibration curve (n =20). Scale bars, 10 µm. Data are from at least 2-3 independent experiments. *, $P < 0.05$; ***, $P < 0.001$; two-tailed, unpaired t test.

3.4.6 MFF knockdown in neuronal cells increases peroxisomal clustering

Peroxisomal disorders are typically associated with neurological alterations (Berger et al. 2016), including disorders with a deficiency in peroxisomal dynamics and plasticity such as PEX11β, DRP1 and MFF (Waterham et al. 2007; Shamseldin et al. 2012; Ebberink et al. 2012; Koch et al. 2016; Sheffer et al. 2016; Nasca et al. 2018). To investigate morphological alterations of peroxisomes after MFF depletion in neuronal cells, primary mouse hippocampal neurons were transfected with a plasmid encoding EGFP-SKL and MFF-specific or control siRNA. After 48 hours, cells were processed for immunofluorescence using anti-MAP2 as a neuronal dendrite marker (Figure 3.5). With control siRNA, peroxisomes in neuronal cells were typically punctate, with an even distribution in the soma (Figure 3.5, CT). In contrast, peroxisomes in MFF-depleted cells appeared clustered and enlarged with a brighter fluorescence, losing the even distribution throughout the cell (Figure 3.5, siMFF) (approx. 77% of MFF-siRNA-treated cells showed this altered phenotype). In contrast to loss of MFF in fibroblasts, peroxisomes in neuronal cells did not hyper-elongate, but form smaller, rod-shaped structures in addition to peroxisomal aggregates. It is possible that an altered peroxisomal phenotype in neurons may contribute to the neurological abnormalities observed in MFF-deficiency.

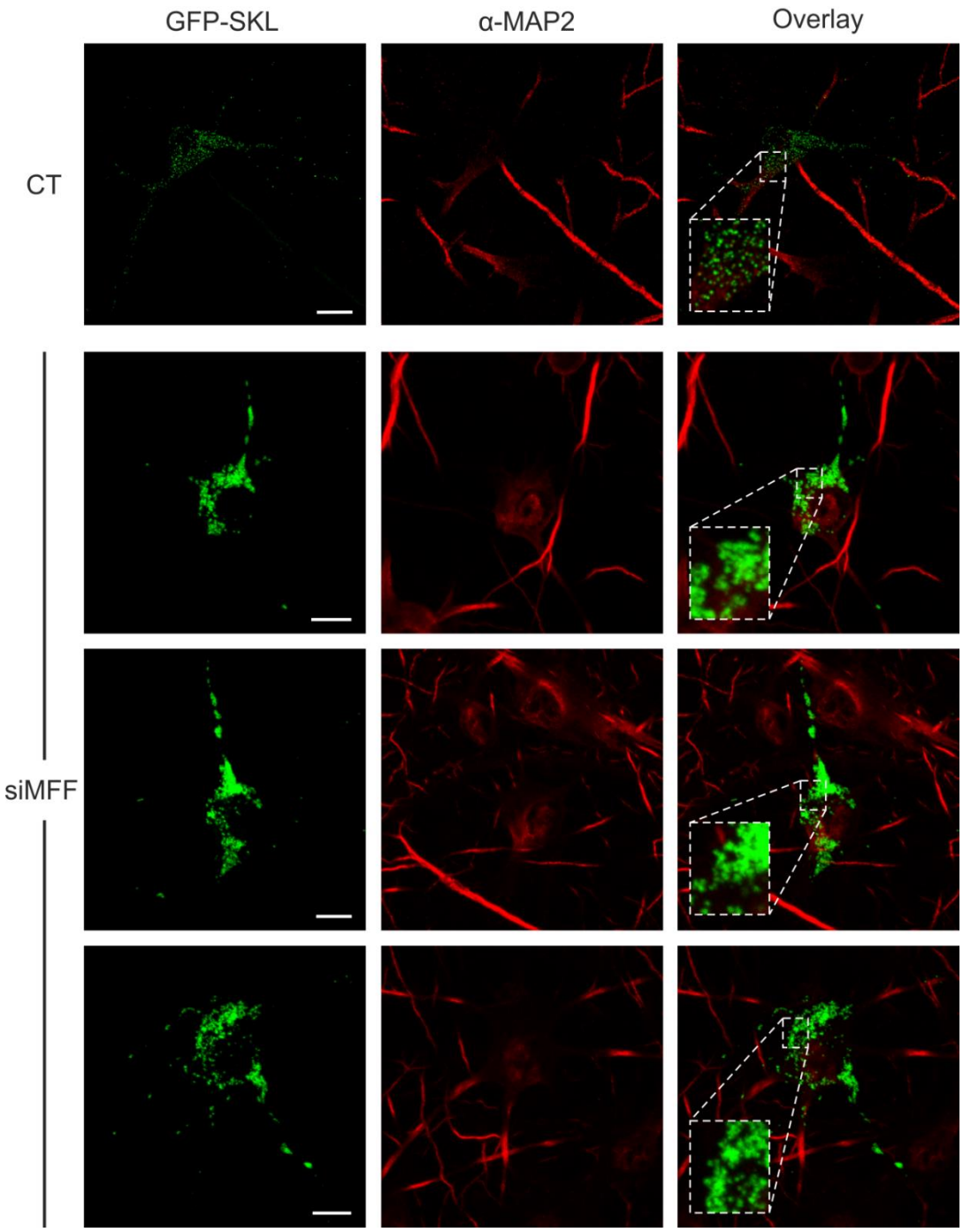

Figure 3.5: Alterations to peroxisomal morphology in MFF-depleted neuronal cells. (**A**) Primary mouse hippocampal neurons were transfected with plasmids encoding EGFP-SKL and MFF-specific (siMFF) or control (CT) siRNAs. After 48 hours, cells were processed for immunofluorescence using anti-MAP2 as a neuronal dendrite marker. Representative images are shown. Note that peroxisomes in MFF-depleted cells appear clustered and enlarged with a brighter fluorescence, losing their uniform distribution when compared to controls (see inset images). All images (CT, siMFF) were captured with the same exposure time. Scale bars, 10 µm.

3.4.7 Highly elongated peroxisomes in MFF-deficient fibroblasts can be degraded by autophagic processes

Autophagic processes are important for the maintenance of cellular homeostasis and the integrity of organelles (Anding and Baehrecke 2017). Peroxisome homeostasis is achieved via a tightly regulated interplay between peroxisome biogenesis and degradation via selective autophagy (pexophagy) (Eberhart and Kovacs 2018). It is still unclear if highly elongated peroxisomes are spared from pexophagy, e.g. due to physical limitations, as the elongated peroxisomes may not fit into the autophagosome. Such a scenario would prevent degradation of peroxisomes and could have pathophysiological consequences.

To examine if highly elongated peroxisomes in MFF-deficient fibroblasts can be degraded by autophagic processes, we first induced pexophagy by the expression of a fragment of peroxisomal biogenesis protein PEX3. Expression of the first 44 amino acids of the peroxin PEX3, which can insert into the peroxisome membrane, was observed to cause complete removal of peroxisomes (Soukupova et al. 1999). When expressing *Hs*PEX3(1-44)-EGFP in control fibroblasts (Figure 3.6A, B), peroxisomes were greatly reduced in number, with many GFP expressing cells showing almost complete loss of PEX14 labelling (Figure 3.6A, C109). As reported earlier, loss of peroxisomes resulted in mistargeting of HsPEX3(1-44)-EGFP to the mitochondria (Soukupova et al. 1999). Interestingly, in MFF-deficient fibroblasts, expression of *Hs*PEX3(1-44)-EGFP also caused a marked reduction of peroxisomes (Figure 3.6A, middle panel, B) or complete loss of PEX14 labelling (Figure 3.6A, lower panel, B). Increased mitochondrial mistargeting of *Hs*PEX3(1-44)-EGFP was observed with increased loss of peroxisomes (Figure 3.6A).

To examine peroxisome degradation under more physiological conditions, we applied nutrient deprivation. Limiting amino acids in the growth media of cells has been previously shown to induce removal of peroxisomes (Sargent et al. 2016). For assessing peroxisome degradation, controls and MFF-deficient fibroblasts were cultured in Hanks' Balanced Salt Solution (HBSS), which lacks amino acids. After 0, 24 and 48 hours, cells were processed for immunofluorescence using anti-PEX14 as a peroxisomal marker (Figure 3.6C). In control cells, we observed a marked decrease in spherical peroxisomes, with often only a few organelles

remaining after 48 hours in HBSS (Figure 3.6C, D). As with *Hs*PEX3(1-44)-EGFP, we also observed a decrease in peroxisomes in nutrient-deprived MFF-deficient cells, which was accompanied by a significant reduction in peroxisomal length (mean peroxisomal length, 0 hours HBSS: 6.08 ± 4.90 µm, 48 hours HBSS: 1.55 ± 1.43 µm) (Figure 3.6C, E). The reduction in peroxisomes was accompanied by a reduction in peroxisomal marker proteins (Figure 3.6F). Peroxisomes and protein levels recovered in control and MFF-deficient cells after switching to complete culture medium for 24 hours (Figure 3.6C-F). Interestingly, the switch to complete growth medium resulted in the recovery of elongated peroxisomes (mean peroxisomal length, 24 hours recovery: 3.84 ± 3.40 µm) (Figure 3.6E), indicating that peroxisomes in MFF-deficient fibroblasts are still dynamic under certain conditions. Overall, these data show that highly elongated peroxisomes in MFF-deficient cells are not spared from autophagic processes and can be degraded similar to controls. It is thus unlikely that impaired peroxisome degradation contributes to the pathology of MFF-deficiency.

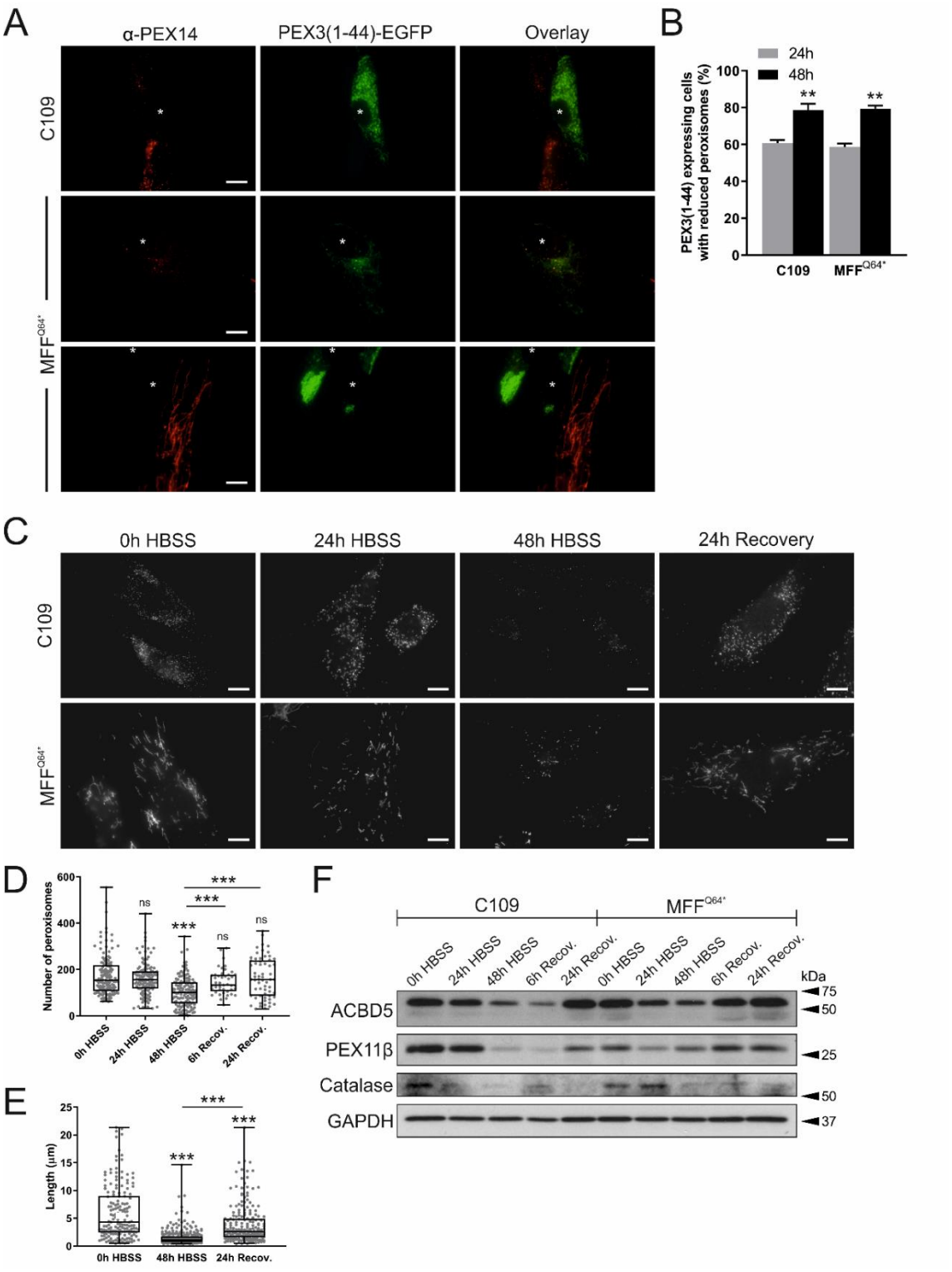

Figure 3.6: Degradation of peroxisomes in MFF-deficient patient fibroblasts. (**A**) Human control (C109) or MFF-deficient (MFF^{Q64*}) fibroblasts were transfected with a plasmid coding for *Hs*PEX3(1-44)-EGFP to induce peroxisome degradation and processed for immunofluorescence after 24 and 48 hours using antibodies against PEX14. Note the almost complete loss of PEX14, and mistargeting of *Hs*PEX3(1-44)-EGFP to mitochondria when peroxisomes are lost (Soukupova et al. 1999). Asterisks indicate *Hs*PEX3(1-44)-EGFP expressing cells. Scale bars, 10 µm. (**B**) Quantification of HsPEX3(1-44)-EGFP expressing cells (control fibroblasts, CON; MFF-deficient, MFF^{Q64*}) showing reduced peroxisomes after 24 and 48 hours (n = 150). (**C**) Human control (C109) and MFF-deficient fibroblasts (MFF^{Q64*}) were incubated in Hanks' Balanced Salt Solution (HBSS) to induce peroxisome degradation and processed for immunofluorescence after

0, 24 and 48 hours and after 24 hours recovery in complete culture medium using antibodies against PEX14. Scale bars, 10 µm. (**D**) Quantification of the number of peroxisomes in C109 control fibroblasts following incubation in HBSS and recovery in complete culture medium (see (C)) [n = 62 (24h Recovery) to 139 (48h HBSS)]. (**E**) Quantification of peroxisome length in MFF^{Q64*} fibroblasts following 0, 48 hours of HBSS treatment, and after 24 hours of recovery in complete culture medium [n = 167 (0h HBSS) to 297 (48h HBSS)]. Data are from at least 3 independent experiments. ***, P < 0.001; ns, not significant; two-tailed, unpaired t test. (**F**) Immunoblot of cell lysates from control (C109) and MFF-deficient fibroblasts (MFF^{Q64*}) which were incubated in HBSS for 0, 24, and 48 hours, and after 6 and 24 hours of recovery in complete culture medium. Antibodies against the peroxisomal membrane proteins ACBD5, PEX11β and catalase were applied. Anti-GAPDH was used as a loading control. Equal amounts of protein were loaded. Molecular mass markers (kDa) are indicated on the right.

3.5 Discussion

Whereas dysfunctional peroxisome metabolism and associated diseases are generally well studied, the consequences and pathophysiology caused by specific disruption to peroxisome dynamics and plasticity are less clear. Mutations in DRP1, MFF or PEX11β have been linked to defects in the membrane dynamics and division of peroxisomes rather than to loss of metabolic functions (Waterham et al. 2007; Shamseldin et al. 2012; Ebberink et al. 2012; Koch et al. 2016; Taylor et al. 2017; Nasca et al. 2018). This is in contrast to the classical peroxisome biogenesis disorders (e.g. Zellweger spectrum disorders) or single enzyme deficiencies and can complicate diagnosis through metabolic biomarkers. Despite considerable progress in the field, the precise molecular functions of several of the proteins regulating peroxisomal plasticity remain to be determined as well as the contribution of impaired peroxisomal dynamics to the pathophysiology of the above disorders. In line with this, depletion of PEX11β in epidermal cells was recently reported to result in abnormal mitosis and organelle inheritance, thus affecting cell fate decisions (Asare et al. 2017). As DRP1 and MFF also localise to mitochondria, and as loss of DRP1 or MFF function also inhibits mitochondrial division, focus has so far mainly been on mitochondrial properties under those conditions. Here, we assessed the extent to which peroxisomal functions and properties are altered in MFF-deficient cells.

There are currently six patients with MFF-deficiency identified, with various mutations in the MFF protein shown; c.C190T:p.Q64* (Shamseldin et al. 2012); c.184dup:p.L62Pfs*13 combined with c.C892T:p.R298* (Koch et al. 2016); c.453_454del:p.E153Afs*5 (Koch et al. 2016); and most recently

c.C892T:p.R298* alone (Nasca et al. 2018). Patient skin fibroblasts show a loss of MFF function with mitochondrial and peroxisomal hyper-elongation, and the patients themselves present with neurological abnormalities, showing developmental delay, peripheral neuropathy, optic atrophy, and Leigh-like encephalopathy (Shamseldin et al. 2012; Koch et al. 2016; Nasca et al. 2018). We confirmed a similar degree of peroxisomal hyper-elongation in skin fibroblasts from three different patients suffering from MFF-deficiency when maintained under the same culture conditions. Furthermore, peroxisomal biochemical parameters related to fatty acid α- and β-oxidation, plasmalogen biosynthesis, or matrix protein import/processing did not reveal any deficiencies in fibroblasts from those patients. This is in agreement with biochemical studies in other MFF-deficient patient fibroblasts (Koch et al. 2016; Nasca et al. 2018). Overall, these findings support the notion that defects in the membrane dynamics and division of peroxisomes rather than loss of metabolic functions contribute to the disease pathophysiology.

Similar observations in PEX11β- or DRP1-deficient cells (Waterham et al. 2007; Ebberink et al. 2012) have led to the general assumption that defects in peroxisomal dynamics and division result in elongated peroxisomes, which are, however, largely functional and otherwise normal. We now reveal in MFF-deficient cells that this is not the case. We show that the elongated peroxisomes in those cells are composed of a spherical body, which represents a mature, import-competent peroxisome, and of thin, tubular extensions, which likely represent pre-peroxisomal membrane compartments; not yet fully import-competent for peroxisomal matrix proteins. An alternative interpretation may be that the tubular structures are to some degree import-competent but lack mechanisms to retain the imported matrix proteins. Such a mechanism for retaining matrix proteins may be provided by membrane constriction, which is impaired in MFF-deficient cells.

These observations are consistent with the proposed multi-step maturation model of peroxisomal growth and division and with previous data on tubular membrane extensions after expression of PEX11β (Delille et al. 2010; Schrader et al. 2012, 2016b). In this respect, elongated peroxisomes in MFF-deficient cells resemble those observed after expression of a division-incompetent PEX11β, which also results in elongated peroxisomes with an import-competent spherical body and a

pre-peroxisomal membrane expansion. In contrast, elongated peroxisomes in DRP1-depleted cells are constricted, with a “beads-on-a string” like appearance, and the interconnected spherical peroxisomes (“beads”) are import-competent for matrix proteins (Koch et al. 2004). These constrictions may therefore provide a mechanism to retain matrix proteins. This indicates that a defect in MFF influences peroxisome division earlier than a defect in DRP1, and results in a maturation defect of elongated peroxisomes, which are unable to constrict and to subsequently import and/or retain matrix proteins. In line with this, it has recently been shown that MFF can act as a sensor but also potentially as an inducer of mitochondrial constriction (Helle et al. 2017). We propose that MFF deficiency, which impairs peroxisomal membrane constriction and proper assembly of the division machinery, blocks further maturation of the pre-peroxisomal membrane compartment.

This means that, although the number of fully functional peroxisomes is reduced and matrix proteins are largely restricted to the mature spherical bodies, membrane surface area and volume of the peroxisomal compartment are increased in MFF-deficient cells (mean estimated total surface area, control fibroblasts: $1.55x10^7 \pm 7.29x10^6$ nm^2, dMFF: $1.15x10^8 \pm 6.57x10^8$ nm^2; mean estimated total volume, control fibroblasts: $4.1x10^8 \pm 1.94x10^8$ nm^3, dMFF $2.5x10^9 \pm 1.45x10^9$ nm^3) (Figure 3.7), as well as the surface area to volume ratio (mean estimated SA:V, control fibroblasts: 0.038 ± 0.001, dMFF: 0.046 ± 0.005) (Figure 3.7). This likely explains why biochemical functions of elongated peroxisomes are overall normal under standard conditions. However, it can be speculated that sudden environmental changes (e.g. an increase in peroxisomal substrates via nutrients/diet or stress conditions), which require increased peroxisomal metabolic activity and number, will overwhelm the capacity of the peroxisomal compartment in MFF-deficient cells. This may also explain why mild alterations of peroxisomal metabolism are occasionally observed in patients with defects in peroxisomal dynamics and division (Waterham et al. 2007; Ebberink et al. 2012; Taylor et al. 2017). Furthermore, peroxisomes in patient cells may be less able to cope with increased expression of peroxisomal matrix enzymes or PMPs. Those may accumulate in the cytoplasm and may be degraded or

mistargeted (e.g. to mitochondria) due to the reduced number of import-competent peroxisomes (Ebberink et al. 2012).

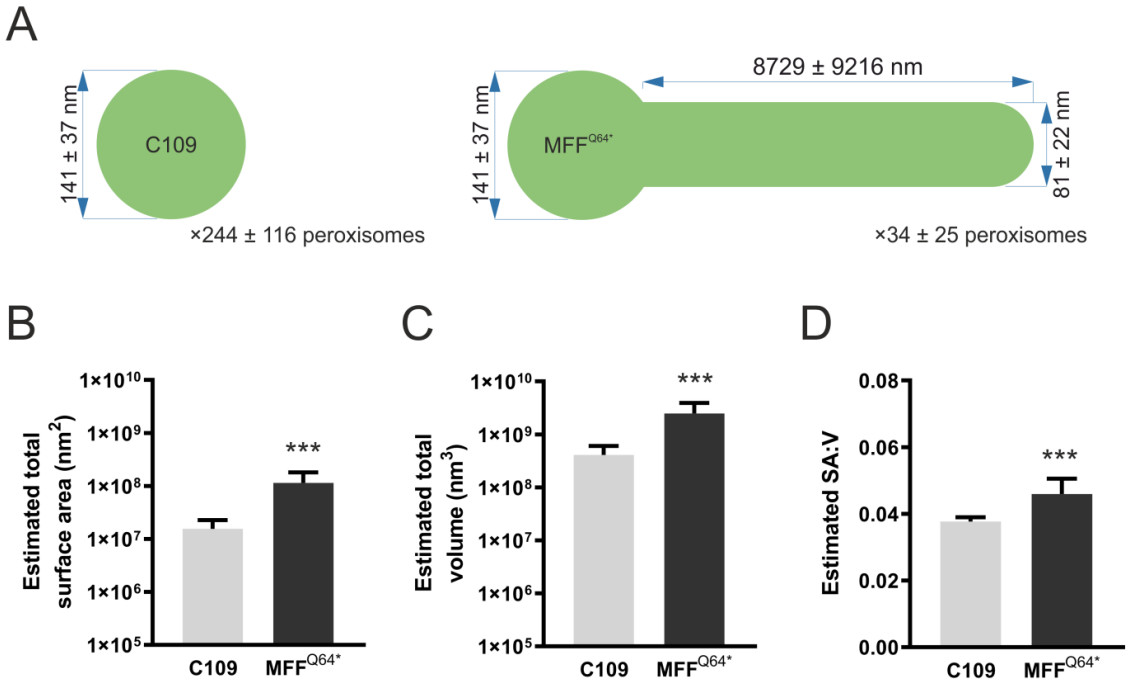

Figure 3.7: Calculations of peroxisomal surface area, volume, and surface area to volume ratio. (**A**) Values used for calculations (mean ± SD). Control peroxisome body diameter was used as the calculated dMFF body diameter. (**B**) Estimated total peroxisomal surface area in control (C109) and MFF-deficient (dMFF) fibroblasts, based on an average of a computer-generated population of peroxisomes using values taken from the distributions shown in (**A**). (**C**) Estimated total peroxisomal volume, and (**D**) estimated surface area to volume ratio (SA:V). Error bars show the mean + SD for 10,000 generated peroxisome populations. ***, $p < 0.001$; two-tailed, unpaired *t* test.

We also show that peroxisomal matrix and membrane proteins do not distribute evenly along the elongated peroxisomes in MFF-deficient cells. Endogenous catalase or exogenously expressed GFP-SKL predominantly localise to the spherical body, whereas PEX14 localises predominantly to the tubular membrane extensions. A heterogeneous distribution of peroxisomal proteins during membrane growth and division has been reported previously (Delille et al. 2010; Cepińska et al. 2011). The specific mechanisms which restrict the mobility of the peroxisomal proteins and keep them within the spherical or tubular membrane domains are still unknown, but may depend on protein oligomerization and/or a specific lipid environment. However, the prominent localisation of PEX14, a component of the docking/translocation complex for matrix protein import, to the tubular peroxisomal membranes in MFF-deficient cells is unusual. It is possible that PEX14, which has been reported to interact with microtubules (Bharti et al.

2011; Theiss et al. 2012), may also act as a peroxisome-microtubule docking factor: it predominantly localises to the peroxisomal membrane extensions in MFF patient cells and may anchor them to microtubules in order to stabilise those highly elongated, delicate membrane structures and to facilitate membrane extension. The membrane topology of PEX14 is poorly defined, but a recent study suggested that the N-terminal domain is protease-protected and may not be exposed to the cytoplasm (Barros-Barbosa et al. 2019). Such a topology may be inconsistent with tubulin-binding, but it is possible that different populations or complexes of PEX14 exist which may fulfil different functions at the peroxisomal membrane.

Peroxisomes are oxidative organelles with important roles in cellular redox homeostasis (Fransen and Lismont 2018). Alterations in their redox metabolism have been suggested to contribute to aging and the development of chronic diseases such as neurodegeneration, diabetes, and cancer (Fransen and Lismont 2019). Using genetically encoded fluorescent sensors with ratiometric readout in live-cell approaches, we revealed alterations in the glutathione redox potential within peroxisomes of MFF-deficient fibroblasts, which was less oxidising compared to controls. Interestingly, in previous studies the intra-peroxisomal redox state in tubular peroxisomal compartments was also observed to be slightly lower than in spherical bodies (Lismont et al. 2017). In line with this, we also detected reduced levels of peroxisomal H_2O_2 in MFF-deficient cells. The reason for this is unclear, but given that (i) peroxisome-derived H_2O_2 can easily cross the peroxisomal membrane (Lismont et al. 2019a), and (ii) the surface to volume ratio is larger in the tubular structures, we hypothesize that H_2O_2 can diffuse faster out of the tubular structures than out of the spherical bodies. Importantly, the glutathione redox balance and hydrogen peroxide levels in the cytosol and mitochondria were similar to controls, indicating peroxisome-specific alterations due to loss of MFF-function. Peroxisome-derived H_2O_2 may be an important signalling messenger that controls cellular processes by modulating protein activity through cysteine oxidation (Fransen and Lismont 2019). However, the precise interrelationship between peroxisomal redox metabolism, cell signalling, and human disease remains to be elucidated. Further insight may come from the identification of primary targets for peroxisome-derived H_2O_2. We also revealed changes in the peroxisomal pH in MFF-deficient fibroblasts, which

was more alkaline than in controls. The pI of most peroxisomal enzymes is basic, and consistent with this, an alkaline pH has been reported for the peroxisomal lumen (Dansen et al. 2000; van Roermund et al. 2004; Godinho and Schrader 2017). Studies addressing peroxisomal pH under disease conditions are scarce, but a more acidic peroxisomal pH has been reported in fibroblasts from patients suffering from Rhizomelic Chondrodysplasia Punctata type 1, a PBD based on a defect in the import receptor PEX7 and impaired matrix protein import of PTS2-containing cargo (Dansen et al. 2000). It remains to be determined if those changes are the result of slightly altered metabolic activity and/or changes in membrane properties which impact on peroxisomal membrane channels/transporters. In line with this, calcium influx into peroxisomes has been reported to induce a minor increase of peroxisomal pH (Lasorsa et al. 2008). Whether peroxisomes possess a proton pump is still debated, but it has been suggested that a peroxisomal proton gradient may be needed to drive other transport processes across the peroxisomal membrane (Rottensteiner and Theodoulou 2006).

It is suggested that a block in peroxisome fission (e.g., due to mutations in MFF or DRP1), which results in the formation of larger, elongated organelles, may have deleterious effects on the mobility of peroxisomes, on synaptic homeostasis, and pexophagy (Schrader et al. 2014). We show here that highly elongated peroxisomes in MFF-deficient fibroblasts can be degraded by autophagic processes, which were induced by expression of a fragment of PEX3 [*Hs*PEX3(1-44)] (Soukupova et al. 1999) or by amino acid starvation. Highly elongated mitochondria, for example, were reported to be spared from mitophagy under starvation conditions (Rambold et al. 2011; Gomes et al. 2011). Our data reveal that elongated peroxisomes are not spared from autophagic processes, e.g. due to physical limitations, and indicate that impaired peroxisome degradation may not contribute to the pathology of MFF-deficiency. Interestingly, a shortening of elongated peroxisomes was observed during amino acid starvation in HBSS, which was accompanied by a reduction in peroxisomal marker proteins, e.g. the PMPs ACBD5 and PEX11β, which are required for membrane expansion and elongation. PEX11β mediates membrane deformation and elongation of the peroxisomal membrane (Delille et al. 2010; Opaliński et al. 2011), whereas ACBD5 has recently been shown to mediate membrane contact sites between

peroxisomes and the ER by interacting with ER-resident VAP proteins (Costello et al. 2017b; Hua et al. 2017). Depletion of ACBD5 (or VAP) in MFF-deficient fibroblasts resulted in a shortening of elongated peroxisomes, likely due to disruption of the peroxisome-ER contact sites and reduced transfer of lipids from the ER to peroxisomes, which are required for peroxisomal membrane expansion (Costello et al. 2017b; Schrader et al. 2019). Our findings are in line with these previous observations and indicate that elongated peroxisomes in MFF-deficient cells are not fully static, but still dynamic under certain conditions. It is possible that a shortening/fragmentation of elongated peroxisomes under conditions of amino acid starvation facilitates their subsequent removal by autophagy.

Mitochondrial and peroxisomal dynamics are particularly important for brain development and function (Berger et al. 2016; Khacho and Slack 2018), likely explaining why MFF-deficient patients show primarily neurological defects. In neuronal cells, there is a strict regulation of the size and number of mitochondria, with smaller, uniform mitochondria in the axon in contrast to longer, elongated mitochondria in the dendrites (Popov et al. 2005). In mice, this regulation of mitochondrial size in the axon has recently been reported to be dependent on MFF (Lewis et al. 2018). Importantly, loss of MFF did not significantly alter the mitochondrial membrane potential, ATP levels or the redox potential of the matrix, but was important for limiting presynaptic Ca^{2+} dynamics, affecting neurotransmitter release, terminal axonal branching and circuit connectivity. We show here that depletion of MFF in primary mouse hippocampal neurons alters peroxisomal morphology and distribution. In contrast to fibroblasts, peroxisomes do not hyper-elongate, but appear enlarged and tend to cluster, affecting their uniform distribution within the soma. Neuronal peroxisomes preferentially accumulate in axon terminals during early postnatal development (Arnold and Holtzman 1978) but are virtually absent from the axon in mature projection neurons (Kassmann et al. 2011). Changes in ACBD5 expression have recently been shown to alter peroxisome motility and distribution in mouse hippocampal neurons, but independent of the ACBD5-VAPB interaction (Wang et al. 2018). Neuronal peroxisomes are required for axonal integrity of Purkinje cells (De Munter et al. 2018), and peroxisomal ROS metabolism was reported to influence activities of pro-opiomelanocortin producing neurons in the hypothalamus (Diano et al. 2011) and synaptic transmission at neuromuscular junctions (Giniatullin et

al. 2019) underlining the physiological importance of peroxisomes in neurons. It remains to be determined if the altered peroxisomal phenotype in neurons contributes to the neurological abnormalities observed in MFF-deficiency. However, loss of PEX11β, which is not a mitochondrial protein, also causes neurological abnormalities in patients and mouse models highlighting the importance of peroxisomal dynamics and plasticity in the brain (Li et al. 2002; Ebberink et al. 2012; Taylor et al. 2017).

In contrast to the more prevalent neurological features in human patients with MFF-deficiency, mice without MFF die of heart failure at week 13, as a result of severe cardiomyopathy, which is likely based on mitochondrial alterations (Chen et al. 2015). However, removal of MFF exacerbated neuronal loss, astrogliosis and neuroinflammation in a Huntington's disease mouse model (Cha et al. 2018). Similar to patient fibroblasts, peroxisomes (and mitochondria) in MFF-deficient mouse embryonic fibroblasts were highly elongated (Chen et al. 2015). Interestingly, peroxisomal length was not substantially altered in MFF-deficient mouse cardiomyocytes (Chen et al. 2015). This strongly indicates that peroxisome morphology and division is affected in a cell type-specific manner. It should also be considered that environmental changes and related signalling events that trigger peroxisomal membrane expansion and division (e.g. metabolic alterations and certain stress conditions) can potentially promote the formation of hyper-elongated peroxisomes in formerly unaffected cell types and contribute to the pathophysiology of MFF-deficiency.

Chapter 4 Modelling Peroxisomal Membrane Dynamics

4.1 Introduction

In order to address biological questions and understand biological complexity, a purely experimental approach is not always optimal. Experiments can be time-consuming, resource intensive, expensive, technically challenging, difficult to replicate, or simply sometimes not possible at all. In contrast, an *in silico* approach to biology, through a combination of mathematical modelling and computer simulations, has the potential to be a faster, more high-throughput, cheaper, more adaptable method with a greater scope for more objective predictions.

A theoretical model in biology utilises mathematics, physics and computing to describe observed data and to make predictions about future outcomes. Assessing to what extent predictions are valid by carrying out experimental work where possible enables (i) reassurance that untestable predictions are reliable, and/or (ii) model refinement/improvement following analysis and incorporation of new data. In this way, a combined experimental-modelling approach can be an extremely powerful tool in understanding the complex nature of biological systems (Thorne et al. 2007).

Due to this, a cross-disciplinary approach to research has become more and more popular, and numerous mathematical models and quantitative approaches have now been developed in cell biology, covering a wide range of scales (Mogilner et al. 2006). At the intracellular level, models can be molecular (focusing on, for example, the physical motion and arrangements of individual atoms and molecules using molecular dynamics simulations (MDS) (Kumari et al. 2017) or the interplay of intracellular signal transduction pathways in systems biology (Klipp and Liebermeister 2006)), or more organelle-based (such as investigating organelle formation (Binder et al. 2009), organelle morphology (Dalmasso et al. 2017), or organelle positioning (Lin and Steinberg 2017)). At a higher level, models can encapsulate the behaviour of the cell as a whole, such as modelling cell shape changes during chemotaxis (Tweedy et al. 2013) or phagocytic cell membrane dynamics during engulfment (Richards and Endres 2017). Models can also investigate multicellular dynamics at the tissue level, for example the response of a tissue layer to hypoxic conditions (Morshed and Dutta

2017), or the growth of tumours and response to radiation therapy (Watanabe et al. 2016).

4.1.1 Modelling in Peroxisome Biology

Compared to the numerous models developed for other organelles such as mitochondria (Kowald and Klipp 2014), there are relatively few models of peroxisomal dynamics, the majority of which focus very specifically on certain aspects of peroxisome biology.

Although there are only a handful of models of peroxisome biology, the few there are have shown the utility of such an approach to help understand and characterise peroxisome function, morphology, motility, plasticity and regulation. An overview of peroxisome-focused studies utilising mathematical modelling is presented below.

Studies can look at specific peroxisomal proteins in more detail, for example using tools such as molecular dynamics simulations. Su *et al.* used an MDS model of the yeast peroxisomal membrane, and observed the association of a conserved N-terminal amphipathic helix of Pex11p with peroxisomes *in silico* (Su et al. 2018), suggesting that Pex11p forms aggregates on membranes in order to facilitate membrane remodelling in peroxisomal growth and division. Similarly, computationally modelling the recruitment of autophagy receptor proteins to peroxisomes hinted at the importance of size-selectivity in pexophagy, by showing that larger peroxisomes may be preferentially degraded due to increased NBR1 clustering on the membrane (Brown and Rutenberg 2017). The shared mitochondrial-peroxisomal yeast AAA ATPase Msp1p removes tail-anchored membrane proteins on organelle membranes (Chen et al. 2014a). Using a mathematical model of protein degradation (McShane et al. 2016), it was shown that experimentally measured clearance of tail-anchored PMP Pex15p by Msp1p better fits a model whereby Pex15p has two distinct populations, nascent and mature, which carry Msp1p sensitivity and resistance, respectively (Weir et al. 2017).

In fungal hyphal cells, peroxisome motility is regulated by passive and active diffusion, combined with microtubule-directed transport. Mathematical modelling of peroxisome spatial distribution suggested that a combination of directed

transport and active diffusion ensures an even distribution of peroxisomes, but also allows for frequent interaction, required for peroxisome function in fungal hyphae (Lin and Steinberg 2017).

In addition to these specific peroxisome models, mathematical models have also been utilised in an attempt to understand the regulation of peroxisome number, by assigning rate parameters to peroxisomal behaviours, as often used for chemical reactions. This approach was first presented by Mukherji and O'Shea to characterise organelle biogenesis, and later extended by Craven, breaking down the regulation of any organelle number into four parameters; *de novo* biogenesis ($k_{de\ novo}$), fission ($k_{fission}$) and fusion (k_{fusion}) of pre-existing organelles, and degradation (γ), generating an overall equation to model organelle number stochastically over time (Mukherji and O'Shea 2014; Craven 2016). As peroxisomes do not fuse to each other (Motley and Hettema 2007; Huybrechts et al. 2009; Bonekamp et al. 2012), peroxisome proliferation can be assumed to be governed by only the rates $k_{de\ novo}$, $k_{fission}$, and γ. In order to test the model, comparison of experimentally measured peroxisome proliferation in yeast in response to growth on either glucose- or oleic acid-containing medium with a k_{fusion}-less variant of the original organelle model was performed (Mukherji and O'Shea 2014). The model suggested that peroxisomes may switch from more *de novo* dominated maintenance of peroxisome number in glucose-containing medium, to fission dominated proliferation in oleic acid-containing medium. This result was validated experimentally by observing that division-protein knockout yeast grown in the presence of oleic acid, show the same behaviour as wild-type yeast grown in the presence of glucose (Mukherji and O'Shea 2014). An experimental data-driven expansion of this model focusing on inferring rate parameter values for mammalian cell peroxisomes indicated a low basal rate of *de novo* biogenesis, with a peroxisome population maintained primarily by the opposing fission and degradation rate parameters (Galitzine et al. 2018). Application of this model to viral infection led to the conclusion that growth and division is likely the preferred mechanism for the rapid increase in peroxisome number during the cell's viral response (Jean Beltran et al. 2018). Further exploring several variations of the original organelle model (Mukherji and O'Shea 2014; Craven 2016), failed to fit experimental data to the k_{fusion}-less variant model, suggesting that peroxisomes in yeast must have some level of fusion (Choubey

et al. 2019). However this suggestion has never previously been observed, suggesting the need for modification to this model.

One important aspect of peroxisome biology that previous models have failed to address is that of peroxisome morphology. Alterations in peroxisomal membrane shape is important not only in elongation during growth and division (Schrader et al. 2016a), but is involved in peroxisome interaction and coordination with other organelles and the cytoskeleton (Costello et al. 2017b; Kustatscher et al. 2019) (see Chapter 2, Chapter 3), resistance to changes in the intracellular environment (Schrader and Fahimi 2006a), and role in cell fate decisions (Asare et al. 2017). Several disorders have now been identified due to a defect in membrane dynamics (see section 1.1.11.3), and a combined experimental-modelling approach focusing on peroxisome shape and its contribution to peroxisome number is needed in order to understand the complex regulation of these processes. In addition, peroxisomes are often heterogeneous in shape (Islinger et al. 2018), with some cells showing mixed populations of spherical/elongated peroxisomes, not reflected in any of the above models. A stochastic agent- or individual-based modelling approach (Thorne et al. 2007; Macal 2016), in which individual peroxisomes are treated as separate 'agents', but all governed by the same parameters, will allow this heterogeneity to be captured.

4.2 Materials and Methods

4.2.1 Modelling Approach

As mentioned above, the aim is, through an agent-based modelling approach motivated by real measured experimental data, to investigate changes in peroxisomal membrane dynamics. This approach will describe the number, shape and size of peroxisomes in various cellular conditions and patient cells. Treating peroxisomes as separate entities allows the simulation to be implemented in a stochastic manner, which is important in biology due to the inherent complexity, heterogeneity, randomness, and noisiness of nature (Tsimring 2014). Although each peroxisome is taken individually and the number and shape of individual peroxisomes in each simulation will have variation due to this stochasticity, there is likely to be some quasi-steady state, where the number and size of the population can be described by a stable mean and standard

deviation over time. It is changes in these steady states that are likely to be altered in patients, and which will allow the model parameters that must be changed to capture various patient phenotypes to be determined.

The goal of this mathematical modelling approach is to condense the complex system of a population of peroxisomes into as few fundamental processes as possible (such as division, growth and degradation). If, through manipulation of these few parameters, both wild-type and various mutant cells can be described, this suggests the model is sufficient to capture the basic biophysics of peroxisome morphology. If, however, the peroxisomes in various situations cannot be described by simply changing the values of model parameters (for example, in the case of the k_{fusion}-less model failing to replicate peroxisome biogenesis (Choubey et al. 2019)), this shows that important components of the system are missing from the model. Therefore, by building upon experimental data, the hope is that the model will give a better understanding of what governs peroxisome proliferation, allowing links to be made between experimental observations and the physical processes underlying regulation of peroxisome abundance and morphology. This carries therapeutic value, as the model may infer, for example, the best way to increase peroxisome number in a patient with a defect in peroxisome biogenesis.

Once the model is established, and can accurately reflect experimental data, it will then be useful for prediction of future outcomes, particularly those that are unable or difficult to measure *in vitro* (e.g. the effects of increasing lipid flow into the peroxisomes). Accurate prediction of peroxisomal membrane alterations, for example the response of the peroxisomal population in a patient cell to an altered intracellular environment (e.g. high ROS levels), also has the potential to give insights into therapeutic treatment of patients through a better understanding of the disease.

4.2.2 Model Description

4.2.2.1 Individual Peroxisomes

Each individual peroxisome is described as a sphere (with radius r) and an optional attached hemispherical-capped cylinder (with length L and width w). For simplicity, for the simulation of the model peroxisomes (which move in the three

dimensions of the cell) are projected onto a two-dimensional plane with coordinates described by x and y, and the angle of the peroxisomal elongation with respect to the x-axis is represented by θ (Figure 4.1).

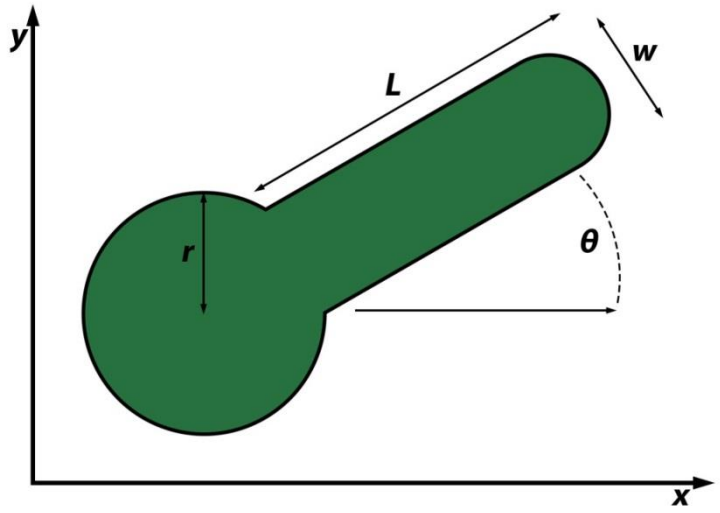

Figure 4.1: Model representation of a single peroxisome. Each peroxisome is described by a spherical body (of radius r), a cylindrical elongation (of length L, width w and angle θ) and an (x,y) position of the centre of the body.

4.2.2.2 Model Parameters

In order to build a mathematical model of peroxisome dynamics, which biophysical processes to include in order to describe the dynamics of each individual peroxisome need to be determined. The growth and division process of peroxisomes can be described by only a few steps and appears relatively self-contained by a small number of proteins (see section 1.1.5.2). These are (i) growth of the peroxisome body, (ii) elongation of the peroxisomal elongation, and (iii) constriction and division of the elongation into new 'daughter' peroxisomes.

To ensure that peroxisome division does not result in progressively smaller peroxisomes, there must be a membrane lipid flow into the peroxisome. This is supported by the fact that membrane lipids are likely supplied from the ER, and reduction of peroxisome-ER tethering appears to compromise peroxisome elongation (Costello et al. 2017b). Lipid flow into the peroxisome is represented in the mathematical model by a constant flow rate α (measured in nm^2/s) (Figure 4.2A), which describes the membrane area increase in unit time. By assuming that lipid only flows into the body, the effect of lipid flow is to increase the body radius r whilst leaving the extension parameters w and L unchanged. Since $\alpha \Delta t$

of lipid flows into the body in time Δt, this causes the body radius to increase to $\sqrt{r^2 + \alpha\Delta t/4\pi}$.

In order for an extension to form and grow, there must be force acting on the extension. The exact mechanisms of peroxisome elongation formation are still unclear, but may be, for example, a pulling force such as that from adaptors to cytoskeletal motors (Castro et al. 2018), or the effect of pushing in membrane lipids into the peroxisome, while membrane-deforming proteins such as PEX11β hold the shape of the extension. Regardless of the mechanism, the growth of a peroxisomal elongation can be modelled simply by assuming extensions grow at a constant speed v (measured in nm/s) (Figure 4.2B). In time Δt, assuming extensions always have constant width w, this has the effect of increasing L to $L + v\Delta t$. Importantly, the lipid to increase the extension length can only come from the body, meaning that extension growth must be accompanied by a corresponding decrease in body size. Assuming that there is no change in overall membrane area during extension growth, the body radius r must then decrease to $\sqrt{r^2 - wv\Delta t/4}$ ($\pi wv\Delta t$ is the increase in elongation area in time Δt.). In addition, when the hemispherical cap of the elongation first forms (from a spherical body) the radius of the body shrinks to $\sqrt{r^2 - w^2/8 + 0.5r^2\left(1 - \sqrt{1 - w^2/4r^2}\right)}$, caused by removal of a spherical cap from the body and replacement by the hemispherical cap of radius $w/2$.

The final step in the growth and division of peroxisomes is the constriction and subsequent division of the elongation into new 'daughter' peroxisomes. This is modelled here using constant division rate per unit length β (in /nm/s) (Figure 4.2C), resulting in the probability of division $\beta L\Delta t$ in time Δt. This has the effect that, in a fixed time Δt, longer peroxisomes are more likely to divide (under the assumption that they are more likely to contain more membrane-bound adaptors to attract division machinery). By modelling division in a stochastic manner (a peroxisome will not divide unless a random number $U(0,1)$ is less than or equal to $\beta L\Delta t$), the model allows for a range of peroxisome lengths. An elongation compartment split length λ divides a peroxisomal elongation into daughter peroxisomes all with radius $\sqrt{w\lambda/4}$. Where the elongation length is not divisible

by λ, one daughter peroxisome will contain any leftover membrane area, further resulting in variation in the model.

The first iteration of the model considered only these three basic processes as controlling all aspects of peroxisomal growth and division. Although capturing some aspects of peroxisome morphology (such as a range in elongation lengths and body size), several limitations soon became clear. These issues were resolved by adding two new processes to the model: peroxisome degradation and more realistic lipid flow.

First, in addition to modelling the peroxisome growth and division process, it is important to also include the effect of peroxisome degradation. Without this, the number of peroxisomes over time increases at an exponential rate. Therefore, peroxisome turnover (see section 1.1.7) is modelled by a fixed probability of an individual peroxisome degrading in a given time. In particular, the probability is described by an average peroxisome lifetime τ (in s) (Figure 4.2D), leading to a probability of $\Delta t/\tau$ for an individual peroxisome to degrade in time Δt.

Second, more biologically relevant lipid flow was included. Lipid flow is assumed to be provided by direct contact with the ER. As not all peroxisomes will be tethered to the ER at any given time (~60%) (Costello et al. 2017b; Xiao et al. 2019), and there is likely a limitation in total available cellular membrane lipids, the lipid flow rate of α was replaced by $\alpha e^{-\gamma A}$ where A represents the total surface area of all peroxisomes. This is in order to model a limitation in available cell membrane lipids rather than a constant flow, and γ is a new lipid flow constant (in /nm^2) (Figure 4.2A). This new lipid flow rate is implemented in a stochastic manner: in time Δt, there is a probability $e^{-\gamma A}$ of lipid flow at rate α. This further stochasticity is another way that the model tries to capture the heterogeneity of real peroxisomes. It is worth noting that an early version of the model also considered a lipid flow probability controlled by n (the total number of peroxisomes), rather than A giving an effective lipid flow rate of $\alpha e^{-\gamma n}$. However, this model failed to limit lipid flow correctly at low peroxisome numbers in some extreme cases (such as when there are only a few, very long peroxisomes as in MFF deficiency).

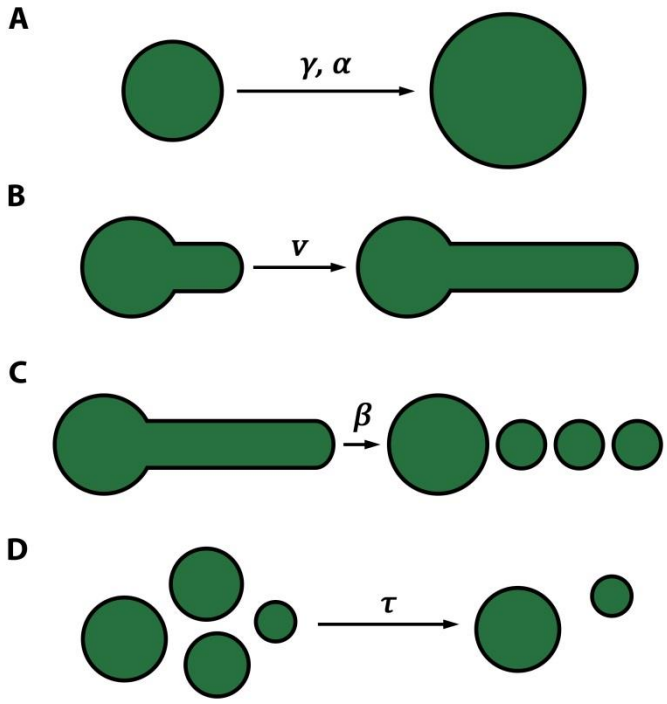

Figure 4.2: Model parameters. (A) An increase in peroxisomal body radius is governed by parameters γ (lipid flow constant) and α (lipid flow rate). **(B)** The rate of increase in elongation length is governed by parameter v (elongation speed). **(C)** Division of a peroxisomal extension into new peroxisomes is governed by parameter β (division rate). **(D)** The rate of degradation of peroxisomes is governed by parameter τ (mean peroxisome lifetime).

4.2.2.3 Model Assumptions

It is important to understand the assumptions that are used in this *in silico* model. Assumptions in mathematical models are needed to ensure simplicity and produce a working model, but should be limited to only those assumptions that are logical, biologically sensible, and backed up with empirical data to avoid bias (Edwards and Hamson 1996). Assumptions determine (i) which components to include, (ii) their relative importance/strength, and (iii) how these components interact with each other. As the model progresses and more experimental data are obtained, these assumptions need to be carefully reviewed, and where needed, reworked.

In the first step of peroxisomal growth and division, provided there is lipid available, the peroxisomal body radius increases at a constant rate, governed by α. The assumption of a constant lipid flow maintains simplicity, and as lipid flow into the ER is likely by direct tethering (Raychaudhuri and Prinz 2008), this assumption is sufficient for a first model. The model assumes that lipid flow only

increases body radius, with no direct effect on the peroxisome elongation. As the ER is predominantly found at the peroxisomal body rather than tubules (Bishop et al. 2019), this assumption is based on empirical data.

Next, during the growth of a peroxisomal tubule, the model assumes that a peroxisome will only elongate when the body is large enough ($r \geq r_{min}$). This is consistent with the fact that all bodies in highly-elongated peroxisomes have a fairly small distribution (Figure 3.1). Similarly, the width of the elongation w is assumed to be constant, as it also appears to have a small distribution as measured in EM (Figure 3.1). The speed of elongation v is assumed constant for simplicity, and also due to the assumption that the mechanism of elongation, while unknown, is the same for individual peroxisomes. Even if this assumption was relaxed, it is unlikely to make much difference to peroxisome morphology.

When a peroxisomal elongation divides into new 'daughter' peroxisomes, the compartment split length (λ) results in peroxisomes all with the radius $\sqrt{w\lambda/4}$. This assumption is for simplicity, and allows for a lower bound on peroxisome size, as peroxisomes are typically noted as being in the range of 0.1-1 μm in diameter (Smith and Aitchison 2013). In order to ensure this lower bound, a peroxisome cannot divide until the length L satisfies the condition $L \geq \lambda$.

For simplicity, the implementation of degradation in this model does not depend on peroxisome size or age. As the model is agent-based, degradation is also independent for each peroxisome, meaning any number of peroxisomes can divide in a given time regardless of the effect on the overall system. Triggers for pexophagy are numerous (see section 1.1.7), leading to the assumption that any peroxisome has the capability to trigger pexophagy at any given time.

Finally, movement of peroxisomes in the simulation of this model is also taken as random and indiscriminate. The motility of peroxisomes may play a role in affecting peroxisome growth and division, as MIRO1 has the capacity to extend elongations, which combined with tethering forces may help to mediate proliferation (Castro et al. 2018). However, this behaviour is likely encapsulated by the elongation parameter v.

4.2.2.4 Parameter Values

The established first-generation model should accurately reflect a wild-type peroxisomal population, which requires fitting the parameter values to the wild-type population data (such as average peroxisome number and size). Wild-type values for the average peroxisome number, radius, elongation length, and fraction of peroxisomes elongated were either obtained from experimental data or motivated by biological considerations (Table 4.1). The number of peroxisomes n, and the average peroxisome body radius $\langle r \rangle$ were measured experimentally (see Chapter 3). As peroxisome elongations are rarely seen by immunofluorescence in a wild-type cell at steady state, the average non-zero elongation length $\langle L \rangle$ is taken as 40 nm, a value small in comparison to the average body size. Similarly, the fraction of elongated peroxisomes is estimated as an intermediate value of $f = 25\%$. Since these values match well with real wild-type data and since different values are unlikely to substantially alter the conclusions, they are sufficient at this stage.

Parameter	Value
n	250
$\langle r \rangle$	80 nm
$\langle L \rangle$	40 nm
f	0.25

Table 4.1: Population values and averages used to fit a wild-type *in silico* model. Values are the estimated averages of wild-type cells at a steady state, used as a baseline for a wild-type model. n, the number of peroxisomes. $\langle r \rangle$, the average peroxisome radius. $\langle L \rangle$ the average peroxisome elongation length. f, the fraction of peroxisomes that are elongated at any given time.

Wild-type parameters were fixed either by (i) using values directly measured from experimental data (for w), (ii) calculating from the approximate steady-state equations given below (for λ, r_{min}, β, γ and τ), (iii) deriving from biologically-sensible values of hard-to-measure quantities like the transient period length (for α), or (iv) fitting to the measured data (for v) (Table 4.2).

Parameter	Value
α	75 nm^2/s
γ	2.4×10^{-7} $/nm^2$
v	0.3 nm/s
β	2×10^{-5} /nm/s
τ	1.5×10^5 s
w	80 nm
λ	80 nm
r_{min}	110 nm

Table 4.2: Values chosen for parameters and constants for the wild-type *in silico* model. Model parameters α, γ, v, β and τ, and constants w, λ and r_{min} were inferred from experimental data, or calculated using wild type values (Table 4.1) as targets.

First, the peroxisome elongation diameter w was taken as 80 nm, as measured previously in dMFF cells (Chapter 3). This also corresponds to previously measured peroxisomal elongations (Delille et al. 2010). Based on the elongation split length λ, the smallest new peroxisomes have an initial radius of $\sqrt{w\lambda/4}$. Using a minimum peroxisome radius as 40 nm (the minimum body radius measured in Figure 3.1D), solving for λ the above equation, with w as 80 nm, results in the estimation of λ also as 80 nm.

Using the assumption that all available lipid flow into a peroxisome when elongating is used for extension elongation, the average body radius can be estimated as $\langle r \rangle = (1-f)(\sqrt{w\lambda/4} + r_{min})/2 + f r_{min}$ (here, the first term represents the average radius of non-elongated peroxisomes assuming an even distribution of radii between $\sqrt{w\lambda/4}$ and r_{min}, and the second term represents the average radius of elongated peroxisomes). Solving for r_{min} using $\langle r \rangle$ as 80 nm, f as 0.25, w as 80 nm, and λ as 80 nm results in the estimation of r_{min} as approximately 110 nm.

Peroxisome turnover in mammalian cells has previously been estimated as approximately two days (Huybrechts et al. 2009). In order to obtain a more specific value for the peroxisome mean lifetime τ, it was derived as follows. The

total lipid entering the whole peroxisome population in time Δt is given by the product of the probability of lipid flow ($e^{-\gamma A}$), the lipid flow per peroxisome ($\alpha \Delta t$) and the number of peroxisomes (n). Since the total area A can be given by n⟨A⟩, where ⟨A⟩ is the average area per peroxisome, the resulting total inwards lipid flow is $e^{-\gamma n\langle A\rangle} n\alpha\Delta t$. Conversely, lipid leaving the peroxisome population only occurs through pexophagy, and is therefore given by $n\langle A\rangle \Delta t/\tau$. At steady state, the total lipid entering the system should be balanced by the total lipid leaving the system: $e^{-\gamma n\langle A\rangle} n\alpha\Delta t = n\langle A\rangle \Delta t/\tau$, which simplifies to give $e^{-\gamma n\langle A\rangle}\, \alpha = \langle A\rangle/\tau$. Assuming a constant lipid flow, the time before a new peroxisome (radius $\sqrt{w\lambda/4}$) begins to elongate (radius r_{min}) is approximately given by $(4\pi {r_{min}}^2 - \pi w\lambda)/(e^{-\gamma n\langle A\rangle}\alpha)$ (here, the first term represents the area of lipid needed to increase from $\sqrt{w\lambda/4}$ to r_{min}, and the second term represents the effective lipid flow rate that allows this area increase). The second term can be replaced, as $e^{-\gamma n\langle A\rangle}\alpha = \langle A\rangle/\tau$, so the time can also be written as $(4\pi {r_{min}}^2 - \pi w\lambda)/(\langle A\rangle/\tau)$. The majority of peroxisomes are not elongated and are assumed to be in this stage of growth before reaching r_{min}. Estimating this time as three days, the average peroxisome area ⟨A⟩ as $4\pi\langle r\rangle^2 + f\pi w\langle L\rangle$, and the wild-type and parameter values as derived above, results in an estimate of τ of around 1.5 × 10^5 s, fitting well with previous data (Huybrechts et al. 2009).

In a wild-type cell (e.g. skin fibroblasts), peroxisomal elongations are rarely seen. Therefore, it is likely that the division rate is high, and a peroxisome does not spend a large amount of time in an elongated state once reaching a length whereby it is possible to divide. This time waiting for division once λ has been reached can be represented by $1/\beta\lambda$. An estimation of this time of around 10 minutes (which would mean elongations in wild-type cells are rarely seen), β can be estimated at 2×10^{-5} /nm/s.

In the above analysis of the mathematical model, the parameters α and γ only appear in the combination $e^{-\gamma n\langle A\rangle}\alpha$, the effective lipid flow rate for the average peroxisome. These parameters are also hard to fit experimentally. This means that steady state cannot be used to determine their values. Instead, the length of the transient period (the time it takes the system to reach the quasi-steady state) can be used to estimate α and γ. Estimating a biologically-sensible transient period of a few tens of hours results in a value of α of 75 nm^2/s. Once fixed, the

equation $e^{-\gamma n\langle A\rangle}\, n\alpha\Delta t = n\langle A\rangle\Delta t/\tau$, equating lipid flow into and out of the system, can be used to derive γ, and results in a value of approximately 2.4×10^{-7} /nm^2.

In order for all lipid flowing into the peroxisome when elongating to only be used for elongation growth, the value for elongation speed v must satisfy $\pi w v > e^{-\gamma n\langle A\rangle}\alpha$. Using the derived values of w, α, γ, n and $\langle A\rangle$ as previously, a lower bound of 7×10^{-4} nm/s is obtained. With all other wild-type parameters fixed, a value of 0.3 nm/s results in the best match for reflecting the target steady state values when simulated.

4.2.3 Model Simulation

The programming language MATLAB (version R2017a, The MathWorks Inc.) was used for simulation of the mathematical model. The workflow of numerical simulation of the model (Figure 4.3) is as follows.

Before the main loop (over time), constants and variables need to be defined, using the derivations described above for the wild-type model. The initial starting conditions of the peroxisomal population are also set up (Table 4.3), drawing the dimensions of each individual peroxisome from a truncated normal distribution (whilst also ensuring unphysical negative values are avoided).

	μ	**σ**	**Truncation**
n	215	0	-
f	0.25	0	-
r	80	30	$50 \leq r \leq 110$
L	30	50	$0 \leq L \leq 80$

Table 4.3: Distributions used for initial conditions of the model simulation. μ, mean, σ, standard deviation, n, number of peroxisomes, f, fraction of peroxisomes elongated, r, peroxisome body radius, L, peroxisome elongation length.

As simulation time progresses in the main loop, at each timestep i, a single peroxisome (labelled by j) will go through each of the steps in growth and division in sequence, governed by the main modelling parameters (Figure 4.2). Firstly, if lipid is available, the peroxisome body radius will increase in size. Secondly, provided the peroxisome body radius is large enough (both larger than r_{min}, and with enough area to form an extension), the elongation length will increase. Next,

if the peroxisome elongation has reached λ and a randomly-chosen number is less than $\beta L \Delta t$, the peroxisome elongation will split into new peroxisomes all with diameter $\sqrt{w\lambda/2}$. Any leftover membrane area whereby the length of the elongation is not exactly divisible by λ will go into one daughter peroxisome, to avoid a peroxisome with diameter less than λ. After the division step, the peroxisome (x,y) position and the elongation angle (θ) both diffuse, whilst always keeping the body and elongation within the cell boundary. Finally, the peroxisome may be degraded governed by parameter τ.

The main loop will progress until one of the following situations arise: (i) a maximum time limit has been reached, (ii) a maximum peroxisome number has been reached, (iii) all peroxisomes have been degraded, or (iv) steady state has been reached. Steady state is determined by sufficiently small fluctuations in n, $\langle \mathrm{r} \rangle$ and $\langle \mathrm{L} \rangle$ over time, assessed by tracking the relative standard deviation (standard deviation σ divided by mean μ) for each of the three characteristics over a period of time. When the average relative standard deviation of all three over this time is below a cut-off value (taken as 0.01), the system is considered to have reached steady state.

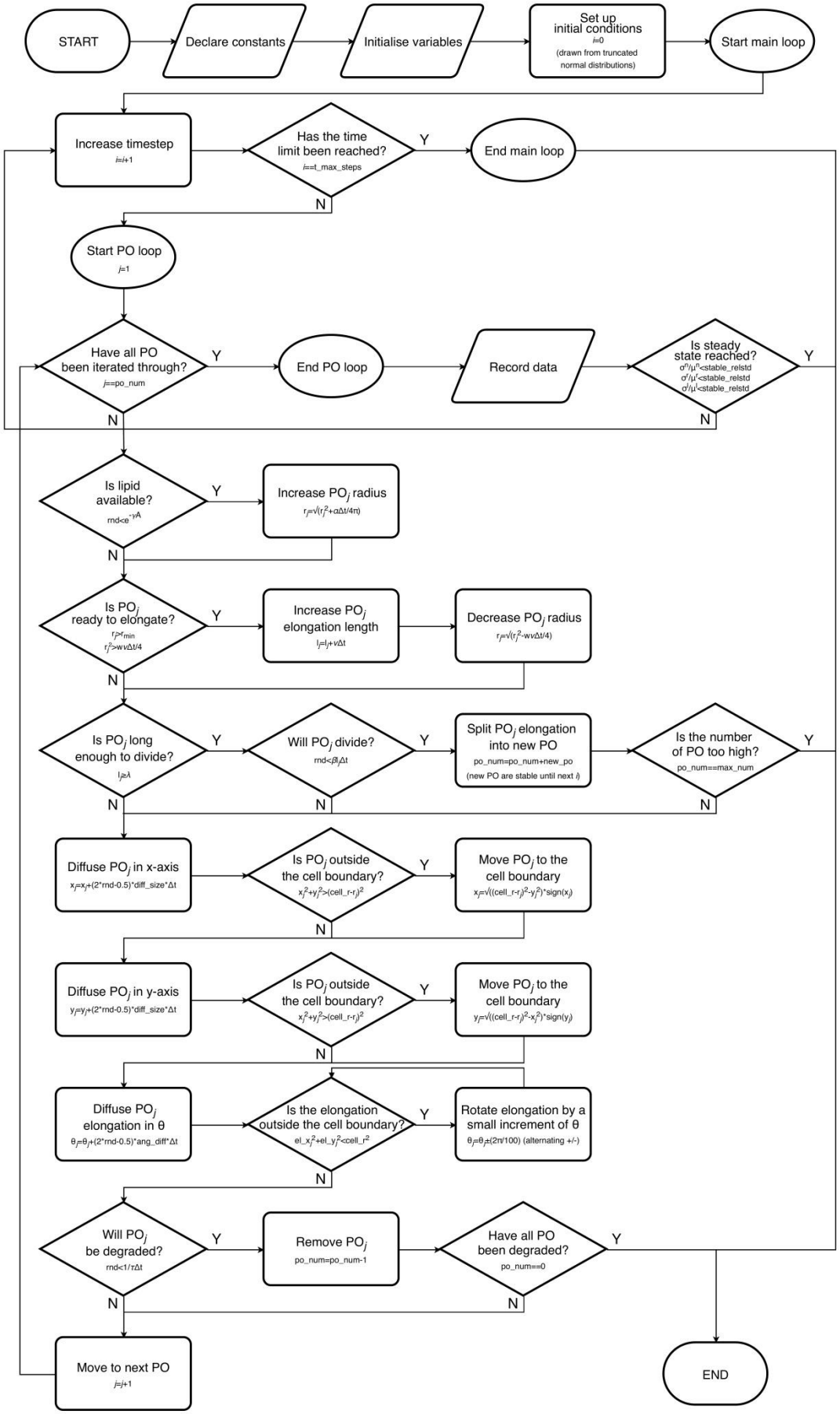
START
Declare constants
Initialise variables
Set up initial conditions
i=0
(drawn from truncated normal distributions)
Start main loop
Increase timestep
i=i+1
Has the time limit been reached?
i==t_max_steps
Y
End main loop
N
Start PO loop
j=1
Have all PO been iterated through?
j==po_num
Y
End PO loop
Record data
Is steady state reached?
σ^n/μ^n<stable_relstd
σ^l/μ^l<stable_relstd
σ^l/μ^l<stable_relstd
Y
N
Is lipid available?
rnd<e^-γA
Y
Increase PO_j radius
r_j=√(r_j^2+aΔt/4π)
N
Is PO_j ready to elongate?
r_j>r_min
r_j^2>wvΔt/4
Y
Increase PO_j elongation length
l_j=l_j+vΔt
Decrease PO_j radius
r_j=√(r_j^2-wvΔt/4)
N
Is PO_j long enough to divide?
l_j≥λ
Y
Will PO_j divide?
rnd<βl_jΔt
Y
Split PO_j elongation into new PO
po_num=po_num+new_po
(new PO are stable until next i)
Is the number of PO too high?
po_num==max_num
Y
N
N
N
Diffuse PO_j in x-axis
x_j=x_j+(2*rnd-0.5)*diff_size*Δt
Is PO_j outside the cell boundary?
x_j^2+y_j^2>(cell_r-r_j)^2
Y
Move PO_j to the cell boundary
x_j=√((cell_r-r_j)^2-y_j^2)*sign(x_j)
N
Diffuse PO_j in y-axis
y_j=y_j+(2*rnd-0.5)*diff_size*Δt
Is PO_j outside the cell boundary?
x_j^2+y_j^2>(cell_r-r_j)^2
Y
Move PO_j to the cell boundary
y_j=√((cell_r-r_j)^2-x_j^2)*sign(y_j)
N
Diffuse PO_j elongation in θ
θ_j=θ_j+(2*rnd-0.5)*ang_diff*Δt
Is the elongation outside the cell boundary?
el_x_j^2+el_y_j^2<cell_r^2
Y
Rotate elongation by a small increment of θ
θ_j=θ_j±(2π/100) (alternating +/-)
N
Will PO_j be degraded?
rnd<1/τΔt
Y
Remove PO_j
po_num=po_num-1
Have all PO been degraded?
po_num==0
Y
N
N
Move to next PO
j=j+1
END

Figure 4.3: The peroxisome model flow. Shape meanings: parallelograms – input/output, rectangles – actions, ellipses – loops, diamonds – decisions. Abbreviations: PO – peroxisome, Y – yes, N – no, *i* – current timestep, t_max_steps – maximum time limit, *j* – current peroxisome, po_num – current number of peroxisomes, stable_relstd – relative standard deviation when system is considered stable, rnd – randomly generated number between 0 and 1, new_po – number of 'daughter' peroxisomes, max_num – maximum peroxisome number, diff_size – diffusion jump in x and y, cell_r – radius of cell, sign(x) – sign of variable x (+1 or -1), ang_diff – diffusion jump in θ, el_x – x position of end of peroxisome elongation, el_y – y position of end of peroxisome elongation.

4.3 Results

4.3.1 The Model can Describe a Wild-Type Peroxisome Population

Using the parameter values derived above from the wild-type target values, time-course simulations were performed, following the simulation rules outlined in section 4.2.2, continuing until the model reached a steady state. A snapshot of the model at steady state revealed that the *in silico* model looks remarkably similar to a wild-type peroxisome population; peroxisomes were mostly punctate, with a narrow distribution of radii, and few small elongations visible (Figure 4.4).

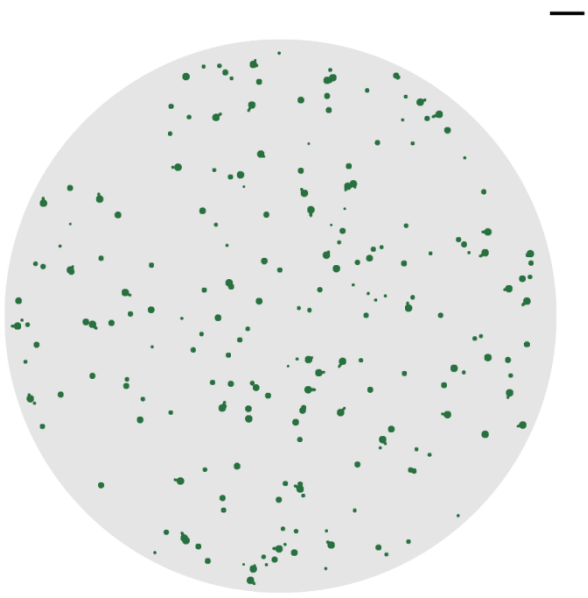

Figure 4.4: Snapshot of model simulation at steady state with wild-type parameters. The model was run with wild-type parameters (α = 75 nm^2/s, γ = 2.4 × 10^{-7} /nm^2, β = 2 × 10^{-5} /nm/s, v = 0.3 nm/s, τ = 1.5 × 10^5 s) until steady state was reached. Scale bar, 1 μm.

To investigate further, during the whole model simulation, the peroxisome number n, the average radius $\langle r \rangle$, the average length $\langle L \rangle$, and the fraction of peroxisomes with extensions f were tracked and plotted (Figure 4.5A-D). In addition, the distribution of peroxisome radii and length at steady state were

recorded (Figure 4.5E, F). Note the similarities between the average values obtained from the model (dashed lines) with the desired wild-type values in Table 4.1, suggesting that the model is able to capture a wild-type peroxisome population.

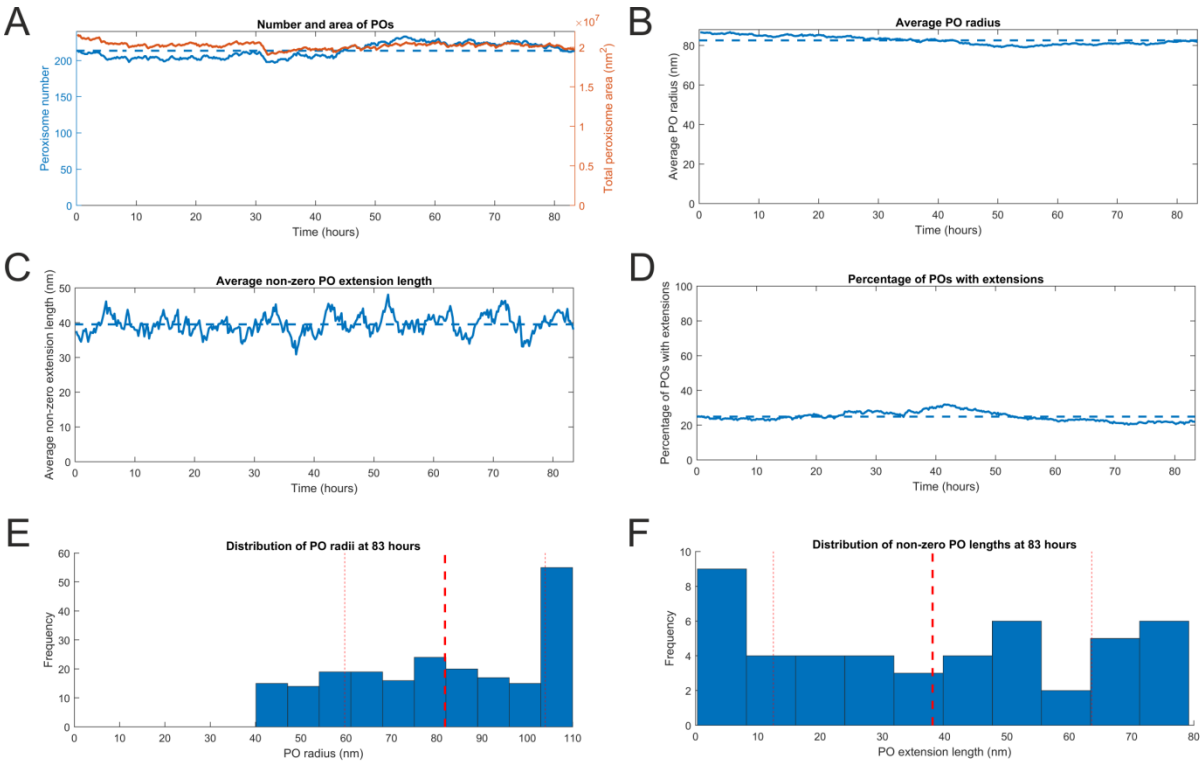

Figure 4.5: Peroxisome population characteristics over a single time-course simulation of the wild-type peroxisome model. A) The number (blue line) and total area (red line) of peroxisomes (POs) over the same single time-course simulation of the model as in Figure 4.4, with wild-type parameters (α = 75 nm^2/s, γ = 2.4 × 10^{-7} /nm^2, β = 2 × 10^{-5} /nm/s, v = 0.3 nm/s, τ = 1.5 × 10^5 s). The simulation was performed until the model reached steady state. The dotted line represents the mean number over the whole simulation. **B-D**) As in A, for the mean PO radius, mean (non-zero) PO length, and percentage of POs elongated, respectively. **E**) Histogram representing the distribution of PO radii at steady state. Dotted lines represent the mean (thick line) ± standard deviation (thin lines). **F**) As in E, for the distribution of non-zero elongation lengths.

Due to the stochastic nature of the model, the simulation output will change from run-to-run. To get accurate estimates for n, $\langle r \rangle$, $\langle L \rangle$ and f (including the r and L steady-state distributions), the simulation was run 500 times for 100 hours each, with values averaged at the end (Figure 4.6). All 500 simulations reached steady-state within this 100 hour time period. The mean values at 100 hours following 500 simulations again confirm the chosen wild-type parameter values accurately reflect a wild-type peroxisome population.

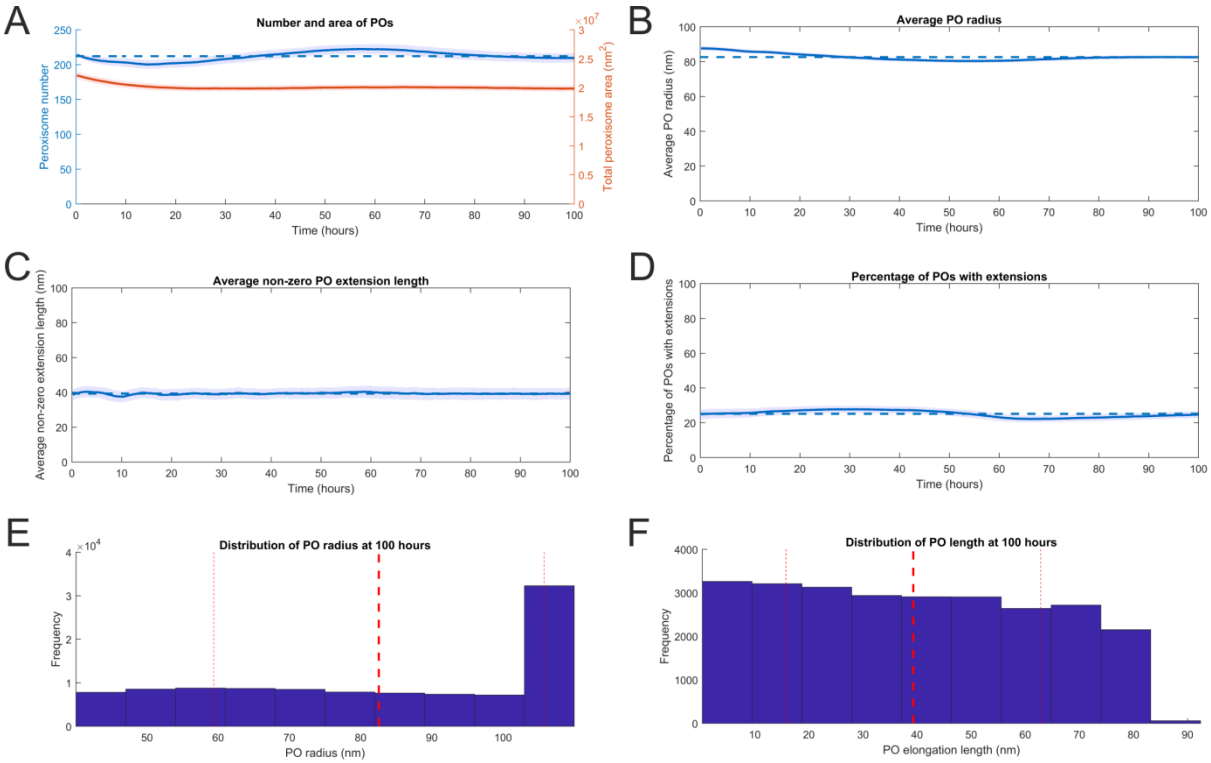

Figure 4.6: Average peroxisome population characteristics over 500 time-course simulations of the wild-type peroxisome model. A) The mean number (blue line) and mean total area (red line) of peroxisomes (POs) over 500 individual time-course simulations of the model run for 100 hours (past steady state) with wild-type parameters (α = 75 nm^2/s, γ – 2.4 × 10^{-7} /nm^2, β = 2 × 10^{-5} /nm/s, ν = 0.3 nm/s, τ = 1.5 × 10^5 s). Shaded areas represent the mean (line) ± standard deviation. The dotted line represents the mean number over the whole of the time-course simulations. **B-D**) As in A, for the mean PO radius, mean (non-zero) PO length, and mean percentage of POs elongated, respectively. **E**) Histogram representing the distribution of all PO radii from all 500 simulations at steady state. Dotted lines represent the mean (thick line) ± standard deviation (thin lines). **F**) As in E, for the distribution of non-zero elongation lengths.

Initial conditions (Table 4.3) were chosen close to the desired wild-type values in order to reduce the length of the transient period between the start of the simulation and reaching steady state. To verify that there are no other steady states (other than the trivial n = 0 steady state) i.e. to check the steady state of the model is not influenced by the initial starting conditions, the simulation was performed with various initial conditions (Figure 4.7). Varying the initial conditions in this way varied the time that the simulation reached steady state but showed that the final steady state values all converged over time. Varying the initial peroxisome number (Figure 4.7A) and initial mean non-zero peroxisome extension length (Figure 4.7C) resulted in steady state being reached within normal times (<100 hours). Interestingly, varying the initial mean peroxisome radius (Figure 4.7B) and initial percentage of peroxisomes with extensions (Figure 4.7D) by the same factors resulted in a much longer time to reach steady

state (>100 hours). Despite this, all lines reached the same steady state over time, suggesting that each parameter set leads to only one non-zero steady state regardless of initial conditions.

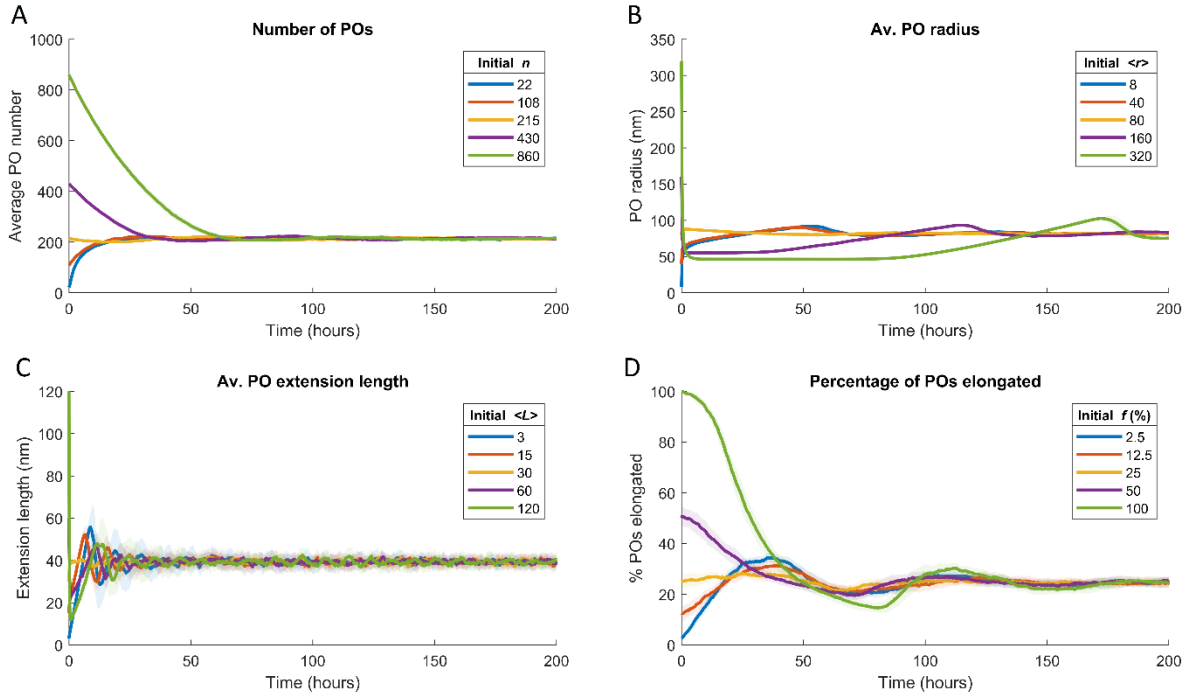

Figure 4.7: Varying initial conditions results in the same steady state for the wild-type peroxisome model. A) Time-course simulations of the wild-type peroxisome model (α = 75 nm^2/s, γ = 2.4 × 10^{-7} /nm^2, β = 2 × 10^{-5} /nm/s, v = 0.3 nm/s, τ = 1.5 × 10^5 s) were performed for 200 hours of simulation time varying the initial number of peroxisomes (POs) n. The line represents the mean PO number of 20 simulations, with shaded area representing ± standard deviation of the mean. B-D) as in A, with variations in mean PO radius $\langle r \rangle$, mean PO (non-zero) elongation length $\langle L \rangle$, and percentage of POs with extensions f, respectively. Note the convergence of all lines to the same steady state values over time.

4.3.2 Individual Parameters Affect the Steady State in Distinct Ways

To assess the influence of parameters on the model steady state, a range of the parameters α, γ, β, v, and τ were used for time-course simulations, and the mean and standard deviation of the final steady state values from 10 runs recorded (Figure 4.8).

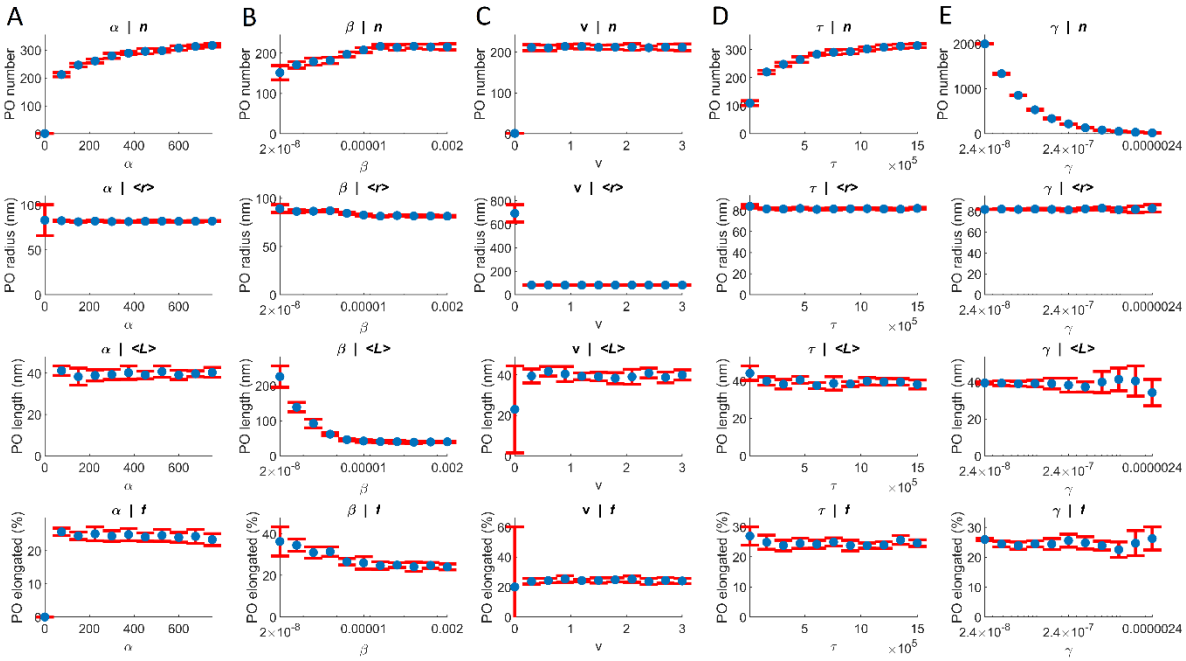

Figure 4.8: Varying parameters changes the steady state. A) Time-course simulations were run of the wild-type model parameters, varying the value of α only. The number of peroxisomes n, the average peroxisome radius ⟨r⟩, the average non-zero peroxisome elongation length ⟨L⟩, and the percentage of peroxisomes elongated f at the end the time-course simulations were tracked. Dots represent the mean of 10 simulations, and error bars show the standard deviation of the mean. **B-E)** As in A, varying the values of parameter β, v, τ and γ, respectively.

First, an increased lipid flow rate α interestingly does not result in an increased steady-state peroxisome radius, despite α directly influencing peroxisome radius in the mathematical model (Figure 4.8A). Instead, an increase in α results in an increase in peroxisomal number (Figure 4.8A). This is likely due to the effect of α in the equation $e^{-\gamma n\langle A\rangle}\,\alpha = \langle A\rangle/\tau$, equating lipid flow into and out of the system. As changing α does not affect the amount of lipid leaving the system (the radius and length of individual peroxisomes are unchanged, leaving ⟨A⟩ unchanged), an increase in α means that the exponent $e^{-\gamma n\langle A\rangle}$ must decrease in order to conserve lipid. With ⟨A⟩ and γ unchanged, the number of peroxisomes must then increase.

High values of β do not affect the steady-state values (Figure 4.8B), because as β increases, the probability of division, $\beta L\Delta t$, effectively becomes 1. At low values of β this probability of division is greatly reduced, resulting in an increase in peroxisome elongation length and a greater frequency of elongated peroxisomes, accompanied by a decrease in peroxisome number, as expected (Figure 4.8B).

Interestingly, except for the situation of v = 0 nm/s (or for very low values of v, whereby extensions cannot effectively form, resulting in a large radius increase

until all peroxisomes are degraded), changing v without changing other parameters has no effect on the overall steady state (Figure 4.8C). Even for high values of v, where the extension should grow quickly, the non-zero elongation length is unchanged. This is most likely due to the fact that at high speeds, elongations cannot grow due to lack of available lipid. In addition, due to the high wild-type value of β elongations almost instantly divide, removing the possibility for large extension elongation. Therefore, while v appears to have no effect when changed on its own, it is likely that effects will only be seen when changed in combination with other parameters.

As expected, increasing the average peroxisome lifetime τ results in an increase in peroxisome number, while the peroxisome radius, elongation length and frequency of elongations are unchanged (Figure 4.8D). As with α, this increase appears not to be exponential, and appears to begin to level above 300 peroxisomes. This is likely due to the effect of γ in limiting the available lipid flow. It is possible that changing γ in addition to τ or α will result in a higher increase in steady-state peroxisome number.

Confirming this, reducing the limitation on lipid flow by reducing the lipid flow constant γ results in a large increase in peroxisome number, even with α and τ unchanged (Figure 4.8E).

Several simulations finished without reaching a typical steady state, either because (i) the maximum number of peroxisomes was reached, (ii) all peroxisomes were degraded (steady state $n = 0$), or (iii) the simulation did not reach steady state within the maximum time limit (Figure 4.9). For example, with $\alpha = 0$ nm^2/s lipid cannot flow into the peroxisomes to increase body radius, all peroxisomes were removed (Figure 4.9A). With a low value of γ, where the lack of limitation on lipid results in a large increase of steady-state peroxisome number, the maximum number of peroxisomes was reached at $\gamma = 2.4 \times 10^{-8}$ /nm^2 (Figure 4.9E), however it can be expected that the simulation would have reached steady state if this maximum number was increased. The division rate β at low values results in an increase of peroxisome length at steady state. As there is still some chance of peroxisome degradation in the values chosen, steady state is possible (Figure 4.9B). However, it can be expected that as β approaches 0 /nm/s, the inability to divide will lead to the steady state of $n = 0$ peroxisomes. Similarly to α

and β, when v = 0 nm/s, no extensions are formed, meaning pexophagy degrades all peroxisomes and the steady state is again n = 0 peroxisomes (Figure 4.9C). Interestingly, while τ appears to increase steady state peroxisome number with a similar affect as α, high values of τ caused the simulation to fail due to the maximum time limit being reached (Figure 4.9D). This indicates that a sudden increase in α reaches the new steady state quicker than an equivalent sudden increase in τ (here, equivalent is meaning values of α and τ that result in the same steady-state number of peroxisomes).

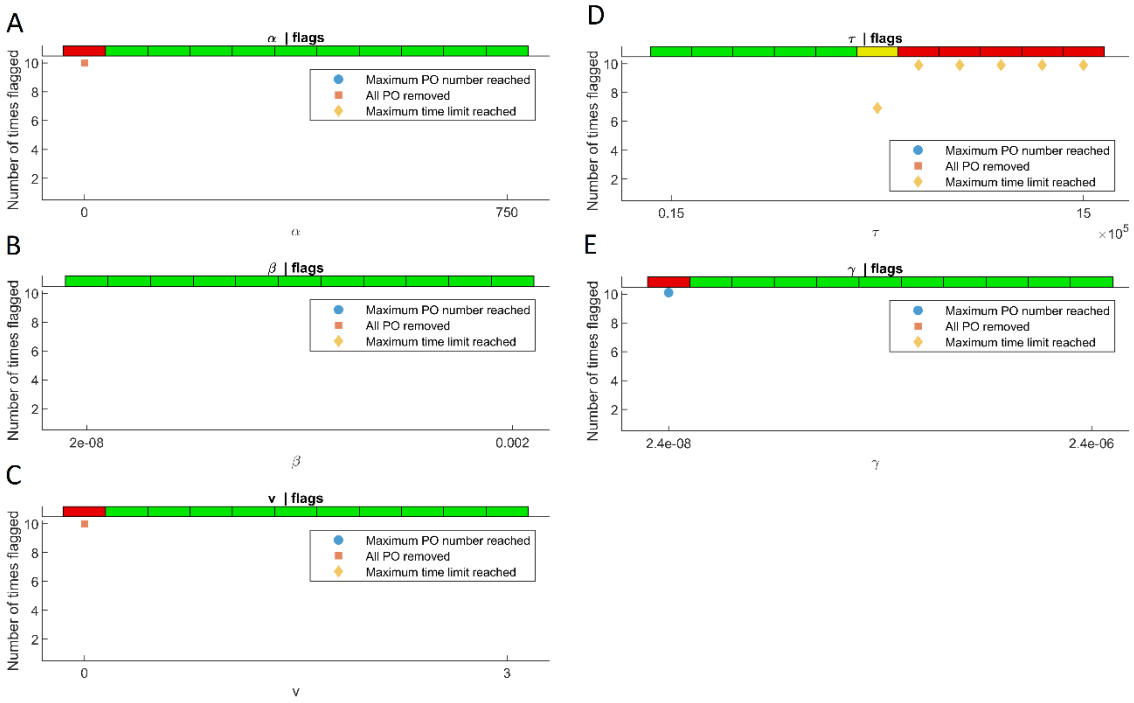

Figure 4.9: Varying parameter values results in several situations where steady state is not reached. A) Time-course simulations were run using wild-type parameter values, varying the value of α only (corresponding to Figure 4.8). The reason for termination (flag) of each time-course simulation was recorded. Top panel represents the number of times the simulation was flagged for each value of α (green – 0 times, yellow – between 0 and 10 times, red – 10 times). Bottom panel displays the reason for termination and how many times the model failed for this reason (blue circle – maximum peroxisome number reached, orange square – peroxisomes all degraded, yellow diamond – maximum time limit reached). **B-E)** As in A, varying the values of parameter β, v, τ and γ, respectively.

Assessing the effect of individual parameters allows for preliminary conclusions to be drawn on the main parameters influencing peroxisome growth and division, and potentially gives insight into which parameters may be affected in patients with a certain peroxisome phenotype.

4.3.3 Peroxisomal Alterations can be Reliably Modelled

4.3.3.1 Modelling Patient Cells - Mitochondrial Fission Factor (MFF)

Patients with a defect in dual-localised peroxisome-mitochondrial tail-anchored membrane protein MFF show fewer, highly elongated peroxisomes compared to controls (see Chapter 2). MFF is a major component of the peroxisome division machinery (Itoyama et al. 2013), meaning alterations in MFF levels are therefore likely to be captured by alterations in the division rate parameter β. Model simulations were performed using the same parameters as the wild-type peroxisome model, but with β reduced to effectively zero (from 2×10^{-5} /nm/s to 2×10^{-15} /nm/s), in order to simulate a loss-of-function in MFF. A snapshot of this model at 100 hours revealed an altered morphological phenotype in a similar manner to that of patients with MFF deficiency; reduced peroxisome number and a substantial increase in peroxisome elongation length (Figure 4.10). Due to the stochastic way the model was implemented, a range of peroxisome lengths are produced, as also observed in MFF-deficient patient cells (Figure 3.1).

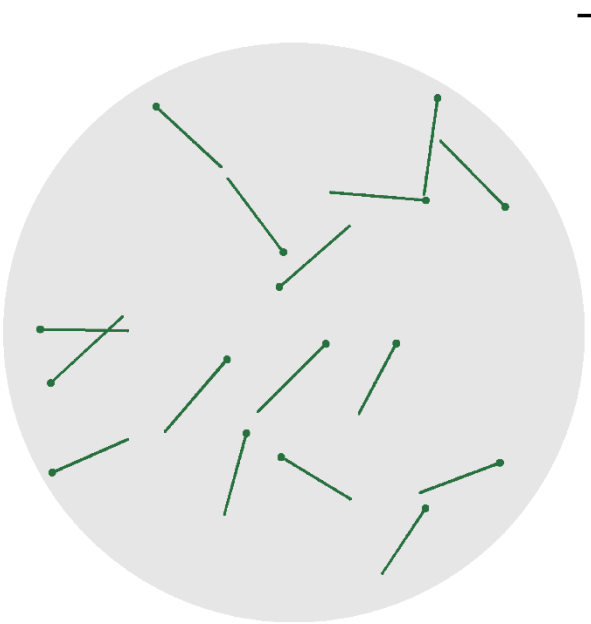

Figure 4.10: Snapshot of the MFF-deficient patient cell model simulation at 100 hours. The model was run with MFF parameters (α = 75 nm^2/s, $\gamma = 2.4 \times 10^{-7}$ /nm^2, $\beta = 2 \times 10^{-15}$ /nm/s, ν = 0.3 nm/s, $\tau = 1.5 \times 10^5$ s) for 100 hours. Scale bar, 1 μm.

Further simulation of the MFF-deficient model revealed that the steady state was $n = 0$, due to the presence of a steady peroxisome turnover with practically no capability to increase peroxisome number through division. As this is not observed in MFF-deficient cells, but peroxisomes in these cells are capable of being degraded by autophagic processes (Figure 3.6), this indicates that either (i) there is a mechanism whereby peroxisomes can increase in number without MFF (*de novo* peroxisome biogenesis, or MFF-independent fission), (ii) that MFF-deficient cells, while capable of it, have a reduced degradation of peroxisomes, or (iii) that pexophagy rate is not constant, but decreases when there are only a few peroxisomes (i.e. $\tau = \tau(n)$). In order to model scenario (ii), simulation of the MFF-deficient model with no peroxisome degradation (i.e. an infinite average peroxisome lifetime τ) was performed (Figure 4.11). Under these conditions, there is effectively no mechanism for peroxisomes to increase or decrease in number, so the initial number of peroxisomes will not change. Therefore, to match with measured values, the initial number of peroxisomes was set to 30.

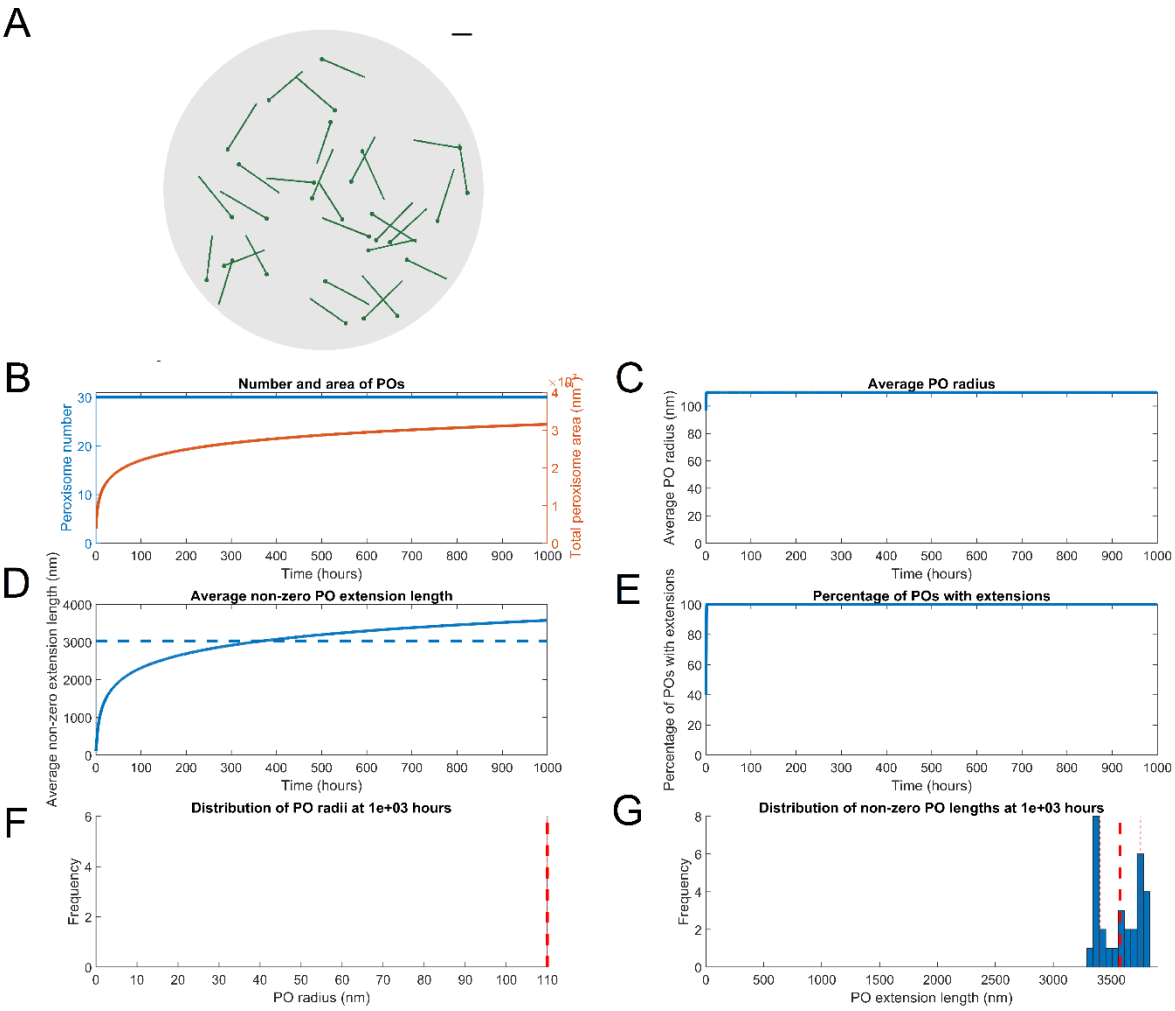

Figure 4.11: The MFF-deficient patient cell model, with peroxisome degradation removed. A) A snapshot of the MFF-deficient patient model with pexophagy removed (i.e. an infinite average peroxisome lifetime τ) removed (α = 75 nm^2/s, γ = 2.4 × 10^{-7} /nm^2, β = 2 × 10^{-15} /nm/s, v = 0.3 nm/s, $\tau = \infty$) at 100 hours. **B)** The number (blue line) and total area (red line) of peroxisomes (POs) over a single time-course simulation. The simulation was performed until the model reached the maximum time limit (1000 hours). The dotted line represents the mean number over the whole time-course simulation. **B-E**) As in B, for the mean PO radius, mean (non-zero) PO length, and percentage of POs elongated, respectively. **F**) Histogram representing the distribution of PO radii at steady state. Dotted lines represent the mean (thick line) ± standard deviation (thin lines). **G**) As in F, for the distribution of non-zero elongation lengths.

Modelling MFF-deficient cells with no peroxisome turnover again resulted in a population of peroxisomes with increased elongation at 100 hours (Figure 4.11A) as expected. With no possibility for peroxisome degradation, the steady state can no longer be that of no peroxisomes ($n = 0$). However, in this situation, steady-state was not reached within the maximum time limit (Figure 4.11B-G) as peroxisome elongations continued to elongate (Figure 4.11D). Due to the limitation on lipid availability imposed by γ, the rate of elongation growth declines over time, and the system can be expected to reach steady state after a long period of simulation time. It is therefore likely that additional components are needed to more accurately model the experimentally measured MFF-deficient cells' steady state.

Despite the inability of the MFF-deficient model to reflect the MFF-deficient cell steady state, it is still able to reliably reflect changes to morphological observations with an alteration in only one parameter. To explore this further, further alterations in protein levels in the same cells were modelled. A reduction in peroxisome-ER tethering in MFF-deficient patient cells (by silencing the peroxisome-ER tethering protein ACBD5), results in a reduction of peroxisome length in these cells, while still maintaining the reduced peroxisome number due to lack of division components (Costello et al. 2017b). As peroxisome-ER physical tethering likely facilitates the flow of membrane lipid from the ER into the peroxisome, to model the reduction of ACBD5 in MFF-deficient cells the lipid flow rate α was reduced (from 75 nm^2/s to 5 nm^2/s), in addition to reducing β to 2 × 10^{-15} /nm/s. Simulations of the MFF-deficient, ACBD5 silenced model showed a morphological phenotype as expected from the experimental observations; reduced peroxisome number in a similar manner to the MFF-deficient model, but a less remarkable increase in peroxisome elongation length (Figure 4.12). In addition to the MFF-deficient model, the MFF-deficient, ACBD5 silenced model

also reaches the steady state of $n = 0$ in the same time due to peroxisome turnover.

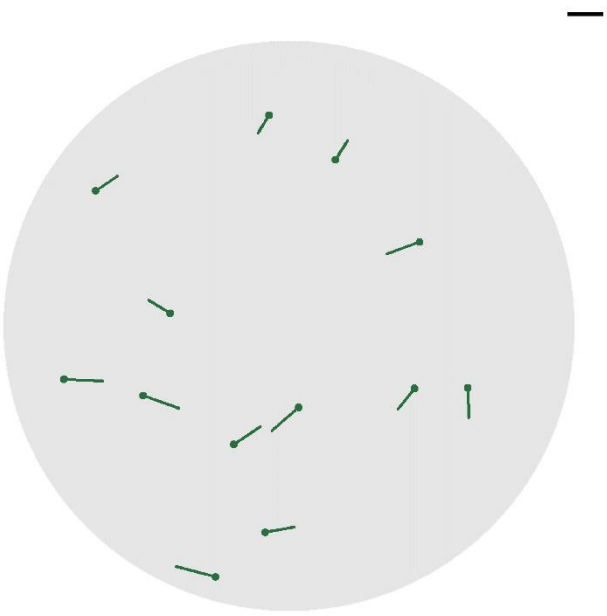

Figure 4.12: Snapshot of the MFF-deficient, siACBD5 patient cell model simulation at 100 hours. The model was run with MFF parameters, with reduced lipid flow to simulate silencing of ACBD5 (α – 5 nm^2/s, γ – 2.4 × 10^{-7} /nm^2, β – 2 × 10^{-15} /nm/s, v – 0.3 nm/s, τ – 1.5 × 10^5 s) for 100 hours. Scale bar, 1 μm.

Overall these results show that this simple, preliminary model can accurately reflect changes in morphology in MFF-deficient cells, as well as the more complex case of ACBD5 silencing in these cells. These changes in patient cells were captured by changing only single parameters, demonstrating the ability of the model to predict which processes in cells are likely to be disturbed under various conditions, including in patients.

4.3.3.2 Modelling Protein Expression - Mitochondrial Rho GTPase 1 (MIRO1)

To further understand the ability of the model to reflect alterations in cells induced by protein levels, the effects of MIRO1 levels in various cell types were investigated. MIRO1 is a regulator of mitochondrial motility, through the formation of a motility complex with the adaptor proteins TRAK1 and 2, and molecular motors kinesin and dynein (Fransson et al. 2006). MIRO1 can also bind PEX19, has some peroxisomal localisation, and overexpression in COS-7 and HeLa causes peroxisomes to localise to the cell periphery, inhibited in the presence of nocodazole (Castro et al. 2018; Okumoto et al. 2018). This effect is also seen when kinesin motors are recruited to peroxisomes (Kapitein et al. 2010). Together,

these data point towards a role of MIRO1 in the regulation of peroxisome motility through facilitating the interaction of peroxisomes with microtubules. When expressed in fibroblasts, MIRO1 induces proliferation of peroxisomes, likely due to pulling forces increasing elongation, which can then quickly divide into new peroxisomes (Castro et al. 2018). These elongations can be seen when MIRO1 is expressed in cells with impaired lipid metabolism (PEX5 deficient cells) causing compromised peroxisome proliferation (Castro et al. 2018). PEX5 deficient cells typically show enlarged peroxisomal 'ghosts' that are fewer in number, but following MIRO1 expression, a mixed phenotype is seen, with a mix of spherical and elongated peroxisomes, and a range of peroxisome lengths.

The various effects of MIRO1 in inducing changes in peroxisome membrane morphology and dynamics present an interesting modelling challenge. In order to see if the model can encapsulate these phenotypes, and then therefore allow conclusions to be inferred on the physical processes underlying these alterations, the model was used to simulate MIRO1 expression in wild-type COS-7 cells, MIRO1 expression in fibroblasts, PEX5 deficient fibroblasts, and MIRO1 expression in PEX5 deficient fibroblasts.

As MIRO1 likely links peroxisomes to the microtubules, and overexpression causes observable peroxisome elongations, MIRO1 overexpression is modelled by an increase in peroxisome elongation speed v (from 0.3 nm/s to 3 nm/s). As demonstrated previously (Figure 4.8), an increase in v does not typically induce any significant change in peroxisome morphology. Therefore, a MIRO1 overexpression model changing only parameter v results in a morphological phenotype similar to the wild-type model (Figure 4.13). This is consistent with the observation that in wild-type COS-7 cells, overexpression of MIRO1 has no effect on peroxisome number or morphology, instead only inducing accumulation of peroxisomes at the cell periphery (Castro et al. 2018).

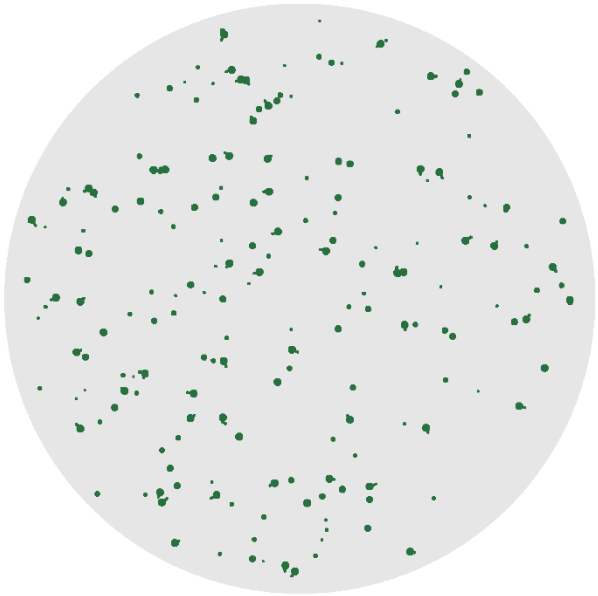

Figure 4.13: Snapshot of the MIRO1 expression in COS-7 cells model simulation at 100 hours. The model was run with wild-type parameters, with increased elongation extension speed to simulate expression of MIRO1 in COS-7 cells (α = 75 nm^2/s, γ = 2.4 × 10^{-7} /nm^2, β = 2 × 10^{-5} /nm/s, v = 3 nm/s, τ = 1.5 × 10^5 s) for 100 hours. Scale bar, 1 µm.

Conversely, MIRO1 overexpression in wild-type fibroblasts induces peroxisome proliferation, with no overall effect on peroxisome morphology (Castro et al. 2018). In order to model this phenotype, manipulation of v alone is insufficient, and requires an accompanying decrease in the lipid flow constant γ (from 2.4 × 10^{-7} /nm^2 to 1.2 × 10^{-7} /nm^2) to observe an increased peroxisome number with no other alteration to peroxisome characteristics (Figure 4.14).

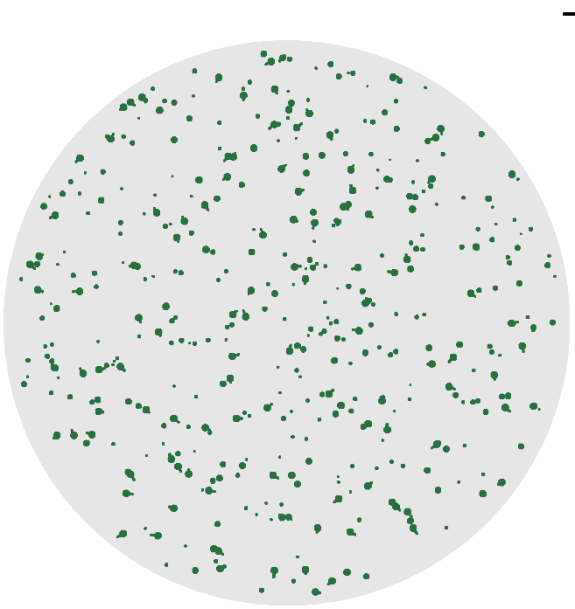

Figure 4.14: Snapshot of the MIRO1 expression in fibroblasts model simulation at 100 hours. The model was run with wild-type parameters, with increased elongation extension speed and decreased lipid constant to simulate expression of MIRO1 in fibroblasts (α = 75 nm^2/s, γ = 1.2 × 10^{-7} /nm^2, β = 2 × 10^{-5} /nm/s, v = 3 nm/s, τ = 1.5 × 10^5 s) for 100 hours. Scale bar, 1 μm.

The peroxisome phenotype in PEX5 deficient cells is that of an enlarged body, and fewer total number (Castro et al. 2018). The impaired lipid metabolism in these patient cells likely impacts the elongation and division pathways but not growth; peroxisomal ghosts such as those with PEX5 deficiency are incapable of elongation and subsequent division when supplemented with DHA, in contrast to controls and those of a single enzyme deficiency (Itoyama et al. 2012), but are enlarged, consistent with an unaltered lipid supply to the peroxisome. Therefore, PEX5 deficient fibroblasts are modelled by reducing both the elongation speed v (from 0.3 nm/s to 3 × 10^{-5} nm/s) and the division rate β (from 2 × 10^{-5} /nm/s to 2 × 10^{-9} /nm/s). Simulation of the PEX5 deficient fibroblast model results in a phenotype as expected, reduced in number and enlarged in size, with very short elongations (Figure 4.15). Similar to the MFF deficient model, steady state in the PEX5 deficient model is at zero peroxisomes due to the reduced division capability, again highlighting the limitation of the model in being able to reflect steady state under certain mutant conditions.

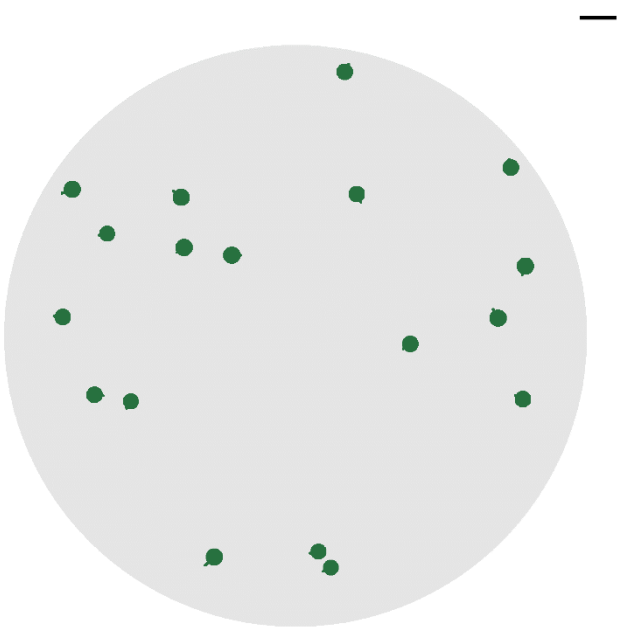

Figure 4.15: Snapshot of the PEX5 deficient patient fibroblasts model simulation at 100 hours. The model was run with wild-type parameters, with decreased elongation extension speed and decreased division rate to simulate loss of PEX5 in fibroblasts (α = 75 nm^2/s, γ = 2.4 × 10^{-7} /nm^2, β = 2 × 10^{-9} /nm/s, v = 3 × 10^{-5} nm/s, τ = 1.5 × 10^5 s) for 100 hours. Scale bar, 1 μm.

To assess the capability of the model to simulate more complex situations and combine confirmed model parameters, MIRO1 expression in PEX5 deficient fibroblasts was modelled by combining the two previously validated models. The MIRO1 expression model includes an increase in v, and the PEX5 deficiency model contains a decrease in v. As MIRO1-induced peroxisome elongations are artificial, v is taken as the MIRO1 expressed value of 3 nm/s. The other parameter values changed from wild-type for the PEX5 deficient and MIRO1 expressed models are γ and β, which are used as previously described, 1.2 × 10^{-7} /nm^2 and 2 × 10^{-9} /nm/s, respectively. Following simulation, the model again can reflect the morphological observations seen in these cells; a mixed population of elongated and spherical peroxisomes, with no change in overall peroxisome number (Figure 4.16).

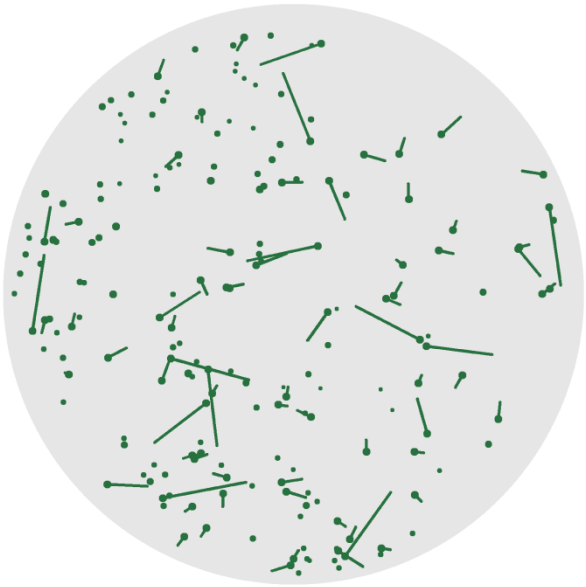

Figure 4.16: Snapshot of the PEX5 deficient, MIRO1 expressed fibroblast model simulation at 100 hours. The model was run with wild-type parameters, with increased elongation extension speed, decreased lipid flow constant and decreased devision rate to simulate loss of PEX5 and expression of MIRO1 in fibroblasts (α = 75 nm^2/s, γ = 1.2 × 10^{-7} /nm^2, β = 2 × 10^{-9} /nm/s, ν = 3 × 10^{-5} nm/s, τ = 1.5 × 10^5 s) for 100 hours. Scale bar, 1 μm.

Overall, these results show that in addition to modelling simple cases of patient cells with a defect in growth and division, where only a single parameter needs to be altered, the model can also reflect more complex cell types and protein expression.

4.4 Discussion

4.4.1 Discussion of Results

While what is presented here is a first-generation mathematical model of peroxisome membrane dynamics, it has been shown to already have the ability to encapsulate phenotypes seen in multiple scenarios and conditions.

Importantly, the model is not sensitive to changes in the initial conditions, with only a single (non-trivial) steady state for each set of parameter values. Therefore, it should only be through changing these parameters that any peroxisomal phenotype should be able to be reflected. Identifiability of the model, i.e. whether multiple sets of substantially-different parameter values yield similar steady states, is an important concern in understanding a mathematical model. For this

preliminary model, identifiability has not yet been extensively investigated but is unlikely to affect the qualitative conclusions.

When assessing the effects on these individual parameter changes, several notable unexpected patterns are observed, particularly (i) the effect of increasing α (rate of lipid flow into the body) is to increase peroxisome number rather than body radius, (ii) changing v (speed of elongation) on its own has no effect but requires multiple parameter changes to affect the steady state, and (iii) decreasing the rate of pexophagy increases peroxisome number at a slower rate than increasing α. These results shed further light on the complex relationship between these parameters, and possibly indicate cellular processes that are better targets for rescuing peroxisomal dysfunction. For example, in a patient with a decrease in peroxisome number, a naïve approach may be to target pexophagy in an attempt to reduce peroxisome turnover. However, the modelling indicates that a more efficient approach may be to increase lipid flow into the peroxisomes through, for example, manipulation of peroxisome-ER tethering components such as ACBD5.

Throughout these studies, results have been obtained by averaging multiple model simulations. Introducing noise, by implementing the mathematical model in a stochastic manner, adds a more realistic biological complexity. Some peroxisomal characteristics show more noise, particularly the peroxisomal non-zero elongation length. This is due to the stochastic way division is implemented, introducing a probability of division at any given time, influenced by the peroxisome length. This results in a distribution of lengths at any given time, with the mean length fluctuating following division of an elongated peroxisome. However, despite this noise, the mean peroxisomal elongation length at steady state varies little over time.

Patient cells with a defect in peroxisomal division protein MFF can be modelled by changing only one parameter, the division rate β. From this, the model suggests several conclusions on the underlying biophysical processes in these cells. The observation that control fibroblasts display large numbers of small, spherical peroxisomes, which turn into few, extremely elongated organelles upon blocking of peroxisomal division, indicates that membrane lipid flow rate, elongation growth speed and division rate must be high in fibroblasts under

normal conditions, allowing for quick growth and division. This may also suggest that peroxisome turnover is also high in fibroblasts in order to avoid an unchecked increase in peroxisome number. Despite a block in division, and the capability of peroxisomes in MFF deficient fibroblasts to be degraded (Figure 3.6), peroxisomes are still present in these cells. This suggests that in MFF deficiency, either (i) peroxisome turnover is altered to avoid complete degradation, (ii) that *de novo* peroxisome biogenesis or MFF-independent division provides a constant rate of new peroxisomes, or (iii) rates of pexophagy may be dependent on peroxisome number. In contrast, low membrane lipid flow rate, elongation speed or division rate in other cell types may result in a population of peroxisomes with reduced numbers and lengths. This is reflected by depletion of ACBD5, which impacts on peroxisome-ER tethering and membrane expansion, resulting in shorter peroxisomes in MFF-deficient cells (Costello et al. 2017b). This morphological change can also be captured in the model by reducing the lipid flow rate α in the MFF-deficient model, giving further evidence to the hypothesis of high lipid flow and division rates in fibroblasts, as well as suggesting that lipid flow, likely mediated by peroxisome-ER interactions, is a major contributor to peroxisome growth and division dynamics.

Through modelling further cellular alterations, MIRO1 expression in three different cell types (COS-7, fibroblasts, and PEX5 deficient fibroblasts), this relationship between cell types and cellular processes can be explored further. When expressed in COS-7, MIRO1 has no effect on peroxisome morphology. This model can capture this with an increase in v, as changing v alone does not affect peroxisome morphology due to insufficient lipid flow for expansion of the elongation. When expressed in fibroblasts, MIRO1 induces peroxisome proliferation. As expected, due to limitations of increasing v, this phenotype cannot be captured without also increasing lipid flow through altering the lipid flow constant γ. This further suggests that fibroblasts have an increased lipid flow compared to other cell types. Peroxisomes in fibroblasts deficient in PEX5 are larger and fewer in number. As previously identified, despite directly causing an increase in radius in the mathematical model, increasing the lipid flow rate itself is insufficient to increase peroxisome radius. Instead, this phenotype can be modelled by reducing the elongation speed v and the division rate β, in line with previous data of impaired elongation and division in peroxisomes from a patient

with Zellweger syndrome (Itoyama et al. 2012). In this case, a peroxisome morphological alteration can be modelled without directly equating the proteins involved to cellular processes, but still gives an insight into which processes are disturbed in these cells, confirmed by experimental data. This very clearly highlights the way in which this model could be useful in the future for the prediction of altered cellular processes in specific patient cells. MIRO1 expression in these cells results in a mixed spherical/elongated phenotype, which can also be modelled by combining the mathematical models for PEX5 deficient fibroblasts and MIRO1 expression in fibroblasts. This again emphasises the importance of introducing stochasticity; such a range of peroxisomes with different morphologies would not be possible without a degree of randomness in the model. The ability of the model to combine several alterations into one model highlights further future uses, in predicting morphological changes in patient cells under certain conditions.

Altogether, the results presented here demonstrate that this model, while preliminary, has enormous future potential in various aspects of peroxisome membrane dynamics, being able to reflect changes in peroxisome number, morphology and movement. It is hoped that in the future, a more mature iteration of the model can be used as a tool for (i) aiding in the understanding of the key processes underlying peroxisome dynamics in various cell types, (ii) helping to decipher which of these key processes are disturbed in patient cells with different peroxisomal alterations, (iii) investigating how peroxisomes in wild-type and patient cells may respond to various intracellular conditions and challenges, and (iv) understanding the precise way in which proteins with unknown or less well understood functions may interact with the peroxisomes to cause changes in peroxisome dynamics.

4.4.2 Further work

While the model presented shows great potential for future, there are clearly several limitations and areas that can be improved, checked, and added. These are summarised here.

First, some validation and investigation of the wild-type model is still to be performed. While the model appears not to give the same steady states for different parameter sets, a more sophisticated approach could be used to check

this in the future (Calvez and Hutzler 2005). This also links to the fact that the effects on the steady state of changing more than one parameter at a time were not investigated. While looking at individual parameters gives some idea of the specific effects of the parameters on the overall system, it is likely that parameters influence each other, affecting model outcomes. When investigated in full, it may then be easier to model more complex scenarios inside the cell.

As previously described, each individual peroxisome is taken simply as a sphere with an attached capped cylinder of constant width w. While this is similar to many peroxisomes viewed with EM (Figure 3.1), this idealised shape does not always accurately describe peroxisomes. For example, peroxisomes in cells devoid of DRP1 show a 'beads on a string' phenotype (Koch et al. 2004), which is unable to be captured in the current version of the model. In order to model this phenotype, an extra step of constriction would need to be added to the model rules, in addition to further changing the model representation of peroxisomal tubules. Constriction also appears to represent an important step in producing mature peroxisomes (see Chapter 2). In implementing constriction, further additions can be made, such as introducing a time lag waiting for the import of matrix proteins to pre-peroxisomal elongations, or the recruitment/competition of different machinery for constriction/division.

At present, the spatial position of peroxisomes has been largely ignored in the model, both in terms of motility and distribution of peroxisomes inside the cell. The effects of MIRO1 highlight that peroxisome growth and division is likely not so independent of peroxisome motility. It is also likely that motile peroxisomes are not tethered to the ER (Costello et al. 2017b), which is predominantly perinuclear. Therefore, it may be that peroxisomes are more likely to grow and divide closer to the centre of the cell, so a future extension of the model could take this into account by introducing an effect whereby motility and spatial distribution influences lipid flow into the peroxisome.

Cell division could also be included in the model. Analysing the effect of altering initial conditions of the model suggests that the peroxisomes can recover from large sudden changes in state, for example in reducing the peroxisome number by half as may happen during cell division. By implementing cell division as a sudden decrease by half of peroxisome number, it may give further insight into

the challenges that cells face when needing to proliferate peroxisomes after division. This may also give insights into ageing, by investigating how the peroxisome population can handle many repeated cell divisions.

An important limitation that was raised following investigation of MFF deficient patient fibroblasts is that the steady state of any model with a substantial block in division is $n = 0$. This led to the conclusion that there must be either *de novo* biogenesis of peroxisomes to maintain numbers, or that peroxisomes are somewhat protected from pexophagy when low numbers arise. To accurately model this, more investigation *in vitro* needs to be performed to discover the mechanisms of peroxisome retention in MFF deficient cells. Pexophagy in the model could be implemented in a less impartial manner, for example by ensuring that older peroxisomes are preferentially degraded (Cavallini et al. 2017). Pexophagy could also be implemented in a similar manner to the lipid flow constant γ, where it is influenced by the total peroxisome area in the cell.

Finally, several additions to the model could improve the aesthetics of the simulation. Peroxisomal elongations are rarely completely straight, with many extensions being curved or kinked. This is particularly noticeable in the case of the MFF deficient model. In addition, a more realistic cell shape, and the inclusion of a nuclear region, would improve model aesthetics.

4.5 Conclusion

In conclusion, this first-generation agent-based mathematical biophysical model of peroxisome membrane dynamics has provided a solid proof-of-concept that this approach is a useful tool for peroxisome research. By using a combined experimental-modelling approach, with the model both being based on and guiding experimental data, the model has already generated hypotheses of mechanisms of peroxisome regulation in various cell types, leading to conclusions on how this regulation is disturbed in patient cells, and aided in expanding the overall picture of growth and division of peroxisomes in mammalian cells. After addressing the limitations described above, future iterations of the model are likely to be powerful tools for helping in the understanding of peroxisomes, and the underlying cellular pathophysiology of patient cells.

Chapter 5 General Discussion

5.1 The Importance of Peroxisomal Membrane Dynamics

Peroxisomal membrane dynamics have been extensively studied over the past years, and the key proteins involved in peroxisomal growth and division described. However, (i) the contribution of this remodelling of the peroxisome membrane to other cellular processes than peroxisome proliferation, (ii) the exact way in which defects in peroxisome membrane dynamics contribute to health and disease, and (iii) the precise relationship between other cellular processes such as lipid flow into the peroxisome and regulation of peroxisomal growth and division are emerging topics.

Chapter 2 demonstrates that despite the close redox-sensitive relationship between peroxisomes and mitochondria, and that mitochondrial morphology and function is disturbed when peroxisomes undergo oxidative stress, peroxisome membrane dynamics are unaffected by ROS produced in the mitochondria. Instead, the respiratory chain inhibitor rotenone alters peroxisome morphology and distribution through its microtubule-destabilising activity, further highlighting the still unclear relationship between the cytoskeleton and the regulation of peroxisomal membrane dynamics. This study indicates that compounds known for affecting specific components of the cell such as mitochondria may also affect peroxisomes, and therefore that looking at how peroxisome membrane dynamics are altered may indicate other cellular alterations (e.g. an observed increase in peroxisomal elongation and clustering may suggest microtubule disruption). Rotenone is often used as a model for Parkinson's disease-like symptoms *in vivo*. However, as this study shows, it also affects peroxisomal dynamics, which have potential links to Parkinson's disease. Therefore, this may suggest that alterations to peroxisome dynamics play a more prominent role in the pathophysiology of the disease than previously thought. At a time when more diseases that affect peroxisome dynamics are being found and characterised more thoroughly, it is important that we understand the cellular consequences of defects in peroxisome dynamics.

Chapter 3 explores this further, by looking more in depth at one of the most drastic alterations to peroxisome morphology, loss of MFF. While MFF is a shared peroxisome-mitochondrial protein, much of the work investigating cellular consequences of lack of MFF has thus far focussed on the mitochondria. It was

shown in this chapter that in addition to mitochondrial elongation, peroxisomal abnormalities also arise, and may be major contributors to the pathophysiology of the disease. Peroxisomal metabolism in these cells is normal, but patients still display symptoms that are similar to those of PBDs (e.g. developmental delay, encephalopathy and peripheral neuropathy), highlighting the importance of maintaining proper peroxisome membrane dynamics inside the cell. Disruption of peroxisomal membrane dynamics by blocking division leads to hyper-elongated peroxisomes, which comprise mostly of membrane that displays reduced presence of matrix proteins, indicating MFF is a critical regulator of peroxisome maturation. This study also provides evidence that there are not only changes in peroxisome morphology, which impacts peroxisome positioning and motility, but also other peroxisomal parameters such as redox state and pH. This proves that peroxisome membrane dynamics are important in more than just the growth and division process affecting peroxisome morphology, and is adding to the growing amount of data suggesting peroxisome membrane dynamics are important in maintaining other peroxisome parameters.

Therefore, it is crucial that peroxisomal membrane dynamics are fully understood. Experimental approaches only allow for direct manipulation of cells and organelles to a certain point; more is needed to fully characterise and understand the regulation of peroxisome membrane dynamics. Chapter 4 provides a modelling workflow in which to do this; peroxisomal membrane dynamics can be described by a few simple parameters, and a mathematical, biophysical model built around these parameters. Simple manipulation of these parameters in a preliminary model already revealed several predictions of which processes are needed for maintenance of peroxisome growth and division, for example suggesting that lipid flow is a major contributor to maintenance of peroxisomes, and that peroxisome number is possibly more efficiently manipulated by targeting this lipid flow. Several case studies using experimental data on peroxisomal morphological alterations revealed further insight. For example, MFF-deficient patient cells likely have altered peroxisome turnover due to the reduced capability to increase in number. In addition, the various effects of the adaptor for microtubule-based motility MIRO1 in different cell types highlights that differences in peroxisomal dynamics between cell types are likely due to alterations in these model parameters; again the lipid flow into the peroxisome by

peroxisome-ER tethering was revealed as a crucial player, possibly providing a mechanism whereby peroxisomes can undergo growth and division more quickly in fibroblasts. While a first-generation model, this study serves as proof that it not only has the capacity when more developed to characterise peroxisomal membrane dynamics to help with future therapeutics, but also that this combined experimental-modelling approach is a powerful tool for investigating organelle dynamics.

In conclusion, this thesis provides evidence that alterations in peroxisomal membrane dynamics are important in health and disease, and the extent to which these dynamics contribute to cell physiology is currently underestimated. Also demonstrated is that the regulation (and dysregulation) of peroxisomal membrane dynamics need to be explored in more detail; a combined experimental-modelling approach being one such useful tool.

Bibliography

Publications

Passmore JB, Pinho S, Gomez-Lazaro M, Schrader M. (2017) The respiratory chain inhibitor rotenone affects peroxisomal dynamics via its microtubule-destabilising ability. *Histochem Cell Biol*. 148(3):331-341. DOI: 10.1007/s00418-017-1577-1

Castro IG, Richards DM, Metz J, Costello JL, **Passmore JB**, Schrader TA, Gouveia A, Ribeiro D, Schrader M. (2018) A role for MIRO1 in motility and membrane dynamics of peroxisomes. *Traffic*. 19(3):229-242. DOI: 10.1111/tra.12549. (among *Traffic*'s most influential research articles of the past 20 years; https://onlinelibrary.wiley.com/doi/toc/10.1111/(ISSN)1600-0854.20th-anniversary-research-articles)

Costello JL, **Passmore JB**, Islinger M, Schrader M. (2018) Multi-localized proteins: the peroxisome-mitochondria connection. *Subcell Biochem*. 89:382-415. DOI: 10.1007/978-981- 13-2233-4_17

Wang Y, Metz J, Costello JL, **Passmore JB**, Schrader M, Schultz C, Islinger M. (2018) Intracellular redistribution of neuronal peroxisomes in response to ACBD5 expression. *PLoS One* 13(12):e0209507. DOI: 10.1371/journal.pone.0209507

Bishop A, Kamoshita M, **Passmore JB**, Hacker C, Schrader TA, Waterham HR, Costello JL, Schrader M. (2019) Fluorescent tools to analyse peroxisome-ER interactions in mammalian cells. *Contact* [Epub ahead of print 15/05/19]. DOI: 10.1177/2515256419848641

Kustatscher G, Grabowski P, Schrader TA, **Passmore JB**, Schrader M, Rappsilber J. (2019) The human proteome co-regulation map reveals functional relationships between proteins. *Nature Biotechnol* 37:1361-1371. DOI: 10.1038/s41587-019-0298-5.

Passmore JB, Godinho L, Ferdinandusse S, Lismont C, Wang Y, Hacker C, Islinger M, Fransen M, Waterham HR, Schrader M. Mitochondrial Fission Factor (MFF) is a critical regulator of peroxisome maturation. *BBA Mol Cell Res* [under review Sep 2019].

Oral Presentations

"Modelling peroxisome dynamics in health and disease". *6th Open European Peroxisome Meeting*, 25-26 Oct 2018. Groningen, Netherlands.

The above presentation was featured in the OEPM meeting report:
Costello JL, Zalckvar E, Kemp S, di Cara F, Kim PK, Linka N, van der Klei IJ (2019) Peroxisomes: new insights into proten sorting, dynamics, quality control, signalling and roles in health and disease. *Histochem Cell Biol* 151(4):283-289. DOI: 10.1007/s00418-019-01780-w.

"Peroxisomes in health and disease". *CLESCon: Addressing Modern Challenges in Life & Environmental Sciences*, 18 Oct 2018. University of Exeter, Exeter, UK.

Poster Presentations

Passmore JB, Richards DM, Schrader M. "Modelling peroxisome dynamics and interaction in health and disease". *EMBO Workshop: Membrane Contact Sites in Health and Disease,* 21-25 Sep 2018. Arosa, Switzerland.

Passmore JB, Richards DM, Metz J, Castro IG, Schrader M. "Modelling peroxisomal dynamics in health and disease". *Exe-BioCon*, 13 Apr 2018. University of Exeter, Exeter, UK. "Best in Show" poster award.

Passmore JB, Richards DM, Schrader M. "Modelling peroxisome membrane dynamics in health and disease" *Postgraduate Research Showcase*, 15-17 May 2017. University of Exeter, Exeter, UK.

References

Agrawal G, Subramani S (2016) De novo peroxisome biogenesis: Evolving concepts and conundrums. Biochim Biophys Acta - Mol Cell Res 1863:892–901. doi: 10.1016/j.bbamcr.2015.09.014

Alam M, Schmidt WJ (2002) Rotenone destroys dopaminergic neurons and induces parkinsonian symptoms in rats. Behav Brain Res 136:317–24

Alexander A, Cai S-L, Kim J, et al (2010) ATM signals to TSC2 in the cytoplasm to regulate mTORC1 in response to ROS. Proc Natl Acad Sci 107:4153–4158. doi: 10.1073/pnas.0913860107

Anderson GJ, Connor WE, Corliss JD (1990) Docosahexaenoic Acid Is the Preferred Dietary n-3 Fatty Acid for the Development of the Brain and Retina. Pediatr Res 27:89–97. doi: 10.1203/00006450-199001000-00023

Anding AL, Baehrecke EH (2017) Cleaning House: Selective Autophagy of Organelles. Dev Cell 41:10–22. doi: 10.1016/j.devcel.2017.02.016

Antonenkov VD, Hiltunen JK (2012) Transfer of metabolites across the peroxisomal membrane. Biochim Biophys Acta - Mol Basis Dis 1822:1374–1386. doi: 10.1016/j.bbadis.2011.12.011

Appelkvist EL, Brunk U, Dallner G (1981) Isolation of peroxisomes from rat liver using sucrose and Percoll gradients. J Biochem Biophys Methods 5:203–17

Aranovich A, Hua R, Rutenberg AD, Kim PK (2014) PEX16 contributes to peroxisome maintenance by constantly trafficking PEX3 via the ER. J Cell Sci 127:3675–86. doi: 10.1242/jcs.146282

Argyriou C, D'Agostino MD, Braverman N (2016) Peroxisome biogenesis disorders. Transl Sci rare Dis 1:111–144. doi: 10.3233/TRD-160003

Arias JA, Moser AB, Goldfischer SL (1985) Ultrastructural and cytochemical demonstration of peroxisomes in cultured fibroblasts from patients with peroxisomal deficiency disorders. J Cell Biol 100:1789–92

Arnold G, Holtzman E (1978) Microperoxisomes in the central nervous system of the postnatal rat. Brain Res 155:1–17

Asare A, Levorse J, Fuchs E (2017) Coupling organelle inheritance with mitosis to balance growth and differentiation. Science (80-) 355:eaah4701. doi: 10.1126/science.aah4701

Bagattin A, Hugendubler L, Mueller E (2010) Transcriptional coactivator PGC-1alpha promotes peroxisomal remodeling and biogenesis. Proc Natl Acad

Sci U S A 107:20376–20381. doi: 10.1073/pnas.1009176107

Baker A, Carrier DJ, Schaedler T, et al (2015) Peroxisomal ABC transporters: functions and mechanism. Biochem Soc Trans 43:959–965. doi: 10.1042/BST20150127

Banker G, Goslin K, Stevens CF (1998) Culturing nerve cells. MIT Press

Barøy T, Koster J, Strømme P, et al (2015) A novel type of rhizomelic chondrodysplasia punctata, RCDP5, is caused by loss of the PEX5 long isoform. Hum Mol Genet 24:5845–5854. doi: 10.1093/hmg/ddv305

Barrientos A, Moraes CT (1999) Titrating the effects of mitochondrial complex I impairment in the cell physiology. J Biol Chem 274:16188–97. doi: 10.1074/jbc.274.23.16188

Barros-Barbosa A, Ferreira MJ, Rodrigues TA, et al (2019) Membrane topologies of PEX13 and PEX14 provide new insights on the mechanism of protein import into peroxisomes. FEBS J 286:205–222. doi: 10.1111/febs.14697

Beard ME, Baker R, Conomos P, et al (1985) Oxidation of oxalate and polyamines by rat peroxisomes. J Histochem Cytochem 33:460–464. doi: 10.1177/33.5.3921604

Berger J, Dorninger F, Forss-Petter S, Kunze M (2016) Peroxisomes in brain development and function. Biochim Biophys Acta - Mol Cell Res 1863:934–955. doi: 10.1016/j.bbamcr.2015.12.005

Berger J, Moller DE (2002) The Mechanisms of Action of PPARs. Annu Rev Med 53:409–435. doi: 10.1146/annurev.med.53.082901.104018

Betarbet R, Sherer TB, MacKenzie G, et al (2000) Chronic systemic pesticide exposure reproduces features of Parkinson's disease. Nat Neurosci 3:1301–1306. doi: 10.1038/81834

Bharti P, Schliebs W, Schievelbusch T, et al (2011) PEX14 is required for microtubule-based peroxisome motility in human cells. J Cell Sci 124:1759–1768. doi: 10.1242/jcs.079368

Bigay J, Antonny B (2012) Curvature, Lipid Packing, and Electrostatics of Membrane Organelles: Defining Cellular Territories in Determining Specificity. Dev Cell 23:886–895. doi: 10.1016/J.DEVCEL.2012.10.009

Binder B, Goede A, Berndt N, Holzhütter H-G (2009) A Conceptual Mathematical Model of the Dynamic Self-Organisation of Distinct Cellular Organelles. PLoS One 4:e8295. doi: 10.1371/journal.pone.0008295

Bishop A, Kamoshita M, Passmore JB, et al (2019) Fluorescent Tools to Analyze Peroxisome–Endoplasmic Reticulum Interactions in Mammalian Cells. Contact 2:251525641984864. doi: 10.1177/2515256419848641

Bonekamp N a, Grille S, Cardoso MJ, et al (2013a) Self-interaction of human Pex11p$β$ during peroxisomal growth and division. PLoS One 8:e53424. doi: 10.1371/journal.pone.0053424

Bonekamp N a, Sampaio P, de Abreu FV, et al (2012) Transient complex interactions of mammalian peroxisomes without exchange of matrix or membrane marker proteins. Traffic 13:960–978. doi: 10.1111/j.1600-0854.2012.01356.x

Bonekamp NA, Islinger M, Lázaro MG, Schrader M (2013b) Cytochemical detection of peroxisomes and mitochondria. Methods Mol Biol 931:467–482. doi: 10.1007/978-1-62703-056-4_24

Bonet-Ponce L, Saez-Atienzar S, da Casa C, et al (2016) Rotenone Induces the Formation of 4-Hydroxynonenal Aggresomes. Role of ROS-Mediated Tubulin Hyperacetylation and Autophagic Flux Disruption. Mol Neurobiol 53:6194–6208. doi: 10.1007/s12035-015-9509-3

Bota DA, Davies KJA (2002) Lon protease preferentially degrades oxidized mitochondrial aconitase by an ATP-stimulated mechanism. Nat Cell Biol 4:674–680. doi: 10.1038/ncb836

Bradford M (1976) A Rapid and Sensitive Method for the Quantitation of Microgram Quantities of Protein Utilizing the Principle of Protein-Dye Binding. Anal Biochem 72:248–254. doi: 10.1006/abio.1976.9999

Braschi E, Goyon V, Zunino R, et al (2010) Vps35 Mediates Vesicle Transport between the Mitochondria and Peroxisomes. Curr Biol 20:1310–1315. doi: 10.1016/j.cub.2010.05.066

Braverman N, Dodt G, Gould SJ, Valle D (1998) An isoform of pex5p, the human PTS1 receptor, is required for the import of PTS2 proteins into peroxisomes. Hum Mol Genet 7:1195–1205. doi: 10.1093/hmg/7.8.1195

Braverman NE, Moser AB (2012) Functions of plasmalogen lipids in health and disease. Biochim Biophys Acta. doi: 10.1016/j.bbadis.2012.05.008

Braverman NE, Moser AB, Steinberg SJ (1993) Rhizomelic Chondrodysplasia Punctata Type 1

Braverman NE, Raymond G V, Rizzo WB, et al (2016) Peroxisome biogenesis disorders in the Zellweger spectrum: An overview of current diagnosis,

clinical manifestations, and treatment guidelines. Mol Genet Metab 117:313–21. doi: 10.1016/j.ymgme.2015.12.009

Brinkley BR, Barham SS, Barranco SC, Fuller GM (1974) Rotenone inhibition of spindle microtubule assembly in mammalian cells. Exp Cell Res 85:41–46. doi: 10.1016/0014-4827(74)90210-9

Brown AI, Rutenberg AD (2017) A Model of Autophagy Size Selectivity by Receptor Clustering on Peroxisomes. Front Phys 5:14. doi: 10.3389/FPHY.2017.00014

Brown FR, McAdams AJ, Cummins JW, et al (1982) Cerebro-hepato-renal (Zellweger) syndrome and neonatal adrenoleukodystrophy: similarities in phenotype and accumulation of very long chain fatty acids. Johns Hopkins Med J 151:344–51

Brown L-A, Baker A (2008) Shuttles and cycles: transport of proteins into the peroxisome matrix (review). Mol Membr Biol 25:363–375. doi: 10.1080/09687680802130583

Calvez B, Hutzler G (2005) Parameter Space Exploration of Agent-Based Models. In: Khosla R, RJ H, LC J (eds) Knowledge-Based Intelligent Information and Engineering Systems, 3684th edn. Springer, Berlin, Heidelberg, pp 633–639

Cartelli D, Ronchi C, Maggioni MG, et al (2010) Microtubule dysfunction precedes transport impairment and mitochondria damage in MPP+-induced neurodegeneration. J Neurochem 115:247–258. doi: 10.1111/j.1471-4159.2010.06924.x

Castro IG, Richards DM, Metz J, et al (2018) A role for Mitochondrial Rho GTPase 1 (MIRO1) in motility and membrane dynamics of peroxisomes. Traffic 19:229–242. doi: 10.1111/tra.12549

Cavallini G, Donati A, Taddei M, Bergamini E (2017) Peroxisomes proliferation and pharmacological stimulation of autophagy in rat liver: evidence to support that autophagy may remove the “older” peroxisomes. Mol Cell Biochem 431:97–102. doi: 10.1007/s11010-017-2979-z

Cepińska MN, Veenhuis M, van der Klei IJ, Nagotu S (2011) Peroxisome fission is associated with reorganization of specific membrane proteins. Traffic 12:925–37. doi: 10.1111/j.1600-0854.2011.01198.x

Cha MY, Chen H, Chan D (2018) Removal of the Mitochondrial Fission Factor Mff Exacerbates Neuronal Loss and Neurological Phenotypes in a

Huntington’s Disease Mouse Model. PLoS Curr 10:. doi: 10.1371/currents.hd.a4e15b80c4915c828d39754942c6631f

Chang C-L, Weigel A V, Ioannou MS, et al (2019) Spastin tethers lipid droplets to peroxisomes and directs fatty acid trafficking through ESCRT-III. J Cell Biol jcb.201902061. doi: 10.1083/jcb.201902061

Chen D, Zhang X-Y, Shi Y (2006) Identification and functional characterization of hCLS1, a human cardiolipin synthase localized in mitochondria. Biochem J 398:169–76. doi: 10.1042/BJ20060303

Chen H, Ren S, Clish C, et al (2015) Titration of mitochondrial fusion rescues Mff-deficient cardiomyopathy. J Cell Biol 211:795–805. doi: 10.1083/jcb.201507035

Chen Y-C, Umanah GKE, Dephoure N, et al (2014a) Msp 1 / ATAD1 maintains mitochondrial function by facilitating the degradation of mislocalized tail-anchored proteins. 33:

Chen Y, Pieuchot L, Loh RA, et al (2014b) Hydrophobic handoff for direct delivery of peroxisome tail-anchored proteins. Nat Commun 5:5790. doi: 10.1038/ncomms6790

Choubey S, Das D, Majumdar S (2019) Cell-to-cell variability in organelle abundance reveals mechanisms of organelle biogenesis. Phys Rev E 100:022405. doi: 10.1103/PhysRevE.100.022405

Chu B-B, Liao Y-C, Qi W, et al (2015) Cholesterol Transport through Lysosome-Peroxisome Membrane Contacts. Cell 161:291–306. doi: 10.1016/j.cell.2015.02.019

Cichocki BA, Krumpe K, Vitali DG, Rapaport D (2018) Pex19 is involved in importing dually targeted tail-anchored proteins to both mitochondria and peroxisomes. Traffic 19:770–785. doi: 10.1111/tra.12604

Cohen Y, Klug YA, Dimitrov L, et al (2014) Peroxisomes are juxtaposed to strategic sites on mitochondria. Mol Biosyst 10:1742–1748. doi: 10.1039/c4mb00001c

Cook KC, Moreno JA, Jean Beltran PM, Cristea IM (2019) Peroxisome Plasticity at the Virus–Host Interface. Trends Microbiol. doi: 10.1016/J.TIM.2019.06.006

Costello JL, Castro IG, Camões F, et al (2017a) Predicting the targeting of tail-anchored proteins to subcellular compartments in mammalian cells. J Cell Sci 130:1675–1687. doi: 10.1242/jcs.200204

Costello JL, Castro IG, Hacker C, et al (2017b) ACBD5 and VAPB mediate membrane associations between peroxisomes and the ER. J Cell Biol 216:331–342. doi: 10.1083/jcb.201607055

Costello JL, Castro IG, Schrader TA, et al (2017c) Peroxisomal ACBD4 interacts with VAPB and promotes ER-peroxisome associations. Cell Cycle 16:1039–1045. doi: 10.1080/15384101.2017.1314422

Costello JL, Passmore JB, Islinger M, Schrader M (2018) Multi-localized Proteins: The Peroxisome-Mitochondria Connection. In: Sub-cellular biochemistry. pp 383–415

Costello JL, Schrader M (2018) Unloosing the Gordian knot of peroxisome formation. Curr Opin Cell Biol 50:50–56. doi: 10.1016/j.ceb.2018.02.002

Craven CJ (2016) Evaluation of predictions of the stochastic model of organelle production based on exact distributions. Elife 5:e10167. doi: 10.7554/eLife.10167

Dacremont G, Cocquyt G, Vincent G (1995) Measurement of very long-chain fatty acids, phytanic and pristanic acid in plasma and cultured fibroblasts by gas chromatography. J Inherit Metab Dis 18 Suppl 1:76–83

Dalmasso G, Marin Zapata PA, Brady NR, Hamacher-Brady A (2017) Agent-Based Modeling of Mitochondria Links Sub-Cellular Dynamics to Cellular Homeostasis and Heterogeneity. PLoS One 12:e0168198. doi: 10.1371/journal.pone.0168198

Dansen TB, Wirtz KWA, Wanders RJA, Pap EHW (2000) Peroxisomes in human fibroblasts have a basic pH. Nat Cell Biol 2:51–53. doi: 10.1038/71375

De Duve C, Baudhuin P (1966) Peroxisomes (microbodies and related particles). Physiol Rev 46:323–357

De Munter S, Bamps D, Malheiro AR, et al (2018) Autonomous Purkinje cell axonal dystrophy causes ataxia in peroxisomal multifunctional protein-2 deficiency. Brain Pathol. doi: 10.1111/bpa.12586

De Vos KJ, Grierson AJ, Ackerley S, Miller CCJ (2008) Role of axonal transport in neurodegenerative diseases. Annu Rev Neurosci 31:151–173. doi: 10.1146/annurev.neuro.31.061307.090711

Dean JM, Lodhi IJ (2018) Structural and functional roles of ether lipids. Protein Cell 9:196–206. doi: 10.1007/s13238-017-0423-5

Defourny J, Aghaie A, Perfettini I, et al (2019) Pejvakin-mediated pexophagy

protects auditory hair cells against noise-induced damage. Proc Natl Acad Sci 201821844. doi: 10.1073/pnas.1821844116

Delille HK, Agricola B, Guimaraes SC, et al (2010) Pex11pbeta-mediated growth and division of mammalian peroxisomes follows a maturation pathway. J Cell Sci 123:2750–2762. doi: 10.1242/jcs.062109

Delille HK, Schrader M (2008) Targeting of hFis1 to peroxisomes is mediated by Pex19p. J Biol Chem 283:31107–31115. doi: 10.1074/jbc.M803332200

Delmaghani S, Defourny J, Aghaie A, et al (2015) Hypervulnerability to Sound Exposure through Impaired Adaptive Proliferation of Peroxisomes. Cell 163:894–906. doi: 10.1016/j.cell.2015.10.023

Deosaran E, Larsen KB, Hua R, et al (2013) NBR1 acts as an autophagy receptor for peroxisomes. J Cell Sci 126:939–952. doi: 10.1242/jcs.114819

Diano S, Liu Z-W, Jeong JK, et al (2011) Peroxisome proliferation–associated control of reactive oxygen species sets melanocortin tone and feeding in diet-induced obesity. Nat Med. doi: 10.1038/nm.2421

Diczfalusy U, Kase BF, Alexson SE, Björkhem I (1991) Metabolism of prostaglandin F2 alpha in Zellweger syndrome. Peroxisomal beta-oxidation is a major importance for in vivo degradation of prostaglandins in humans. J Clin Invest 88:978–84. doi: 10.1172/JCI115401

Dietrich D, Seiler F, Essmann F, Dodt G (2013) Identification of the kinesin KifC3 as a new player for positioning of peroxisomes and other organelles in mammalian cells. Biochim Biophys Acta - Mol Cell Res. doi: 10.1016/j.bbamcr.2013.08.002

Dixit E, Boulant S, Zhang Y, et al (2010) Peroxisomes are signaling platforms for antiviral innate immunity. Cell 141:668–681. doi: 10.1016/j.cell.2010.04.018

Djordjević VB (2004) Free Radicals in Cell Biology. Int Rev Cytol 237:57–89. doi: 10.1016/S0074-7696(04)37002-6

Dodt G, Gould SJ (1996) Multiple PEX genes are required for proper subcellular distribution and stability of Pex5p, the PTS1 receptor: Evidence that PTS1 protein import is mediated by a cycling receptor. J Cell Biol 135:1763–1774. doi: 10.1083/jcb.135.6.1763

Donaldson RP, Tolbert NE, Schnarrenberger C (1972) A comparison of microbody membranes with microsomes and mitochondria from plant and animal tissue. Arch Biochem Biophys 152:199–215. doi: 10.1016/0003-9861(72)90208-1

Dorninger F, Forss-Petter S, Berger J (2017) From peroxisomal disorders to common neurodegenerative diseases - the role of ether phospholipids in the nervous system. FEBS Lett 591:2761–2788. doi: 10.1002/1873-3468.12788

Ebberink MS, Koster J, Visser G, et al (2012) A novel defect of peroxisome division due to a homozygous non-sense mutation in the PEX11β gene. J. Med. Genet. 49:307–313

Eberhart T, Kovacs WJ (2018) Pexophagy in yeast and mammals: an update on mysteries. Histochem Cell Biol 150:473–488. doi: 10.1007/s00418-018-1724-3

Edwards D, Hamson M (1996) Mathematical Modelling Skills. Macmillan Press LTD

Fabelo N, Martín V, Santpere G, et al (2011) Severe Alterations in Lipid Composition of Frontal Cortex Lipid Rafts from Parkinson's Disease and Incidental Parkinson's Disease. Mol Med 17:1107–1118. doi: 10.2119/molmed.2011.00119

Fahimi HD (1973) Diffusion artifacts in cytochemistry of catalase. J Histochem Cytochem 21:999–1009. doi: 10.1177/21.11.999

Fan J, Li X, Issop L, et al (2016) ACBD2/ECI2-Mediated Peroxisome-Mitochondria Interactions in Leydig Cell Steroid Biosynthesis. Mol Endocrinol 30:763–82. doi: 10.1210/me.2016-1008

Fan Y, Wali G, Sutharsan R, et al (2014) Low dose tubulin-binding drugs rescue peroxisome trafficking deficit in patient-derived stem cells in Hereditary Spastic Paraplegia. Biol Open 3:494–502. doi: 10.1242/bio.20147641

Fang Y, Morrell JC, Jones JM, Gould SJ (2004) PEX3 functions as a PEX19 docking factor in the import of class I peroxisomal membrane proteins. J Cell Biol 164:863–875. doi: 10.1083/jcb.200311131 jcb.200311131 [pii]

Farré J, Mahalingam SS, Proietto M, Subramani S (2019) Peroxisome biogenesis, membrane contact sites, and quality control. EMBO Rep 20:e46864. doi: 10.15252/embr.201846864

Faust PL, Kovacs WJ (2014) Cholesterol biosynthesis and ER stress in peroxisome deficiency. Biochimie 98:75–85. doi: 10.1016/j.biochi.2013.10.019

Ferdinandusse S, Denis S, Dacremont G, Wanders RJA (2009a) Toxicity of peroxisomal C27-bile acid intermediates. Mol Genet Metab 96:121–128. doi:

10.1016/j.ymgme.2008.11.165

Ferdinandusse S, Denis S, Faust PL, Wanders RJA (2009b) Bile acids: the role of peroxisomes. J Lipid Res 50:2139–47. doi: 10.1194/jlr.R900009-JLR200

Ferdinandusse S, Ebberink MS, Vaz FM, et al (2016) The important role of biochemical and functional studies in the diagnostics of peroxisomal disorders. J Inherit Metab Dis 39:531–543. doi: 10.1007/s10545-016-9922-4

Ferdinandusse S, Falkenberg KD, Koster J, et al (2017) ACBD5 deficiency causes a defect in peroxisomal very long-chain fatty acid metabolism. J Med Genet 54:330–337. doi: 10.1136/jmedgenet-2016-104132

Fodor K, Wolf J, Erdmann R, et al (2012) Molecular Requirements for Peroxisomal Targeting of Alanine-Glyoxylate Aminotransferase as an Essential Determinant in Primary Hyperoxaluria Type 1. PLoS Biol 10:e1001309. doi: 10.1371/journal.pbio.1001309

Francisco T, Rodrigues TA, Dias AF, et al (2017) Protein transport into peroxisomes: Knowns and unknowns. BioEssays 39:1700047. doi: 10.1002/bies.201700047

Fransen M, Lismont C (2018) Peroxisomes and Cellular Oxidant/Antioxidant Balance: Protein Redox Modifications and Impact on Inter-organelle Communication. In: Sub-cellular biochemistry. pp 435–461

Fransen M, Lismont C (2019) Redox Signaling from and to Peroxisomes: Progress, Challenges, and Prospects. Antioxid Redox Signal 30:95–112. doi: 10.1089/ars.2018.7515

Fransen M, Lismont C, Walton P (2017) The Peroxisome-Mitochondria Connection: How and Why? Int J Mol Sci 18:1126. doi: 10.3390/ijms18061126

Fransen M, Nordgren M, Wang B, et al (2013) Aging, age-related diseases and peroxisomes. In: Peroxisomes and their Key Role in Cellular Signaling and Metabolism. Springer, pp 45–65

Fransen M, Nordgren M, Wang B, Apanasets O (2012) Role of peroxisomes in ROS/RNS-metabolism: Implications for human disease. Biochim Biophys Acta 1822:1363–1373. doi: 10.1016/j.bbadis.2011.12.001

Fransen M, Wylin T, Brees C, et al (2001) Human pex19p binds peroxisomal integral membrane proteins at regions distinct from their sorting sequences. Mol Cell Biol 21:4413–24. doi: 10.1128/MCB.21.13.4413-4424.2001

Fransson A, Ruusala A, Aspenström P (2006) The atypical Rho GTPases Miro-1 and Miro-2 have essential roles in mitochondrial trafficking. Biochem Biophys Res Commun 344:500–510. doi: 10.1016/j.bbrc.2006.03.163

Freitas MO, Francisco T, Rodrigues TA, et al (2011) PEX5 protein binds monomeric catalase blocking its tetramerization and releases it upon binding the N-terminal domain of PEX14. J Biol Chem 286:40509–40519. doi: 10.1074/jbc.M111.287201

Fujiki Y, Fowler S, Shio H, et al (1982) Polypeptide and phospholipid composition of the membrane of rat liver peroxisomes: comparison with endoplasmic reticulum and mitochondrial membranes. J Cell Biol 93:103–10

Galbusera C, Orth P, Fedida D, Spector T (2006) Superoxide radical production by allopurinol and xanthine oxidase. Biochem Pharmacol 71:1747–1752. doi: 10.1016/J.BCP.2006.02.008

Galiani S, Waithe D, Reglinski K, et al (2016) Super-resolution Microscopy Reveals Compartmentalization of Peroxisomal Membrane Proteins. J Biol Chem 291:16948–62. doi: 10.1074/jbc.M116.734038

Galindo MF, Jordán J, González-García C, Ceña V (2003) Chromaffin cell death induced by 6-hydroxydopamine is independent of mitochondrial swelling and caspase activation. J Neurochem 84:1066–1073. doi: 10.1046/j.1471-4159.2003.01592.x

Galitzine C, Beltran PMJ, Cristea IM, Vitek O (2018) Statistical Inference of Peroxisome Dynamics. In: Raphael B (ed) Research in Computational Molecular Biology. Springer, Cham, pp 54–74

Gandre-Babbe S, van der Bliek AM (2008) The novel tail-anchored membrane protein Mff controls mitochondrial and peroxisomal fission in mammalian cells. Mol Biol Cell 19:2402–2412. doi: 10.1091/mbc.E07

Gerber S, Charif M, Chevrollier A, et al (2017) Mutations in DNM1L, as in OPA1, result indominant optic atrophy despite opposite effectson mitochondrial fusion and fission. Brain 140:2586–2596. doi: 10.1093/brain/awx219

Geuze HJ, Murk JL, Stroobants AK, et al (2003) Involvement of the Endoplasmic Reticulum in Peroxisome Formation. Mol Biol Cell 14:2900–2907. doi: 10.1091/mbc.e02-11-0734

Gibellini F, Smith TK (2010) The Kennedy pathway-De novo synthesis of phosphatidylethanolamine and phosphatidylcholine. IUBMB Life 62:n/a-n/a.

doi: 10.1002/iub.337

Giniatullin A, Petrov A, Giniatullin R (2019) Action of Hydrogen Peroxide on Synaptic Transmission at the Mouse Neuromuscular Junction. Neuroscience 399:135–145. doi: 10.1016/j.neuroscience.2018.12.027

Glaser PE, Gross RW (1994) Plasmenylethanolamine Facilitates Rapid Membrane Fusion: A Stopped-Flow Kinetic Investigation Correlating the Propensity of a Major Plasma Membrane Constituent to Adopt an HII Phase with Its Ability to Promote Membrane Fusion. Biochemistry 33:5805–5812. doi: 10.1021/bi00185a019

Godinho LF, Schrader M (2017) Determination of Peroxisomal pH in Living Mammalian Cells Using pHRed. In: Methods in molecular biology (Clifton, N.J.). pp 181–189

Goldman BM, Blobel G (1978) Biogenesis of peroxisomes: intracellular site of synthesis of catalase and uricase. Proc Natl Acad Sci U S A 75:5066–70. doi: 10.1073/pnas.75.10.5066

Gomes LC, Benedetto G Di, Scorrano L (2011) During autophagy mitochondria elongate, are spared from degradation and sustain cell viability. Nat Cell Biol 13:589–598. doi: 10.1038/ncb2220

Gomez-Lazaro M, Bonekamp N a, Galindo MF, et al (2008) 6-Hydroxydopamine (6-OHDA) induces Drp1-dependent mitochondrial fragmentation in SH-SY5Y cells. Free Radic Biol Med 44:1960–1969. doi: 10.1016/j.freeradbiomed.2008.03.009

Grant P, Ahlemeyer B, Karnati S, et al (2013) The biogenesis protein PEX14 is an optimal marker for the identification and localization of peroxisomes in different cell types, tissues, and species in morphological studies. Histochem Cell Biol 140:423–442. doi: 10.1007/s00418-013-1133-6

Halbach A, Lorenzen S, Landgraf C, et al (2005) Function of the PEX19-binding site of human adrenoleukodystrophy protein as targeting motif in man and yeast. PMP targeting is evolutionarily conserved. J Biol Chem 280:21176–21182. doi: 10.1074/jbc.M501750200

Hara-Kuge S, Fujiki Y (2008) The peroxin Pex14p is involved in LC3-dependent degradation of mammalian peroxisomes. Exp Cell Res 314:3531–3541. doi: 10.1016/j.yexcr.2008.09.015

Harano T, Nose S, Uezu R, et al (2001) Hsp70 regulates the interaction between the peroxisome targeting signal type 1 (PTS1)-receptor Pex5p and PTS1.

Biochem J 357:157–65

Hardeman D, Versantvoort C, van den Brink JM, van den Bosch H (1990) Studies on peroxisomal membranes. Biochim Biophys Acta 1027:149–54. doi: 10.1016/0005-2736(90)90078-3

Helle SCJ, Feng Q, Aebersold MJ, et al (2017) Mechanical force induces mitochondrial fission. Elife 6:. doi: 10.7554/eLife.30292

Hettema EH, Erdmann R, van der Klei IJ, Veenhuis M (2014) Evolving models for peroxisome biogenesis. Curr Opin Cell Biol 29:25–30. doi: 10.1016/j.ceb.2014.02.002

Hettema EH, Girzalsky W, van den Berg M, et al (2000) Saccharomyces cerevisiae Pex3p and Pex19p are required for proper localization and stability of peroxisomal membrane proteins. EMBO J 19:223–233. doi: 10.1093/emboj/19.2.223

Heymans HS, Schutgens RB, Tan R, et al (1983) Severe plasmalogen deficiency in tissues of infants without peroxisomes (Zellweger syndrome). Nature 306:69–70

Hirst J, King MS, Pryde KR (2008) The production of reactive oxygen species by complex I. Biochem Soc Trans 36:976–980. doi: 10.1042/BST0360976

Honsho M, Tamura S, Shimozawa N, et al (1998) Mutation in PEX16 is causal in the peroxisome-deficient Zellweger syndrome of complementation group D. Am J Hum Genet 63:1622–1630. doi: S0002-9297(07)61606-1 [pii] 10.1086/302161

Horvath SE, Daum G (2013) Lipids of mitochondria. Prog Lipid Res 52:590–614. doi: 10.1016/J.PLIPRES.2013.07.002

Hosoi K, Miyata N, Mukai S, et al (2017) The VDAC2–BAK axis regulates peroxisomal membrane permeability. J Cell Biol 216:709–722. doi: 10.1083/jcb.201605002

Hu A, Zhao X-T, Tu H, et al (2018) PIP4K2A regulates intracellular cholesterol transport through modulating PI(4,5)P $_2$ homeostasis. J Lipid Res 59:507–514. doi: 10.1194/jlr.M082149

Hua R, Cheng D, Coyaud É, et al (2017) VAPs and ACBD5 tether peroxisomes to the ER for peroxisome maintenance and lipid homeostasis. J Cell Biol 216:367–377. doi: 10.1083/jcb.201608128

Huang T-Y, Zheng D, Houmard JA, et al (2017) Overexpression of PGC-1α

increases peroxisomal activity and mitochondrial fatty acid oxidation in human primary myotubes. Am J Physiol Metab 312:E253–E263. doi: 10.1152/ajpendo.00331.2016

Huber C, Saffrich R, Anton M, et al (1997) A heterotrimeric G protein-phospholipase A2 signaling cascade is involved in the regulation of peroxisomal motility in CHO cells. J Cell Sci 110 (Pt 2:2955–2968

Huber N, Guimaraes S, Schrader M, et al (2013) Charcot-Marie-Tooth disease-associated mutants of GDAP1 dissociate its roles in peroxisomal and mitochondrial fission. EMBO Rep 14:545–552. doi: 10.1038/embor.2013.56

Huitema K, van den Dikkenberg J, Brouwers JFHM, Holthuis JCM (2004) Identification of a family of animal sphingomyelin synthases. EMBO J 23:33–44. doi: 10.1038/sj.emboj.7600034

Huybrechts SJ, Van Veldhoven PP, Brees C, et al (2009) Peroxisome dynamics in cultured mammalian cells. Traffic 10:1722–1733. doi: 10.1111/j.1600-0854.2009.00970.x

Hwang J, Qi L (2018) Quality Control in the Endoplasmic Reticulum: Crosstalk between ERAD and UPR pathways. Trends Biochem Sci 43:593–605. doi: 10.1016/j.tibs.2018.06.005

Imoto Y, Abe Y, Honsho M, et al (2018) Onsite GTP fuelling via DYNAMO1 drives division of mitochondria and peroxisomes. Nat Commun 9:4634. doi: 10.1038/s41467-018-07009-z

Islinger M, Voelkl A, Fahimi HD, Schrader M (2018) The peroxisome: an update on mysteries 2.0. Histochem Cell Biol 150:443–471. doi: 10.1007/s00418-018-1722-5

Itoyama A, Honsho M, Abe Y, et al (2012) Docosahexaenoic acid mediates peroxisomal elongation, a prerequisite for peroxisome division. J Cell Sci 125:589–602. doi: 10.1242/jcs.087452

Itoyama A, Michiyuki S, Honsho M, et al (2013) Mff functions with Pex11p and DLP1 in peroxisomal fission. Biol Open. doi: 10.1242/bio.20135298

Ivashchenko O, Van Veldhoven PP, Brees C, et al (2011) Intraperoxisomal redox balance in mammalian cells: oxidative stress and interorganellar cross-talk. Mol Biol Cell 22:1440–1451. doi: 10.1091/mbc.E10-11-0919

Iwata JI, Ezaki J, Komatsu M, et al (2006) Excess peroxisomes are degraded by autophagic machinery in mammals. J Biol Chem 281:4035–4041. doi: 10.1074/jbc.M512283200

Janmey PA, Kinnunen PKJ (2006) Biophysical properties of lipids and dynamic membranes. Trends Cell Biol 16:538–546. doi: 10.1016/J.TCB.2006.08.009

Jansen GA, Oftnan R, Ferdinandusse S, et al (1997) Refsum disease is caused by mutations in the phytanoyl–CoA hydroxylase gene. Nat Genet 17:190–193. doi: 10.1038/ng1097-190

Jansen RLM, van der Klei IJ (2019) The peroxisome biogenesis factors Pex3 and Pex19: multitasking proteins with disputed functions. FEBS Lett. doi: 10.1002/1873-3468.13340

Jean Beltran PM, Cook KC, Hashimoto Y, et al (2018) Infection-Induced Peroxisome Biogenesis Is a Metabolic Strategy for Herpesvirus Replication. Cell Host Microbe 24:526–541.e7. doi: 10.1016/j.chom.2018.09.002

Jiang L, Hara-Kuge S, Yamashita S-I, Fujiki Y (2014) Peroxin Pex14p is the key component for coordinated autophagic degradation of mammalian peroxisomes by direct binding to LC3-II. Genes Cells 6–10. doi: 10.1111/gtc.12198

Jiang Q, Yan Z, Feng J (2006) Neurotrophic Factors Stabilize Microtubules and Protect against Rotenone Toxicity on Dopaminergic Neurons. J Biol Chem 281:29391–29400. doi: 10.1074/jbc.M602740200

Jones JM, Morrell JC, Gould SJ (2001) Multiple distinct targeting signals in integral peroxisomal membrane proteins. J Cell Biol 153:1141–1149. doi: 10.1083/jcb.153.6.1141

Jones JM, Morrell JC, Gould SJ (2004) PEX19 is a predominantly cytosolic chaperone and import receptor for class 1 peroxisomal membrane proteins. J Cell Biol 164:57–67. doi: 10.1083/jcb.200304111

Kapitein LC, Schlager M a, Kuijpers M, et al (2010) Mixed microtubules steer dynein-driven cargo transport into dendrites. Curr Biol 20:290–299. doi: 10.1016/j.cub.2009.12.052

Kassmann CM, Quintes S, Rietdorf J, et al (2011) A role for myelin-associated peroxisomes in maintaining paranodal loops and axonal integrity. FEBS Lett 585:2205–2211. doi: 10.1016/j.febslet.2011.05.032

Kawai T, Takahashi K, Sato S, et al (2005) IPS-1, an adaptor triggering RIG-I- and Mda5-mediated type I interferon induction. Nat Immunol 6:981–988. doi: 10.1038/ni1243

Kawałek A, Jagadeesan C, van der Klei IJ (2016) Impaired biosynthesis of the

non-bilayer lipids phosphatidylethanolamine or cardiolipin does not affect peroxisome biogenesis and proliferation in Saccharomyces cerevisiae. Biochem Biophys Res Commun 480:228–233. doi: 10.1016/j.bbrc.2016.10.033

Keller GA, Warner TG, Steimer KS, Hallewell RA (1991) Cu,Zn superoxide dismutase is a peroxisomal enzyme in human fibroblasts and hepatoma cells. Proc Natl Acad Sci U S A 88:7381–5. doi: 10.1073/pnas.88.16.7381

Kemp S, Berger J, Aubourg P (2012) X-linked adrenoleukodystrophy: Clinical, metabolic, genetic and pathophysiological aspects. Biochim Biophys Acta - Mol Basis Dis 1822:1465–1474. doi: 10.1016/J.BBADIS.2012.03.012

Kemp S, Valianpour F, Mooyer PAW, et al (2004) Method for measurement of peroxisomal very-long-chain fatty acid beta-oxidation in human skin fibroblasts using stable-isotope-labeled tetracosanoic acid. Clin Chem 50:1824–6. doi: 10.1373/clinchem.2004.038539

Khacho M, Slack RS (2018) Mitochondrial dynamics in the regulation of neurogenesis: From development to the adult brain. Dev Dyn 247:47–53. doi: 10.1002/dvdy.24538

Khaminets A, Behl C, Dikic I (2016) Ubiquitin-Dependent And Independent Signals In Selective Autophagy. Trends Cell Biol 26:6–16. doi: 10.1016/J.TCB.2015.08.010

Kiel JAKW, Emmrich K, Meyer HE, Kunau W-H (2005) Ubiquitination of the Peroxisomal Targeting Signal Type 1 Receptor, Pex5p, Suggests the Presence of a Quality Control Mechanism during Peroxisomal Matrix Protein Import. J Biol Chem 280:1921–1930. doi: 10.1074/jbc.M403632200

Kikuchi M, Hatano N, Yokota S, et al (2004) Proteomic Analysis of Rat Liver Peroxisome. J Biol Chem 279:421–428. doi: 10.1074/jbc.M305623200

Kim PK, Hailey DW, Mullen RT, Lippincott-Schwartz J (2008) Ubiquitin signals autophagic degradation of cytosolic proteins and peroxisomes. Proc Natl Acad Sci U S A 105:20567–20574. doi: 10.1073/pnas.0810611105

Kim PK, Hettema EH (2015) Multiple pathways for protein transport to peroxisomes. J Mol Biol 427:1176–1190. doi: 10.1016/j.jmb.2015.02.005

Kim PK, Mullen RT, Schumann U, Lippincott-Schwartz J (2006) The origin and maintenance of mammalian peroxisomes involves a de novo PEX16-dependent pathway from the ER. J Cell Biol 173:521–532. doi: 10.1083/jcb.200601036

Kirkin V, Lamark T, Sou Y-S, et al (2009) A role for NBR1 in autophagosomal degradation of ubiquitinated substrates. Mol Cell 33:505–516. doi: 10.1016/j.molcel.2009.01.020

Klipp E, Liebermeister W (2006) Mathematical modeling of intracellular signaling pathways. BMC Neurosci 7 Suppl 1:S10. doi: 10.1186/1471-2202-7-S1-S10

Kobayashi S, Tanaka A, Fujiki Y (2007) Fis1, DLP1, and Pex11p coordinately regulate peroxisome morphogenesis. Exp Cell Res 313:1675–1686. doi: 10.1016/j.yexcr.2007.02.028

Koch A, Schneider G, Lüers GH, Schrader M (2004) Peroxisome elongation and constriction but not fission can occur independently of dynamin-like protein 1. J Cell Sci 117:3995–4006. doi: 10.1242/jcs.01268

Koch A, Yoon Y, Bonekamp NA, et al (2005) A Role for Fis1 in Both Mitochondrial and Peroxisomal Fission in Mammalian Cells. Mol Biol Cell 16:5077–5086. doi: 10.1091/mbc.E05

Koch J, Brocard C (2012) PEX11 proteins attract Mff and hFis1 to coordinate peroxisomal fission. J Cell Sci 125:3813–3826

Koch J, Feichtinger RG, Freisinger P, et al (2016) Disturbed mitochondrial and peroxisomal dynamics due to loss of MFF causes Leigh-like encephalopathy, optic atrophy and peripheral neuropathy. J Med Genet 53:270–278. doi: 10.1136/jmedgenet-2015-103500

Koepke JI, Wood CS, Terlecky LJ, et al (2008) Progeric effects of catalase inactivation in human cells. Toxicol Appl Pharmacol 232:99–108. doi: 10.1016/j.taap.2008.06.004

Komen JC, Duran M, Wanders RJA (2005) Characterization of phytanic acid ω-hydroxylation in human liver microsomes. Mol Genet Metab 85:190–195. doi: 10.1016/J.YMGME.2005.02.005

Kowald A, Klipp E (2014) Mathematical Models of Mitochondrial Aging and Dynamics. Prog Mol Biol Transl Sci 127:63–92. doi: 10.1016/B978-0-12-394625-6.00003-9

Kumari I, Sandhu P, Ahmed M, Akhter Y (2017) Molecular Dynamics Simulations, Challenges and Opportunities: A Biologist's Prospective. Curr Protein Pept Sci 18:. doi: 10.2174/1389203718666170622074741

Kustatscher G, Grabowski P, Schrader TA, et al (2019) The human proteome co-regulation map reveals functional relationships between proteins. bioRxiv

582247. doi: 10.1101/582247

LaBelle EF, Hajra AK (1974) Purification and kinetic properties of acyl and alkyl dihydroxyacetone phosphate oxidoreductase. J Biol Chem 249:6936–44

Ladds E, Whitney A, Dombi E, et al (2018) De novo DNM1L mutation associated with mitochondrial epilepsy syndrome with fever sensitivity. Neurol Genet 4:e258. doi: 10.1212/NXG.0000000000000258

Lasorsa FM, Pinton P, Palmieri L, et al (2008) Peroxisomes as novel players in cell calcium homeostasis. J Biol Chem 283:15300–15308. doi: 10.1074/jbc.M800648200

Laurenti G, Benedetti E, D'Angelo B, et al (2011) Hypoxia induces peroxisome proliferator-activated receptor α (PPARα) and lipid metabolism peroxisomal enzymes in human glioblastoma cells. J Cell Biochem 112:3891–3901. doi: 10.1002/jcb.23323

Law KB, Bronte-Tinkew D, Di Pietro E, et al (2017) The peroxisomal AAA ATPase complex prevents pexophagy and development of peroxisome biogenesis disorders. Autophagy 13:868–884. doi: 10.1080/15548627.2017.1291470

Lee JN, Dutta RK, Maharjan Y, et al (2018) Catalase inhibition induces pexophagy through ROS accumulation. Biochem Biophys Res Commun 501:696–702. doi: 10.1016/j.bbrc.2018.05.050

Lee MY, Sumpter R, Zou Z, et al (2017) Peroxisomal protein PEX13 functions in selective autophagy. EMBO Rep 18:48–60. doi: 10.15252/embr.201642443

Lewis TL, Kwon S-K, Lee A, et al (2018) MFF-dependent mitochondrial fission regulates presynaptic release and axon branching by limiting axonal mitochondria size. Nat Commun 9:5008. doi: 10.1038/s41467-018-07416-2

Li X, Baumgart E, Morrell JC, et al (2002) PEX11β Deficiency Is Lethal and Impairs Neuronal Migration but Does Not Abrogate Peroxisome Function. Mol Cell Biol 22:4358–4365

Li X, Gould SJ (2003) The dynamin-like GTPase DLP1 is essential for peroxisome division and is recruited to peroxisomes in part by PEX11. J Biol Chem 278:17012–17020. doi: 10.1074/jbc.M212031200

Li X, Han H, Zhou M-T, et al (2017) Proteomic Analysis of the Human Tankyrase Protein Interaction Network Reveals Its Role in Pexophagy. Cell Rep 20:737–749. doi: 10.1016/J.CELREP.2017.06.077

Lin C, Steinberg G (2017) Spatial organization of organelles in fungi: Insights from mathematical modelling. Fungal Genet Biol 103:55–59. doi:

10.1016/j.fgb.2017.03.006

Lismont C, Koster J, Provost S, et al (2019a) Deciphering the potential involvement of PXMP2 and PEX11B in hydrogen peroxide permeation across the peroxisomal membrane reveals a role for PEX11B in protein sorting. Biochim Biophys Acta - Biomembr. doi: 10.1016/J.BBAMEM.2019.05.013

Lismont C, Nordgren M, Brees C, et al (2019b) Peroxisomes as Modulators of Cellular Protein Thiol Oxidation: A New Model System. Antioxid Redox Signal 30:22–39. doi: 10.1089/ars.2017.6997

Lismont C, Walton PA, Fransen M (2017) Quantitative Monitoring of Subcellular Redox Dynamics in Living Mammalian Cells Using RoGFP2-Based Probes. In: Methods in molecular biology (Clifton, N.J.). pp 151–164

Liu R, Chan DC (2015) The mitochondrial fission receptor Mff selectively recruits oligomerized Drp1. Mol Biol Cell 26:4466–77. doi: 10.1091/mbc.E15-08-0591

Long B, Wang K, Li N, et al (2013) miR-761 regulates the mitochondrial network by targeting mitochondrial fission factor. Free Radic Biol Med 65:371–9. doi: 10.1016/j.freeradbiomed.2013.07.009

Loo Y-M, Gale M, Jr. (2011) Immune signaling by RIG-I-like receptors. Immunity 34:680–92. doi: 10.1016/j.immuni.2011.05.003

Luoma AM, Kuo F, Cakici O, et al (2015) Plasmalogen phospholipids protect internodal myelin from oxidative damage. Free Radic Biol Med 84:296–310. doi: 10.1016/j.freeradbiomed.2015.03.012

Ma H, Yang Y, Cherng S (2008) Peroxisome proliferator-activated receptors. Nat Sci 6:64–70

Macal CM (2016) Everything you need to know about agent-based modelling and simulation. J Simul 10:144–156. doi: 10.1057/jos.2016.7

Magalhães AC, Ferreira AR, Gomes S, et al (2016) Peroxisomes are platforms for cytomegalovirus' evasion from the cellular immune response. Sci Rep 6:26028. doi: 10.1038/srep26028

Magalhaes MAO, Glogauer M (2010) Pivotal Advance: Phospholipids determine net membrane surface charge resulting in differential localization of active Rac1 and Rac2. J Leukoc Biol 87:545–555. doi: 10.1189/JLB.0609390

Marcassa E, Kallinos A, Jardine J, et al (2018) Dual role of USP30 in controlling

basal pexophagy and mitophagy. EMBO Rep 19:e45595. doi: 10.15252/embr.201745595

Marggraf W-D, Alfred Anderer F, Kanfer JN (1981) The formation of sphingomyelin from phosphatidylcholine in plasma membrane preparations from mouse fibroblasts. Biochim Biophys Acta - Lipids Lipid Metab 664:61–73. doi: 10.1016/0005-2760(81)90028-X

Marshall LE, Himes RH (1978) Rotenone inhibition of tubulin self-assembly. Biochim Biophys Acta 543:590–4. doi: 10.1016/0304-4165(78)90315-x

Mashek DG, Li LO, Coleman RA (2017) Long-Chain Acyl-Coa Synthetases And Fatty Acid Channeling. Future Lipidol 2:465–476. doi: 10.2217/17460875.2.4.465

Matsunaga T, Endo S, Maeda S, et al (2008) Characterization of human DHRS4: An inducible short-chain dehydrogenase/reductase enzyme with 3β-hydroxysteroid dehydrogenase activity. Arch Biochem Biophys 477:339–347. doi: 10.1016/J.ABB.2008.06.002

Matsuzaki T, Fujiki Y (2008) The peroxisomal membrane protein import receptor Pex3p is directly transported to peroxisomes by a novel Pex19p- and Pex16p-dependent pathway. J Cell Biol 183:1275–1286. doi: 10.1083/jcb.200806062

Matsuzono Y, Kinoshita N, Tamura S, et al (1999) Human PEX19: cDNA cloning by functional complementation, mutation analysis in a patient with Zellweger syndrome, and potential role in peroxisomal membrane assembly. Proc Natl Acad Sci U S A 96:2116–2121. doi: 10.1073/pnas.96.5.2116

Mattiazzi Ušaj M, Brložnik M, Kaferle P, et al (2015) Genome-Wide Localization Study of Yeast Pex11 Identifies Peroxisome–Mitochondria Interactions through the ERMES Complex. J Mol Biol 427:2072–2087. doi: 10.1016/j.jmb.2015.03.004

Mayerhofer PU (2016) Targeting and insertion of peroxisomal membrane proteins: ER trafficking versus direct delivery to peroxisomes. Biochim Biophys Acta - Mol Cell Res 1863:870–880. doi: 10.1016/j.bbamcr.2015.09.021

McDonough MA, Kavanagh KL, Butler D, et al (2005) Structure of human phytanoyl-CoA 2-hydroxylase identifies molecular mechanisms of Refsum disease. J Biol Chem 280:41101–10. doi: 10.1074/jbc.M507528200

McShane E, Sin C, Zauber H, et al (2016) Kinetic Analysis of Protein Stability

Reveals Age-Dependent Degradation. Cell 167:803–815.e21. doi: 10.1016/J.CELL.2016.09.015

Mears J a, Lackner LL, Fang S, et al (2011) Conformational changes in Dnm1 support a contractile mechanism for mitochondrial fission. Nat Struct Mol Biol 18:20–26. doi: 10.1038/nsmb.1949

Meisner HM, Sorensen L (1966) Metaphase arrest of Chinese hamster cells with rotenone. Exp Cell Res 42:291–295. doi: 10.1016/0014-4827(66)90292-8

Mercer TJ, Gubas A, Tooze SA (2018) A molecular perspective of mammalian autophagosome biogenesis. J Biol Chem 293:5386–5395. doi: 10.1074/jbc.R117.810366

Meurers BH, Zhu C, Fernagut PO, et al (2009) Low dose rotenone treatment causes selective transcriptional activation of cell death related pathways in dopaminergic neurons in vivo. Neurobiol Dis 33:182–192. doi: 10.1016/j.nbd.2008.10.001

Meylan E, Curran J, Hofmann K, et al (2005) Cardif is an adaptor protein in the RIG-I antiviral pathway and is targeted by hepatitis C virus. Nature 437:1167–1172. doi: 10.1038/nature04193

Mogilner A, Wollman R, Marshall WF (2006) Quantitative Modeling in Cell Biology: What Is It Good for? Dev Cell 11:279–287. doi: 10.1016/J.DEVCEL.2006.08.004

Morshed A, Dutta P (2017) Mathematical Model for Tissue-Level Hypoxic Response in Microfluidic Environment. J Biomech Eng 140:011009. doi: 10.1115/1.4037915

Motley AM, Hettema EH (2007) Yeast peroxisomes multiply by growth and division. J Cell Biol 178:399–410. doi: 10.1083/jcb.200702167

Motley AM, Ward GP, Hettema EH (2008) Dnm1p-dependent peroxisome fission requires Caf4p, Mdv1p and Fis1p. J Cell Sci 121:1633–1640. doi: 10.1242/jcs.026344

Mounsey RB, Teismann P (2011) Mitochondrial Dysfunction in Parkinson's Disease: Pathogenesis and Neuroprotection. Parkinsons Dis 2011:1–18. doi: 10.4061/2011/617472

Mukherji S, O'Shea EK (2014) Mechanisms of organelle biogenesis govern stochastic fluctuations in organelle abundance. Elife 2014:1–17. doi: 10.7554/eLife.02678.001

Nagan N, Zoeller RA (2001) Plasmalogens: biosynthesis and functions. Prog Lipid Res 40:199–229. doi: 10.1016/S0163-7827(01)00003-0

Nasca A, Legati A, Baruffini E, et al (2016) Biallelic Mutations in DNM1L are Associated with a Slowly Progressive Infantile Encephalopathy. Hum Mutat 37:898–903. doi: 10.1002/humu.23033

Nasca A, Nardecchia F, Commone A, et al (2018) Clinical and Biochemical Features in a Patient With Mitochondrial Fission Factor Gene Alteration. Front Genet 9:625. doi: 10.3389/fgene.2018.00625

Nazarko TY, Ozeki K, Till A, et al (2014) Peroxisomal Atg37 binds Atg30 or palmitoyl-CoA to regulate phagophore formation during pexophagy. J Cell Biol 204:541–557. doi: 10.1083/jcb.201307050

Neuspiel M, Schauss AC, Braschi E, et al (2008) Cargo-selected transport from the mitochondria to peroxisomes is mediated by vesicular carriers. Curr Biol 18:102–108. doi: 10.1016/j.cub.2007.12.038

Nguyen T, Bjorkman J, Paton BC, Crane DI (2006) Failure of microtubule-mediated peroxisome division and trafficking in disorders with reduced peroxisome abundance. J Cell Sci 119:636–645. doi: 10.1242/jcs.02776

Nordgren M, Francisco T, Lismont C, et al (2015) Export-deficient monoubiquitinated PEX5 triggers peroxisome removal in SV40 large T antigen-transformed mouse embryonic fibroblasts. Autophagy 11:1326–1340. doi: 10.1080/15548627.2015.1061846

Nordgren M, Fransen M (2014) Peroxisomal metabolism and oxidative stress. Biochimie 98:56–62. doi: 10.1016/j.biochi.2013.07.026

Ofman R, Wanders RJ (1994) Purification of peroxisomal acyl-CoA: dihydroxyacetonephosphate acyltransferase from human placenta. Biochim Biophys Acta 1206:27–34

Ohh M, Park CW, Ivan M, et al (2000) Ubiquitination of hypoxia-inducible factor requires direct binding to the β-domain of the von Hippel–Lindau protein. Nat Cell Biol 2:423–427. doi: 10.1038/35017054

Okumoto K, Kametani Y, Fujiki Y (2011) Two Proteases, Trypsin Domain-containing 1 (Tysnd1) and Peroxisomal Lon Protease (PsLon), Cooperatively Regulate Fatty Acid β-Oxidation in Peroxisomal Matrix. J Biol Chem 286:44367–44379. doi: 10.1074/jbc.M111.285197

Okumoto K, Ono T, Toyama R, et al (2018) New splicing variants of mitochondrial Rho GTPase-1 (Miro1) transport peroxisomes. J Cell Biol 217:619–633. doi:

10.1083/jcb.201708122

Opaliński L, Kiel JAKW, Williams C, et al (2011) Membrane curvature during peroxisome fission requires Pex11. EMBO J 30:5–16

Otera H, Wang C, Cleland MM, et al (2010) Mff is an essential factor for mitochondrial recruitment of Drp1 during mitochondrial fission in mammalian cells. J Cell Biol 191:1141–1158. doi: 10.1083/jcb.201007152

Palmer CS, Elgass KD, Parton RG, et al (2013) Adaptor proteins MiD49 and MiD51 can act independently of Mff and Fis1 in Drp1 recruitment and are specific for mitochondrial fission. J Biol Chem 288:27584–93. doi: 10.1074/jbc.M113.479873

Passmore JB, Pinho S, Gomez-Lazaro M, Schrader M (2017) The respiratory chain inhibitor rotenone affects peroxisomal dynamics via its microtubule-destabilising activity. Histochem Cell Biol 148:. doi: 10.1007/s00418-017-1577-1

Pause B, Diestelkötter P, Heid H, Just WW (1997) Cytosolic factors mediate protein insertion into the peroxisomal membrane. FEBS Lett 414:95–8

Pinho SA de A (2010) Induction and determination of ROS and their effect on peroxisome dynamics. University of Aveiro (Master's Thesis)

Pinto MP, Grou CP, Alencastre IS, et al (2006) The Import Competence of a Peroxisomal Membrane Protein Is Determined by Pex19p before the Docking Step. J Biol Chem 281:34492–34502

Pinto MP, Grou CP, Fransen M, et al (2009) The cytosolic domain of PEX3, a protein involved in the biogenesis of peroxisomes, binds membrane lipids. Biochim Biophys Acta - Mol Cell Res 1793:1669–1675. doi: 10.1016/J.BBAMCR.2009.08.007

Piperno G (1987) Microtubules containing acetylated alpha-tubulin in mammalian cells in culture. J Cell Biol 104:289–302. doi: 10.1083/jcb.104.2.289

Platta HW, Grunau S, Rosenkranz K, et al (2005) Functional role of the AAA peroxins in dislocation of the cycling PTS1 receptor back to the cytosol. Nat Cell Biol 7:817–822. doi: 10.1038/ncb1281

Poirier Y, Antonenkov VD, Glumoff T, Hiltunen JK (2006) Peroxisomal beta-oxidation--a metabolic pathway with multiple functions. Biochim Biophys Acta 1763:1413–1426

Popov V, Medvedev NI, Davies HA, Stewart MG (2005) Mitochondria form a

filamentous reticular network in hippocampal dendrites but are present as discrete bodies in axons: A three-dimensional ultrastructural study. J Comp Neurol 492:50–65. doi: 10.1002/cne.20682

Post JA, Verkleij AJ, Roelofsen B, Op de Kamp JA (1988) Plasmalogen content and distribution in the sarcolemma of cultured neonatal rat myocytes. FEBS Lett 240:78–82

Rabanal-Ruiz Y, Otten EG, Korolchuk VI (2017) mTORC1 as the main gateway to autophagy. Essays Biochem 61:565–584. doi: 10.1042/EBC20170027

Rakhshandehroo M, Knoch B, Michael M, Kersten S (2010) Peroxisome Proliferator-Activated Receptor Alpha Target Genes. PPAR Res. doi: 10.1155/2010/612089

Rambold AS, Kostelecky B, Elia N, Lippincott-schwartz J (2011) Tubular network formation protects mitochondria from autophagosomal degradation during nutrient starvation. Proc Natl Acad Sci U S A 108:10190–10195. doi: 10.1073/pnas.1107402108/-/DCSupplemental.www.pnas.org/cgi/doi/10.1073/pnas.1107402108

Rapp S, Saffrich R, Anton M, et al (1996) Microtubule-based peroxisome movement. J Cell Sci 109:837–849

Raychaudhuri S, Prinz WA (2008) Nonvesicular phospholipid transfer between peroxisomes and the endoplasmic reticulum. Proc Natl Acad Sci U S A 105:15785–15790

Raymond G V, Moser AB, Fatemi A (1993) X-Linked Adrenoleukodystrophy

Ren Y, Liu W, Jiang H, et al (2005) Selective Vulnerability of Dopaminergic Neurons to Microtubule Depolymerization. J Biol Chem 280:34105–34112. doi: 10.1074/jbc.M503483200

Reuber BE, Karl C, Reimann SA, et al (1997) Cloning and functional expression of a mammalian gene for a peroxisomal sarcosine oxidase. J Biol Chem 272:6766–76. doi: 10.1074/jbc.272.10.6766

Rhee SG (2006) H2O2, a necessary evil for cell signaling. Science 312:1882–3. doi: 10.1126/science.1130481

Rhodin J (1954) Correlation of ultrastructural organization and function in normal and experimentally changed proximal convoluted tubule cells of the mouse kidney. Aktiebolaget Godvil

Ribeiro D, Castro I, Fahimi HD, Schrader M (2012) Peroxisome morphology in pathology. Histol Histopathol 27:661–676

Riccio V, Demers N, Hua R, et al (2019) Deubiquitinating enzyme USP30 maintains basal peroxisome abundance by regulating pexophagy. J Cell Biol jcb.201804172. doi: 10.1083/jcb.201804172

Richards DM, Endres RG (2017) How cells engulf: a review of theoretical approaches to phagocytosis. Reports Prog Phys 80:126601. doi: 10.1088/1361-6633/aa8730

Rokka A, Antonenkov VD, Soininen R, et al (2009) Pxmp2 Is a Channel-Forming Protein in Mammalian Peroxisomal Membrane. PLoS One 4:e5090. doi: 10.1371/journal.pone.0005090

Rottensteiner H, Kramer A, Lorenzen S, et al (2004) Peroxisomal membrane proteins contain common Pex19p-binding sites that are an integral part of their targeting signals. Mol Biol Cell 15:3406–3417. doi: 10.1091/mbc.E04–03–0188

Rottensteiner H, Theodoulou FL (2006) The ins and outs of peroxisomes: Co-ordination of membrane transport and peroxisomal metabolism. Biochim Biophys Acta (BBA)-Molecular Cell Res 1763:1527–1540. doi: 10.1016/j.bbamcr.2006.08.012

Rucktäschel R, Thoms S, Sidorovitch V, et al (2009) Farnesylation of Pex19p Is Required for Its Structural Integrity and Function in Peroxisome Biogenesis. J Biol Chem 284:20885–20896. doi: 10.1074/JBC.M109.016584

Russell DW (2003) The enzymes, regulation, and genetics of bile acid synthesis. Annu Rev Biochem 72:137–74. doi: 10.1146/annurev.biochem.72.121801.161712

Sacksteder K a., Jones JM, South ST, et al (2000) PEX19 binds multiple peroxisomal membrane proteins, is predominantly cytoplasmic, and is required for peroxisome membrane synthesis. J Cell Biol 148:931–944. doi: 10.1083/jcb.148.5.931

Santos MJ, Imanaka T, Shio H, et al (1988) Peroxisomal membrane ghosts in Zellweger syndrome--aberrant organelle assembly. Science 239:1536–8

Sargent G, van Zutphen T, Shatseva T, et al (2016) PEX2 is the E3 ubiquitin ligase required for pexophagy during starvation. J Cell Biol 214:677–690. doi: 10.1083/jcb.201511034

Schell-Steven A, Stein K, Amoros M, et al (2005) Identification of a Novel, Intraperoxisomal Pex14-Binding Site in Pex13: Association of Pex13 with the

Docking Complex Is Essential for Peroxisomal Matrix Protein Import. Mol Cell Biol 25:3007–3018. doi: 10.1128/MCB.25.8.3007-3018.2005

Schneider CA, Rasband WS, Eliceiri KW (2012) NIH Image to ImageJ: 25 years of image analysis. Nat Methods 9:671–5

Schrader M, Baumgart E, Fahimi HD (1995) Effects of fixation on the preservation of peroxisomal structures for immunofluorescence studies using HepG2 cells as a model system. Histochem J 27:615–9

Schrader M, Bonekamp NA, Islinger M (2012) Fission and proliferation of peroxisomes. Biochim Biophys Acta - Mol Basis Dis 1822:1343–1357. doi: 10.1016/j.bbadis.2011.12.014

Schrader M, Burkhardt JK, Baumgart E, et al (1996) Interaction of microtubules with peroxisomes. Tubular and spherical peroxisomes in HepG2 cells and their alteractions induced by microtubule-active drugs. Eur J Cell Biol 69:24–35

Schrader M, Castro I, Fahimi HD, Islinger M (2014) Peroxisome morphology in pathologies. In: Molecular Machines Involved in Peroxisome Biogenesis and Maintenance. Springer, pp 125–151

Schrader M, Costello JL, Godinho LF, et al (2016a) Proliferation and fission of peroxisomes — An update. Biochim Biophys Acta - Mol Cell Res 1863:971–983. doi: 10.1016/j.bbamcr.2015.09.024

Schrader M, Costello JL, Godinho LF, et al (2016b) Proliferation and fission of peroxisomes - An update. Biochim Biophys Acta - Mol Cell Res 1863:971–983. doi: 10.1016/j.bbamcr.2015.09.024

Schrader M, Fahimi HD (2006a) Peroxisomes and oxidative stress. Biochim Biophys Acta - Mol Cell Res 1763:1755–1766. doi: 10.1016/j.bbamcr.2006.09.006

Schrader M, Fahimi HD (2004) Mammalian peroxisomes and reactive oxygen species. Histochem Cell Biol 122:383–393. doi: 10.1007/s00418-004-0673-1

Schrader M, Fahimi HD (2006b) Growth and division of peroxisomes. Int Rev Cytol 255:237–290. doi: S0074-7696(06)55005-3 [pii] 10.1016/S0074-7696(06)55005-3

Schrader M, Godinho LF, Costello JL, Islinger M (2015) The different facets of organelle interplay—an overview of organelle interactions. Front Cell Dev Biol 3:56. doi: 10.3389/fcell.2015.00056

Schrader M, Kamoshita M, Islinger M (2019) Organelle interplay-peroxisome interactions in health and disease. J Inherit Metab Dis. doi: 10.1002/jimd.12083

Schrader M, King SJ, Stroh TA, Schroer TA (2000) Real time imaging reveals a peroxisomal reticulum in living cells. J Cell Sci 113:3663–3671

Schrader M, Krieglstein K, Dariush Fahimi H (1998) Tubular peroxisomes in HepG2 cells: Selective induction by growth factors and arachidonic acid. Eur J Cell Biol 75:87–96. doi: 10.1016/S0171-9335(98)80051-4

Schrader M, Pellegrini L (2017) The making of a mammalian peroxisome, version 2.0: mitochondria get into the mix. Cell Death Differ 24:1148–1152. doi: 10.1038/cdd.2017.23

Schrader M, Thiemann M, Fahimi HD (2003) Peroxisomal Motility and Interaction With Microtubules. Microsc Res Tech 61:171–178. doi: 10.1002/jemt.10326

Schrader M, Wodopia R, Fahimi HD (1999) Induction of Tubular Peroxisomes by UV Irradiation and Reactive Oxygen Species in HepG2 Cells. J Histochem Cytochem 47:1141–1148. doi: 10.1177/002215549904700906

Schrader TA, Schrader M (2017) siRNA-mediated Silencing of Peroxisomal Genes in Mammalian Cells. In: Methods in molecular biology (Clifton, N.J.). pp 69–79

Schrul B, Kopito RR (2016) Peroxin-dependent targeting of a lipid-droplet-destined membrane protein to ER subdomains. Nat Cell Biol 18:740–751. doi: 10.1038/ncb3373

Schueller N, Holton SJ, Fodor K, et al (2010) The peroxisomal receptor Pex19p forms a helical mPTS recognition domain. EMBO J 29:2491–2500. doi: 10.1038/emboj.2010.115

Sepasi Tehrani H, Moosavi-Movahedi AA (2018) Catalase and its mysteries. Prog Biophys Mol Biol 140:5–12. doi: 10.1016/J.PBIOMOLBIO.2018.03.001

Sexton JZ, He Q, Forsberg LJ, Brenman JE (2010) High content screening for non-classical peroxisome proliferators. Int J High Throughput Screen 2010:127–140. doi: 10.2147/IJHTS.S10547

Shai N, Yifrach E, van Roermund CWT, et al (2018) Systematic mapping of contact sites reveals tethers and a function for the peroxisome-mitochondria contact. Nat Commun 9:1761. doi: 10.1038/s41467-018-03957-8

Shamseldin HE, Alshammari M, Al-Sheddi T, et al (2012) Genomic analysis of

mitochondrial diseases in a consanguineous population reveals novel candidate disease genes. J Med Genet 49:234–241. doi: 10.1136/jmedgenet-2012-100836

Sheffer R, Douiev L, Edvardson S, et al (2016) Postnatal microcephaly and pain insensitivity due to a de novo heterozygous DNM1L mutation causing impaired mitochondrial fission and function. Am J Med Genet A 170:1603–7. doi: 10.1002/ajmg.a.37624

Sherer TB, Betarbet R, Testa CM, et al (2003) Mechanism of toxicity in rotenone models of Parkinson's disease. J Neurosci 23:10756–64

Shiao YJ, Lupo G, Vance JE (1995) Evidence that phosphatidylserine is imported into mitochondria via a mitochondria-associated membrane and that the majority of mitochondrial phosphatidylethanolamine is derived from decarboxylation of phosphatidylserine. J Biol Chem 270:11190–8. doi: 10.1074/JBC.270.19.11190

Shimozawa N, Suzuki Y, Zhang Z, et al (2000) Identification of PEX3 as the gene mutated in a Zellweger syndrome patient lacking peroxisomal remnant structures. Hum Mol Genet 9:1995–1999. doi: 10.1093/hmg/9.13.1995

Singh AK, Dhaunsi GS, Gupta MP, et al (1994) Demonstration of Glutathione Peroxidase in Rat Liver Peroxisomes and Its Intraorganellar Distribution. Arch Biochem Biophys 315:331–338. doi: 10.1006/ABBI.1994.1508

Smith JJ, Aitchison JD (2013) Peroxisomes take shape. Nat Rev Mol Cell Biol 14:803–817. doi: 10.1038/nrm3700

Soliman K, Göttfert F, Rosewich H, et al (2018) Super-resolution imaging reveals the sub-diffraction phenotype of Zellweger Syndrome ghosts and wild-type peroxisomes. Sci Rep 8:7809. doi: 10.1038/s41598-018-24119-2

Soukupova M, Sprenger C, Gorgas K, et al (1999) Identification and characterization of the human peroxin PEX3. Eur J Cell Biol 78:357–374. doi: 10.1016/S0171-9335(99)80078-8

South ST, Gould SJ (1999) Peroxisome Synthesis in the Absence of Preexisting Peroxisomes. J Cell Biol 144:255–266

Srivastava P, Panda D (2007) Rotenone inhibits mammalian cell proliferation by inhibiting microtubule assembly through tubulin binding. FEBS J 274:4788–4801. doi: 10.1111/j.1742-4658.2007.06004.x

Stamer K, Vogel R, Thies E, et al (2002) Tau blocks traffic of organelles, neurofilaments, and APP vesicles in neurons and enhances oxidative stress.

J Cell Biol 156:1051–63. doi: 10.1083/jcb.200108057

Stolz D, Zamora R, Vodovotz Y, et al (2002) Peroxisomal localization of inducible nitric oxide synthase in hepatocytes. Hepatology 36:81–93. doi: 10.1053/jhep.2002.33716

Su HM, Moser AB, Moser HW, Watkins PA (2001) Peroxisomal straight-chain Acyl-CoA oxidase and D-bifunctional protein are essential for the retroconversion step in docosahexaenoic acid synthesis. J Biol Chem 276:38115–20. doi: 10.1074/jbc.M106326200

Su J, Thomas AS, Grabietz T, et al (2018) The N-terminal amphipathic helix of Pex11p self-interacts to induce membrane remodelling during peroxisome fission. Biochim Biophys Acta - Biomembr. doi: 10.1016/j.bbamem.2018.02.029

Sugiura A, Mattie S, Prudent J, McBride HM (2017) Newly born peroxisomes are a hybrid of mitochondrial and ER-derived pre-peroxisomes. Nature 542:251–254. doi: 10.1038/nature21375

Sun M, Bernard LP, DiBona VL, et al (2013) Calcium Phosphate Transfection of Primary Hippocampal Neurons. J Vis Exp e50808. doi: 10.3791/50808

Suzuki Y, Orii T, Takiguchi M, et al (1987) Biosynthesis of Membrane Polypeptides of Rat Liver Peroxisomes. J Biochem 101:491–496. doi: 10.1093/oxfordjournals.jbchem.a121935

Tanaka H, Okazaki T, Aoyama S, et al (2019) Peroxisomes control mitochondrial dynamics and the mitochondrion-dependent apoptosis pathway. J Cell Sci 132:jcs224766. doi: 10.1242/jcs.224766

Tantama M, Hung YP, Yellen G (2011) Imaging Intracellular pH in Live Cells with a Genetically Encoded Red Fluorescent Protein Sensor. J Am Chem Soc 133:10034–10037. doi: 10.1021/ja202902d

Taylor RL, Handley MT, Waller S, et al (2017) Novel PEX11B Mutations Extend the Peroxisome Biogenesis Disorder 14B Phenotypic Spectrum and Underscore Congenital Cataract as an Early Feature. Invest Ophthalmol Vis Sci 58:594–603. doi: 10.1167/iovs.16-21026

Testa CM, Sherer TB, Greenamyre JT (2005) Rotenone induces oxidative stress and dopaminergic neuron damage in organotypic substantia nigra cultures. Mol Brain Res 134:109–118. doi: 10.1016/j.molbrainres.2004.11.007

Theiss C, Neuhaus A, Schliebs W, Erdmann R (2012) TubStain: a universal

peptide-tool to label microtubules. Histochem Cell Biol 138:531–540. doi: 10.1007/s00418-012-0992-6

Thiemann M, Schrader M, Volkl A, et al (2000) Interaction of peroxisomes with microtubules In vitro studies using a novel peroxisome-microtubule binding assay. Eur J Biochem 267:6264–6275

Thorne BC, Bailey AM, Peirce SM (2007) Combining experiments with multi-cell agent-based modeling to study biological tissue patterning. Brief Bioinform 8:245–257. doi: 10.1093/bib/bbm024

Titorenko VI, Terlecky SR (2011) Peroxisome metabolism and cellular aging. Traffic 12:252–259. doi: 10.1111/j.1600-0854.2010.01144.x

Trujillo M, Clippe A, Manta B, et al (2007) Pre-steady state kinetic characterization of human peroxiredoxin 5: Taking advantage of Trp84 fluorescence increase upon oxidation. Arch Biochem Biophys 467:95–106. doi: 10.1016/j.abb.2007.08.008

Tsimring LS (2014) Noise in biology. Rep Prog Phys 77:026601. doi: 10.1088/0034-4885/77/2/026601

Tweedy L, Meier B, Stephan J, et al (2013) Distinct cell shapes determine accurate chemotaxis. Sci Rep 3:2606. doi: 10.1038/srep02606

van de Beek M-C, Ofman R, Dijkstra I, et al (2017) Lipid-induced endoplasmic reticulum stress in X-linked adrenoleukodystrophy. Biochim Biophys Acta - Mol Basis Dis 1863:2255–2265. doi: 10.1016/j.bbadis.2017.06.003

van der Zand A, Braakman I, Tabak HF (2010) Peroxisomal membrane proteins insert into the endoplasmic reticulum. Mol Biol Cell 21:2057–2065. doi: 10.1091/mbc.E10

van Leyen K, Duvoisin RM, Engelhardt H, Wiedmann M (1998) A function for lipoxygenase in programmed organelle degradation. Nature 395:392–395. doi: 10.1038/26500

van Roermund CWT, de Jong M, IJlst L, et al (2004) The peroxisomal lumen in Saccharomyces cerevisiae is alkaline. J Cell Sci 117:4231–7. doi: 10.1242/jcs.01305

Vance JE (2015) Phospholipid Synthesis and Transport in Mammalian Cells. Traffic 16:1–18. doi: 10.1111/tra.12230

Vanstone JR, Smith AM, McBride S, et al (2016) DNM1L-related mitochondrial fission defect presenting as refractory epilepsy. Eur J Hum Genet 24:1084–1088. doi: 10.1038/ejhg.2015.243

Vastiau IMK, Anthonio EA, Brams M, et al (2006) Farnesylation of Pex19p is not essential for peroxisome biogenesis in yeast and mammalian cells. Cell Mol Life Sci C 63:1686–1699. doi: 10.1007/s00018-006-6110-y

Votyakova T V., Reynolds IJ (2008) ΔΨm-Dependent and -independent production of reactive oxygen species by rat brain mitochondria. J Neurochem 79:266–277. doi: 10.1046/j.1471-4159.2001.00548.x

Walbrecq G, Wang B, Becker S, et al (2015) Antioxidant cytoprotection by peroxisomal peroxiredoxin-5. Free Radic Biol Med 84:215–226. doi: 10.1016/j.freeradbiomed.2015.02.032

Wali G, Sutharsan R, Fan Y, et al (2016) Mechanism of impaired microtubule-dependent peroxisome trafficking and oxidative stress in SPAST-mutated cells from patients with Hereditary Spastic Paraplegia. Sci Rep 6:27004. doi: 10.1038/srep27004

Walker CL, Pomatto LCD, Tripathi DN, Davies KJA (2018) Redox Regulation of Homeostasis and Proteostasis in Peroxisomes. Physiol Rev 98:89. doi: 10.1152/PHYSREV.00033.2016

Walter KM, Schönenberger MJ, Trötzmüller M, et al (2014) Hif-2α promotes degradation of mammalian peroxisomes by selective autophagy. Cell Metab 20:882–897. doi: 10.1016/j.cmet.2014.09.017

Walter T, Erdmann R (2019) Current Advances in Protein Import into Peroxisomes. Protein J 38:351–362. doi: 10.1007/s10930-019-09835-6

Walton P a., Pizzitelli M (2012) Effects of peroxisomal catalase inhibition on mitochondrial function. Front Physiol 3:1–10. doi: 10.3389/fphys.2012.00108

Walton PA, Wendland M, Subramani S, et al (1994) Involvement of 70-kD heat-shock proteins in peroxisomal import. J Cell Biol 125:1037–46

Wanders RJ, Denis S, Ruiter JP, et al (1995) Measurement of peroxisomal fatty acid beta-oxidation in cultured human skin fibroblasts. J Inherit Metab Dis 18 Suppl 1:113–24

Wanders RJ, Van Roermund CW (1993) Studies on phytanic acid alpha-oxidation in rat liver and cultured human skin fibroblasts. Biochim Biophys Acta 1167:345–50

Wanders RJ, Waterham HR, Leroy BP (2006) Refsum Disease. University of Washington, Seattle

Wanders RJA (2018) Peroxisomal disorders: Improved laboratory diagnosis, new

defects and the complicated route to treatment. Mol Cell Probes 40:60–69. doi: 10.1016/j.mcp.2018.02.001

Wanders RJA, Komen J, Ferdinandusse S (2011) Phytanic acid metabolism in health and disease. Biochim Biophys Acta 1811:498–507. doi: 10.1016/j.bbalip.2011.06.006

Wanders RJA, Waterham HR, Ferdinandusse S (2016) Metabolic Interplay between Peroxisomes and Other Subcellular Organelles Including Mitochondria and the Endoplasmic Reticulum. Front Cell Dev Biol Front Cell Dev Biol 3:833383–833389. doi: 10.3389/fcell.2015.00083

Wang B, Van Veldhoven PP, Brees C, et al (2013a) Mitochondria are targets for peroxisome-derived oxidative stress in cultured mammalian cells. Free Radic Biol Med 65:882–894. doi: 10.1016/j.freeradbiomed.2013.08.173

Wang W, Wu Z, Dai Z, et al (2013b) Glycine metabolism in animals and humans: implications for nutrition and health. Amino Acids 45:463–477. doi: 10.1007/s00726-013-1493-1

Wang X, Schwarz TL (2009) The Mechanism of Ca2+ -Dependent Regulation of Kinesin-Mediated Mitochondrial Motility. Cell 136:163–174. doi: 10.1016/j.cell.2008.11.046

Wang Y, Metz J, Costello JL, et al (2018) Intracellular redistribution of neuronal peroxisomes in response to ACBD5 expression. PLoS One 13:e0209507. doi: 10.1371/journal.pone.0209507

Watanabe Y, Dahlman EL, Leder KZ, Hui SK (2016) A mathematical model of tumor growth and its response to single irradiation. Theor Biol Med Model 13:6. doi: 10.1186/s12976-016-0032-7

Waterham HR, Ebberink MS (2012) Genetics and molecular basis of human peroxisome biogenesis disorders. Biochim Biophys Acta 1822:1430–1441. doi: 10.1016/j.bbadis.2012.04.006

Waterham HR, Ferdinandusse S, Wanders RJA (2016) Human disorders of peroxisome metabolism and biogenesis. Biochim Biophys Acta - Mol Cell Res 1863:922–933. doi: 10.1016/j.bbamcr.2015.11.015

Waterham HR, Koster J, van Roermund CWT, et al (2007) A lethal defect of mitochondrial and peroxisomal fission. N Engl J Med 356:1736–1741

Weir NR, Kamber RA, Martenson JS, Denic V (2017) The AAA protein Msp1 mediates clearance of excess tail-anchored proteins from the peroxisomal membrane. Elife 6:. doi: 10.7554/eLife.28507

Westin MAK, Hunt MC, Alexson SEH (2008) Short- and medium-chain carnitine acyltransferases and acyl-CoA thioesterases in mouse provide complementary systems for transport of beta-oxidation products out of peroxisomes. Cell Mol Life Sci 65:982–90. doi: 10.1007/s00018-008-7576-6

Wiemer EAC, Wenzel T, Deerinck TJ, et al (1997) Visualization of the peroxisomal compartment in living mammalian cells: dynamic behavior and association with microtubules. J Cell Biol 136:71–80

Williams C, Opalinski L, Landgraf C, et al (2015) The membrane remodeling protein Pex11p activates the GTPase Dnm1p during peroxisomal fission. Proc Natl Acad Sci U S A 112:6377–6382. doi: 10.1073/pnas.1418736112

Wong CP, Xu Z, Power C, Hobman TC (2018) Targeted Elimination of Peroxisomes During Viral Infection: Lessons from HIV and Other Viruses. DNA Cell Biol 37:417–421. doi: 10.1089/dna.2018.4153

Wriesnegger T, Gubitz G, Leitner E, et al (2007) Lipid composition of peroxisomes from the yeast Pichia pastoris grown on different carbon sources. Biochim Biophys Acta - Mol Cell Biol Lipids 1771:455–461. doi: 10.1016/j.bbalip.2007.01.004

Xiao J, Luo J, Hu A, et al (2019) Cholesterol transport through the peroxisome-ER membrane contacts tethered by PI(4,5)P2 and extended synaptotagmins. Sci China Life Sci. doi: 10.1007/s11427-019-9569-9

Xu L-G, Wang Y-Y, Han K-J, et al (2005) VISA Is an Adapter Protein Required for Virus-Triggered IFN-β Signaling. Mol Cell 19:727–740. doi: 10.1016/j.molcel.2005.08.014

Xu Z, Asahchop EL, Branton WG, et al (2017) MicroRNAs upregulated during HIV infection target peroxisome biogenesis factors: Implications for virus biology, disease mechanisms and neuropathology. PLOS Pathog 13:e1006360. doi: 10.1371/journal.ppat.1006360

Yagita Y, Shinohara K, Abe Y, et al (2017) Deficiency of a Retinal Dystrophy Protein, Acyl-CoA Binding Domain-containing 5 (ACBD5), Impairs Peroxisomal β-Oxidation of Very-long-chain Fatty Acids. J Biol Chem 292:691–705. doi: 10.1074/jbc.M116.760090

Yamashita S, Abe K, Tatemichi Y, Fujiki Y (2014) The membrane peroxin PEX3 induces peroxisome-ubiquitination-linked pexophagy. 3:1549–1564

Yang Y, Lee M, Fairn GD (2018) Phospholipid subcellular localization and

dynamics. J Biol Chem 293:6230–6240. doi: 10.1074/jbc.R117.000582

Yeldandi A V, Chu R, Pan J, et al (1996) Peroxisomal purine metabolism. Ann N Y Acad Sci 804:165–75

Yeung T, Gilbert GE, Shi J, et al (2008) Membrane phosphatidylserine regulates surface charge and protein localization. Science 319:210–3. doi: 10.1126/science.1152066

Yokota S, Haraguchi CM, Oda T (2008) Induction of peroxisomal Lon protease in rat liver after di-(2-ethylhexyl)phthalate treatment. Histochem Cell Biol 129:73–83. doi: 10.1007/s00418-007-0328-0

Yokota S, Oda T, Fahimi HD (2001) The role of 15-lipoxygenase in disruption of the peroxisomal membrane and in programmed degradation of peroxisomes in normal rat liver. J Histochem Cytochem 49:613–622. doi: 10.1177/002215540104900508

Yoon G, Malam Z, Paton T, et al (2016) Lethal Disorder of Mitochondrial Fission Caused by Mutations in DNM1L. J Pediatr 171:313–316.e2. doi: 10.1016/j.jpeds.2015.12.060

Yoon Y, Krueger EW, Oswald BJ, Mcniven MA (2003) The mitochondrial protein hFis1 regulates mitochondrial fission in mammalian cells through an interaction with the dynamin-like protein DLP1. Mol Cell Biol 23:5409–5420. doi: 10.1128/MCB.23.15.5409

Yoshida Y, Niwa H, Honsho M, et al (2015) Pex11mediates peroxisomal proliferation by promoting deformation of the lipid membrane. Biol Open 4:710–21. doi: 10.1242/bio.201410801

Zhang J, Kim J, Alexander A, et al (2013) A tuberous sclerosis complex signalling node at the peroxisome regulates mTORC1 and autophagy in response to ROS. Nat Cell Biol 15:1–13. doi: 10.1038/ncb2822

Zhang J, Tripathi DN, Jing J, et al (2015) ATM functions at the peroxisome to induce pexophagy in response to ROS. Nat Cell Biol 17:1259–1269. doi: 10.1038/ncb3230

Zhang Z, Naughton D, Winyard PG, et al (1998) Generation of Nitric Oxide by a Nitrite Reductase Activity of Xanthine Oxidase: A Potential Pathway for Nitric Oxide Formation in the Absence of Nitric Oxide Synthase Activity. Biochem Biophys Res Commun 249:767–772. doi: 10.1006/bbrc.1998.9226

Zheng C, Su C (2017) Herpes simplex virus 1 infection dampens the immediate early antiviral innate immunity signaling from peroxisomes by tegument

protein VP16. Virol J 14:35. doi: 10.1186/s12985-017-0709-5

Zinser E, Sperka-Gottlieb CD, Fasch E V, et al (1991) Phospholipid synthesis and lipid composition of subcellular membranes in the unicellular eukaryote Saccharomyces cerevisiae. J Bacteriol 173:2026–34

Zoeller RA, Lake AC, Nagan N, et al (1999) Plasmalogens as endogenous antioxidants: somatic cell mutants reveal the importance of the vinyl ether. Biochem J 338 (Pt 3):769–76